Journal of Engineering

ISSN 1726-4073

A Scientific Refereed Journal
Published by College of
Engineering University of
Baghdad

July

2014

Number 7

Volume 20

ISSN 1726-4073

مجلة الهندسة

مجلة علمية محكمة تصدرها
كلية الهندسة ـ جامعة بغداد

تموز
2014

العدد 7
المجلد 20

ENGINEERING

College of Engineering University of Baghdad

List of Contents

English Section:

Assessing Durability of Roller Compacted Concrete

Prof. Saad Issa Sarsam
Department of Civil Engineering
College of Engineering
Baghdad University
Email: saadisasarsam3@yahoo.com

Lect. Dr. Abeer Abdulqader Salih
Department of Civil Engineering
College of Engineering
Baghdad University
drabeeraslih@yahoo.com

Sura Dheyaa Tawfee
Department of Civil Engineering
College of Engineering
Baghdad University

ABSTRACT

Roller Compacted Concrete (RCC) is a technology characterized mainly by the use of rollers for compaction; this technology achieves significant time and cost savings in the construction of dams and roads. The primary scope of this research is to study the durability and performance of roller compacted concrete that was constructed in the laboratory using roller compactor manufactured in local market. A total of (60) slab specimen of (38×38×10) cm was constructed using the roller device, cured for 28 days, then 180 sawed cubes and 180 beams are obtained from RCC slab. Then, the specimens are subjected to 60 cycles of freezing and thawing, sulfate attack test and wetting and drying. The degree of effect of the type of coarse aggregate (crushed and rounded), cement type (OPC and SRPC) and cement content on the durability of RCC were investigated. The results indicated that RCC that contain SRPC has beneficial effects on properties of RCC as compared to RCC that contain OPC after durability testing. Based on the testing results, it was concluded that the resistance of RCC specimens to freezing and thawing, wetting and drying and sulfate attack test increase as cement content increase. The results also indicate that using RCC that contain crushed aggregate has a positive effect on the overall properties of RCC, as compared with RCC that contain rounded aggregate after durability testing.

Keywords: roller compacted concrete, durability, freezing and thawing, sulfate attack test, wetting and drying.

تقييم ديمومة الخرسانة المرصوصة بالحدل

ا. سعد عيسى سرسم
قسم الهندسة المدنية
كلية الهندسة/جامعة بغداد

م.د.عبير عبد القادر صالح
قسم الهندسة المدنية
كلية الهندسة/جامعة بغداد

سرى ضياء توفيق
قسم الهندسة المدنية
كلية الهندسة/جامعة بغداد

الخلاصة

تعتبر الخرسانة المرصوصة بالحدل من التقنيات التي تعتمد بالدرجة الأكبر خاصية إستعمال الحادلات لرص الخرسانة،هذه التقنية توفر وتحفظ الوقت المهم والكلفة في إنشاء السدود و الطرق. ان الهدف الرئيسي من هذا البحث هو دراسة ديمومة واداء الخرسانة المرصوصة بالحدل التي تم تصنيعها مختبريا بأستخدام جهاز حدل صنع في الاسواق المحلية. 0يتضمن الجزء العملي تحضير (60) بلاطة خرسانية مرصوصة بالحادلة بأبعاد (٣٨×٣٨×١٠) سم،بعد ذلك انضجت لمدة 28 يوم، ثم تم تقطيع هذه البلاطات الى (180) مكعب و (180)عتبة. تم تعريض النماذج الى 30و60 دوره من الانجماد والذوبان , فحص تأثير الكبريتات و الترطيب والتجفيف. تم دراسة نوع السمنت (السمنت البورتلاندي الاعتيادي و السمنت المقاوم للكبريتات) وتأثير محتوى السمنت على ديمومة الخرسانة المرصوصة بالحادلة. من خلال النتائج التي تم الحصول عليها وجد ان مقاومة النماذج الحاوية على السمنت المقاوم للكبريتات له تأثير ايجابي على خواص الخرسانة المرصوصة بالحدل مقارنة مع النماذج الحاوية على السمنت البورتلاندي الاعتيادي بعد تعريض النماذج الى فحوصات الديمومة. اعتمادا على نتائج الفحوصات تم الاستنتاج ايضا بأن مقاومة نماذج الخرسانة المرصوصة بالحدل لدورات الانجماد والذوبان , الترطيب و التجفيف و فحص مقاومة تأثير الكبريتات تزداد بزيادة محتوى السمنت .

1. INTRODUCTION

The American Concrete Institute (ACI) defines RCC as "concrete compacted by roller compaction; in its unhardened state, will support a roller while being compacted." Properties of hardened RCC can be similar to those of conventionally placed concrete. The term "roller compaction" is also defined by ACI as "a process for compacting concrete using a roller, often a vibrating roller. **USACE , 2000.**

Kreuer ,2006, defined Roller Compacted Concrete as a dry concrete consisting of more aggregate and less cement paste than conventional concrete. Because cement is the most expensive constituent of concrete, RCC is less expensive in terms of cost of materials.

Due to its dry nature, RCC has a zero slump and it is placed without forms or finishing. RCC pavements do not require joints, dowels, or reinforcing steel. Relatively large quantities of RCC pavement can be placed rapidly with minimal labor and equipment, enabling speedy completion of tightly scheduled pavements.

RCC is used for the construction of dams and pavements, **Chun et al , 2008**. RCC first was used to build dams. Besides the reduced construction cost resulting mainly from labor and equipment savings, its principal advantage for mass construction is the low cement content of the mixture which greatly reduces problems due to the heat of hydration of cement, **PCA , 2004.**

RCC pavement is much stronger and durable than asphalt pavement. RCC will not rut from high axle loads, or shove or tear from turning or braking of operating equipment. It will not soften from heat generated by hot summer sun or material stored on RCC floors. RCC resists degradation from materials such as diesel fuel, **Naik et al , 2001**.

The primary differences in proportions of RCC pavement mixtures and conventional concrete pavement mixtures are, **ACI 325-10R-, 1995.**

• RCC is generally not air-entrained;
• RCC has lower water content;
• RCC has lower cement paste content;
• RCC generally requires a larger amount of fine aggregate in order to produce a combined aggregate that is well-graded and stable under the action of a vibratory roller. RCC pavements, like all other types of concrete elements, can be subjected to many types of deterioration such as abrasion/erosion, freezing and thawing, wetting and drying, and other factors such as alkali-silica reaction, and sulfate attack. RCC is now increasingly used for the construction of pavements exposed to very severe loading and environmental conditions, **PCA , 2004**.

RCC is not just more economical than the currently used pavement alternatives, but has also shown high durability and early gain of mechanical strength in both the field and the laboratory, **Kreuer 2006**.

RCC has been used in Iraq in mid-eighties below the foundations of the medical drug factory near Mosul and also in the AL-Adaim Dam, **Ahmed , 2001**. Another reported use was in the construction of extra lane for Mosul- Duhok highway in 1988, **Sarsam , 2002**.

1.1 Objective of the Study

The objective of this research is to assess durability and performance of a test slab that was constructed by using roller compactor machine. The main aims of this study are as follows:

1- Studying degree of effect of freezing and thawing cycles, wetting and drying cycles and sulfate attack on the modulus of rupture of RCC slabs.
2- Investigating degree of effect of cement type and cement content on the performance of RCC slabs during durability testing.

2 . EXPERIMENTAL WORK

2.1 Material Characteristics

2.1.1 Cement

Both ordinary Portland cement (OPC) and sulfate resisting Portland cement (SRPC) manufactured in Iraq with a commercial name of (Tasluga, Al-jesser) is used for RCC mixes throughout the present work.

2.1.2 Aggregate

Crushed gravel with a nominal size of (19 mm) brought from Nibaai region is used in this work. The aggregate is washed and cleaned by water. Later, it is air dried and separated into different sizes. Fine aggregate (passing sieve No.4 BS.) brought from Al-Ukhaider region are used in this work. The sand is washed and cleaned by water. Later, it is air dried and separated into different sizes.

2.1.2.1 Gradation of Coarse and Fine Aggregate

Dense gradation usually used for asphalt concrete pavement in Iraq has been adopted for this investigation. The coarse and fine aggregates are sieved to different sizes; the desired weight of each size of aggregate is taken and combined to satisfy the requirements of gradation**.** The design over all gradation of aggregate is selected by using of State Commission of Roads and Bridges **SCRB , 2004.** The grain size distribution is illustrated in **Table 1.**

2.1.3 Water

The water used in RCC mixes was drinking water of Baghdad area. This water was also used for curing**.**

2.2 Mix Design and Proportions of RCC Samples

The concrete mix is designed according to previous experience **Abdullah , 2011.** .Three different percentages of cement content has been selected (10 %, 12 %, and16 %) by weight of air dried aggregate and three different percentages of moisture content are used. The details of dry density at different moisture and cement contents are summarized in **Table 2**. Four types of mixes are adopted with three percentages of cement and
three percentages of moisture content for each mix; the types of mixes are as following:

1- Crushed aggregate + Natural sand + Ordinary Portland cement
2- Crushed Aggregate + Natural Sand + Sulfate resisting Portland cement.

2.3 Casting of RCC Slab Samples

2.3.1 The Molds

The steel molds manufactured in local workshop are used in this investigation. It consists of four sides made from angle section steel of (100×100×10 mm) with steel plate of (650×600×10 mm)**,** the sides and plate are connected together by bolts and two handles are welded with the plate to easy lift the mold and put on the vibrating table, the total weight of one mold is 51kg. A slab specimen having size of (380×380×100mm) is obtained from this mold. Molds details of slab specimens are shown in **Fig.1**.

2.3.2 The Roller Device

The device consists of a steel roller of 160mm diameter, 330 mm in length and 15 kg in weight is fixed by two bolts with device ,steel box of (600 ×460×180) mm is used to add various standard weights up to 138kg for applying loads on the roller to simulate the field conditions ,this box is connected by welding above the device, and two small wheels connected in the back direction for easy transporting the device during the work and two hands support is welded in the back of the device to easing push the device during the rolling as shown in **Fig.2** The total weight of this apparatus is 36 Kg.

2.3.3 Mixing

Before mixing the materials molds are prepared by cleaning, and their internal surfaces are covered by using nylon sheets to prevent loss of the water or material from sides during the rolling and to prevent adhesion with concrete after
hardening, after that for two minutes the cement and aggregate are dried mixed by hand mixing then a hole is formed at the mixture in the middle .Then required amount of water is poured and mixed for five to six minutes to achieve homogeneous mixture.

2.3.4 Compaction

2.3.4.1 Compaction by vibrating table

The mixture is placed in the mold and subjected to initial compaction on a vibrating table for 3 layers of 30 seconds time interval.

2.3.4.2 Compaction by using a roller device:

The mold is fixed in front of the roller compactor device and subjected to three stages of rolling based on the work done by **Sarsam ,2002. Abdullah ,2011.** and **Abdulrahim ,2011.** for each stage10 passes is applied .This number of passes is suitable to achieve the good rolling with low labor , and the rolling action is taken in x-x direction , then the same sequence have been repeated in the y- y direction as shown in the **Fig.3** . This is to insure the compaction of the slab sides. The first stage represent the initial compaction in the field, a total load of 1.1 kg/cm width (by using roller compactor weight only) is applied with 10 passes of the roller in each direction. The concrete is settled in a level position and completely fill the slab mold and gives a level surface, the compaction by using a roller device is shown in **Fig.4**.

The second stage may simulate the intermediate field compaction; a total load of 3.2 kg/cm width (by using 6 standard loads each load of 11.5 kg plus roller compactor weight) is applied with 10 passes of the roller in each direction. The final stage represents the finishing compaction in the field a total load of 5.3kg/cm width (by using 12 standard loads each load of 11.5 kg plus roller compactor weight) is applied with 10 passes of the roller in each direction.

2.3.5 Curing

After molding and finishing the compaction, the surface of casted samples is leveled by hand trawling and covered with polyethylene sheet to prevent evaporation of moisture from the fresh concrete, and left in lab

at room temperature of 30±5˚c to next day for setting then, the samples are taken out of the molds. Then, the specimens are immersed in the curing tank for (28) days at 30±5˚c. Part of RCC slab specimens after 28 day curing is shown in **Fig. 5**.

2.3.6 Cutting of RCC slab specimens

By using the procedure of **ASTM C42/C42M-(2003)** sawed cubes and beams are obtained from RCC slab specimens, a total of 180 cubes of (100×100×100 mm) are obtained from slab specimens, and 180 beams of (380×80×100mm) are also obtained from slabs specimens. Samples obtained from RCC slab is shown in **Fig. 6**.

2.4 Durability Investigations

2.4.1 Freezing and thawing test

The freezing and thawing test is carried out according to ASTM C-666-(2002) procedure B, (rapid freezing in air and thawing in water). Freezing and thawing tests are started by placing the specimens (4 cubes and 4 beams from each mixes) in the thawing water at the beginning of the thawing phase of the cycle at temperature 30 ± 3 ◦ C for 2 ½ hr to ensure that the specimens are completely thawed then, the specimens are taken out of water and are placed in deep freezer at temperature (-11± 1◦ C) for 4 ± ½ hr as the beginning of the freezing phase of the cycle. This procedure is repeated for 60 cycles of freezing and thawing**.**

2.4.2 Sulfate attack test

Resistance of RCC specimens to disintegrate by saturated solution of sodium sulfate is determined according to ASTM C –88 (1999).

2.4.3 Wetting and drying cycles

The RCC specimens are subjected to cycles of wetting and drying in the light of many research works **Mahmoud ,1977. AL-Delaimee , 1989. Ahmed, 2001, and Riyadh , 2005.** The cycles are started by placing the specimens (4 cubes and 4 beams from each mixture) in the oven at temperature 70 ◦ C for 24 hr. Then, it is removed from oven and it is immersed in water for 24 hr at

28 ◦ C .The alternate immersion and drying of specimens are repeated for 60 cycles.

2.5 Modulus of Rupture Test

The modulus of rupture is determined by using sawed beams of sizes (380×100×80) mm according to **ASTM C293-(2003).**

3. ANALYSIS AND DISCUSSION OF TEST RESULTS

3.1 Effect of Type of Cement and Cement Content on Modulus of Rupture of RCC during Freezing and Thawing Cyclic

Modulus of rupture of RCC that made of sulfate resisting Portland cement shows higher values than that RCC made of ordinary Portland cement before and after subjected to freezing and thawing cycles as shown in **Table 3**.

When testing beam specimen with 16% sulfate resisting Portland cement at 60 cycles of freezing and thawing the modulus of rupture is higher than that of specimens that have ordinary Portland cement by 14.285% as shown in **Fig.7**.This happens because the strength is developed rapidly for finer cement since the rate of hydration depends on the fineness of cement particles, where the surface area of cement represents the material available for hydration. This affects the resistance of cement paste and amount of water that able to freeze in it.

It can be seen that the modulus of rupture of sawed beams which obtained from RCC slab samples increases with increasing cement content. Specimens tested after 60 cycles of freezing and thawing shows increasing in modulus of rupture as cement content increase, the range of this increase is (22.43 -11.36%) for (OPC) **.**This may be attributed to the cement availability for hydration filling the voids, this will give better permeability and create stronger bonds within the concrete matrix and thus provide more resistance to frost damage in concrete were based up on the expansion of ice upon freezing and the subsequent stress , This agrees with **stutzman , 1999.** The durability can be improved by increasing cement content, Balaguru **and Ramakrishnan , 1986.**

Table 4 shows percentage of decrease in modulus of rupture of RCC that subjected to alternate freezing and thawing cycles, while **Fig. 8** shows the relationship between percentages of decrease in modulus of rupture with cement content for RCC made of OPC and SRPC**.**

The result also shows that the modulus of rupture of RCC decreases as the cycles increase. It can be seen from **Table 4** that the modulus of rupture at 60 cycles for beam specimens with 10% ordinary Portland cement shows maximum reduction of 12.213% , while beam specimens with 10% sulfate resisting Portland cement shows maximum reduction at 60 cycles of 6.619% . The reason of decreasing in strength is internal damage result from freezing and thawing cycles causes microscopic cracks in the cement paste leading to change in mechanical parameters of the concrete. This agrees with **Petersen , 2007.**

3.2 Effect of Type of Cement and Cement Content on Modulus of Rupture of RCC during Wetting and Drying Cyclic

It is clear from the test results that the modulus of rupture of RCC made of SRPC cement is higher than that OPC before and after subjecting specimens to cycles of wetting and drying as shown in **Table 5** .

When 16% sulfate resisting Portland cement is used the results show modulus of rupture higher than that ordinary Portland cement by 14.602% at 60 cycles of wetting and drying. This may be attributed to that

the rate of hydration will be reduced at each drying period for ordinary and sulfate resisting Portland cement but the strength of sulfate resisting Portland cement still developed faster than that ordinary Portland cement because SRPC is finer than OPC and the rate of hydration depends on the fineness of cement particles. **Fig. 9** shows the relationship between modulus of rupture and number of cycles for RCC made of ordinary and sulfate resisting Portland cement.

From the results in **Table 5**, it can clearly be seen that the modulus of rupture increases with increasing cement content before and after cycles of wetting and drying. The percentage of increasing in modulus of rupture is 21.815% when ordinary Portland cement content changes from 10% to 12% and 9.885% increasing in modulus of rupture when cement content changes from 12% to 16%. This trend may be attributed to higher cement content created stronger bonds within the concrete matrix and this provide more resistance to microcracks that result from drying process.

Table 6 shows percentage of decrease in modulus of rupture of RCC that subjected to wetting and drying cycles, **Fig.10** shows the relationship between percentage of decrease in modulus of rupture with cement content for RCC made of OPC and SRPC.

It can be seen that the modulus of rupture decrease as the cycles increase. The percentage of decrease in modulus of rupture at 30 and 60 cycles for RCC made of 12% ordinary Portland cement is 4.545% and 9.350% respectively than modulus of rupture at zero cycle, and the percentage of decrease in modulus of rupture at 30 and 60 cycles for RCC made of 12% sulphate resisting Portland cement is 3.899% and 8.050% respectively than modulus of rupture at no cycle. The reduction in strength is due to induces microcracks in RCC material and the rate of hydration will be reduced at each drying period.

3.3 Effect of Type of Cement and Cement Content on Modulus of Rupture of RCC during Sulfate Attack Cyclic

It is clear from the test results that modulus of rupture of RCC made of SRPC is higher than that RCC made of OPC before and after subjecting 60 cycles of wetting in sodium sulfate solution and drying as shown in **Table 7** . RCC made of 16% SRPC shows modulus of rupture higher than RCC made of OPC by 17.227% at 60 cycles .This is because sulfate resisting Portland cement have lower content of C_3A that react with sulfate ion and form ettringite. **Fig. 11** shows the relationship between modulus of rupture and number of cycles for RCC made of ordinary and sulfate resisting Portland cement.

It is clear from the test result that the modulus of rupture before and after 30 and 60 cycles of wetting in sulfate solution and drying increase as cement content increase , specimens tested after 30 cycles and that content 12% and 16% OPC shows increasing in modulus of rupture as compared to reference RCC mix at 10% by 19.7% and 30.4% respectively ,and specimens tested after 60 cycles and that content 12% and 16% SRPC shows increasing in modulus of rupture as compared to reference RCC mix at 10% by 21.26% and 33.8% respectively. This happens because at high cement content the concrete is higher density than that low cement content and this leads to make the concrete less permeability and the resistance of concrete to sulfate attack is depended on its permeability, **Neville , 1995.**

It can be seen from **Table 8** that after 30 and 60 cycles of immersion in sodium sulfate solution and drying RCC made of 12% ordinary Portland cement shows percentage of decrease in modulus of rupture by 6.103% and 12.597 % respectively than that modulus of rupture at no cycles, and specimens which have 12% sulfate resisting Portland cement shows after 30 and 60 cycles of immersion and drying percentage of decrease in modulus of rupture by 4.150% and 7.924% respectively than that modulus of rupture at zero cycles. The reduction in modulus of rupture can be attributed to the same reasons of decrease in compressive strength. Fig. 12 shows the relationship between percentage of decrease in modulus of rupture with cement content for RCC made of OPC and SRPC.

4. CONCLUSIONS

1- The modulus of rupture RCC mixes decrease with the increase in freezing and thawing cycles, alternating wetting and drying cycles, and with increasing the number of immersion cycles in sodium sulfate solution and then drying.
2- The resistance of RCC to freezing and thawing cycles, wetting and drying cycles and sulfate attack test increases with increasing cement content.
3- RCC made of sulfate resisting Portland cement gave better durability than RCC made of ordinary Portland cement when subjecting the specimens to 60 cycles of freezing and thawing. Modulus of rupture was higher for samples containing sulfate-resisting cement, as compared with ordinary Portland cement by 14.285% at 16% cement content.
4- Resistance of RCC mixes to sulfate attack test cycles was improved when using Sulfate resisting Portland cement as compared with the ordinary Portland cement, the modulus of rupture of samples exposed for 60 cycles and containing Sulfate resisting cement is higher than the resistance of samples containing ordinary Portland cement by 17.227% at 16% cement content.
5- Resistance of RCC containing sulfate-resisting cement is better than specimens containing ordinary Portland cement when exposed to cycles of wetting and drying. The increase in the

modulus of rupture of the samples containing Sulfate resisting cement when exposed to 60 cycles of wetting and drying is 14.602% at 16% cement content.

REFRENCES

Abdullah, S., G., 2011, *Effect Of Additives On The Properties Of Roller Compacted Concrete*, MSc Thesis, Department of Civil Engineering, University of Baghdad, January.

Abdulrahim,A.,S., 2011, *Laboratory Investigation On Roller Compaction Technique In Concrete Construction*, MSC Thesis, Department of Civil Engineering, University of Baghdad, January.

ACI Committee 325.10R-95, 1995**,** *State-of-the-Art Report on Roller-Compacted Concrete Pavements*., ACI Manual of Concrete Practice, 31 page.

Ahmed H.K, 2001, *Factors Influencing the Properties of Roller Compacted Concrete*, Ph.D. Thesis, Department of Building and Construction, University of Technology.

AL-Delaimee,H.A., 1989**,** *Effect Of External Salts On High-Strength Concrete*, M.SC., Thesis, Department of Civil Engineering , University Of Baghdad ,September .

ASTM C 666, 1997, *Standard Test Method for Resistance of Concrete to Rapid Freezing and Thawing*, Annual Book of ASTM Standards American Society for Testing and Materials, vol.04.02.

ASTM C- 88, 1999, *Standard Test Method for Soundness of Aggregates by Use of Sodium Sulfate or Magnesium Sulfate*, Annual Book of ASTM Standards American Society for Testing and Materials, vol.04.02.

ASTM C-293, 2002**,** *Standard Test Method for Flexural Strength of Concrete (Using Simple Beam with Center-Point Loading*, Annual Book of ASTM Standards American Society for Testing and Materials, vol.04.02.

ASTM C42/42M 2003, *Standard Test Method for Obtaining and Testing Drilled Cores and Sawed Beams of Concrete*, Annual Book of ASTM Standards, Vol. (04.02), West Conshohocken, PA., Issued October.

ASTM C-597, 2002, *Standard Test Method for Pulse Velocity through Concrete*, Annual Book of ASTM Standards American Society for Testing and Materials, vol.04.02.

ASTM C-642, 1997, *Standard Test Method for Density, Absorption, and Voids in Hardened Concrete*, Annual Book of ASTM Standards American Society for Testing and Materials, vol.04.02.

Balaguru, P.,N., and Ramakrishnan, V. , 1986, *Freeze -thaw durability of fiber reinforced concrete* , journal of the American concrete institute , vol. (83) No.(3) may. June, 1986, pp(374-382).

British Standard B.S. 1881, 1983**,** *Method for Determination of Compressive strength of Concrete Cubes***,** part 116.

Chun,Y. M. , Naik, T. R. and Kraus, R. N. , 2008 , *Roller-Compacted Concrete Pavements*, Department of Civil Engineering and Mechanics, College of Engineering and Applied Science ,The University Of Wisconsin, Report No. CBU-2008-03, March.

Kreuer, B., 2006, *Bond Shear Strength Of A Rigid Pavement System With A Roller Compacted Concrete Base*, department of Civil Engineering, Cleveland State University, PCA , Serial No.2990, May.

Mahmoud, T.K., 1977, *The Effect Of Sulfates And Cyclic Wetting And Drying On The Physical Properties Of Concrete*, M.SC., Thesis, Department Of Civil Engineering, University Of Baghdad, June.

Naik, T.R., Chun, Y-M., Kraus, R.N., Singh, S.S., Pennock, L-L.C., and Ramme, B.W., 2001, *Strength and Durability of Roller-Compacted HVFA Concrete Pavements*, Department of Civil Engineering and Mechanics, College of Engineering and Applied Science, The University of Wisconsin – Milwaukee, Accepted for Publication in the ASCE's Practice Periodical on Structural Design and Construction, Report No. CBU-2001-08, REP-434, March .

Neville, A. M., 1995, P*roperties of Concrete", 4th Edition, Pittman Publishing Limited, London.*

PCA 2004, *Frost Durability of Roller-Compacted Concrete Pavements,* RD135, Portland Cement Association, Skokie, Illinois, USA, 2004, 148 pages

Petersen, L, Lohaus, L., and polak, M.A. , 2007, I*nfluence Of Freezing And Thawing Damage On Behavior Of Reinforced Concrete Elements*, ACI Materials journal, Vol. (104), No. (4), July-august, 2007**,**pp(369-378).

Riyadh, M .J., 2005**,** S*ome Factors Affecting Properties And Behavior Of Roller Compacted Concrete In Embankments*, Ph.D., Thesis, Department of Civil Engineering, University of Baghdad, January.

Sarsam S.I., 2002 *Evaluation of Roller Compacted Concrete pavement Properties* Engineering and Development Scientific Journal of Al-Mustansiria University, Vol. (6), No. (1), March, 2002, pp. (59-74).

SCRB, 2004 ,*State commission of roads and bridges* Ministry of Housing and construction, 2004, Iraq.

Stutzman, P. E. , 1999, *Deterioration of Iowa Highway Concrete Pavements: A Petrographic Study*, Building And Fire Research Laboratory ,National Institute of Standards And Technology, United States Department Of Commerce Technology Administration, December.

USACE (U.S. Army Corps of Engineers), 2000," *Roller-Compacted Concrete*", Engineer Manual, Department of the Army, Washington, DC 20314-1000, January.

Sarsam S., AL-Rawi A. and Tawfeeq S. , 2014, *Durability Assessment of Roller Compacted Concrete Using NDT*,American Journal of Civil and Structural Engineering AJCSE2014, 1(1):11-17, Sciknow Publications Ltd. USA.

List of Abbreviations

Mc_1 Crushed Aggregate + Sand + 10% OPC
Mc_2 Crushed Aggregate + Sand + 12% OPC
Mc_3 Crushed Aggregate + Sand + 16% OPC
Mcr_1 Crushed Aggregate + Sand + 10% SRPC
Mcr_2 Crushed Aggregate + Sand + 12% SRPC
Mcr_3 Crushed Aggregate + Sand +16% SRPC

Table 1. Grain size distributed used for RCC.

Sieve Size (mm)	% Passing by Weight
19	98
12.5	85
9.5	76.5
4.75	62.5
0.6	26.5
0.075	9

Table 2. Details of the design mixes of RCC Samples,Abdullah, 2011.

Moisture content %	Dry Density (gm. / cm^3)				
	Cement content %				
	10	12	14	16	18
4	2.167	-	-	-	-
5	2.240	2.270	2.290	-	-
6	2.270	**2.390**	2.320	-	-
7	**2.330**	2.350	2.355	2.268	2.360
8	2.310	2.330	2.346	**2.272**	2.370
9	2.268	2.300	2.320	2.260	2.320
10	-	-	2.290	2.240	-
11	-	-	-	2.190	-

Table 3. Modulus of rupture of freezing and thawing cycles for RCC made of (OPC) and (SRPC).

Mix Symbol	Modulus of Rupture (MPa)		
	Number of freezing and thawing cycles		
	No cycle	30 cycles	60 cycles
Mc_1	6.55	6.16	5.75
Mc_2	7.7	7.41	7.04
Mc_3	8.31	8.1	7.84
Mcr_1	7.1	6.88	6.63
Mcr2	7.95	7.72	7.43
Mcr3	9.3	9.2	8.96

Table 4. Modulus of rupture after alternate freezing and thawing cycles for RCC made of (OPC) and (SRPC).

Mix Symbol	Modulus of Rupture (MPa)		
	Number of wetting and drying cycles		
	No cycles	30 Cycles	60 Cycles
Mc_1	6.55	6.15	5.73
Mc_2	7.7	7.35	6.98
Mc_3	8.31	8	7.67
Mcr_1	7.1	6.73	6.37
Mcr2	7.95	7.64	7.31
Mcr3	9.3	9.05	8.79

Table 5. Modulus of rupture of wetting and drying cycles for RCC made of (OPC) and (SRPC).

Mix symbol	Percent decrease after 30 cycles	Percent decrease after 60 cycles
Mc_1	6.1	12.5
Mc_2	4.5	9.3
Mc_3	3.7	7.7
Mcr_1	5.2	10.2
Mcr2	3.8	8.0
Mcr3	2.6	5.4

Table 6. Modulus of rupture after alternate wetting and drying cycles for RCC made of (OPC) and (SRPC).

Mix symbol	Percent decrease after 30 cycles	Percent decrease after 60 cycles
Mc_1	5.9	12.2
Mc_2	3.7	8.5
Mc_3	2.5	5.6
Mcr_1	3.0	6.6
Mcr2	2.8	6.5
Mcr3	1.0	3.6

Table 7. Modulus of rupture of sulfate attack test for RCC made of (OPC) and (SRPC).

Mix symbol	Percent decrease after 30 cycles	Percent decrease after 60cycles
Mc_1	7.7	15.2
Mc_2	6.1	12.5
Mc_3	5.1	10.5
Mcr_1	5.7	11.6
Mcr2	4.1	7.9
Mcr3	3.0	6.3

Table 8. Modulus of rupture after sulfate attack test for RCC made of (OPC) and (SRPC).

Mix Symbol	Modulus of Rupture (MPa)		
	Number of freezing and thawing cycles		
	No cycle	30 cycles	60 cycles
Mc_1	6.55	6.16	5.75
Mc_2	7.7	7.41	7.04
Mc_3	8.31	8.1	7.84
Mcr_1	7.1	6.88	6.63
Mcr2	7.95	7.72	7.43
Mcr3	9.3	9.2	8.96

Figure1. RCC mold .

Figure 2. The roller device.

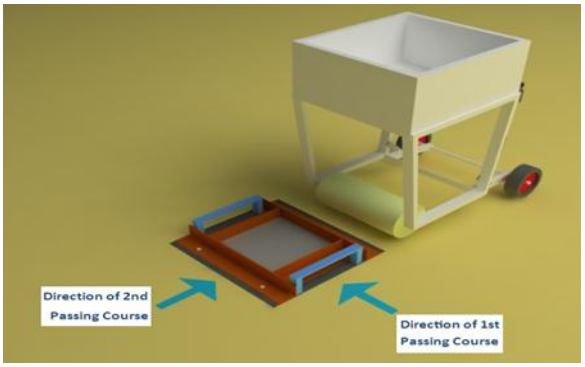

Figure 3. The rolling directions.

Figure 4. The compaction with a roller device.

Figure 5. Part of RCC slab specimens.

Figure 6. Part of samples obtained from RCC slab.

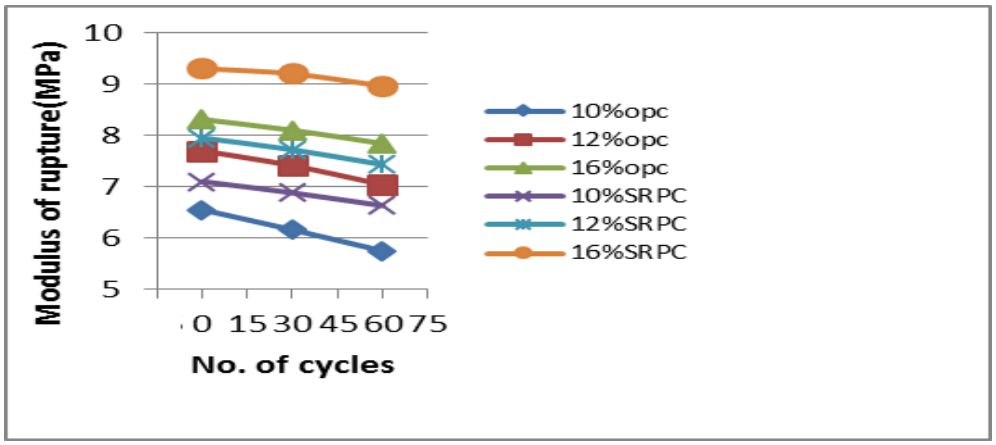

Figure 7 . Variation in modulus of rupture with No. of cycle after freezing and thawing for RCC made of (OPC) and (SRPC).

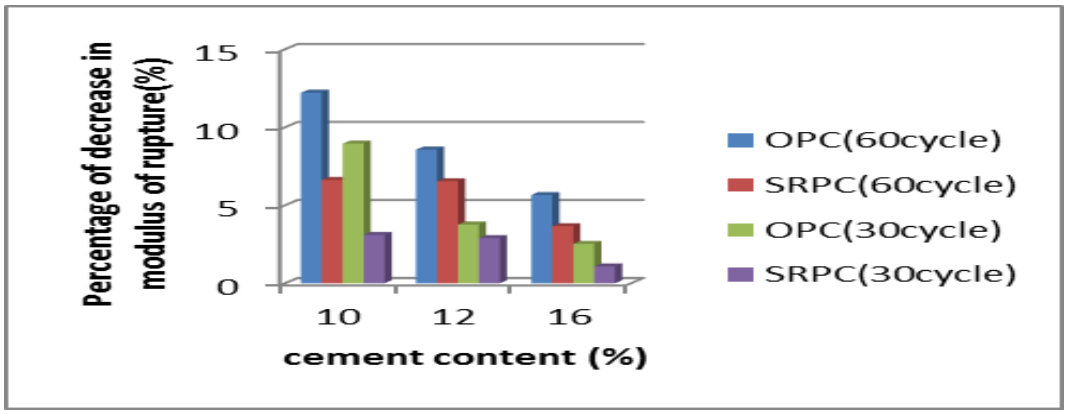

Figure 8. percentage of decrease in modulus of rupture with cement content for RCC made of(OPC) and (SRPC) after freezing and thawing cycles.

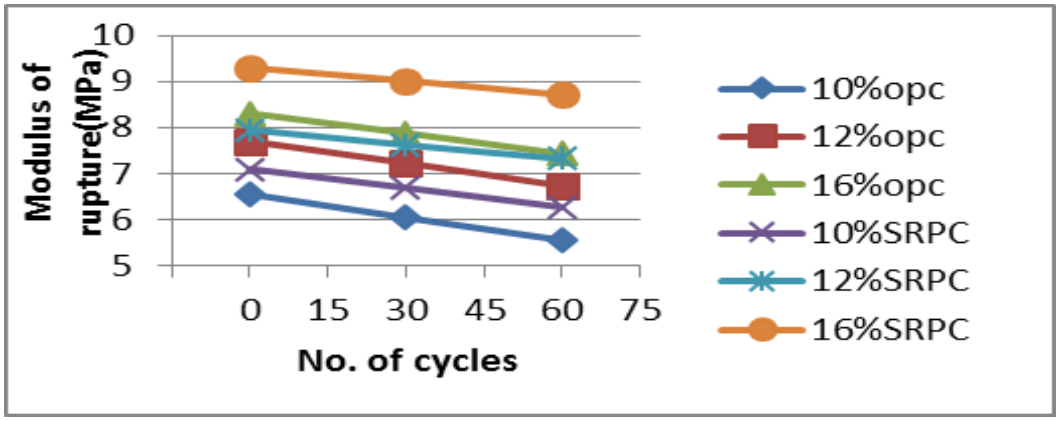

Figure 9. Variation in modulus of rupture with No. of cycle after wetting and drying for RCC made of (OPC) and (SRPC).

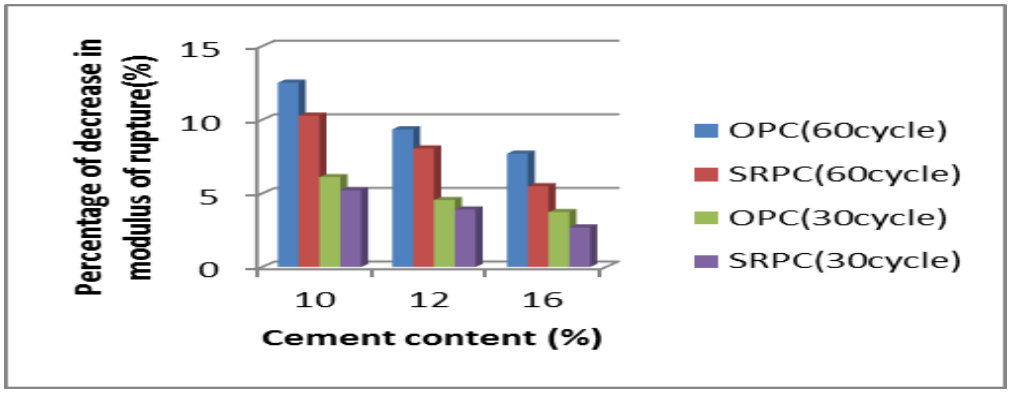

Figure 10. percentage of decrease in modulus of rupture with cement content for RCC made of (OPC) and (SRPC) after wetting and drying cycles.

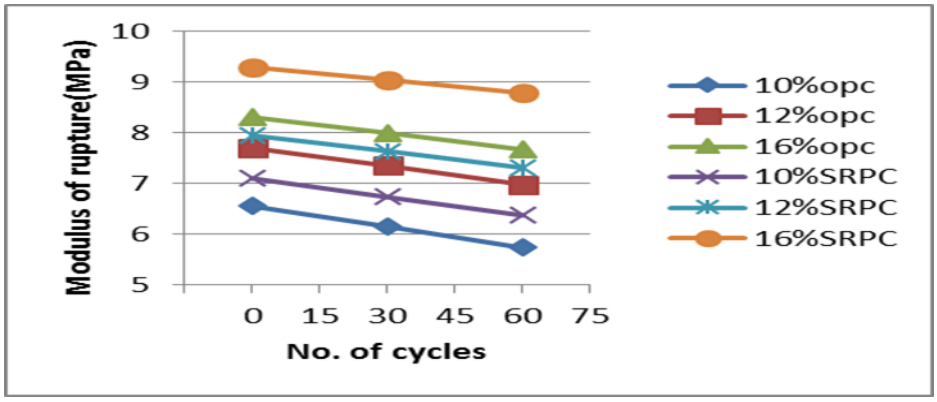

Figure 11. Variation in modulus of rupture with No. of cycle after sulfate attack test for RCC made of (OPC) and (SRPC).

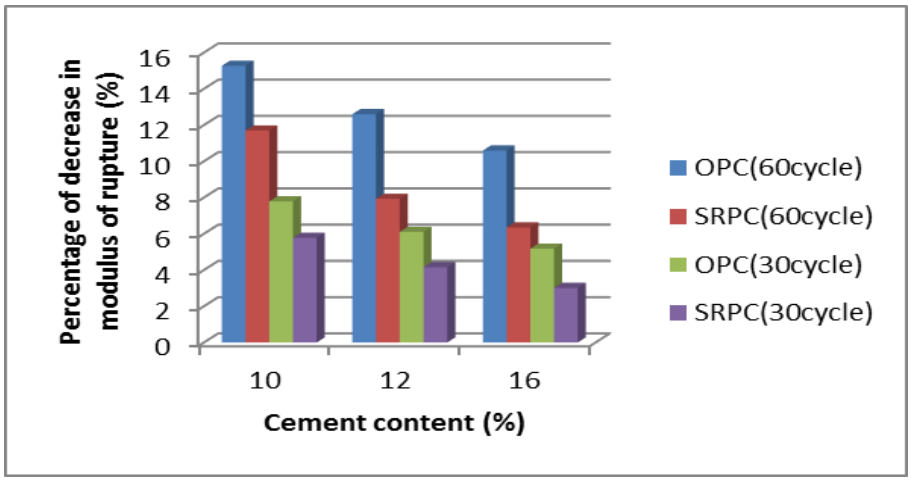

Figure 12 . percentage of decrease in modulus of rupture with cement content for RCC made of (OPC) and (SRPC) after sulfate attack test.

A Proposed Management System for Construction Practices during Sustainable Buildings Life Cycle

Dr. Angham E. Al-Saffar

Professor
Engineering College - Baghdad University
Email:anghamalsaffar@yahoo.com

Zeena Hameed Salman

Master Degree
Ministry of Municipalities and Public Work
Email : zinaheng@yahoo.com

ABSTRACT

For many years, the construction industry damages have been overlooked such as unreasonable consumption of resources in addition to producing a lot of construction waste but with global awareness growth towards the sustainable development issues, the sustainable construction practices have been adopted, taking into account the environment and human safety. The research aims to propose a management system for construction practices which could be adopted during constructing different types of sustainable buildings besides formulating flowcharts which clarify the required whole phases of sustainable buildings life cycle. The research includes two parts: theoretical part which generally ,handles the sustainability concepts at construction industry and specially buildings .But the practical part comprises investigating the professional opinions in construction industry about applications possibility of sustainable requirements and global criteria to construction of sustainable buildings in Iraq where the weakness and strength points in the essential requirements for achieving the sustainable construction practices have been diagnosed and the development need has been specified. The utilized statistical analysis of questionnaire results show readiness of buildings sectors to implement the sustainable practices. The different strategies and techniques in the proposed management have been employed for getting the sustainable procedures of sequences practices within project life cycle.

Key words: system, practices, sustainable buildings, phases.

نظام إداري مقترح للتطبيقات الانشائية خلال دورة حياة المباني المستدامة

د. أنغام عز الدين الصفار
استاذ
كلية الهندسة – جامعة بغداد

زينة حميد سلمان
درجة الماجستير
وزارة البلديات والاشغال العامة

الخلاصة

خلال سنوات عديدة , تم اغفال اضرار الصناعة الانشائية كالاستهلاك اللامعقول للموارد فضلا عن انتاج الكثير من المخلفات الانشائية , لكن مع تنامي الوعي العالمي نحو قضايا التنمية المستدامة تم تبني فعاليات انشائية مستدامة (تطبيقات) تاخذ في الحسبان سلامة البيئة والأنسان.يهدف البحث الى اقتراح نظام اداري للفعاليات الانشائية يمكن إعتماده خلال إنشاء انواع مختلفة من الابنية المستدامة الى جانب صياغة مخططات انسيابية توضح الأجراءات المطلوبة لكافة مراحل دورة حياة المباني المستدامة . تضمن البحث جزئين أساسيين : الجزء النظري , حيث تناول مفاهيم الأستدامة في الصناعة الأنشائية بشكل عام والمباني بشكل خاص وأما الجزء العملي فشمل أستطلاع أراء المختصين في الصناعة الأنشائية حول إمكانية تطبيق متطلبات ومعايير الأستدامة العالمية في إنشاء المباني المستدامة في العراق حيث تم تشخيص نقاط القوة والضعف في تطبيق المتطلبات

اللازمة لتحقيق الفعاليات الأنشائية المستدامة وتحديد مدى الحاجة للتطوير .اظهر التحليل الاحصائي المستخدم لنتائج الأستبيان استعداد قطاع الابنية لتنفيذ متطلبات الفعاليات المستدامة . وتم توظيف استراتيجيات وتقنيات مختلفة في النظام الاداري المقترح إعتمادا على معايير تقييم المباني المستدامة للحصول على أساليب إجرائية مستدامة للفعاليات المتتالية ضمن دورة حياة المشروع .

1 - INTRODUCTION

The present global environmental conditions are consequence of the increasing consumption of natural resources whose depletion exceeds what is physically possible to sustain in the long term. The effects resulting in damage of eco-systems are very evident. Therefore the need arises to find clean friendly sources for energy with environment and other strategies for protecting both of the environment and the opportunities of next generation for sharing with these resources within sustainability frame.

The construction sector is complex and has, therefore, a tendency to resist changes towards sustainability. Designers and project managers are facing barriers to the application of sustainability, e.g. lack of pro-active sustainable measures, conflicts in real and perceived costs and inadequate implementation expertise.

The sustainable construction practices are modern subject and the sustainable construction captures interesting position of the researchers but until now there is no management system for sustainable construction practices. In this research the researcher will propose management system for managing them during sustainable buildings life cycle therefore this research is considered the first thesis interested in this subject. The research scope of the sustainable buildings includes commercial buildings, public services (non-housing) buildings, multi-residential buildings and managerial buildings.

2- SUSTAINABLE CONSTRUCTION

The goals of sustainable construction are to maximize resource efficiency and minimize waste in the building assembly, operation, and disposal processes. Sustainable construction seeks to dovetail the construction industry into the global sustainable development movement by moving it onto a path where it adheres to principles that are able to provide a good quality of life for future generations **, Panagiotakopoulos,2005**.

2-1 Management of Sustainable Construction

The management team of a sustainable construction work project should consider the entire process from an early design stage towards the final product, and the benefits and negative impacts regarding the triple bottom-lines of sustainability that are to be expected during the lifetime of the final product, i.e. the facility **, Persson , 2009**.

2-2 The Sustainable Construction Practices

Sustainable construction practice refers to various methods in the process of implementing construction projects that involve less harm to the environment - i.e. prevention of waste production, increased reuse of waste in the production of construction material - i.e. waste management, beneficial to the society, and profitable to the company **,Akadiri , 2011.** To create a competitive advantage using environment-friendly construction practices and the whole life-cycle of buildings should be adopted also, **Akadiri et al., 2012.**

3- LIFE CYCLE OF SUSTAINABLE BUILDING

The term “Sustainable buildings” is often used interchangeably with “green buildings” or “eco-buildings” **,ADUPC,2010**. Construction activities affect the environment throughout the life cycle of a construction project. This life-cycle concept refers to all activities from extraction of

resources through product manufacture and use and final disposal or recycle, i.e. from "cradle to grave" **, Akadiri, 2011**.

The Whole Building Life-Cycle that guides current practices comprises processes of feasibility ,design, construction, operation, renovation, and demolition of buildings **,Panagiotakopoulos,2005**, **Randolph et al., 2008,** and **Mer'eb, 2008. Bauer et al.,2010,** attempted to extend this thinking even further by considering the regenerative and productive reuse of products and materials in what they call a "cradle-to- cradle" approach**.**

As a result of advance, the researcher supposes the sustainable buildings life cycle should include the phases: planning, design, procurement, implementation, operation and maintenance, post operation and maintenance (which could include deconstruction / reusing / disposal/ demolition).

3-1 Cost of Sustainable Buildings

The opinions about the cost of sustainable buildings are divided into three attitudes:

1) **Halliday, 2008,** refers the overriding assumption that sustainable building inevitably costs more or is less profitable based on the market-driven economies and doesn't adopt them besides the innovation required has a cost implication of time, planning, risk and enhanced information requirements, and the innovators will be penalized and their profit margins reduced when put in direct competition with unsustainable practices.

2) **Persson , 2009,** opposes **,Halliday, 2008,** by saying "*there is a common misunderstanding that sustainability in construction works is more expensive in terms of investment costs compared to 'normal' mainstream buildings.",* based on survey conducted by the World Business Council for Sustainable Development in 2008 which investigated the difference in investment cost between a 'normal' building and a certified sustainable building which is about 17% for the last and **,Persson , 2009,**added that the initial costs do not necessarily increase if energy consumption (one of the most significant factors in building sustainability) is reduced by about 50%.

3) **Myers, 2008,** takes the neutral side when he clarified that cost-benefit analysis is a way of appraising an investment proposal. It involves taking into account the external costs and benefits of a proposed development as well as the conventional private costs and benefits. This is done by estimating monetary values for aspects such as health, time, and pollution.

3-2 Tools of Sustainable Buildings Projects Management

The researcher notes some tools are used numerously in management of sustainable buildings projects which are:

1) **Life-cycle cost analysis**

Life-cycle cost - sometimes also called - Whole-Life Cost (WLC) is the assessment of all relevant costs and revenues associated with a building over an agreed period, including procurement, operation and sometimes disposal. Whole-life cost looks at the life cycle from the start of design and construction, and might include**:** procurement costs, operating costs, recurring, end-of-life and revenue **,Halliday, 2008**.

2) **Value engineering**

In sustainable perspective, in value engineering all alternatives can be compared using life-cycle costing because the alternatives for each project component (systems, materials, plant, and processes) are defined to satisfy the same basic function or set of functions. When the alternatives all satisfy the required function, then the best value alternative can be identified by comparing the first costs and life-cycle costs of each alternative for achieving lowest life-cycle

cost consistent with the required performance. Value engineering has been used at sustainability issues as siting factor, energy issues, water, facility costs **,Federal Facilities Council, 2001**.

3) Computer simulation

During the planning and construction process, computer-based simulation programs are used ,**Bauer et al., 2010. Site** and **Project Planning Group, 2002,** showed that computer simulation is used at pre-design, schematic design, design development, construction, commissioning, post-occupancy. Computer simulations serve to define the following practices **,Bauer et al., 2010**:

a. Maximum and minimum air temperature settings or indoor heating and/or cooling load, for thermal indoor comfort.
b. The operating behavior of a given building under real-life and variable conditions for defining energy efficiency.
c. For evaluation and optimization of a building and its envelope.
d. Using most efficiency water strategies.

4) Rating systems

Rating systems have been developed to measure the sustainability level of green buildings and provide best-practice experience in their highest certification level. With benchmarks, the design, construction and operation of sustainable buildings will be certified using several criteria **,Bauer et al., 2010**.

It is important to realize that any scheme is very good mechanism for encouraging design teams, particularly those unfamiliar with the issues of sustainable design, to focus on a client aspiration **,Halliday, 2008**.These systems often provide a defined format for projects to compare to a baseline to determine how they measure up against other projects **, Sarté, 2010**.

The researcher could draw out some of the most criteria repeatedly, which could search within the following axes: sustainable site, water efficiency, energy and atmosphere, materials and resources, indoor environmental quality and innovation in design.

4- MANAGEMENT OF CONSTRUCTION PRACTICES DURING SUSTAINABLE BUILDINGS LIFE CYCLE

The ways of management the sustainable construction practices could be explored and categorized them during sustainable buildings life cycle phases as follows:

4-1 Planning phase

Every project starts with a vision and a set of objectives. Once the structure is agreed on, a project has been defined and agreed upon, the next step is to establish appropriate design strategies to meet those goals **,Sarté, 2010**. Planning initiate with feasibility study which is carried out by assessing the client's objectives and providing advice and expertise in order to help the client define more precisely what is needed and how it can be achieved **,The Chartered Institute of Building, 2002**.

Federal Facilities Council, 2001, states that ecologically and culturally sensitive areas should be considered at sustainable site planning. The cost plays essential role in water planning .For example, in the tertiary treatment levels, they have improved water quality but they have come at a high energy cost **,Sarté, 2010**.

USGBC, 2009, states that the requirements like on-site renewable energy self-supply, minimum and optimize energy performance, measurement and verification should be considered at this phase.

In selecting sustainable materials, designers should aim to maximize durability, energy efficiency, recyclability, maintainability, and use of local materials to minimize the use of hazardous materials, and synthetic chemicals by using a strategy in the choice **,Akadiri ,2011**.

Life-cycle assessment (LCA)could be used as a method to measure and evaluate the environmental burdens associated with a product system or activity, by describing and assessing the energy and materials used and released to the environment over the life cycle **,Halliday, 2008**.

The planning phase, must take into account outdoor air quality levels, all the possibilities and limits of air supply in respect to natural ventilation via the windows, filtering and cleaning of outdoor air **,Bauer et al., 2010**. Besides using passive cooling strategies, it includes **,Halliday, 2008**.

4-2 Design Phase

Green buildings incorporate three critical factors: energy, environment /ecology, and human health. These factors are keys to the design process **,Panawek, 2007**. In sustainable site design the land, its hydrology, and the complex diversity of living systems are interdependent and cannot be isolated from the design process**, Sarté, 2010**.

Site design begins with the analysis of the site and environmental conditions and integrates them into the program and design solution. Integrating the natural attributes of the site can reduce energy consumption considerably **,Williams, 2007.**

Federal Facilities Council, 2001, considers the following issues:

1) Specifying measures of water use can be taken to ensure is as efficient as possible.
2) Specifying measures to reduce, control, and treat surface runoff.
3) Incorporating rainwater collection cisterns and separate gray water systems for below-ground irrigation to eliminate the use of potable water.

Designers can therefore help reduce operational energy consumption of buildings by adopting designs that reduce heat losses through the building envelop, reduce cooling and heating loads and by introduction of energy saving measures **,Ndungu , 2008**.

The efficient utilization of resources as possible needs to specify the use of renewable and recycled sources in order to close the life-cycle loop of materials and select materials with the least environmental impact throughout their entire lifetime **Akadiri ,2011.**

Design of indoor environment considers the following **,Bauer et al., 2010**:

1) Assuring optimal air quality.
2) The amount of daylight reaching the room.
3) The solar protective device’s automation.

4-3 Procurement Phase

Federal Facilities Council, 2001, states that the following should be considered at procurement phase:

1) Stipulation on specification design criteria.
2) The contract method that will best support the achievement of sustainability objectives.
3) Implications of the choice of project delivery method.
4) Implications of the contract selection procedure.
5) The types of incentives and clauses.
6) Types of evaluations used.
7) The side responsible for sustainable construction practices.

8) The required level of commissioning, the liability for failures to meet the requirements and the remediation method in the failures case.

4-4 Implementation Phase

Implementation stage is the actual execution of what has been planned to be a development project. Implementation is made according to projects agreement and memorandum. During the implementation process complexity and risks come to closer, bureaucratic problems, and conflicts could emerge **,Oyoko et al., 2008**.

Halliday, 2008, mentions that particular attention should be paid to the commissioning operations – not just of innovative technology. Checking that products are of the required quality and that they work as specified is essential. It will become clear at this point how important it is to specify all the testing regimes at the tender period.

The following the procedures could be taken in the construction phase **,Federal Facilities Council, 2001**:

1) Evaluation, analysis, and consideration of change orders that may affect facility sustainability.
2) Study on value engineering of change proposals.
3) Implementation of monitoring procedures.
4) Reduction or elimination of the production of harmful waste.
5) Protection of construction workers from the hazard waste.

4-5 The Occupancy (Operation and Maintenance) Phase

The constructed works are expected to be in service for a long time. Maintenance is defined, according to Standard of International Organization for Standardization (ISO 15686-1), as: *"Combination of all technical and associated administrative actions during service life to retain a building or its parts in a state in which it can perform its required functions"* **,Hallberg , 2005**.

The most important job in maintenance is to make regular checks which might betray a more serious durability threat. Simple visual checking is often all that is required, but it should be thorough and regular. In this way almost all serious problems can be spotted early and dealt with cheaply and simpl, **Halliday ,2008**.

4-6 Post Operation and Maintenance Phase

At the end of life phase, sustainability issues that need to be considered are the reduction of waste when the buildings are demolished. All avenues to recover materials by recycling and reuse should be explored **,Ndungu, 2008**. Accordingly the researcher handled the following aspect:

1) **<u>Deconstruction</u>**

The processes of dismantling a building or site have shifted from demolition to deconstruction **,Calkins, 2009**. Deconstructing a building is the careful dismantling of that building so as to make possible the recovery of construction materials and components, promoting their reuse and recycling **,Couto et al., 2010**. A good deconstruction contractor will be able to reclaim/recycle 75%–95% of the site and building if salvage or recycling markets are available nearby **,Calkins, 2009**.

2) **<u>Source-separated recycling</u>**

Source-separated recycling (also called source separation) is the alternative to commingling. The highest benefits of recycling come from separating waste materials at the jobsite , transporting

and recycling them individually into a different container which is then transported by a recycler, transfer site, or directly to individual markets **,Chiras, 2006**.

3) **Reclaiming and reusing of materials and products**

Reusing materials can add a layer of meaning to a project, revealing the cultural history of a place, which is often difficult to achieve with mass production due to the following **,Calkins ,2009**:

a. Finding appropriate types and quantities of materials.
b. There is often additional design time.
c. A reclaimed material will not be found in a catalog with all specifications listed.

4) **Demolition**

The demolition reduces the building or site to debris without preserving the integrity of its components for reuse **,Calkins, 2009**. During the demolition, rubble and debris are hauled away and disposed into the sea and sometimes at abandoned quarries **,Ndungu, 2008**.

5- FIELD SURVEY

There is a common misunderstanding supposes that the sustainable construction of the buildings is more expensive in terms of investment costs compared to traditional buildings and adoption of sustainable construction in construction works will lead to delay or confusion in methodology. Therefore, proposing a management system for the construction practices during sustainable buildings life cycle aims to correct this misunderstanding and encourage adoption of the sustainable construction practices and solve the avoidance of sustainable buildings.

As a result, the researcher embarked in testing the research hypothesis through field survey .The field investigation passed two stages, as follows:

1-Open questionnaire stage: through personal interview.

2-Closed questionnaire stage: by using questionnaire form.

The closed questionnaire form includes investigation the requirements of sustainable construction practices through six axes of sustainability: site, water efficiency, energy efficiency, and indoor environmental quality, innovation in design and awareness and education. Four determinants facing application the requirements of sustainable construction practices have been used in survey which is application's possibility, difficulty types, influence on cost and influence on time. The results of the first two determinates have been discussed depending on frequency distribution but the last two determinates have been discussed depending on the evaluation of statistical analysis results.

5-1 Statistical Analysis

The statistical analysis is used for analyzing the closed questionnaire results related with participants responses to the two determinants of using axes requirements which concern requirement influence on cost and on time by considering each response type of (always, often, some times and no) a class could give it evaluation range and extraction the class evaluation of degree (class center) as clarified in **Table 1**.The researcher used the following statistical features:

First: – The arithmetic mean

The weighted mean is used to evaluation every requirement of questionnaire axes .It has been calculated from the following equation **,Moore et al., 2009**:

$$M = \sum_{i=1}^{i=n} Xi * Fi/N \quad (1)$$

where:

M = Responses weighted mean about requirement influence on cost or time.
Xi =Evaluation degree of responses class (i) about requirement influence on cost or time.
Fi = Responses frequency for class (i) about requirement influence on cost or time.
N= Sample size in each requirement.

The above equation is applied to influence of every requirement on each the cost and time.

Second: – The conformance ratio

It is used in influence evaluation for every axis of questionnaire axes on the cost and time .It represents congruence extent of axis influence with the ideal status depending on responses frequency for sample individuals by applying the following equation **,Al- Ani, 2006**:

$$Cr = M / X_{max} \quad (2)$$

Where:
Cr = Axis conformance ratio.
M = Arithmetic mean of responses weighted mean.
X_{max}= The maximum evaluation degree which represents the maximum class center for the responses evaluation (8.75).

The analysis and evaluation of the questionnaire results for every axis of questionnaire axes depend on conformance ratio computed for every axis whose value varies from (1.25/8.75 - 1) where the median of these ratios is the average of (0.42) and (0.72) and equals (0.57) and it is considered the lower limit to axis analysis, then the upper quartile will be computed for the values (0.14-1) as follows:

a- If **(Cr < 0.57)**, then evaluation of axis influence is **(poor)** therefore the required development would be **(must)**.
b- If **(0.57≤ Cr ≤ 0.86)**, then evaluation of axis influence is **(accepted-middle)** therefore the required development would be **(wanted)**.
c- If (**Cr > 0.86)**, then axis evaluation is **(good-very good)** therefore the required development would be **(desired)**.

Based on results of total weighted mean listed in **Table 2**, all axes have Cr < 0.86 thus all axes affect cost and time therefore the supposed actions which make the axes affect cost and time need development. Also from **Fig. 1**, it could be noted there is relation between the axis influence on cost and time since whenever the axis affect cost, it affect time too.

As a conclusion from analysis the closed questionnaire results, the building construction sector has the readiness for inclusion of the sustainability aspects but it suffers from absence of management system because of some of difficulties which are summarized by technical difficulties in the first place, followed by managerial difficulties are due to lack of awareness of sustainability targets in addition fear of effect on cost and time of project if the sustainable construction practices have been applied. But the proposed actions of management system could overcome both lack of awareness and some of these effects.

Then the comprehensive view of extent of acceptance of building construction sector has been reached .In addition, the light is shed on fields that need to be developed .Based on the results, the researcher could diagnose the weaknesses and strengths in managing the sustainable construction practices.

6- THE PROPOSED MANAGEMENT SYSTEM OF SUSTAINABLE BUILDINGS

The management system is an approach used to organize the activities and the resources to perform the actions according to a specified cost and time program relating to certain objectives. Since sustainable building life cycle consists of six phases, previously mentioned, the researcher has tracked the construction practices through the sustainability aspects during life cycle phases to find out the procedures and at the end to formulate the proposed management system.

The proposed management actions are based on management strategies and techniques that constitute most difficulties facing the construction practices, as well as the cost and time management through the placed plans and requirements that precede the intended actions, where every criterion of sustainable site, water efficiency, energy and atmosphere, materials and resources, indoor environmental quality, and innovation in design comprise many construction practices.

6-1 The Proposed Planning Actions for Sustainable Buildings

The planning phase is considered the first phase in the project. The project –owner requirements should be defined to clarify the project scope by the planning consultant and the project team (project manager, engineers, geotechnical specialists, other specialists, land surveyors, cost estimator and quantity surveyors etc.). At this point the sustainability features begin to originate from environmental and sustainability objectives such as energy targets, the systems performance requirements, operation and maintenance, occupants' requirements, owner and user requirements that are stipulated in project –owner requirements document as shown in **Fig. 2**.

Fig. 2 shows the main planning actions for sustainable buildings including the following:

1- Establishing the sustainability vision, objectives, and measurements and implementing systems approach.
2- Feasibility study and cost estimations
3- Site selection
4- Value engineering
5- Schematic design
6- Developing the basis of design (BOD)
7- Cost efficiency management system

6-2 The Proposed Design Actions for Sustainable Buildings

For advancing sustainability in design, the following could be achieved:

1- Integrate sustainability vision and values into design.
2- Implement sustainability objectives, measurement system, systems thinking models and sustainability framework.
3- Implement sustainability approaches.
4- Applying Life cycle assessment for sustainability features.

As shown in **Fig. 3**, for conversion to sustainable design the sustainability axes such as sustainable site, water efficiency, energy and atmosphere, material and resources and indoor environmental quality, and innovation in design have been considered. Each of these axes includes more than design set. **Fig. 3** shows actions that should be followed in each axis and how the researcher employed the construction practices related to them in the design phase.

6-3 The Proposed Procurement Actions for Sustainable Buildings

The procurement in construction life cycle of sustainable buildings is related to purchasing of materials, plant, and the correct choice of suppliers and subcontractors. The actions related to procurement could include the following:

1- Integrate sustainability vision and values into procurement.
2- Implement sustainability objectives, measurement system, systems models and sustainability framework.
3- Commit to green purchasing policy.
4- Implement sustainability.
5- Engaging procurement in design for a sustainable supply chain

As a result, the researcher summarized the procurement actions in a proposed flowchart in **Fig. 4**.

6-4 The Proposed Implementation Actions for Sustainable Buildings

The following activities must be followed:

1- Integrate sustainability vision and values into construction.
2- Implement sustainability objectives, measurement system, and sustainability framework.
3- Implement sustainability approaches.
4- Manage and minimize CO_2 emissions in construction.

Fig. 5 describes actions which must be undertaken for managing the implementation of sustainable buildings which are characterized by performing all the previously arranged plans starting from performing time management and ending in performing operation and handover plan.

The most time-consuming activity in the project is the creation of the physical constructing of practices. **Fig. 6** explains the work mechanism that is followed in implementation according to sustainability axes. It is obvious from **Fig. 6** focusing on testing efficiency of all of the installed systems and sustainable practices insures of achieving the cost saving at its performing and environmental targets that are planned before. Many of the management process have been permeated and schemed at the planning phase.

6-5 The Proposed Operation and Maintenance /Occupancy Actions for Sustainable Buildings

The suggested operation and maintenance actions are as follows:

1- Integrate sustainability vision and values into operation and maintenance stage.
2- Implement sustainability objectives and measurement system.
3- Start early in planning and design to provide operation and maintenance input to project development.
4- Implement sustainability approaches.
5- Individual behaviors and individual ownership

This phase is very important in achieving the planned and designed savings therefore it should be of interest. As a result the researcher suggests the flowchart in **Fig. 7** for the operation and maintenance actions.

After operational building life has been finished, the structural element should be sustained through reusing of them at the same site and rehabilitation the capable elements by friendly–environmental materials

6-6 The Proposed Post-Operation and Maintenance Actions for Sustainable Buildings

The sustainability's tendency doesn't end with building occupancy and benefits harvested that had been looked forward but this stage could be exploited to service the building's sustainability in materials arena ,through construction waste management including reusing, recycling ,reprocessing and safety disposal.

Fig. 8 represents the proposed actions for post-operation and maintenance that the researcher proposes where advanced planning for deconstruction or salvage before demolition is crucial for its success.

Building deconstruction supports the waste management in its sequence of preferred options for the management of generated waste materials. If a building is still structurally sound, durable and flexible enough to be adapted for a different use, then waste can be reduced by reusing the whole building. If components and materials of a building can be recovered in high quality condition, then they can be reused. If the building materials are not immediately reusable, they can be used as secondary feedstock in the manufacture of other products, i.e., recycled. The aim is to ensure that the amount of waste that is destined for landfill is reduced to an absolute minimum. This approach closes the loop in material flow thereby contributing to resource efficiency.

At last, the proposed management system flowchart during sustainable buildings life cycle is summarized as shown in **Fig. 9**.

7- CONCLUSIONS

1. As a result of undertaking closed questionnaire, it was determined there was awareness lack about realizing the benefits of a sustainable approach in construction in Iraq which has led to absence of sustainable construction practices.

2. There is a huge lack in understanding the techniques of sustainable construction.

3. There is a relationship between some sustainable construction practices therefore application some of them will be reflected positively or negatively on other practices whether in direct or indirect way.

4. When the aim is to reduce site pollution, achieve indoor environment quality, reduce using the materials and resources this really leads to additional costs but on other hand the increase in cost could be balanced by the efficient use of materials and resources in construction phase, operation and maintenance phase and in the next-phase, moreover efficient use of water, energy at operation phase could save cost too.

5. Although application of the management system of sustainable construction practices may increase initial costs of buildings through design and construction phase, it will lead to cost savings greater than initial investment besides the environmental and social benefits. These savings are due to reduced water costs, lowered energy use, lowered, and decreased waste disposal, reduced operation and maintenance costs, and savings resulting from increasing productivity.

6. Some of sustainable construction practices affect time but as noted in the proposed management system more than sustainable practice can be applied at the same time with each other in addition to traditional practice as a result time as possible as could be saved.

7. Adopting the sustainability principles, especially at the post-operation and maintenance phase (deconstruction /disposal), could help in providing work opportunities and reduce the unemployment.

8- RECOMMENDATIONS

The following recommendations have been drawn to enhance the proposed management system for sustainable construction practices:

1. Applying the proposed management system in all details and actions to the future sustainable buildings projects in Iraq.

2. It should be of interest to develop the current techniques in construction practices in Iraq to be sustainable.

3. It is necessary to make the competition basis between the constructed company according to its commitments about implementing the sustainability's' principles by introducing the related plans within the bid.

4. Holding training courses and workshops to spread the sustainability aspects for both private and public sectors in collaboration with professionals who have experience in construction sustainability from abroad that are very advanced at this arena.

5. Establishing Iraqi sustainable buildings council which will be in charge of rating the sustainable buildings projects and giving recognized certification for this purpose as well as issuing guides for specifying the sustainable buildings similar to what is done in other countries like Abu Dhabi, USA, and Australia etc..

REFERENCES

ADUPC., 2010, *The PEARL Rating System For ESTIDAMA: Building Rating System for Design and Construction,* Version 1.0, Abu Dhabi Urban Planning Council, U.A.E.

Akadiri ,P. O. ,2011, *Development of A Multi- Criteria Approach for The Selection of Sustainable Materials for Building Projects,* Ph.D. Thesis, Wolverhampton University.

Akadiri, P. O. ,Chinyio , E. A. ,and Olomolaiya , P. O. ,2012, *Design of a Sustainable Building: A Conceptual Framework for Implementing Sustainability in the Building Sector*,An Article, Journal of Buildings, Vol.2, May 4, pp.126-152.

Al- Ani, Raad D. N. ,2006. *Development of Construction Designs Quality Assurance Program For Building Projects*, A M.Sc. Thesis, Civil Engineering Department, Al-Mustansiriya University.

Bauer, M., Mösle , P., and Schwarz, M. ,2010, *Green Building: Guidebook for Sustainable Architecture*, Springer, Germany.

Calkins, M. ,2009, *Materials For Sustainable Sites: A Complete Guide to the Evaluation, Selection, And Use Of Sustainable Construction Materials*, John Wiley& Sons, New Jersey.

Chiras, D. ,2006, *The Homeowner's Guide to Renewable Energy: Achieving Energy Independence through Solar, Wind, Biomass and Hydropower*, New Society Publishers, Canada.

Couto,J. And Couto,A.,2010, *Analysis Of Barriers And The Potential For Exploration Of Deconstruction Techniques In Portuguese Construction Sites*,A Review, Journal Of Sustainability, Vol.2, January 27, pp.428-442.

Federal Facilities Council ,2001, *Sustainable Federal Facilities: A Guide To Integrating Value Engineering, Life-Cycle Costing, And Sustainable Development*, A Technical Report No.142, National Academy Press, Washington.

Hallberg, D. ,2005,*Development And Adoption Of A Life Cycle Management System For Constructed Works*, M.Sc. Thesis, KTH Architecture and Built Environment College, University of Gälve, Sweden.

Halliday, S. ,2008, *Sustainable Construction*, First Edition, Elsevier, Slovenia.

Mer'eb, M. M. ,2008, *GREENOMETER-7: A Tool To Assess The Sustainability Of A Building's Life Cycle At The Conceptual Design Phase* , Ph.D. Thesis, Cleveland State University.

Moore, D. S. and Notz W. I. ,2009, *Statistics: Concepts And Controversie*,Seventh Edition, Freeman And Company, New York.

Myers, D. ,2008, *Construction Economics: A New Approach*, Second Edition, Taylor & Francis Group, USA.

Ndungu, P. ,2008, *Sustainable Construction: Comparison Of Environmental Impact Due To Off-Site Vs. On-Site Construction*, M.Sc. Thesis, College of Engineering, University of Cincinnati.

Okoyo, M., Hussein, M. ,2008, *Swedish Aid Policy And Development Projects In Kenya: An Analysis Of Strategy And Organization*, M.Sc. Thesis, School of Sustainable Development of Society and Technology, University of MÄLARDALEN.

Panagiotakopoulos, D. P. ,2005, *A System And Cybernetics Approach To Corporate Sustainability In Construction* , Ph.D. Thesis, School of Built Environment, Heriot – Wat University, Edinburgh.

Panawek, K. ,2007, *Changing 'Light' Green to 'Deep' Green: Mainstreaming Green Building In Hamilton County: An Analysis & Evaluation Of The Constraints Facing The Green Building Housing Market In Hamilton County*, M.Sc. Thesis, College of Design, Architecture, Art and Planning, University of Cincinnati.

Persson, U. ,2009, *Management Of Sustainability In Construction Works*, Ph.D. Thesis, Division Of Construction Management, Lund University, Sweden.

Randolph, J. And Masters, M. G. ,2008, *Energy For Sustainability: Technology, Planning, Policy* ,Island Press, Washington.

Sarté, S. B. ,2010, *Sustainable Infrastructure: The Guide To Green Engineering And Design* , John Wiley& Sons, New Jersey.

Site and Project Planning Group. ,2002, *LANL Sustainable Design Guide*, LANL, New Mexico, United States.

The Chartered Institute of Building. ,2002, *Code Of Practice For Project Management For Construction And Development*, Third Edition, Blackwell, UK.

USGBC. ,2009, *LEED 2009 For New Construction And Major Renovations*,USGBC, Washington.

Williams, E. D. ,2007, *Sustainable Design: Ecology, Architecture, And Planning* ,John Wiley& Sons, New Jersey.

Table 1. Distribution evaluation degree on responses classes.

Response Class	Evaluation Range	Evaluation Degree
No	**(10 - 7.51)**	**8.75**
Sometimes	**(7.5 - 5.1)**	**6.3**
Often	**(5 - 2.51)**	**3.75**
Always	**(2.5 - 0)**	**1.25**

Table 2. The evaluation of influence of axes on cost and time compared with ideal condition. (Researcher)

Axis	Axis Influence on Cost				Axis Influence on Time			
	Total Weighted Mean	Axis Conformance Ratio (Cost)	Evaluation of Axis Influence	Development of Supposed Axis Actions	Total Weighted Mean	Axis Conformance Ratio (Time)	Evaluation of Axis Influence	Development of Supposed Axis Actions
Site	67.39	0.59	accepted-middle	wanted	73.18	0.64	accepted-middle	wanted
Water Efficiency	21.33	0.49	poor	must	24.32	0.56	poor	must
Power and Atmosphere	19.77	0.45	poor	must	23.82	0.54	poor	must

Table 2. continued.

Axis	Axis Influence on Cost				Axis Influence on Time			
	Total Weighted Mean	Axis Conformance Ratio (Cost)	Evaluation of Axis Influence	Development of Supposed Axis Actions	Total Weighted Mean	Axis Conformance Ratio (Time)	Evaluation of Axis Influence	Development of Supposed Axis Actions
Materials and Resources	55.00	0.63	accepted-middle	wanted	59.30	0.68	accepted-middle	wanted
Indoor Environmental Quality	73.46	0.60	accepted-middle	wanted	84.54	0.69	accepted-middle	wanted
Innovation in Design	23.36	0.67	accepted-middle	wanted	25.11	0.72	accepted-middle	wanted
Awareness and Education	17.77	0.68	accepted-middle	wanted	19.92	0.76	accepted-middle	wanted

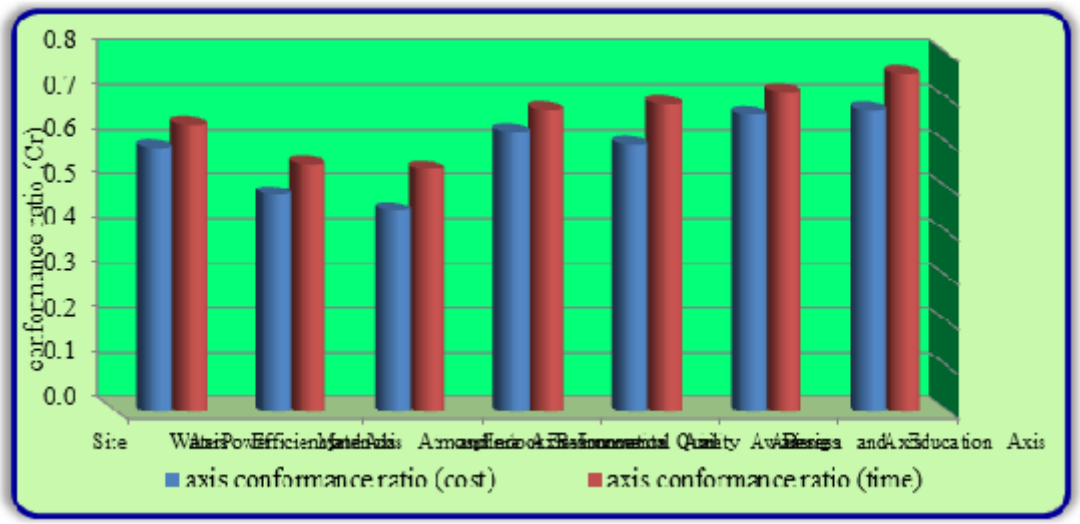

Figure 1. Conformance ratio of axis influence on cost and time compared with ideal condition.

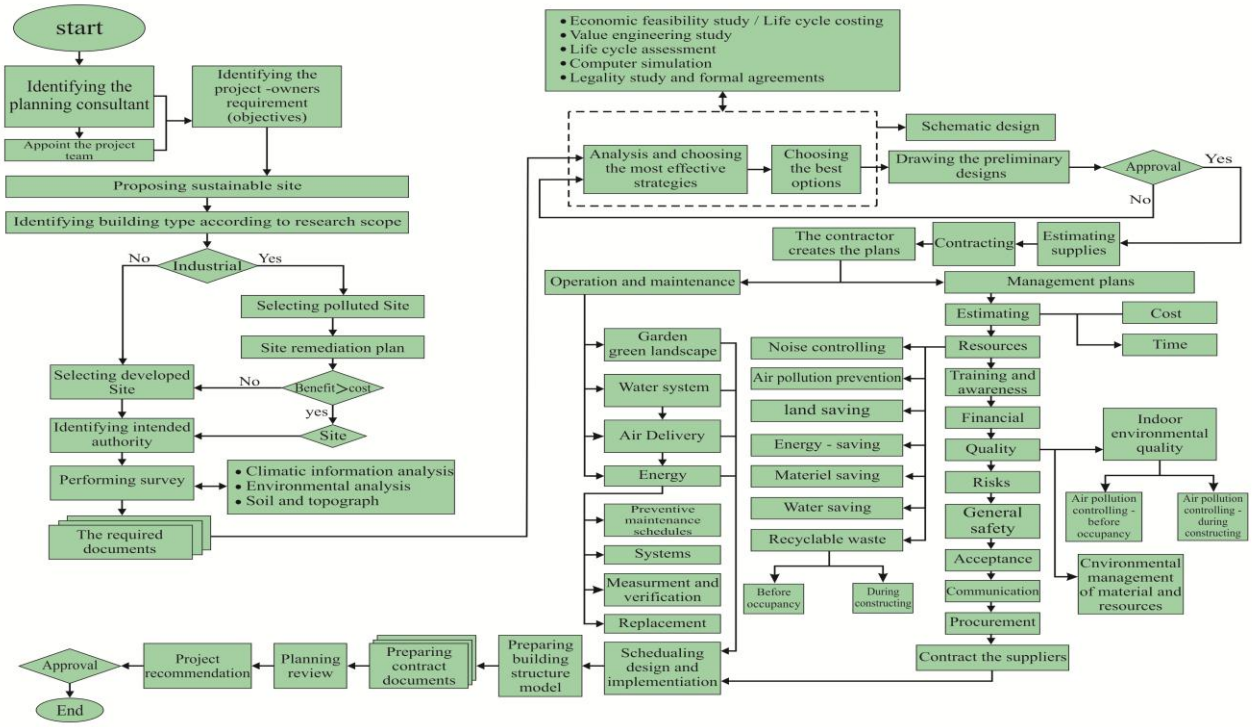

Figure 2. The proposed planning actions flowchart (researcher).

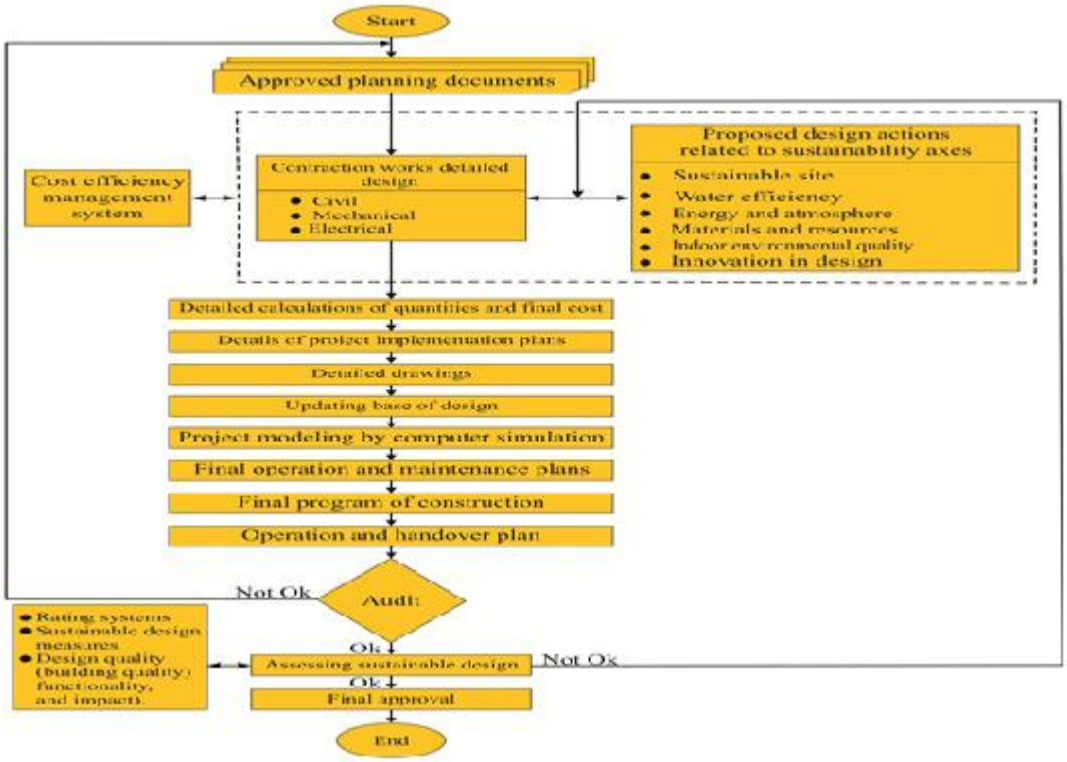

Figure 3. The proposed design actions flowchart (researcher).

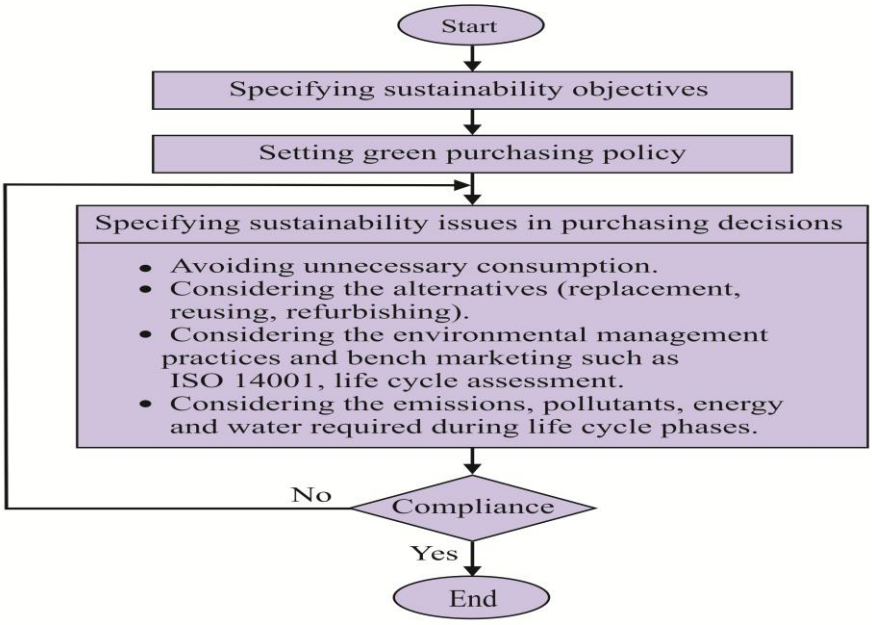

Figure 4. The proposed procurement actions flowchart (researcher).

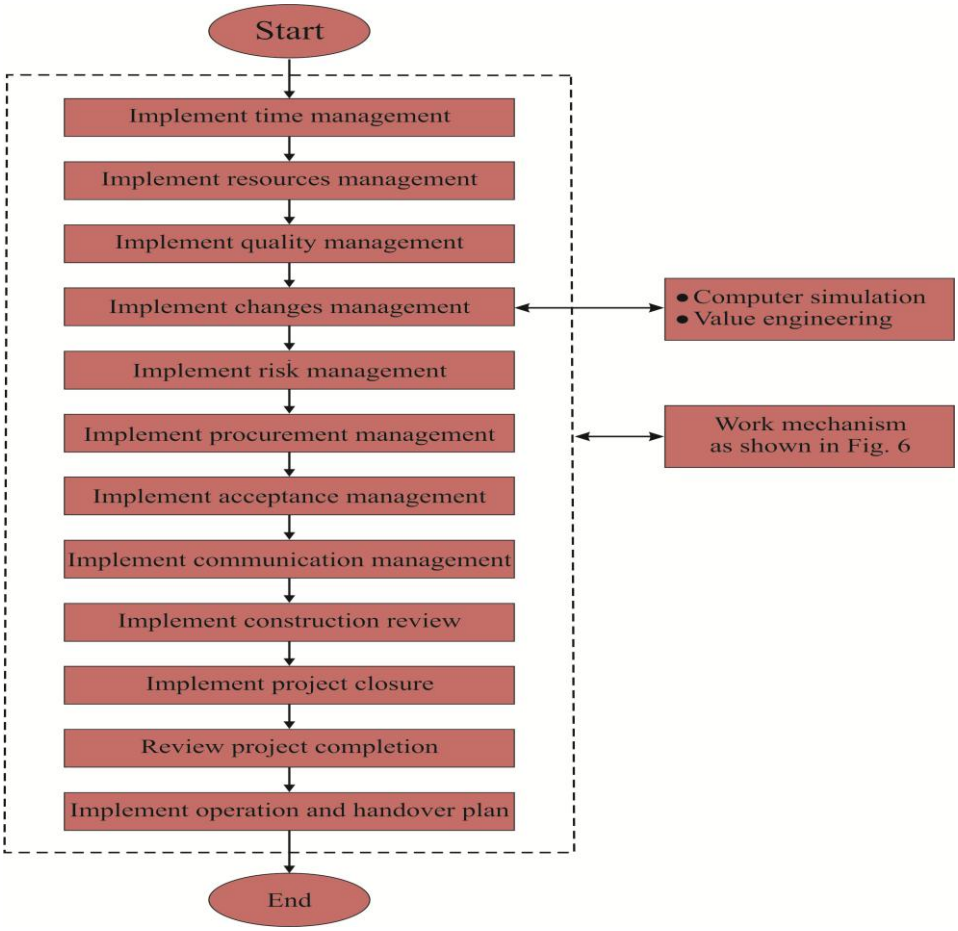

Figure 5. The proposed implementation actions flowchart (researcher).

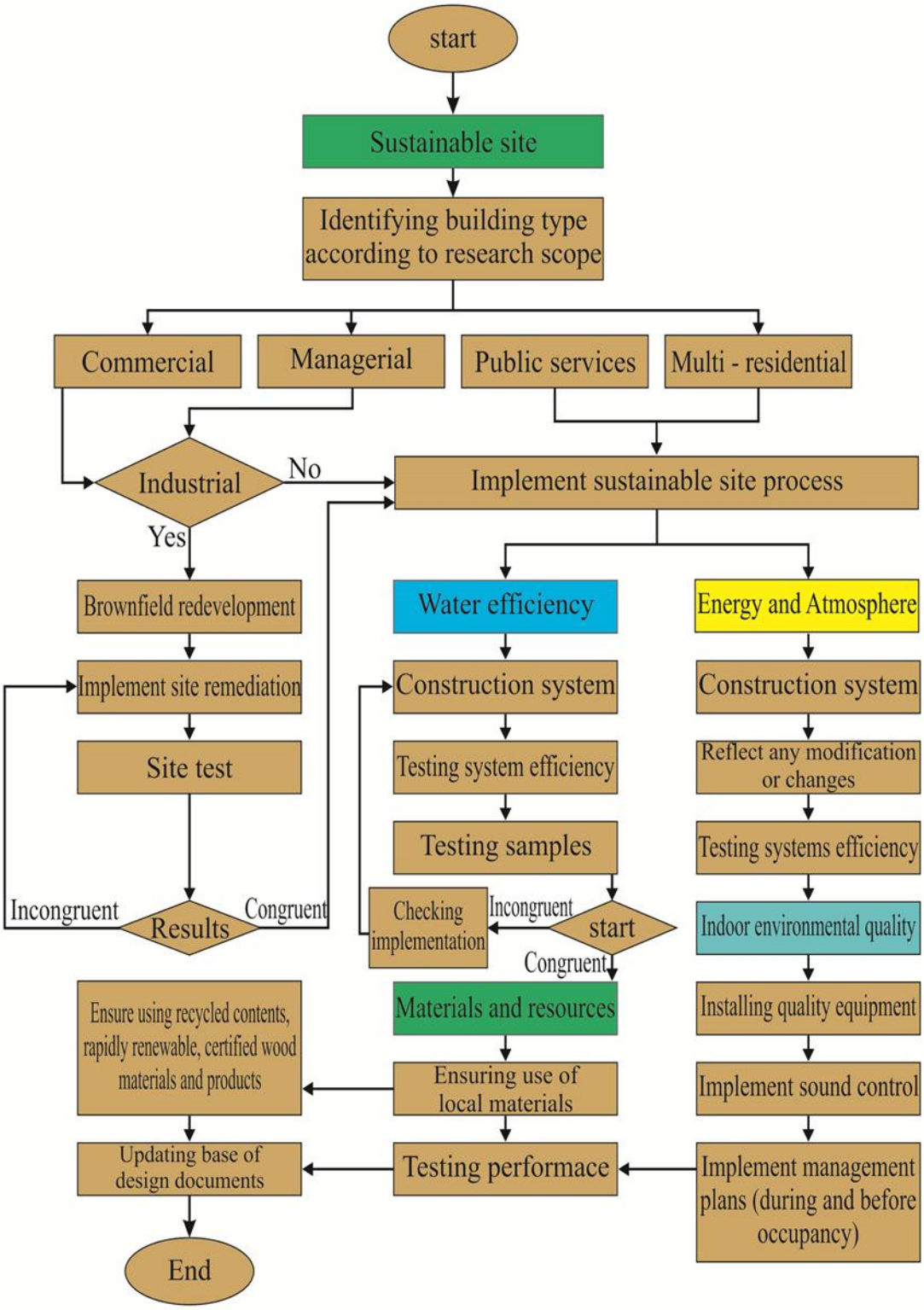

Figure 6. The proposed work mechanism in implementation phase of sustainable buildings (researcher).

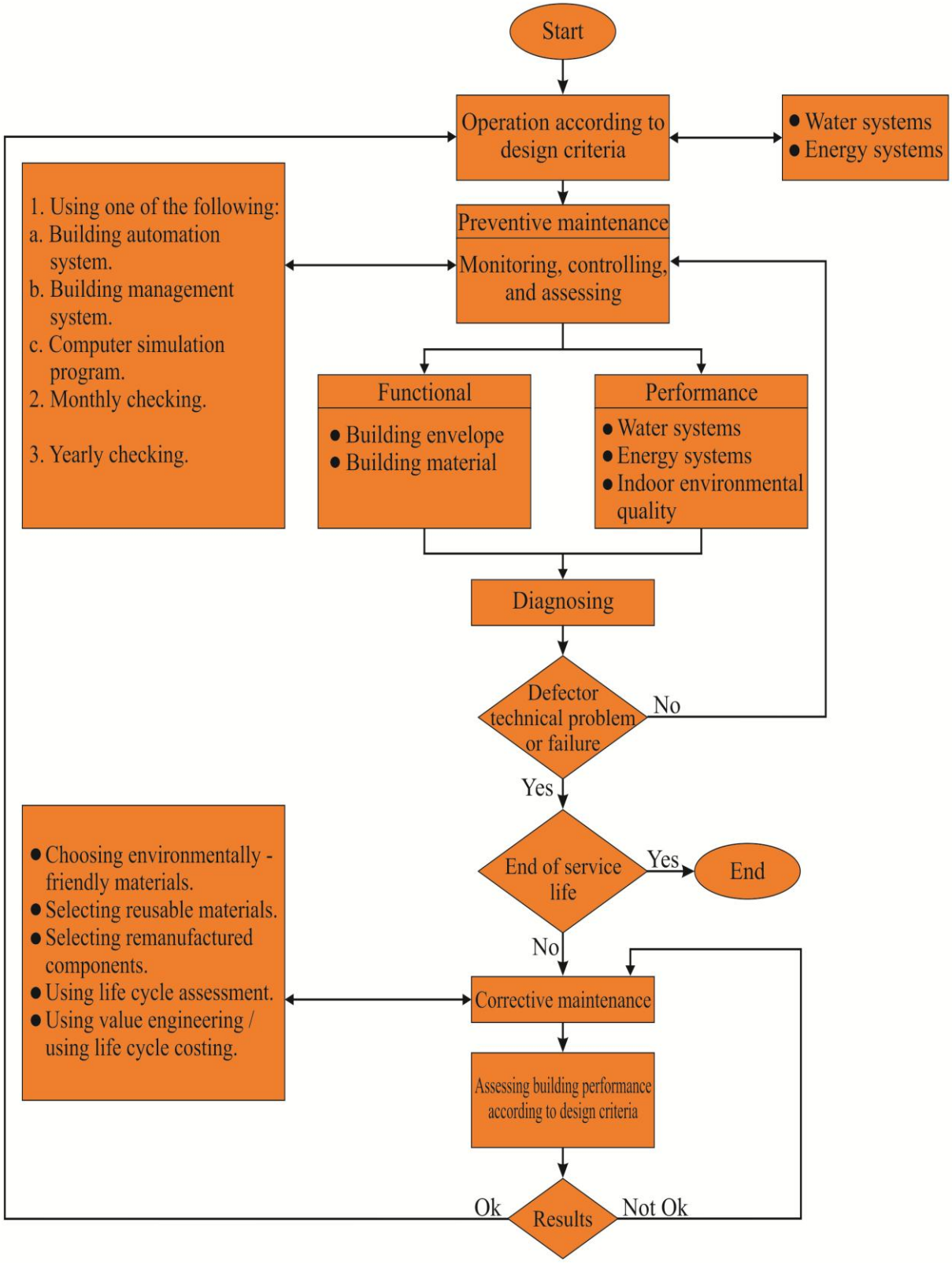

Figure 7. The proposed actions of operation and maintenance for sustainable buildings (researcher).

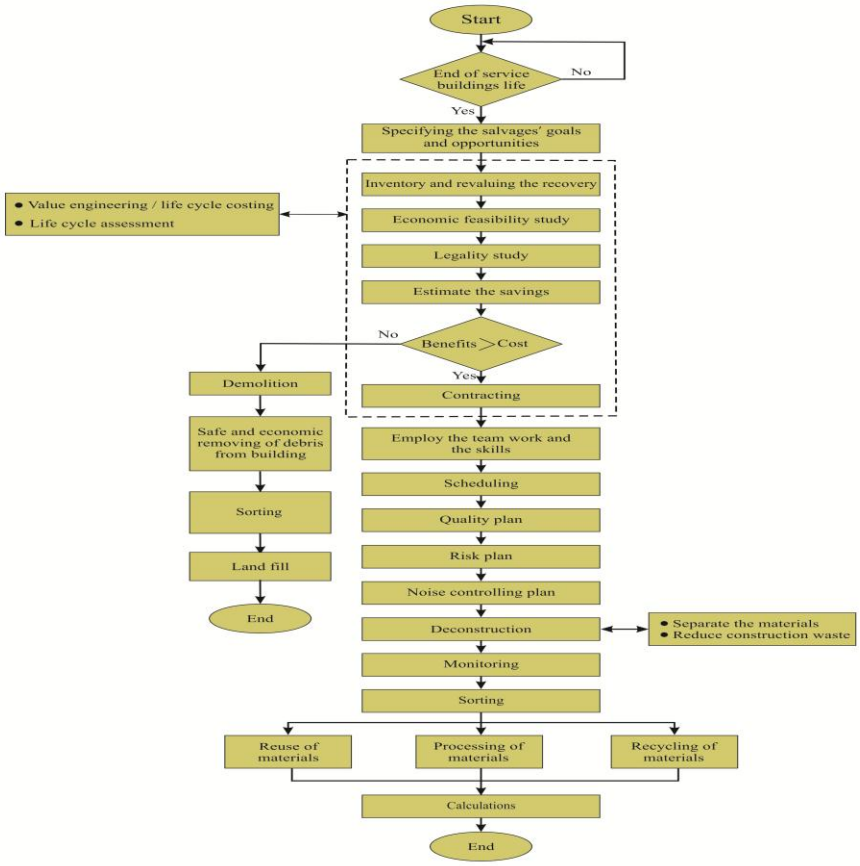

Figure 8. The proposed actions of post-operation and maintenance for sustainable buildings (researcher).

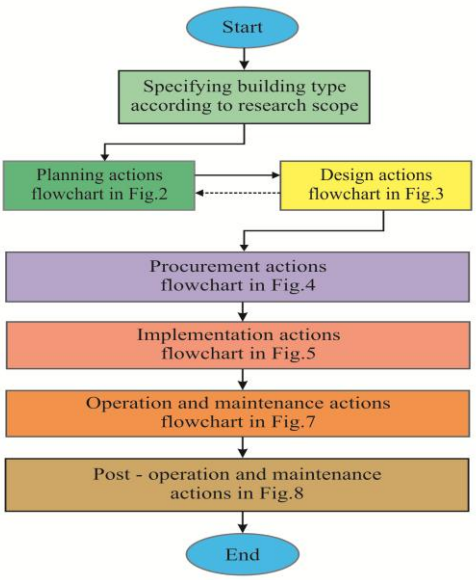

Figure 9. Summary of the proposed management system flowchart during sustainable buildings life cycle (researcher).

Design and Implementation of ICT-Based Recycle-Rewarding System for Green Environment

Dr. Mohammed Issam Younis
Department of Computer Engineering
College of Engineering / University of Baghdad
younismi@coeng.uobaghdad.edu.iq

ABSTRACT

This paper proposes a collaborative system called Recycle Rewarding System (RRS), and focuses on the aspect of using information communication technology (ICT) as a tool to promote greening. The idea behind RRS is to encourage recycling collectors by paying them for earning points. In doing so, both the industries and individuals reap the economical benefits of such system. Finally, and more importantly, the system intends to achieve a green environment for the Earth. This paper discusses the design and implementation of the RRS, involves: the architectural design, selection of components, and implementation issues. Five modules are used to construct the system, namely: database, data entry, points collecting and recording, points rewarding, and web modules. The RRS has been deployed at the Universiti Sains Malaysia (USM) to encourage the collectors to support the green environment.

Keywords: RFID, recycling, information engineering, software engineering, ICT.

تصميم وتنفيذ نظام لاعادة التدوير والمكافأة للبيئة الخضراء المستند على تكنولوجيا المعلومات والاتصالات

م.د. محمد عصام يونس
قسم هندسة الحاسبات
كلية الهندسة / جامعة بغداد

الخلاصة

يقترح هذا البحث تصميم وتنفيذ نظام تعاوني محوسب لاعادة التدوير والمكافأة للبيئة الخضراء, ويركز على جانب استخدام تكنولوجيا المعلومات والاتصالات كأداة لتعزيز تخضير الأرض. الفكرة وراء هذا النظام هي تشجيع جامعي المواد القابلة للتدوير عن طريق احتساب نقاط لهم, ومن ثم دفع أجور مقابلة للنقاط المكتسبة . وبذلك، فإن كلا من المصانع والأفراد تجني فوائد اقتصادية من هذا النظام. والأهم من ذلك, نحقق البيئة الخضراء للأرض. تناقش هذه الورقة تصميم وتنفيذ النظام المقترح، وتتضمن :التصميم المعماري، واختيار المكونات، وقضايا التنفيذ . فضلا عن ذلك, يقترح البحث خمسة وحدات لتشييد النظام، وهي :قاعدة البيانات، وحدة إدخال البيانات ، وحدة جمع وتسجيل النقاط, وحدة مكافأة النقاط، ووحدة شبكة الإنترنت. وقد تم وضع النظام المقترح حيز التطبيق في جامعة الساينس الماليزية لدعم البيئة الخضراء.

الكلمات الرئيسية :تحديد الهوية باستعمال الموجات الراديوية, التدوير، هندسة المعلومات، هندسة البرمجيات، تكنولوجيا المعلومات والاتصالات.

1. INTRODUCTION

During the past decade, radio frequency identification (RFID) systems have been incorporated into a wide range of industrial and commercial systems, **Chen, et al., 2010**. Its low cost provides a wide spectrum of applications that have never been seen in literature, **Akyildiz, et al., 2002**. RFID is a form of automatic contactless data capturing technique that uses radio frequency electromagnetic waves. An RFID system is comprised of a transponder (tag), a reader, and a host computer (software application), which is usually connected to a distributed database. The readers are usually placed in certain places to recognize the tags, **Ali, et al., 2010; Mahmood, et al., 2013**. A wide scale of applications is well studied in the literatures **, Nambiar, 2009; Idris, et al., 2009;** and **Lien, et al., 2012**. These applications involve, but are not limited to, supply chain, production and manufacturing, healthcare and medicine, construction, hospitality, parking management, transportation, attendance, tracing, and tracking. Thus, RFID becomes cost effective because the price of individual tags is reduced with the increase in manufactured volumes. Other opportunities will arise as the technology develops. Building on earlier works, this paper proposes the use of RFID in developing a recycling rewarding system (RRS).

Recycling involves processing the used materials into new products to prevent the wastage of potentially useful materials, reduce the consumption of fresh raw materials, reduce energy usage, reduce air pollution (from incineration) and water pollution (from land filling) by decreasing the need for conventional waste disposal, and lower greenhouse gas emissions compared with virgin production **, Murphy, 1993**. Recycling is a key component of modern waste reduction and is the third component of the "Reduce, Reuse, and Recycle" waste hierarchy **, EPA, 2013**.

To understand the environmental effects of recycling, consider the fact that recycling 1 kg of aluminum saves up to 6 kg of bauxite, 4 kg of chemical products, and 14 kWh of electricity **, EPA, 2013**. In other words, aluminum recycling provides up to 95% savings for both energy **, Murphy, 1993.** and air pollution **, EPA, 2013**. As another example, cited from Proclamation 7250 on America Recycles Day: "Buying recycled products conserves resources, reduces water and air pollution, saves energy, and creates jobs. Producing 1 ton of paper from recycled pulp saves 17 trees, 3 cubic yards of landfill space, and 7000 gallons of water. It also reduces air pollutants by 60 pounds, saves 390 gallons of oil, and conserves 4200 kilowatt hours of energy—enough to heat a home for half a year. Estimates show that 9 jobs are created for every 15,000 tons of solid waste recycled into new products" **, Clinton, 1999**. Thus, the importance of recycling on green environment is summarized as follows:

- Recycling reduces our reliance on landfills and incinerators.
- Recycling protects our health and environment when harmful substances are removed from the waste stream.
- Recycling conserves our natural resources because it reduces the need for raw materials.

An economic value creation in a proactive green manufacturing strategy results from an incremental contribution margin due to the sales of products made from regenerated materials. This measure identifies whether the take-back and regeneration of end-of-life products can also be justified from an economic viewpoint aside from the environmental considerations **, Azzone,**

and Noci, 1998 A; Azzone, and Noci, 1998 B. A second approach for firms involves cost savings. Some examples of potential cost savings include reducing energy consumption, waste reduction, lowering pollution emissions, smaller environmental fines, improving economic efficiency, and decreasing environmental cleanup costs **, Characklis, and Richards, 1999**.

Advances in manufacturing technology have enabled most recycled products to compete both in price and quality, with products made from virgin materials. However, only 12% of consumers are True Greens (regularly involved in recycling), 68% are Light Greens (sometimes involved in recycling), and 20% are Never Greens (never involved in recycling). The so-called True Greens are still a minority, whereas the Light Greens are the majority of consumers. Thus, there is a need to encourage the majority of consumers to be True Greens **, Hanas, 2007**. One way to achieve this objective is through rewards.

Earlier studies on the role of rewards in environmental management indicate a positive effect on environmental performance **, Daily, et al., 2007; Zutshi, and Sohal, 2003;** and **Chinander, 2001**. For instance, supervisor support behaviors advocating rewards motivate employees to introduce novel environmental initiatives, **Ramus, 2002**. Massoud et al. advocate the utilization of the Scanlon Plan as catalyst to green organizations. This institutionalization serves as a potential mechanism to enhance the environmental performance of a firm. In summary, the model is based on the following features: 1) collectiveness and cooperation, 2) employee participation, 3) quantifiable performance and bonus measures, and an equitable reward system. A firm predetermines with its employees an allocation ratio for gains in productivity or cost savings. Employee participation plays an ultimate role in gauging the fairness of the ratio, and as a result, the ratio remains open to adjustments, **Massoud, et al., 2008**.

Recycling is important for green environment because it has economical benefits and provides job opportunities. However, the persons involved in the recycling process, especially the item collectors, need to be encouraged. Thus, a rewards system is required to make them satisfied. This will improve recycling significantly, **Ramus, 2002; Massoud, et al., 2008**. Moreover, both the industries and individuals will reap the economical benefits of such system. Finally and more importantly, the system intends to achieve a green environment for the Earth.

Motivated by such goal, this paper proposes a collaborative system, that is, an RFID-based RRS. The remainder of this paper is organized as follows: Section 2 presents the specification of the RRS; Section 3 gives the architectural design; Section 4 discusses the implementation issues; and finally, Section 5 gives the conclusion and suggestions for future works.

2. RRS SPECIFICATION

To state the RRS specification, an inspection technique is used, by considering the following scenario for recycling in the inspection phase.

A collection center (e.g. a university) is responsible for collecting the recycling material, storing the recycling items, declaring the types of material, determining the points for each material and the formula to convert the points to benefits, and reporting the amount available in stock for each type of material. Recyclable materials include different kinds of glass, paper, metal, plastic, textiles, and electronics. The types of materials, their corresponding points, and the formula are controlled by the supervisor of the center. The materials to be recycled are brought

to a collection center by the collectors. Any person who would like to collect points should register himself/herself in a collection center. After registration, the collector brings the material and identifies himself/herself to the system. The weighting operator weighs the material and selects the type of the collected material from a computerized dialog to update the points for the corresponding collector in the system. The collector can withdraw his/her points from any branch of the collecting center (e.g. a cafeteria in a university). Finally, the industrial tracker tracks the amount of the recycled items available in stock in the recycling center and their corresponding price formula.

The RRS system involves many actors. The role of each actor is illustrated below:

- Supervisor Member(s) – The role of the supervisor is to administrate the whole system. The tasks include the following:
    1. Select the materials to be collected.
    2. Consult the environment, ICT, and economical experts to derive a suitable formula for earning and withdrawing points. There are two formulas based on economics: the first formula is for buying the collected materials from the collectors, and the second formula is for selling the collected materials to the industry.
    3. Decide on the scalability of the center and the members involved in the system (i.e., number of branches for the collecting center, number of operators and their salaries, method for announcement of the available materials, and their price formula).
- Weighing operator – The role of the weighing operator is to obtain the collected materials from the collector or to give the collected materials to the industry. In both cases, the weighing operator selects the material to be weighted and the corresponding (buying or selling) formula.
- Cashier – When the collector wants to withdraw points, he/she identifies himself/herself and then enters the amount of points to be withdrawn. The system calculates the corresponding cash to be given to the collector. Similarly, when an industry wants to buy a material from the collection center, the person who represents the industry identifies the firm, selects the type of the desired materials, and enters the required amount. The system calculates the corresponding cash to be received from the firm.
- Registrar – The role of the registrar is to assign an identity and enter the information (i.e., user name, identity, contact address, e-mail, and mobile phone number) for both the collectors and industries involved in the recycling system.
- Collectors – They are the people involved in collecting the recycled materials. The collectors should register themselves in the collecting center. The collectors are familiar with the materials and the corresponding formula to earn the points. They can withdraw their points from the cashier.
- Industries – These are the firms involved in buying the collected materials from the center. The industrial trackers (employees), similar to the collectors, are familiar with the amount of the materials and their corresponding formula to buy from the center. The

employees either track the availability of the materials or provide material information according to the strategy of the center.

3. RRS ARCHITECTURAL DESIGN

To simplify the work of the operators and save time for the individuals, RRS uses an RFID tag for user identification. This process can significantly improve the automation of identifying the persons in the system. Clearly, many tags are required, and the tag type should have a short distance between the tag and the RFID reader, consume less power, and have low cost, **Ali, et al., 2010**. For these reasons, the passive tags are chosen for person identification.

The RRS consists of five modules, namely, database, data entry, points collecting and recording, points rewarding, and a web module. Each module is described as follows.

3.1. Database Module

The database module is used to store, update, and retrieve all the information on the tags of the industrial firms as well as the collectors and their corresponding points. The database also includes the type of recycling material, the points awarded for each material, the amount available for each type, and the formulas for selling/buying items. For scalability purposes, the database is shared logically with other RRS modules and connected through a reliable network.

3.2. Data Entry Module

The data entry module is the software used to enter data into the database through a graphical user interface (GUI). The data entry module consists of two sub-modules that are described as follows:

3.2.1**. Registrar data entry module** – The registrar uses this module to enter the information for each industry/collector into database, and activate their corresponding identities in the system.

3.2.2. **Supervisor data entry module** – The supervisor uses this module to add/remove material, update the points for each material, and enter/update the name for the payment algorithm (e.g., buying and selling).

3.3. Points Collecting and Recording Module

This module consists of a weighing machine, a passive reader, and a PC. The PC is connected physically to the weighing machine and the passive reader. The PC running the points collecting and recording application software. In addition, this module is logically connected to the database. This module works as follows.

When the collector brings a material for recycling, the operator weighs the material using the weighing machine. Next, the collector presents his/her tag to an antenna attached to the passive reader. The passive reader detects the tag and sends the detected information to the PC. The application software asks the operator through the GUI about the type of the material, in addition, informs the operator the weight of the material. The application then queries the database and determines the points for the corresponding material. Next, the application software displays the old and new points of the collector. The operator can select the type of

material or cancel the detection process. When the operator presses the proceed button in the GUI, the application software updates the database for both the collector points and the available recycling weight of the selected material (i.e., the new weight is added to the old weight). Otherwise, the operator can cancel the transaction. Similarly, the operator can select to withdraw material when a firm would like to buy a material. The procedure is similar for the firm except that the updates of available material are subtracted from the total available material.

3.4. Points Rewarding Module

This module consists of a passive reader and a PC. The PC is physically connected to the passive reader. The PC running the points rewarding application software is logically connected to the database. This module is used by the cashier and works as follows.

In the case of the collector, the cashier selects the collector transaction. The collector then presents his/her tag to an antenna attached to the passive reader. The passive reader detects the tag and sends the detected information to the PC. The application software sends a query to the database and then retrieves the total amount of points. The software calculates the corresponding money of the retrieved points (using the buying formula). The software then displays the user name, total points, and the corresponding money. The application software asks the collector to enter the amount of money to be withdrawn. If the collector agrees on the withdrawn transaction (by clicking proceed), the total number of points and the total money are updated. The cashier gives the cash to the collector. To terminate the transaction, the operator can press a cancel button.

Similarly, in the case of a firm, the cashier selects the firm transaction. The employee then presents his/her tag to an antenna attached to the passive reader. The passive reader detects the tag and sends the detected information to the PC. The application software sends a query to the database and then retrieves the total amount of materials and their corresponding points. The application software asks the employee to select the material(s) and the desired weight through the GUI. Next, the software calculates the corresponding money of the desired amount of materials (using the selling formula). The software then displays the firm name, the weight of materials, the corresponding points, and the amount of money. If the employee agrees on the transaction (by clicking proceed), the total amount of the selected materials is updated. The cashier takes the cash from the employee. To terminate the transaction, the cancel button is pressed.

3.5. Web Module

This module consists of a web server and has a logical connection to the database. The web module retrieves the information stored in the database and displays the name of materials, the corresponding points, the total available amounts of the materials, and the formulas for buying and selling. The web module also displays the desired information for remote users. The user can be the collector (to check their points or the buying formula) or the industry (to see the items provided by the collection center and the corresponding amounts and selling formula).

4. RRS IMPLEMENTATION

This section describes the implementation issues for RRS. It should be noted that various implementations are possible.

The weighing machine is chosen as a third-party commercial machine. MySQL server is selected as the database server and Apache Tomcat as the web server. An in-house USMUHF passive reader serves as the RFID reader, **Ali, et al., 2010**. The Java programming language is used for the software application. These components are selected for their cross-platform functionality, that is, they support different hardware and operating systems.

The weighing machine is connected to the PC using the serial communication port (RS232), whereas the passive RFID reader is connected to the PC through the LAN. The application software has a configuration management feature. This feature is useful in setting the serial port and the TCP/IP port during the first run of the application.

A typical entry to the database for the supervisor is illustrated in **Table 1**. The first column presents the materials, the second column presents the green points for each material, and the third and fourth columns are the buying and selling formulas, respectively. The entry for the buying/selling formula shows the class name and the corresponding method to be invoked for the calculations. The algorithm for buying and selling is simple, that is, paying one cent and two cents, respectively, for each point.

Aside from the monetary benefits, the supervisor offers other incentives for collectors. For example, any collector with more than 300 points can own a locker for one semester for free. Moreover, a gift worth 1000 Malaysian Ringgit (RM) will be given to the green student who can collect the maximum earning points during the semester.

The points collecting and recording GUI starts in the waiting state of the module, that is, no tag is detected. When the tag is detected for a collector, the GUI shows the identity of the tag, the earned points, and the weight displayed by the weighing machine in grams (g). Finally, the GUI enables the operator to select the type of material or even cancel the operation as depicted in **Fig. 1(a)**. When the operator selects the material, a dialog will appear to verify the information entered. The weight shown by the weighing machine, the tag identity, the current points, the points to be given, and the total cumulative points will be shown on the display. The operator can press the "Proceed" button to confirm the information or press the "Cancel" button to terminate the operation and return to the waiting state, as shown in **Fig. 1b**. The updating of the points is conducted using the following formulas:

$$New\ Points = Weight\ (kg) * Green\ Point\ of\ the\ material \quad (1)$$

$$Total\ points = Old\ points + New\ points \quad (2)$$

For instance, when a collector (already with 78.2 points) brings 440 g of metal tin, the operator presses the "Metal tin" button, **Fig.1a**, and then

New points= 440/1000 *15=6.6 points.

Total points=78.2+6.6=84.8 **Fig.1b**.

In the points awarding software, the card's number (CN) can be entered in two ways: manually or through the RFID tag-detection system (depends whether the passive reader is available at the payment branch or not). After identifying the tag for a collector, the payment system enables the cashier to check, enter the amount of points to be withdrawn by the collector, trace the record of the collector, and finally proceed or cancel the transaction, as depicted in **Fig. 2**.

Similarly, when a firm tag is detected, the dialog appears to the employee and enables him/her to enter the desired amount for each material. Next, a dialog displays the total amount of points and the corresponding cash to be paid to the center. For example, consider a firm that wants to buy 1 ton of aluminum tin can, 500 kg of computer paper, and 100 kg of compact disc. In this case:

Total Points=330*1000+500*48+55*100

=359,500 points.

Using the USM_Selling formula, the cash amount=RM 7190.00.

5. CONCLUSION

This paper presented a recycling system called RRS that aims to keep the environment green. The use of low-cost passive tags significantly reduces the cost of modernization and identification automation. This paper also presented the design and implementation of the system. An incremental prototype was discussed as a case study. The modular design of the system makes it scalable, easy to use, and extendable horizontally (by adding more functionality to the system) and vertically (by supporting various implementations of the system). For instance, instead of tracking the available material passively from the web site, an alternative active tracking system can be achieved by sending an e-mail or SMS to the interested firm or industry. Currently, a pilot testing of the system is undergoing in Universiti Sains Malaysia (USM). As part of future work, a web-based material tracking and tracing system is currently being developed to make the industry track and trace materials around different universities and countries.

6. ACKNOWLEDGEMENTS

The author would like to give his sincere gratitude and thanks to the Vice Chancellor of the Universiti Sains Malaysia, and the Auto Identification Laboratory (AIDL) research group at the School of Electrical and Electronics Engineering for granting this research, providing all the required hardware, and putting the RRS at the University.

7. REFERENCES

Akyildiz, I. F., Su, W., Sankarasubramaniam, Y., and Cayirci, E., 2002, *A Survey on Sensor Networks*, IEEE Communications Magazine, Vol. 40, No. 8, PP. 102-114.

Ali, M. F. M., Younis, M. I., Zamli, K. Z., and Ismail, W. , 2010, *Development of Java Based RFID Application Programmable Interface for Heterogeneous RFID System*. Journal of Systems and Software, Vol. 83, No. 11, PP. 2322–2331.

Azzone, G. and Noci, G. , 1998 A, *Identifying Effective PMSs for the Deployment of Green Manufacturing Strategies*, International Journal of Productions & Operations Management, Vol. 18, No. 4, PP. 308-335.

Azzone, G. and Noci, G. , 1998 B, *Seeing Ecology and Green Innovations as a Source of Change*, Journal of Organizational Change Management, Vol. 11, No. 8, PP. 94-111.

Characklis, G. W., and Richards, D. J., 1999, *The Evolution of Industrial Environmental Performance Metrics: Trends and Challenges*, Corporate Environmental Strategy, Vol. 6, No. 4, PP. 387-398.

Chen, M., Gonzalez, S., Zhang, Q., Li, M., and Leung, V., 2010, *A 2G-RFID Based E-healthcare System*, IEEE Wireless Communications Magazine, Vol. 17, No. 1, PP. 37-43.

Chinander, K. R., 2001, *Aligning Accountability and Awareness for Environmental Performance in Operations*, Production and Operations Management, Vol. 10, No. 3, PP. 276-291.

Clinton, W. J., 1999, *America Recycles Day*, in Proclamation 7250 of November 15, USA.

Daily, B. F., Bishop, J. W., and Steiner, R., 2007, *The Mediating Role of EMS Teamwork as it Pertains to HR Factors and Perceived Environmental Performance*, Journal of Applied Business Research, Vol. 23, No. 1, PP. 95-110.

EPA, 2013, *Recycling*, United States Environmental Protection Agency, Annual Report, 2013.

Hanas, J. , 2007, *A World Gone Green*, Speacial Report: Eco-Marketing, Advertising Age.

Idris, M. Y. I., Tamil, E. M., Razak, Z., Noor, N. M., and Km, L. W., 2009, *Smart Parking System using Image Processing Techniques in Wireless Sensor Network Environment*, Information Technology Journal, Vol. 8, No. 2, PP. 114–127.

Lien Y. H., Hsi, C. T., Leng, X., Chiu, J. H., and Chang, K. C., 2012, *An RFID Based Multi-Batch Supply Chain Systems*, Wireless Personal Communications, Vol. 63, No. 2, PP. 393-413.

Mahmood, B. M. R., Younis, M. I., and Ali, H. M., 2013, *Construction of a General Purpose Infrastructure for Rfid-Based Applications*, Journal of Engineering, Vol. 19, No. 11, PP. 1425-1442.

Massoud, J. A., Daily, B. F., and Bishop, J. W., 2008, *Reward for Environmental Performance: Using the Scanlon Plan as Catalyst to Green Organisations*, International Journal of Environment, Workplace and Employment, Vol. 4, No. 4, PP. 15-31.

Murphy, P., 1993, *The Garbage Primer: The League of Women Voters*, New York: Lyons & Burford.

Nambiar, A. N. , 2009, *RFID Technology: a Review of its Applications*, in Proceedings of the World Congress on Engineering and Computer Science 2009 (WCECS 2009), San Francisco, USA, PP. 1-7.

Ramus, C. A. , 2002, *Encouraging Innovative Environmental Actions: What Companies and Managers Must Do*, Journal of World Business, Vol. 37, No. 1, PP. 151- 164.

Zutshi, A., and Sohal, S., 2003, *Stakeholder Involvement in the EMS Adoption Process*, Business Process Management Journal, Vol. 9, No. 2, PP. 133-148.

Table 1. Typical data entry for supervisors in the USM recycling center.

MATERIALS	Green Points/kg	Buying Formula	Selling Formula
All types of paper	25	USM_Buy	USM_Sell
Computer paper	48	USM_Buy	USM_Sell
Mineral water bottles	50	USM_Buy	USM_Sell
Aluminum tin can	330	USM_Buy	USM_Sell
Glass bottles	2	USM_Buy	USM_Sell
Metal tin (milk tin, biscuit tin)	15	USM_Buy	USM_Sell
Mixed-plastics (PVC, water containers)	30	USM_Buy	USM_Sell
Compact Disc (CD-ROM, Audio CD, VCD, DVD)	55	USM_Buy	USM_Sell
Mixed-metals	20	USM_Buy	USM_Sell

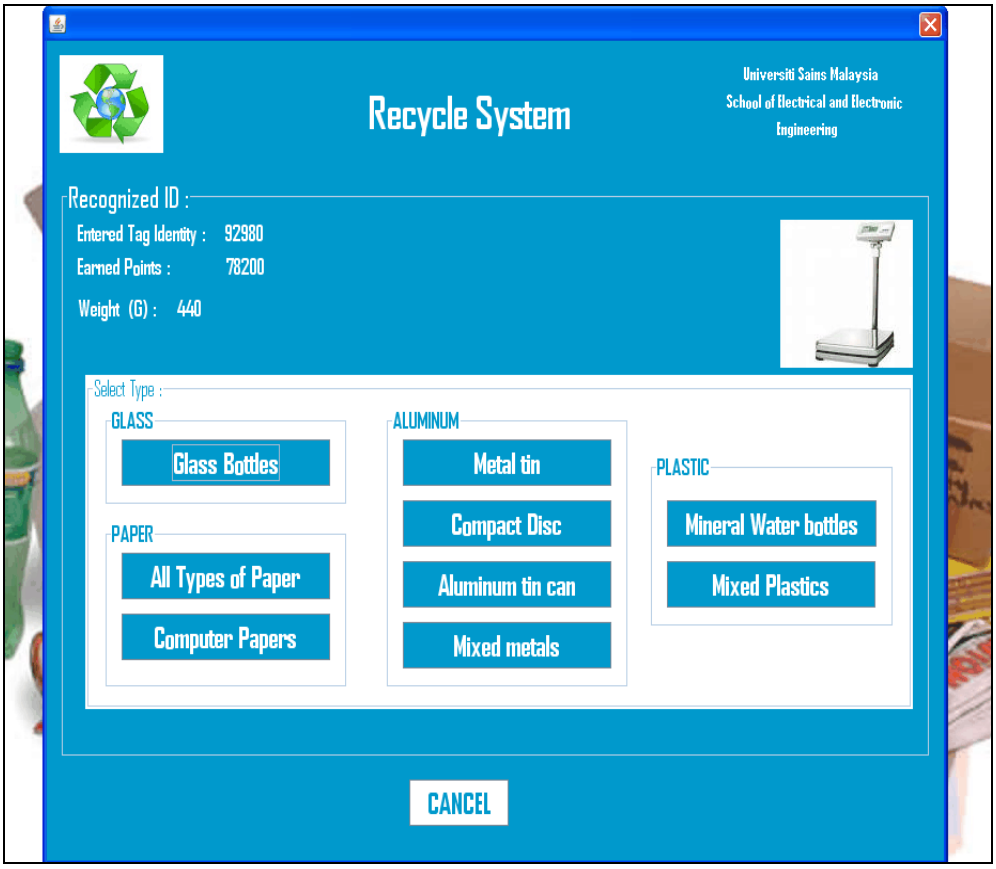

(a) Tag detection and type selection process for an authorized tag.

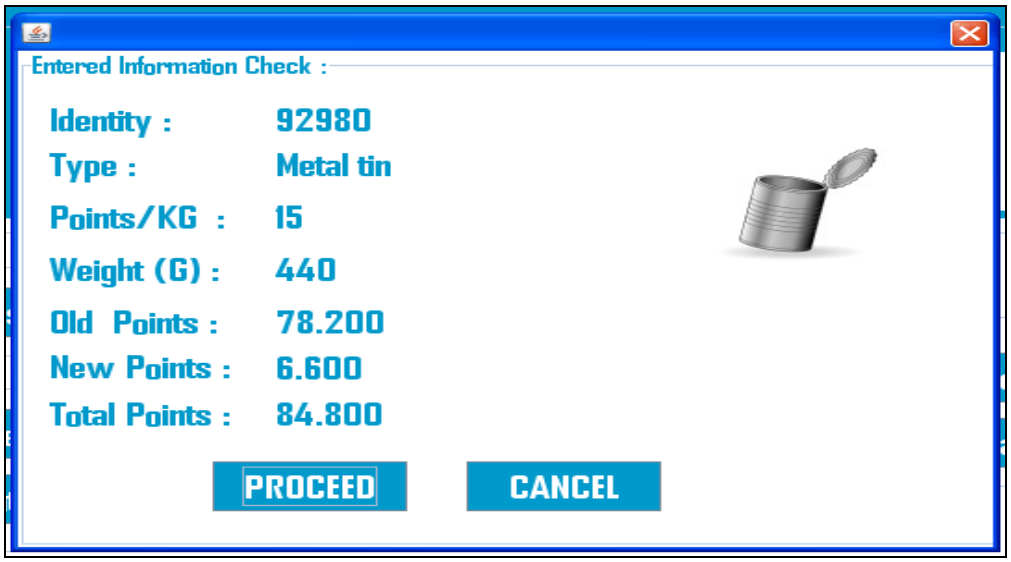

(b) Confirmation dialogue

Figure 1. Snapshots of the points collecting and recording.

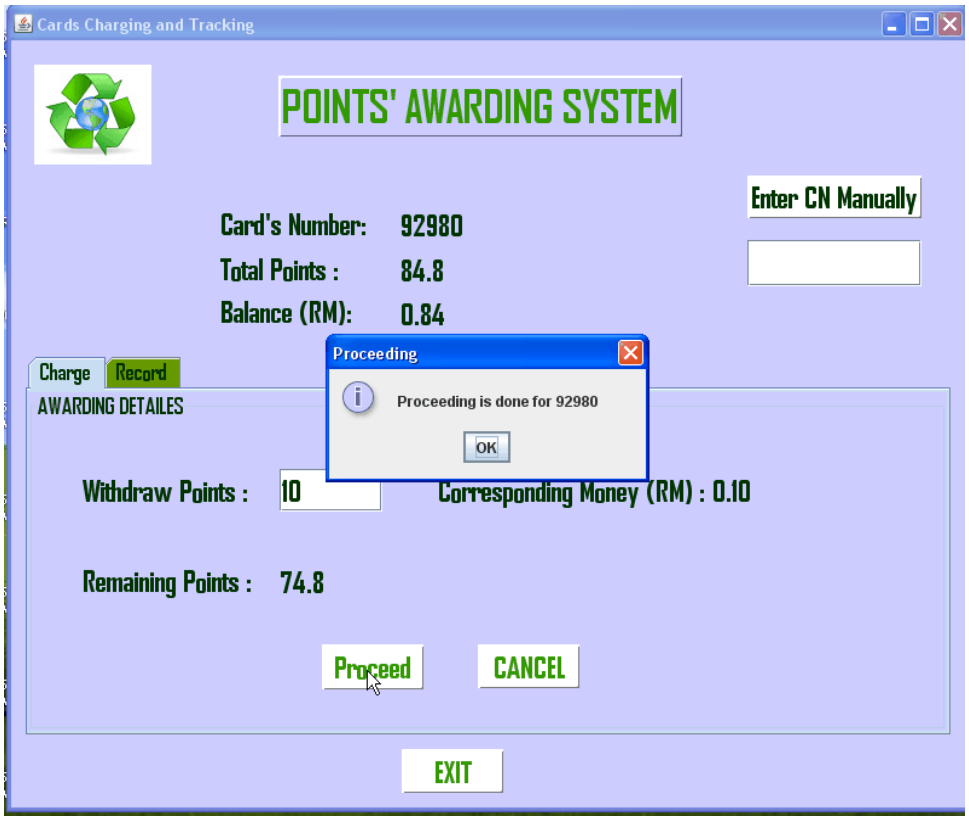

Figure 2. Snapshot of the points awarding system.

Experimental Studies and Finite Element Modeling of Piles and Pile Groups in Dry Sand under Harmonic Excitation

Saad Faik Abbas Al-Wakel
Lecturer
University of Technology-Baghdad
Saadfaik231@yahoo.com

Mahmoud Rasheed Mahmoud
Assistant professor
University of Technology-Baghdad

Ahmed Sameer Abdulrasool
Lecturer
University of Technology-Baghdad

ABSTRUCT

Foundations supporting reciprocating engines, radar towers, turbines, large electric motors, and generators, etc. are subject to vibrations caused by unbalanced machine forces as well as the static weight of the machine. If these vibrations are excessive, they may damage the machine or cause it not to function properly. In the case of block foundation, if changes in size and mass of the foundation do not lead to a satisfactory design, a pile foundation may be used.
In this study, the dynamic response of piles and pile Groups in dry sand is investigated experimentally. The analysis involves the displacement response under harmonic excitation. In addition, a numerical modeling by using finite element method with a three-dimensional formulation is adopted to simulate the experimental model. The results of the numerical model showed that a good agreement is achieved between the predicted dynamic response and that measured from the experimental model.

Key words: dynamic analysis, finite element method, pile foundations.

دراسات عملية ونمذجة العنصر المحدود للركائز ومجموعات الركيزة في الرمل الجاف تحت تأثير الأستثارة المتناسقة

سعد فايق عباس
مدرس
الجامعة التكنولوجية - بغداد

محمود رشيد محمود
أستاذ مساعد
الجامعة التكنولوجية - بغداد

أحمد سمير عبد الرسول
مدرس
الجامعة التكنولوجية - بغداد

الخلاصة

الأسس التي تسند المحركات الترددية، أبراج رادار، توربينات، محرّكات كهربائية كبيرة، ومولّدات، الخ تكون خاضعة للإهتزازاتِ التي تسببها قوى الماكنةِ غير المتوازنةِ بالإضافة إلى الوزنِ الساكنِ للماكنةِ. إذا كانت هذه الإهتزازاتِ مفرطة، قَدْ تسبب ضرر للماكنةَ أو قد لا تشتغلَ بشكل صحيح. في حالة الأسس ذات الكتلة ، إذا كان التغيير في حجمِ وكتلةِ الأساسِ لا يُؤدّيانِ إلى تصميم مقنع , فأن أسس الركائز يمكن أنْ تُستَعملُ.في هذه الدراسةِ، الأستجابة الديناميكية للركيزة ولمجموعة ركائز في الرملِ الجافِ يُتحرّى عنها بشكل عملي. يَتضمّنُ التحليلُ رَدِّ الإزاحةَ تحت الأستثارة المتناسقة. بالإضافة الى ذلك, النمذجة العددية بإستعمال طريقةِ العنصرِ المحدودةِ مَع صياغة ثلاثية الأبعاد تم تبنيها لتمثيل النموذجِ العملي. تبين نَتائِجَ النموذجِ العددي بأنّ هنالك توافق جيد تم تحقيقه في النتائج بين الرَدِّ الديناميكي المُتَوَقّعِ وذلك الذي تم قياسه مِنْ النموذجِ العملي.

1. INTRODUCTION

In the recent years, there is a dramatic progress in the develop-merit of theories for dynamic analysis of piles. The rapid development of pile analysis is prompted by the growing use of pile foundations in traditional areas. As well as it's used as a deep foundation for building, it's used also as a machine foundations and their large scale application used in new application of civil engineering such as nuclear power plants and offshore towers. Many methods have been used to examine the foundation behavior under dynamic loadings; they are basically classified as experimental and theoretical approaches. The experimental approach includes models and field studies on existing foundations while the theoretical approach includes analytical and numerical solutions.

There are various types of dynamic tests of piles are conducted, they differ primarily according to the size of piles, test medium, technique employed, and aim as following **, Novak, 1987.**

(1) Full scale field tests

In these tests full scale piles are installed in natural deposit. Sometimes the piles are instrumented with strain gauges to monitor strains and thus axial forces or bending moments. Often the piles are loaded by a rigid concrete or steel test body. The purpose of this loading is to lower the pile resonant frequencies and to bring them within the frequency range of the exciter, if an exciter is used, and to lower the damping ratio which facilitates the analysis of the experimental data.

(2) Small prototype field tests

Field experiments with small prototype piles are less demanding than full scale experiments in terms of equipment, cost and effort, and make it easier to control the conditions of experiments while still allowing for unobstructed propagation of elastic waves.

(3) Small scale laboratory tests

Small scale laboratory tests are conducted with very small model piles in test bins or tanks. The small scale laboratory tests are popular because they are inexpensive, easy to organize, and independent of the weather. Their deficiencies are their inability to work with an undisturbed natural deposit (which limits the experiments to artificially prepared deposits of sand or remolded clay), the difficulty in achieving meaningful confining pressure on which soil stiffness depends and, finally, the limited size of the test box.

2. THE DYNAMIC RESPONSE OF PILE FOUNDATIONS

Das , 1983. presented a method to determine the natural frequency of vertical vibration of the pile using elastic waves in a bar method. The benefit derived from the use of piles depends on several factors such as the type of piles to be used, the length of piles, and the portion of load carried by each pile. The problem was treated as a vertical rod fixed at the base (i.e., at the rock layer) and free on top.

Novak , 1987. Studied the dynamic behavior of pile and pile groups experimentally. Three types of test are conducted: steady-state vibration tests using a mechanical oscillator, free vibration (plucking) tests, and static deflection tests. The excitation forces are produced by means of a Lazan mechanical oscillator. A typical set of vertical response curves measured with different intensities of harmonic excitation is considered. The experimental response curves are compared with theoretical predictions. The first observation made is that the vertical stiffness of the pile strongly depends on the tip condition unless the pile is quite long or the soil very stiff. Assuming an end bearing pile, where the floating tip condition is more proper, may result in a very substantial overestimation of stiffness and a significant underestimation of damping. A proper

relaxation of the tip, depending on the stiffness of the stratum underlying the tip, is necessary. This observation is in good agreement with theoretical results.

El-Marsafawi et al. 1992. conducted a field experiments on group of piles supporting rigid foundations and subjected to harmonic loading. The objective is to investigate the ability of linear elastic theories of pile-group modeling to predict the response curve characteristics including the resonant frequency and amplitude. Harmonic vibration tests are conducted on the pile group in vertical and horizontal directions. In addition, a single pile is tested under harmonic loading in the vertical direction and in free vibration in the horizontal direction. The theoretical results are also verified using the more rigorous direct analysis approach. The comparison with the experiments shown that, the linear theory gives a good estimate of the group stiffness but overestimates damping of the group.

Boominathan and Lakshmi , 2000. studied the influence of pile-soil interaction on dynamic characteristics of pile groups. The vertical vibration tests are conducted in a carefully designed small scale pile test facilities at the laboratory. The analysis of the test results indicate that the group stiffness increases with increase of frequency up to limiting frequency and then decreases. The damping constants are substantially high at the low frequencies and decreases with the increase of the frequency. In addition, it is found that the stiffness is increasing and the damping is decreasing as the spacing between the piles decreases.

3. PROPERTIS OF MATERIALS USED IN THE EXPERIMENTAL MODEL

The materials used in this study are divided into two parts they are; dry sand and reinforced concrete for the pile foundation. The standard tests are performed to determine the physical properties of the sand as follows:

(1) Relative density: The test is carried out according to the (ASTM-D4253 and D4254) specification.

(2) Specific gravity: The standard test for the specific gravity of the soil particles is performed according to (ASTM-D854) specification using water the pycnometer method. The physical properties of the soil are shown in **Table 1**.

(3) Grain size analysis: The test is carried out according to the (ASTM-D422) specification; the grain size distribution of the soil is shown in **Fig. 1**.

(4) Direct shear test: The direct shear test is used to obtain the stress-strain relationship. In addition, the angle of internal friction (Ø) of the sand with a unit weight of 15.0 kN/m^3 is obtained from the same test.. The mechanical properties of the soil obtained from the test are shown in **Table 2**.

The tests performed to determine the properties of the concrete and the reinforcement is:

(1) Compression test: The standard test of compressive strength according to (ASTM-C39M) specification is performed for three samples of cylinders.

(2) Tensile test: The Tensile test of the reinforcement is carried out according to the (ASTM-E8M) specification.

4. PRPARATION OF EXPERIMENTAL MODEL

The experimental tests are conducted on deep foundations under the effect of harmonic vertical mode of waves with two groups of piles. In addition, a deep foundation consists of single pile is tested. A steel mold is used to construct the frame of the deep foundation. The mold for the single pile consists of two parts linked together with screws. The molds of the experimental model with two and four piles consist of three parts linked together with screws. The reinforcement of the pile consists of four bars with 3.0 mm in diameter and the length of the bar

is 545.0 mm. The spacing between the reinforcement of the pile center to center is 8.0 mm. The yield strength of the reinforcement (fy) is 290 MPa.
A circumferential wire is used as stirrups, and the spacing between stirrups is 136.0 mm center to center. The cap is reinforced in two directions where the number of bars in each direction is 9 bars. The length of each bar is 206.0 mm with diameter of 2.0 mm. The space between the reinforcement center to center is 24 mm and the cover of cap reinforcement is 7.5 mm. The yield strength of the reinforcement (fy) is 175.0 MPa. In addition, the end of each bar is twisted in the vertical direction with length of 15.0 mm, and the reinforcement of the pile and cap are linked together with a wire. The molds and the reinforcement of the experimental model are shown in **Plate 1**. Four screws are used to link the mechanical oscillator with the cap of the foundation to act as a one unit where the screws are fixed at the bottom of the cap. A steel base plate is used to ensure the spacing between the bolts to put a mechanical oscillator at a specific location, and then the plate is lifted up.
A concrete with mix of (1:1.5:3) is used to construct the model of the pile foundation, the gravel is passing through a sieve No.6 (3.35 mm). **Chowdhary** and **Dasgupta , 2009.** Recommended that the water-cement ratio shall be not exceeding 0.45 for a machine foundation. In this work, the water-cement ratio (w/c) was 0.4. An additive of Structuro 520 (Suporplasticisers) is added to the concrete mix with a ratio of 1 liter/m3. This additive allows producing a concrete with a high performance and workability. The concrete of the pile and cap is board continuously and integrally, and then the mold is placed on a vibration table for 45 second to ensure that no voids in the concrete and to have a smooth surface of concrete. After 24 hours, the concrete of the pile foundation is cured for a 28 days.

5. SET-UP OF THE EXPERIMENTAL MODEL

The group interaction factor which has been observed to have a significant effect on the dynamic response on the system especially for the pile spacing between 2.5D to 3D where D is the overall diameter of the pile. To ignore the effect of group interaction factor, the distance between the piles center to center is at least more than 5D **, Chowdhary** and **Dasgupta, 2009**. In this study, the distance between the piles center to center was 6D.
The model of the deep foundations consists of pile with a square cross-section of width 25.0 mm and length of 550.0 mm. The cap of the piles is made of a reinforced concrete of thickness 30.0 mm. The base of the cap is rising 50.0 mm above the soil surface to avoid the effect of pile raft condition. The layout of the deep foundation is shown in **Fig. 2**. A container of steel plate with dimensions of (600×600) mm and 700 mm height is used, so that the distance from the edges of the cap and tip of the piles to the boundary of the container is more than 5D of the pile which is satisfying a non-reflection wave. This behavior can be examined by the numerical model when the displacement response for this type of foundation returns to zero (i.e., no reflection of the wave at the boundary).
To prepare the soil of the experimental model, a sandy soil passing through sieve No.18 (1.0 mm) and retained on sieve No.100 (0.150 mm) is used. In the first stage, a soil of 130.0 mm thickness is placed in the steel container to prepare the bed of soil. Then, the pile foundation is placed in the container so that the base of the cap is resting on a steel plate with fixed ends as shown in Plate (2). After that, the container is filled with sand by five layers with thickness of 100 mm for each layer. The density of the soil used 15.0 kN/m^3 is specified previously. The required amount of the soil is weight, and then put in the container. The general procedure of ASTM-D4253 is adopted to obtain the dry unit weight of the soil. A surcharge load of 37.32 kg/m^2 is added on the surface of the soil to avoid vertical movement of surface particles. An external source of vibration with frequency of 3600 cycles/min is applied up to the soil is

occupying a specific volume (cross-section area of the container with height of the layer) to give the required density of the soil. The time required to apply the vibration was found in the laboratory experimentally and depends on the thickness of layer which is 37 seconds for the bed layer and 30 seconds for each other layers. The steel plate which supports the foundation is removed during the test.

To create a small scale model of a dynamic system, a mechanical oscillator consists of an electrical motor having a maximum rated speed of 6500 rpm through a shift is used to introduce a harmonic vertical mode of sinusoidal wave. The mechanical oscillator consists of a rotating disc manufactured from steel with diameter 70.0 mm and thickness 5.0 mm. A single mass (m_e) is placed on the rotating disc at an eccentricity, e of (25.0) mm from the axis of rotation. This arrangement rotates in one direction when it is driven by a motor having a maximum rated speed of (6500) rpm through a shift, where such an arrangement induces a dynamic force at the base of the oscillator.

The speed of the motor and hence the mechanical oscillator can be varied which, in turn, causes a change in frequency of vibration. In addition, a mechanical assemblage is fixed on the disc of the mechanical oscillator and connected to a tachometer to measure the frequency of the dynamic system. The dynamic force induced is a frequency dependent for a given mass on the rotating disc. By varying the mass by means of an external control, it is possible to change the amplitude of dynamic force for a specific frequency. The amplitude of vertical dynamic force produced as in Eq. (1):

$$F_o = m_e\, e\, \omega^2 \tag{1}$$

where ω = circular frequency of the dynamic system,

The displacement response of the foundation can be measured by a vibration meter which converts the electrical signal to a displacement. The main objective of the apparatus is to apply a harmonic vertical mode of vibration on a pile foundation to determine the displacement response. The frequency of the dynamic force is controlled by a speed control unit which is connected to the mechanical oscillator. The displacement of the foundation is measured by the vibration meter. For all tests, the displacement response is measured at the edge and center of the cap. The amplitude of the applied dynamic force is ± 99.41 and ± 155.34 N and the circular frequency (ω) is 209.4 and 261.7 rad/sec, respectively. The displacement of the foundation is recorded when the steady state is occurred.

The results of the experimental model which are represent the frequency versus displacement of the pile foundation at the edge and center for different values of amplitude of dynamic force are shown in **Tables 3** and **4**. From results of the experimental model, it can be stated that the maximum amplitude of displacement of the deep foundations occurs at the center of the foundation. In addition, as the number of piles increases this will lead to a decrease in the displacement response of the pile foundation due to increase the mass of foundation.

6. THE NUMERICAL SIMULATION OF THE EXPERIMENTAL MODEL BY USING FINITE ELEMENT METHOD

The Finite element method is one of the most popular numerical methods used for obtaining an approximate solution for complex problems in various fields of engineering. In this study, a numerical modeling in prototype scale using a three-dimensional condition is adopted to simulate the physical model. In addition, the numerical simulation is performed by using the finite element method with Tcl command language which is implemented in OpenSees program.

The basic equations of the displacement field in three dimension for the elastic analysis of the finite element method can be written as in Eq. (2), **Zienkiewicz** and **Taylor, 2005**:

$$u = \sum_{i=1}^{n} N_i u_i \quad (2\text{ a})$$

$$v = \sum_{i=1}^{n} N_i v_i \quad (2\text{ b})$$

$$w = \sum_{i=1}^{n} N_i w_i \quad (2\text{ c})$$

where: N_i = the shape function at a given node, u_i, v_i and w_i are the nodal displacement.

In matrix form Eq. (3):

$$\{u\}=[N]\{d_i\} \quad (3)$$

The strain vector can be derived as in Eq. (4)

$$\{\varepsilon\} = [B]\{d_i\} \quad (4)$$

where [B] = nodal strain-displacement matrix.

Then stiffness matrix [K] can be as in Eq. (5)

$$K = \int_v [B]^T D\,[B]\,dv \quad (5)$$

where D = elastic coefficient matrix.

The general equation of motion as in Eq. (6)

$$[M]\{\ddot{u}\} + [C]\{\dot{u}\} + [K]\{u\}=\{F\} \quad (6)$$

where $[M]$ = the mass matrix, [C] = the damping matrix, [K] = the stiffness matrix, $\{\ddot{u}\}$ = nodal acceleration vector, $\{\dot{u}\}$ = nodal velocity vector, $\{u\}$ = nodal displacement vector, and $\{F\}$ = applied load vector.

The considerations of similitude lead to model scale listed in **Table 5**, the linear dimensions are scaled 1 to it and the stresses are represented 1 to 1 **, Novak, 1987**. In this study, the scale factor (n) was 10. For the full scale model, the dimensions of the pile cap are (2.25× 2.25) m with thickness of 0.3 m. The length of pile is 5.5 m with a cross-section of (0.25× 0.25) m. A brick element of 8-node linear isoparametric is used for the finite element discretization. Each node of element has three degrees of freedom for displacements. To achieve a three-dimensional analysis, the boundary conditions are applied so that the bottom of the soil is fixed in displacement while the top surface of the soil is set to be free. To model the steel container, the constraint on displacement in X and Z directions is applied on nodes at the boundary in Y-Z and X-Y planes, respectively and the finite element mesh is shown in **Fig.3**.

The response of pile foundations is greatly affected by the behavior of soil, in which piles are embedded. Considerable research has been conducted for the analysis of pile groups, in most of the literature the behavior of the soil is assumed elastic , **Maheshwari** and **Watanabe, 2005**.The poisson's ratio of the fine-grained sand used in the numerical model is 0.25 **, Kaniraj, 2008**. According to the laboratory experiments the modulus of elasticity of the soil as shown in

Table 2.

The material properties of the concrete of foundation, as shown in **Table 6**, are calculated according to the ACI code (ACI-318-83), where the compression strength of the concrete, f_c is 44.24 MPa. The unit weight of the reinforced concrete is 24.0 kN/m^3.

The dynamic load is applied at the surface of the foundation for a specific node at the edge and center of the cap. The foundation is subjected to a steady state load of sinusoidal function of the form $F = F_o \sin(\omega t)$ with amplitude of force 9.941 and 15.534 kN and circular frequency of 20.94 and 26.17 rad/sec, respectively. To cure the artificial oscillation, the numerical damping is introduced into the analysis which is achieved by using $\gamma = 0.6$ and $\beta = 0.3025$ in the Newmark algorithm, **Jeremic, 2006**. The time step (Δt) of the dynamic analysis for circular frequency 20.94 and 26.17 rad/sec are 0.19882 and 0.31068 second, respectively with a total of 50 steps are performed.

The displacement responses of the deep foundation with a group of four piles obtained from the numerical model are shown in **Figs. 4** to **7** From these figures, it can be seen that the displacement reaches maximum amplitude and then rumbling is occurred after that it is return to zero. This behavior can be attributing to the decay of the wave with time, i.e., the reflection of the wave at the boundary is not occurred. The comparison between the displacement response of the foundation with group of four piles which is obtained from the experimental and the numerical model is shown in **Tables 7** and **8** By comparing these results it can be seen that, a good agreement is achieved.

7. CONCLUSIONS

(1) From the experimental model it can be stated that the maximum amplitude of displacement of pile foundations occurred at the center. In addition, for a specific frequency, the amplitude of displacement of the foundation increased with increasing the amplitude of dynamic force.

(2) The displacement response of the pile foundation under effect of dynamic force, decreases with the increasing in number of piles due to the increase in the mass of foundation

(3) The numerical modeling using the finite element method can be used to analyze pile foundations under effect of harmonic excitation.

8. REFFERENCES

- Boominathan, A, and Lakshmi, T. 2000, *Dynamic Characteristics of Pile Groups under Vertical Vibrations*, Conference, 12WCEE, Australia.
- Chowdhury, I. and Dasgupta, S. 2009, *Dynamics of Structure and Foundation – A Unified Approach*, CRC Press-Balkema, London.
- Das, B. M. 1983, *Fundamentals of Soil Dynamics*, ELSEVIER- New York, Amsterdam, Oxford.
- El-Marsafawi, H., Han, Y.C. and Novak, M. 1992, *Dynamic Experiments on Two Pile Groups*, Journal of Geotechnical Engineering, ASCE, 118, 4, pp.576-592.
- Jeremic, B. 2006, *Computational Geomechanics Inelastic Finite Elements for Pressure Sensitive Materials*," Lecture, University of California, Davis.
- Kaniraj, S. R 2008, *Design Aids in Soil Mechanics and Foundation Engineering*, McGraw.
- Maheshwari, B.K and Watanabe, H. 2005, *Dynamic Analysis of Pile Foundations Effects of Material Nonlinearity of Soil*," Electronic Journal of Geotechnical Engineering, EJGE.

- Novak, M. ,1987, *Experimental Studies of the Dynamic Behavior of Piles and Pile Groups*, Dynamic Behavior of Foundations and Buried Structures, Elsevier Applied Science Publishers (London), pp. 270.

- Zienkiewicz, O.C. and Taylor, R.L. , 2005, *The Finite Element Method*, McGraw-Hill, London, UK.

Table 1. Physical properties of the sand.

Parameters	Value	Units
Max dry unit weight, $\gamma_{dry\ max}$	16.7	kN/m^3
Min dry unit weight, $\gamma_{dry\ min}$	14.3	kN/m^3
Relative density (%)	32.5	_
Specific gravity, Gs	2.661	_

Table 2. Mechanical properties of the sand.

Parameters	Value	Units
Modulus of elasticity, E_s	40202	kN/m^2
Angle of internal friction, Ø	34^o	_

Table 3. Displacement of the pile foundation at the edge obtained from the experimental model .

Type of Model	Frequency (rad/sec)	Amplitude of Dynamic Force (N)	Amplitude of Displacement (mm)
Single Pile	261.7	155.34	0.635
Group of Two Piles	209.4	99.41	0.471
	261.7	155.34	0.581
Group of Four Piles	209.4	99.41	0.048
	261.7	155.34	0.053

Table 4. Displacement of the pile foundation at the center obtained from the experimental model **.**

Type of Model	Frequency (rad/sec)	Amplitude of Dynamic Force (N)	Amplitude of Displacement Edge (mm)
Single Pile	261.7	155.34	0.810
Group of Two Piles	209.4	99.41	0.502
	261.7	155.34	0.710
Group of Four Piles	209.4	99.41	0.051
	261.7	155.34	0.057

Table 5. Scales for centrifugal modeling (after Novak, 1987).

Quantity	Full scale	Centrifugal model
Linear dimension	1	1 / n
Time (in dynamic terms)	1	1 / n
Force	1	$1 / n^2$
Stress	1	1
Strain	1	1
Density	1	1
Frequency	1	n

Table 6. Material properties of the concrete**.**

Parameters	Value	Units
Poisson's ratio, υ	0.20	_
Modulus of elasticity, E	31261184	kN/m^2

Table 7. The displacement response of the pile foundation at the edge.

Frequency (rad/sec)	Scaled Frequency (rad/sec)	Experimental Amplitude of Dynamic Force (kN)	Numerical amplitude of Dynamic Force (kN)	Measured Displacement (mm)	Predicted Displacement (mm)
209.4	20.94	0.09941	9.941	0.0485	0.0543
261.7	26.17	0.15534	15.534	0.0535	0.0609

Table 8. The displacement response of the pile foundation at the center.

Frequency (rad/sec)	Scaled Frequency (rad/sec)	Experimental Amplitude of Dynamic Force (kN)	Numerical Amplitude of Dynamic Force (kN)	Measured Displacement (mm)	Predicted Displacement (mm)
209.4	20.94	0.09941	9.941	0.051	0.0547
261.7	26.17	0.15534	15.534	0.057	0.0628

Plate 1. The molds and reinforcement of the experimental model **.**

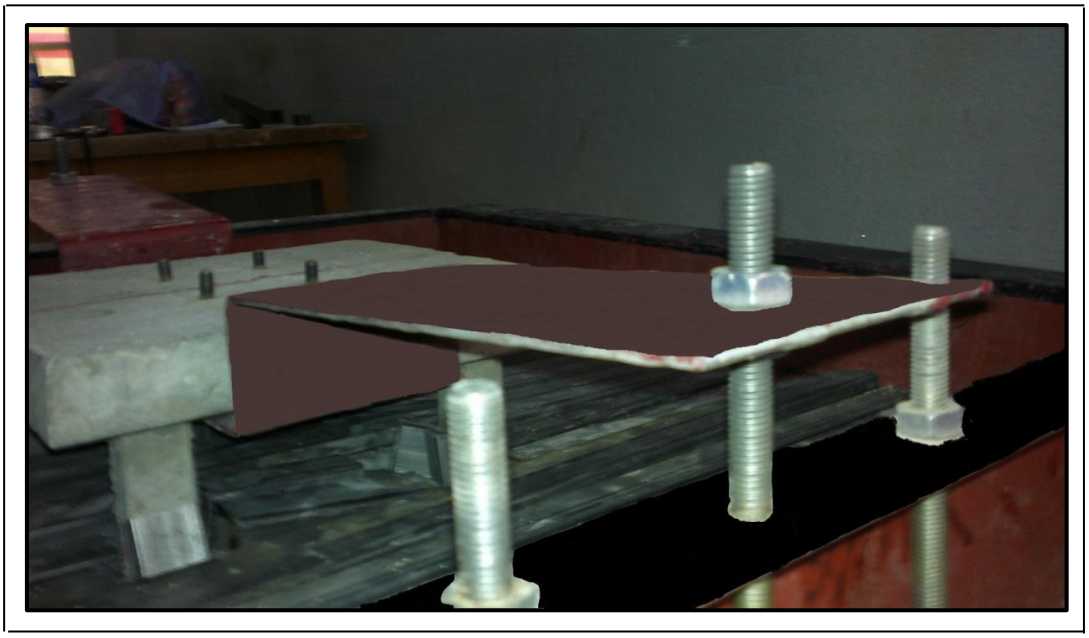

Plate 2. The pile foundation with the steel plate under the cap **.**

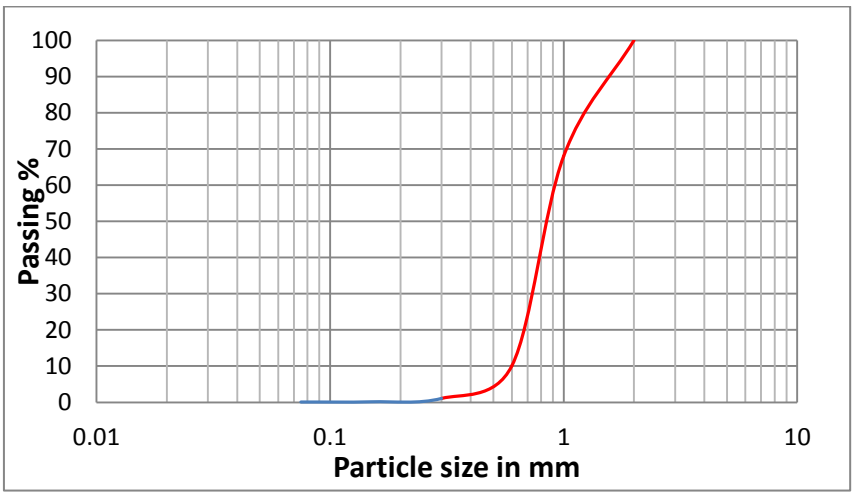

Figure 1. Particle-size distribution curve from the grain size analysis test of sand.

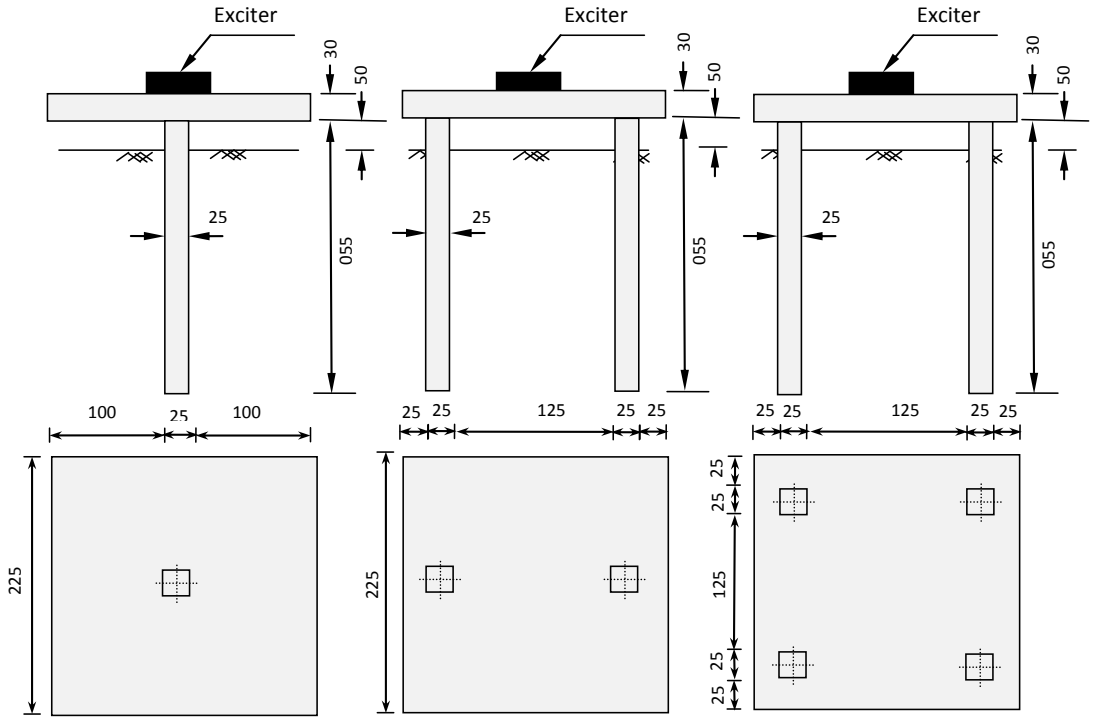

Figure 2. The layout of the deep foundation (All dimensions in mm).

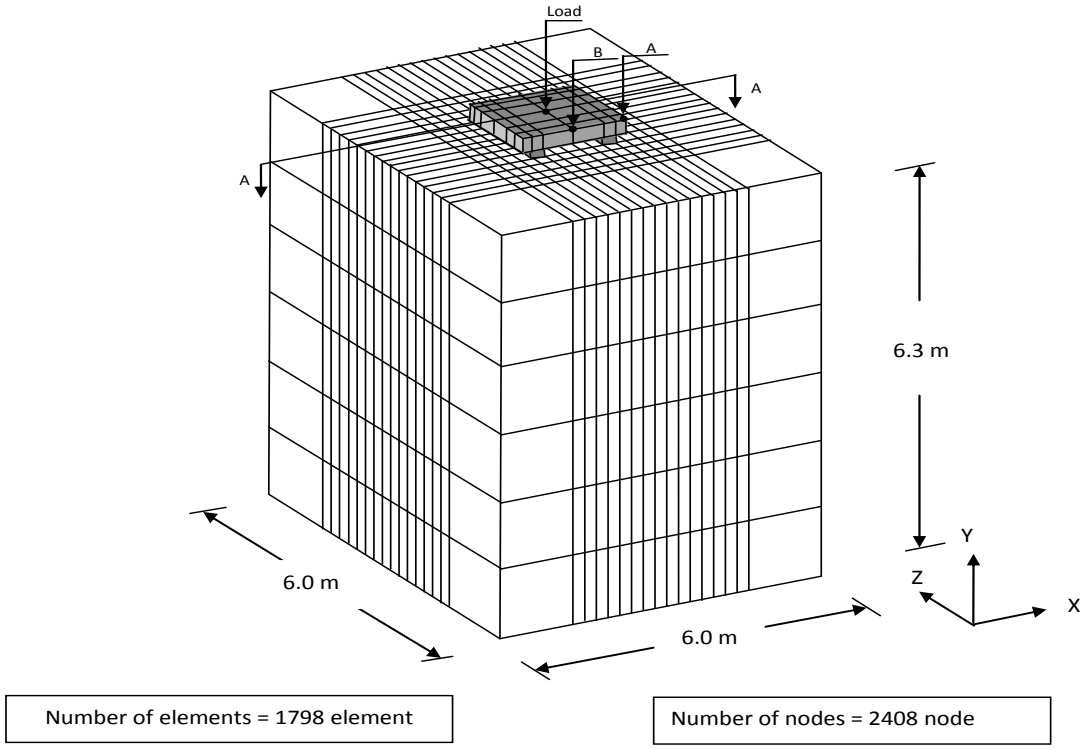

Figure 3. Three-dimensional finite element model.

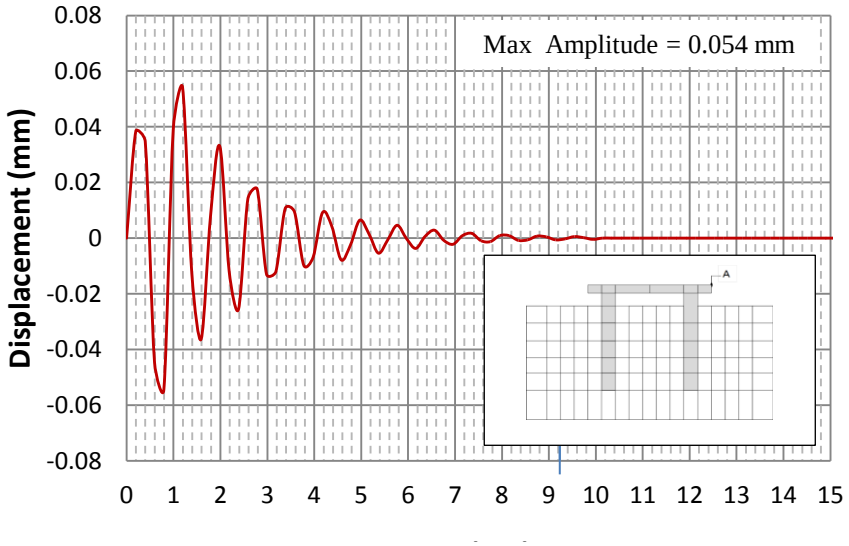

Figure 4. Displacement of foundation with group of four piles at the edge (Point A) of the numerical model (scaled frequency = 20.94 rad/sec).

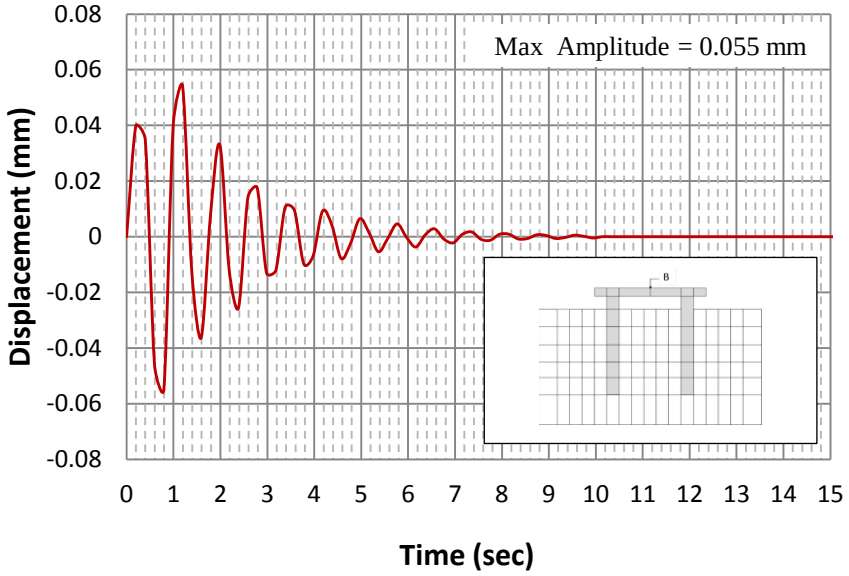

Figure 5. Displacement of foundation with group of four piles at the center (Point B) of the numerical model (scaled frequency = 20.94 rad/sec).

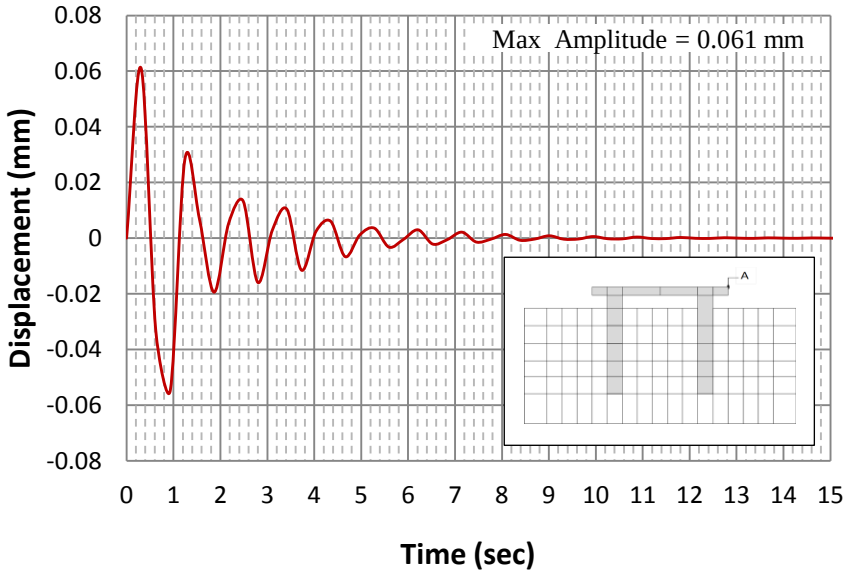

Figure 6. Displacement of foundation with group of four piles at the edge (Point A) of the numerical model (scaled frequency = 26.17 rad/sec).

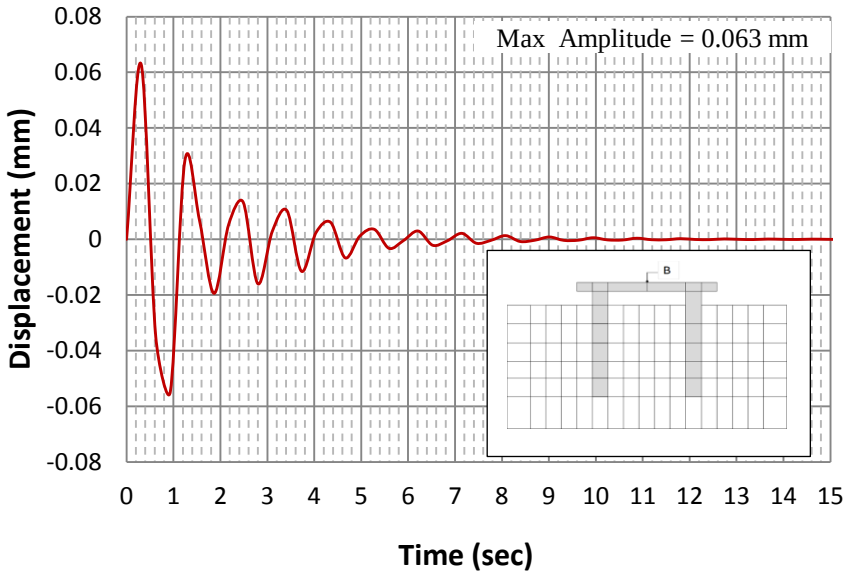

Figure 7. Displacement of foundation with group of four piles at the center (Point B) of the numerical model (scaled frequency = 26.17 rad/sec).

An Experimental Analysis of Embankment on Stone Columns

Dr. Mohammed Y.Fattah
Professor
Building and Construction Department
University of Technology
E-mail:myf_1968@yahoo.com

Dr. Bushra S.Zabar
Assistant Professor
College of Engineering
University of Baghdad
E-mail albusoda@yahoo.com

Hanan A. Hassan
Instructor
College of Engineering
University of Al-Mustansiriya
E-mail: ghassan_hanan@yahoo.com

ABSTRACT

When embankment is constructed on very soft soil, special construction methods are adopted. One of the techniques is a piled embankment. Piled (stone columns) embankments provide an economic and effective solution to the problem of constructing embankments over soft soils. This method can reduce settlements, construction time and cost. Stone columns provide an effective improvement method for soft soils under light structures such as rail or road embankments. The present work investigates the behavior of the embankment models resting on soft soil reinforced with stone columns. Model tests were performed with different spacing distances between stone columns and two lengths to diameter ratios of the stone columns, in addition to different embankment heights. A total number of 21 model tests were carried out on a soil with undrianed shear strength ≈ 10 kPa. The models consist of stone columns embankment at spacing to diameter ratio equal to 2.5, 3 and 4. Three embankment heights; 200 mm, 250 mm and 300 mm were conducted. Three earth pressure cells were used to measure directly the vertical effective stress on column at the top of the middle stone column under the center line of embankment and on the edge stone column for all models while the third cell was placed at the base of embankment between two columns to measure the vertical effective stress in reinforced soft soil directly. The embankment models constructed on soft clay treated with ordinary stone columns at spacing ratio equal 2.5 revealed maximum bearing improvement ratio equals (1.21, 1.44 and 1.7) for 200 mm, 250 mm and 300 embankment heights, respectively and maximum settlement improvement ratio equals (0.78, 0.67 and 0.56) for 200 mm, 250 mm and 300 embankment heights, respectively.

Keywords: stone columns, soft clay, embankment, laboratory models.

تحليل عملي لسدة ترابيه مستندة على أعمدة حجرية

أ.د. محمد يوسف فتاح
قسم البناء والانشاءت
الجامعة التكنولوجية

أ.م.د. بشرى سهيل زبار
قسم الهندسة المدنية
كلية الهندسة/ جامعة بغداد

م. حنان عدنان حسن
قسم الطرق والنقل
كلية الهندسة/ الجامعة المستنصيرية

الخلاصة

ان انشاء سدة على تربة طينية رخوة يحتاج الى طرق خاصة. احدى هذه الطرق هو استخدام الركائز الحجرية تحت السدة. حيث توفر هذه الطريقة حلاً اقتصادياً وفعالاً لمشاكل انشاء السدة فوق تربة طينية رخوة. تقلل هذه الطريقة الهبوط ووقت وكلفة الانشاء, تعتبر الاعمدة الحجرية طريقة تحسين فعالة تحت الاحمال الخفيفة مثل احمال السدة لسكة قطار او الطريق. اجريت هذه الدراسة على مجموعة موديلات بلغت 42 موديل تضمنت تربة طينية رخوة ذات مقاومة قص غير مبزول ≈ 10 كيلوباسكال مع اعمدة

حجرية عادية تم ترتيبها بنمط مربع الشكل مع مسافات مركزية بين عمود واخر تساوي 4 ,3 ,2.5 من قطر العمود كما تم تغيير ارتفاع السدة حيث بلغ 200ملم, 250ملم و300 ملم. وجد من دراسة موديلات لسدة مستندة على تربة طينية رخوة مثبته بأعمدة حجرية ، إن الاعمدة الحجرية المرتبه بمسافة مركزية (2.5) أظهرت أعلى نسبة تحسن في قابلية تحمل التربة حيث بلغت (1.21, 1.44و1.7) لسدة بارتفاع 200ملم, 250ملم و300 ملم. وأقل نسبة تحسن في نسبة الهبوط وبلغت (0.78, 0.67 و 0.56) لسدة بارتفاع 200ملم, 250ملم و300 ملم.

1. INTRODUCTION

The stone column method is the most effective soft soil improvement with undrained shear strength cu > 15 kN/m^2. Stone columns have higher drainage ability and stiffness than sand drains. Therefore, ground reinforcement by stone columns solves the problems of the soft soil by providing advantage of reduced settlement and accelerates consolidation process. Another advantage of this method is the simplicity of its construction. In extremely soft soil conditions, (c_u < 15 kN/m2), lateral support can be problematic for stone columns , **Kempfert, 2003.**

Stone columns provide the primary functions of reinforcement and drainage by improving the strength and deformation properties of the soft soil. Stone columns increase the unit weight of soil (due to densification of surrounding soil during construction), dissipate quickly the excess pore pressures generated and act as strong and stiff elements and carry higher shear stresses , M**adhav et. al., 1994, Yoo, 2010. Juran and Guermazi , 1988.** performed a series of special modified triaxial tests on soil reinforced with stone columns to study the effect of area replacement ratio (a_r) on the settlement reduction ratio. The results showed that the increase of replacement ratio from 0.04 to 0.16 results in a significant increase of the resistance of reinforced soil to the applied vertical load and reduce the settlement reduction ratio. **Rao et al. , 1997.** conducted a series of tests on stone columns installed in remolded soft clay with different soil consistencies (I_C) to study the effect of many parameters such as length to diameter of stone column, effect of the placement moisture content of the surrounding soil, the influence of spacing and the number of columns within the group on the ultimate bearing capacity. The study showed that the most effective length to diameter ratio was found to be ranged from 5 to 10. The consistency of soil (Ic = L.L-wn/PI) is one of the main factors that affect the load carrying capacity of the stone columns and controls the bulb formation.

Al- Shaikhly , 2000. carried out laboratory model tests to investigate the effect of grain size of backfill material, effect of length of stone columns and effect of area replacement ratio. The optimal size of backfill material for achieving the maximum value of improvement ranged from (11-14) % of the column diameter. For all types of the backfill material, the bearing ratio increased with increasing both the area ratio (a_r) and the length to diameter of the columns ratio (L/d).

Al-Qayssi , 2001. conducted model tests to improve the behavior of stone columns by using different patterns of reinforcement consisting of two and three discs connected to a central shaft. Influence of spacing between stone columns, effect of footing shape, effect of area replacement ratio and number of stone columns on ultimate bearing capacity was studied. The circular footing demonstrated a higher bearing ratio at failure followed by the square then by the rectangular model footings. The bearing ratio increased with increasing spacing from 2d, 2.5d and 3d c/c for all the three shapes of model footings. The area replacement ratio showed an insignificant influence on the efficiencies of the single stone column. Increasing number of stone columns caused a delay in the development of the bulging shape and hence improves the granular behavior. The bearing ratios for two and three discs giving an increase of 12% and 40% respectively over the single unreinforced stone columns.

Al-Waily , 2008. and Fattah et al. 2011. conducted a testing program to study the influence of stone column number (single, two, three, and four stone columns) , L/d ratio and undrained shear strength of bed soil on the stress concentration ratio and the bearing improvement ratio ($q_{treared}/q_{untreated}$) of stone columns. The experimental tests showed that the stone columns with L/d=8 provided a stress concentration ratio n of 1.4, 2.4, 2.7, and 3.1 for the soil having a shear strength cu=6 kPa, treated with single, two, three, and four columns, respectively. The values of n were decreased to 1.2, 2.2, 2.5, and 2.8 when the L/d=6. The values of n increase when the shear strength of the treated soil was increased to 9 and 12 kPa. The value of the bearing improvement ratio decreases with increasing the shear strength of the treated soil.

2. EXPERIMENTAL WORK

2.1 Soil Used

A brown clayey silt soil was brought from a depth of 5 m from the site of a bridge in the sport city within Al-Basrah government. The soil was subjected to routine laboratory tests to determine its properties, these tests include: grain size distribution (sieve analysis and hydrometer tests) according ASTM D422 specifications, Atterberg limits (liquid and plastic limits) according to ASTM D4318 and specific gravity according to ASTM D854 specifications. The results show that the soil consists of 6% sand, 46% clay and 48% silt as shown in **Fig. 1**. The soil is classified according to the Unified Soil Classification System USCS as (CL). **Table 1** shows the physical and chemical properties of the soil used.

2.2 Crushed Stone

The crushed stone, used as a backfill material was obtained from a private mosaic factory. The size of the crushed stone was chosen in accordance with the guidelines suggested by **Al-Shaikhly 2000,** where the particle size is about 1/7 to 1/9 of the diameter of stone columns. The particle size distribution is shown in **Fig. 2**, the particle sizes range between 2 to14 mm and found to have Ø value of 41.5º from direct shear test at a dry unit weight of 14.4 kN/m^3 corresponding to a relative density of 55%. The stone is uniform as its uniformity coefficient is less than 4 and considered as poorly graded. The physical properties are presented in **Table 2**.

2.3 Sub-base (Embankment Fill Material)

The granular sub-base was brought from Al-Nibaee quarry, north of Baghdad. The sub-base is commonly used as a fill material for embankment construction. **Fig. 3** shows the grain size distribution of sub-base according to (B.S.1377:1990, Test 7B). The physical and chemical properties of the sub-base used are shown in **Table 3**. The sub-base is classified as class (B) according to the **Iraqi SORB ,2003.** and as (GW) according to USCS.

3. MODEL DESIGN AND MANUFACTURING

To study the behavior of soft clay reinforced by ordinary stone columns underneath embankment; an experimental setup with an approximate scale of 1/20 to 1/30 of the prototype was designed and manufactured to achieve this goal. The setup consists of: steel container, loading frame, hydraulic system, load cell with load indicator, earth pressure cell, piezometer, strain gauge with strain indicator, footing model, dial gauges and data acquisition.

3.1 The Test Setup

***Steel container*:** A movable steel container was constructed to host the bed of soil and all accessories. The internal dimensions are 1500 mm length, 800 mm width and 1000 mm depth. The container was made of steel plates 6 mm in thickness braced externally by angles at their corners, edges and each side. The front side was made from tough glass. The container was provided with four wheels that allow it to move freely, the container is sufficiently rigid and exhibited no lateral deformation during preparation of soil and during the test. **Plate 1** shows details of the container.

Loading frame and axial loading system: The steel frame consists of two columns and a beam, each column is fixed at bottom by casting in a concrete slab. The axial pressure is applied through a hydraulic system which consists of three hydraulic jacks; one in the middle and the others on sides, used to apply the load on the embankment model, the location of the hydraulic jack is shown in **Plate 1**. The maximum stress that can be applied on a model footing (250 mm ×500 mm) reaches about 400 kPa. The pressure is measured by a load cell 50 kN in capacity connected to the digital load indicator as shown in **Plate 2**.

Earth pressure cell and readout: Earth pressure cells provide a direct means of measuring total pressure in or on bridge abutments, diaphragm walls, fills and embankments, retaining walls surfaces, sheet piling, slurry walls and tunnel lining. They may also be used to measure earth bearing pressure on foundation slabs and footings and at the tips of piles. **Plate 3** shows the earth pressure cell model 4800 manufactured by GEOKON company in U.S.A which is used in this study. Earth pressure cells are constructed from two thin stainless steel plates welded together around their periphery and separated by a narrow gap filled with hydraulic fluid. A length of stainless steel tubing connects the fluid filled cavity to a pressure transducer that converts the fluid pressure into an electrical signal transmitted by cable to the readout. They can be positioned in the fill at different orientations so that soil pressure can be measured in two or three directions. The vibrating wire readout box model GK404 manufactured by GEOKON company in U.S.A, used with earth pressure cell and piezometer, is portable, low-power, hand-held that is capable of running for more than 20 hours continuously. It is designed for the readout all GEOKON vibrating wire gages and transducers. **Plate 4** shows the readout device. The model GK404 provides 6 excitation positions (A-F) with display resolution of 0.1 digits. It is displaying the reading of one connector so that a suitable selector was manufactured to read all the instruments at the same time.

3.2 Preparation of Model Tests

3.2.1 Preparation of soil

Prior to the preparation of the soil bed in the container, the variation of shear strength of the clayey soil versus time after mixing at different liquidity indices should be obtained. Therefore; six samples with different liquidity indices were prepared individually; each sample was placed in five layers inside a CBR mould. Each layer was tamped gently with a special hammer to extract any entrapped air. The samples were then covered with polythen sheet and left for a period of eight days. Each day, the undrained shear strength was measured by a portable vane shear device, **Plate 5**. These tests provide the time required for the remolded soil to regain strength after a rest period following the mixing process, **Fig. 4**. The shear strength of soil decreases with the value of liquidity index and the influence of time decreases with liquidity index, **Fig. 5** shows the variation of shear strength of soil with liquidity indices after 96 hour curing.

According to the results obtained from **Fig. 5**, the soil was prepared in the manufactured container at undrained shear strength cu of 10 kPa and liquidity index of (0.48) corresponding to water content

of (34.5%). To perform soil preparation, 660 kg of air dried soil was divided into 30 kg groups; each group was mixed separately with enough quantity of water to get the desired consistency. The mixing operation was conducted using a large mixer manufactured for this purpose till completing the whole quantity. After thorough mixing, the wet soil was kept inside tightened polythen bags for a period of one day to get uniform moisture content. After that, the soil was placed in a steel container (1500×800×1000) mm in eleven layers; each layer was leveled gently using a wooden tamper of dimensions (50×100) mm. This process continues for the eleven layers till reaching a thickness of 560 mm of soil in the steel container. After completing the final layer, the top surface was scraped and leveled to get, as near as possible, a flat surface, then covered with polythen sheet to prevent any loss of moisture as shown in **Plate 6**. A wooden board of area similar to that of the soil surface area (1500× 800) mm was placed on the soil bed. The prepared soil was left for a period of four days to regain its strength reaching (10 kPa) as was suggested by , **Fattah et al. 2011.**

3.2.2 Installation of the stone columns

The position of the stone columns to be placed correctly in their proper locations was marked using a special frame manufactured according to the proposed configuration patterns of stone columns. A hollow steel pipe with external diameter of 70 mm coated with petroleum jelly was pushed down the bed to the specific depth (560 mm in fully penetrated stone column with L/d=8 and 350 mm for partially penetrated stone column with L/d=5) with the aid of the loading system. **Plate 7** shows process of the installation of the stone column. To remove the soil inside the casing, a hand auger, manufactured for this purpose was used. After that, the casing was removed carefully. The stones were carefully charged into the hole in ten layers and compacted at relative density of 55% using 50 mm diameter rod to achieve a dry unit weight of 14.4 kN/m^3 by a tamping rod. Spacing between stone columns for each configuration pattern is shown in **Plate 8**.

3.2.3 Installation of embankment fills

The construction of the embankment fill was started after installation of ordinary stone columns. A predetermined weight of sub-base was mixed with water by a mixer at optimum moisture content of 6.3%, this weight of sub-base is sufficient to create a uniform layer 50 mm thick. Each layer was compacted gently by a wooden tamper of size 75×75 mm to attain a placement maximum dry unit weight of 21.84 kN/m^3 until the desired embankment depth is obtained. Then the top layer was leveled using a piece of plywood. The final upper width of the embankment is 300 mm. **Plate 9** shows the process of preparation of the embankment.

3.2.4 Model testing procedure

The model tests were carried out on natural soil and soil improved with stone columns. The load cell and load readout used in testing program were calibrated by applying different known static loads and measuring values through the load cell before using. A footing (250 mm×600 mm) in dimensions was placed in position on the surface of the embankment model so that the center of the footing coincides with the center of the load cell and hydraulic jack. Two dial gauges with accuracy of (0.01 mm/division) were fixed in position to measure the settlements of plate and one dial gauge was placed in the toe of embankment to measure the soil heave as shown in **Plate 10**. Loads were then applied through a hydraulic jack in the form of load increments and measured by the load cell and recorded by load readout. During each load increment, the readings of the three dial gauges were recorded. The dial gauge readings were recorded at the end of the period of each load increment. Each load increment was left for (5 minutes) or till the rate of settlement became constant. **Plate 11** presents the tested models after completion of the tests.

4. PRESENTATION AND DISCUSSION OF TEST RESULTS

The investigation focuses on influence of parameters like, spacing of stone columns, length of stone column and height of embankment on overall behavior of soft soil treated by stone columns. The analysis of results of all model tests regarding the applied stress and the corresponding settlement is illustrated in terms of (q/c_u) vs (S/B). The (q/c_u) represents the ratio of applied stress to undrained shear strength of the soft clay, denoted as "bearing ratio" and (S/B) represents the corresponding vertical settlement as a percent of the model footing width, denoted as "settlement ratio". To obtain the degree of improvement achieved by each improvement technique, the results are plotted in the form of $(q/c_u)_t$ /($q/c_u)_{unt}$ denoted as "bearing improvement ratio", where $(q/c_u)_t$ is improved bearing ratio and $(q/c_u)_{unt}$ is unimproved bearing ratio.

The improvement in settlement achieved by the model tests is presented in the form of (S_t/S_{unt}) "settlement of treated soil to settlement of untreated soil at the same applied stress" denoted as "settlement improvement ratio", plotted against the bearing ratio (q/c_u).

4.1 Definition of Failure

The failure point is defined when the settlement reaches 36% of the diameter of the stone column or 10% of the width of the model footing. This definition is compatible with **Terzaghi,1947**, **Hughes and Withers,1974, Al-Mosawe et al., 1985 , and Fattah et al. 2011.**

4.1.1 Model tests on untreated embankment

Three model tests were conducted on beds of untreated soil with undrained shear strengths of 10 kPa at different embankment heights (200 mm, 250 mm and 300 mm). These tests are considered as reference to obtain the degree of improvement gained after introducing any other type of improvement technique.

Fig. 6 shows the relationship between the pressure (q) and the surface settlement of embankment (S) for model test, the figure illustrates that the mode of failure of model test is close to local shear pattern, due to the rapid rate of deformation. In this test, the footing model is resting on compacted layer (sub-base) of width relatively ≈ the footing width. The ultimate bearing capacity obtained is 35 kPa, 33 kPa and 30 kPa for the model tests of embankment height 200 mm, 250 mm and 300 mm respectively based on the failure criterion of (10% of footing width). **Fig. 7** shows the bearing ratio plotted against settlement ratio. The figure demonstrates that the soil bed underneath the 200 mm embankment height exhibited higher bearing ratio. The bearing ratios at failure (q/c_u) for the embankment- soft soil model are 3.5, 3.3 and 3.0 corresponding to the settlement ratio of 10% of the footing width and for embankment heights 200, 250 and 300 mm respectively. The results demonstrate a substantial decrease in bearing ratio with increasing thickness of embankment; this is due to the increase in the settlement induced by the load from embankment and applied stress.

4.1.2 Model tests of embankment treated with stone columns

Bearing capacity: This series consists of eighteen model tests performed with 200, 250 and 300 mm embankment overlying soft clay and immediately underneath the model footing. **Figs. 8** to **10** show the relationship between pressure and embankment surface settlement. The results show increase in the surface settlement with increasing spacing of columns for applied pressure. The maximum bearing capacity of soil was observed for soft soil improved with stone columns at (s/d =2.5) and the minimum bearing capacity was for soft soil improved with stone columns at (s/d =4). This may be

explained by the reduction in area ratio from 12.53 % to 4.89 %. Similar conclusions were obtained by **Han and Gabr ,2002, and Murugesan and Rajagopal ,2006.** In addition, it can be noticed that a higher embankment height resting on stone columns would result in a higher bearing pressure. Heave at the end of embankment versus horizontal distance from center line of embankment for different spacing and two L/d ratios are shown in **Figs. 11 to 14**.

Bearing ratio verses settlement ratio: The variation of bearing ratio (q/c_u) versus settlement ratio (S/B) is shown in **Figs. 15 to 17**. The results show the effect of ordinary stone columns on bearing ratio of soil. The spacing ratio (s/d =2.5), demonstrates higher bearing ratio at failure, as compared with spacing ratio (s/d = 4). Such behavior may be explained due to the confinement effect provided by the surrounding soil and the adjacent stone columns. As spacing ratio decreased, the confinement stress provided by the surrounding soil increases. Since the stone columns are stiffer than the surrounding soil, the stress concentration on the stone columns increases with decreasing the spacing of stone and embankment height due to soil arching. The values of bearing ratio at failure are summarized in **Table 4**. The present results are in agreement with the results obtanied by **Juran and Guermazi ,1988, Craig and Al-Kahafaji ,1997, Rahil ,2007, Al-Waily ,2008 and Fattah et al. 2011.**

Bearing improvement ratio verses settlement ratio: To evaluate the amount of improvement achieved by the ordinary stone column for different spacings over untreated soil, the bearing improvement ratio (q_t/q_{unt}) versus settlement ratio S/B% is presented in **Figs. 18 to 20**. Peak values of improvement ratio are observed at nearly S/B about 2% to 4% then drops down and decreased with increasing settlement ratio. This behavior is attributed to the load transfer mechanism, the stress is transferred to the stone columns expressing these peak values then it is gradually transferred to the surrounding soil implied by the drop in the improvement ratio. Also, it can be noticed that the stone columns with spacing ratio (s/d= 2.5) has higher improvement ratio for different embankment heights, which is attributed to the increase in area replacement. **Table 5** summarizes the values of bearing improvement ratio at failure.

Settlement improvement ratio versus bearing ratio: Variation of settlement improvement ratio (S_t/S_{unt}) versus bearing ratio (q/c_u) for different column spacings and embankment heights is shown in **Figs. 21 to 23**.The results imply a decrease in settlement improvement ratio as the bearing ratio increases until reaching (q/c_u) equals 1.48 to 2.8, then a gradual increase in settlement improvement ratio takes place, the decrease in settlement improvement ratio shows the level of improvement. This behavior may be attributed to the fact that the decrease in settlement improvement ratio to about (q/c_u) equals 1.48 to 2.8 associated by the increase in bearing ratio and beyond these values, the excess bulging leads to decrease in load carrying capacity. Also the lower improvement values (high degree of improvement) are observed when the embankment model is treated by ordinary stone columns at (s/d = 2.5) compared with the model at (s/d= 4) that revealed a high value of settlement improvement ratio for different heights of embankment. Settlement improvement ratio at failure is summarized in **Table 6**. The results are in agreement with the results of Craig and **Al-Kahafaji 1997, Rahil, 2007, Al-Waily, 2008, and Fattah et al. ,2011.**

Stress on column versus settlement: The vertical effective stress on column was measured at the top of the middle stone column under the center line of embankment and on the edge stone column using earth pressure cell for all models. The stress-settlement behavior of the stone columns for all spacing ratios is the same as shown in **Figs. 24 to 26**. The bearing capacity of the stone columns at failure

corresponding to settlement ratio of 10% increases with decreasing spacing distance between the columns, as shown in **Table 7**. These results agree with **Hewlett** and **Randolph, 1988, Low et al., 1994, Chen et al., 2007, Britton and Naughton, 2008 and Ellis and Aslam, 2009,** who measured the stress using different experimental models for piled embnkment.

The highest vertical effective stress is obtained in case of the least spacing (s/d = 2.5) is used under the embankment of height 300 mm. This phenomenon is due to the stress concentration occurring between the adjacent columns as well as due to the confinement effect provided by the surrounding soil and the adjacent stone columns therefore, the stress concentration on the stone columns increases with decreasing the spacing of columns. The decrease in vertical effective stress on the stone column as the spacing increases is due to the yielding of the stone column. Once yielded, the stiffness of the column decreases, its radial deformability increases due to dilitancy. Otherwise, the yielding of the column reduces the transfer of vertical load from the soil.

Stress on soft soil versus settlement: The vertical effective stress (σ'_{vc}) in reinforced soft soil was measured at the base of embankment between two columns using earth pressure cells. The relationship of the vertical effective stress with surface settlement of embankment is shown in **Figs. 27 to 29**. The vertical effective stress in the reinforced soft soil increases at a high rate with increasing spacing between stone columns and decreasing embankment fill height. This may be due to the excess bulging that occurs in the stone column which leads to decrease in load carrying capacity. Directly after the embankment construction stages have been finished, the vertical stress in the reinforced soft soil increases at a very small rate, and as stone columns spacing decreases, the vertical stress in the reinforced soil decreases and high stress values are generated in the stone column. This is due to the stress transfer from the soft soil and concentration of the stress in the stone column (soil arching phenomenon). **Table 8** summarizes the values of vertical effective stress on soft soil at failure corresponding to settlement ratio of 10%. These results agree with **Hewlett** and **Randolph, 1988, Low et al., 1994, Chen et al., 2008, Britton and Naughton, 2008, and Ellis and Aslam, 2009,** who measured the stress using different experimental models for piled embankment.

5. CONCLUSIONS

The following points are drawn from the test results:

1. The mode of failure for embankment model resting on untreated very soft clay with cu ≈ 10 kPa is close to local shear failure and the mode gradually changes toward the general shear with using stone columns.
2. The bearing ratio increases with decreasing spacing distance between the stone columns at any embankment height. The rate of increasing in bearing ratio of treated models was found to be within the range (1.08 to 1.2); (1.23 to 1.42) and (1.37 to 1.65) of untreated models for embankment model height of 200 mm, 250 mm and 300 mm, respectively.

3. The bearing improvement ratio increases with decreasing spacing ratio of stone column for given embankment. Higher improvement ratio was achieved for the models treated with stone columns at S=2.5d at any embankment high. The higher values of (q_t / q_{unt}) was found to be (1.21, 1.44 and 1.7) for embankment model of height 200 mm, 250 mm and 300 mm, respectively while lowest improvement was observed at spacing s = 4d especially for embankment height 200 mm.

4. The improvement in settlement ratio increases as the spacing ratio of stone columns increases. The lowest value of settlement improvement ratio at failure was observed at s=2.5d for a given embankment height, which represents higher degree of improvement.

6. REFERENCES

Al-Mosawe, M.J., Abbass, A.J. and Majeed, A.H. ,1985, *Prediction of Ultimate Capacity of a Single and Groups of Stone Columns*, Iraqi Conference on Engineering ICE 85, Vol.1, Baghdad.

Al-Qayssi, M.R. ,2001, *Unreinforced and Reinforced Behavior of Single and Groups of Granular Piles,* Ph.D. Thesis, Civil Engineering Department, Faculty of the Military College of Engineering, Iraq.

Al-Shaikhly, A.A. 2000, *Effect of Stone Grain Size on the Behavior of Stone Column*, M.Sc. Thesis, Building and Construction Engineering Department, University of Technology, Iraq.

Al-Waily, M. J. , 2008, *Stress Concentration Ratio of Model Stone Columns Improved by Additives*, Ph.D. Thesis, Building and Construction Engineering Department, University of Technology, Iraq.

ASTM, D422 2003, *Standard Test Method for Particle-Size Analysis of Soils* Soil and Rock (I), Vol. 04.08.

ASTM, D854 2003, *Standard Test Method for Specific Gravity of Soil Solids by Water Pycnometer*, Soil and Rock (I), Vol. 04.08.

ASTM, D4318 ,2003, *Standard Test Method for Liquid Limit, Plastic Limit, and Plasticity Index of Soils*, Soil and Rock (I), Vol. 04.08.

British Standard B.S.:1377 part 2 ,1990, *Methods of Test for Soils for Civil Engineering Purposes General Requirements and Sample Preparation*, British Standard Institution, London.

Britton, E. and Naughton, P. ,2008, *An Experimental Investigation of Arching in Piled Embankments*, Proceedings of the 4th European Geosynthetics Conference, Edinburgh, UK, September 2008, No. 106, pp. 1-8

Chen, Y.M., Cao, W.P. and Chen, R.P. , 2007, *An Experimental Investigation of Soil Arching within Basal Reinforced and Unreinforced Piled Embankments* Geotextiles and Geomembranes, Vol. 26, pp. 164-174.

Cragi, W.H. and Al-Khafaji, Z.A. , 1997, *Reduction of Soft Clay Settlement by Compacted Sand Piles*, Proceeding of the 3rd International Conference of Ground Improvement, London, pp.218-224.

Chen, R.P., Chen, Y.M., Han, J. and Xu, Z.Z. 2008, *A Theoretical Solution for Pile – Supported Embankments on Soft Soils under One Dimensional Compression*, Canadian Geotechnical Journal, Vol. 45, No. 5, pp. 611-623.

Ellis, E.A. and Aslam, R. , 2009, *Arching in Piled Embankments: Comparison of Centrifuge Tests and Predictive Methods* – Part 1 of 2. Ground Engineering, pp. 34-38.

Fattah, M. Y, Shlash, K. T., and Al-Waily, M.J. 2011, *Stress Concentration Ratio of Model Stone Columns in Soft Clays*, Geotechnical Testing Journal, Vol. 34, No. 1, pp. 61-71.

Han, J. and Gabr, M.A. 2002, *Numerical Analysis of Geosynthetic Reinforced and Pile-Supported Earth Platforms over Soft Soil*, Journal of Geotechnical and Geoenvironmental Engineering, pp. 44-53.

1Hewlett, W.J. and Randolph, M.F. 1988, *Analysis of Piled Embankments*, Ground Engineering, Vol. 21, No. 3, pp. 12-18.

Hughes, J.M.O. and Withers, N.J. 1974, *Reinforcing of Soft Cohesive Soils with Stone Columns*, Ground Engineering Journal, Vol. 7, No. 3, pp. 42-49.
Juran, I. and Guermazi, A. 1988, *Settlement Response of Soft Soil Reinforced by Compacted Sand Columns*, Journal of Geotechnical Engineering, ASCE, Vol.114, No.8, pp.930-943.
Kempfert, H.G. ,2003, *Ground Improvement Methods with Special Emphasis on Column-Type Techniques*, Int. Workshop on Geotechnics of Soft Soils-Theory and Practice. Vermeer, Schweiger, Karstunen & Cudny (eds.).
Low, B.K., Tang, S.K. and Choa, V. ,1994, *Arching in Piled Embankments*, Journal of Geotechnical Engineering, ASCE, Vol. 120, No. 11, pp. 1917-1938.
Madhav, M.R., Alamgir, M. and Miura, N. 1994, *Improving Granular Column Capacity by Geogrid Reinforcement*, Proceedings of the 5th International Conference on Geotextiles, Geomembranes and Related Products, Vol. 1, Singapore, pp. 351-356.
Murugesan, S. and Rajagopal, K. 2006, *Geosynthetic-Encased Stone Columns: Numerical Evaluation*, Geotextiles and Geomembranes, Vol. 24, No.6, pp. 349–358.
Rahil, F.H. 2007, *Improvement of Soft Clay Underneath a Railway Track Model using Stone Columns Technique*, Ph.D. Thesis, Building and Construction Engineering Department, University of Technology, Iraq.
Rao, S.N., Reddy, K.M. and Kummar, P.H. ,1997, *Studies on Group of Stone Columns in Soft Clays.*, Journal of Geotechnical Engineering, Southeast Asian, Vol. 28, No. 2, Dec., pp.165-181.
Yoo C. 2010, *Performance of Geosynthetic-Encased Stone Columns in Embankment Construction: Numerical Investigation*, Journal of Geotechnical and Geoenvironmental Engineering, ASCE, Vol. 136, No. 8, pp. 1148-1160.

Table 1. Physical and chemical properties of natural soil used.

Property	Value
Liquid limit (LL) %	47
Plastic limit (PL) %	23
Plasticity index (PI) %	24
Specific gravity (G_s)	2.7
% Passing sieve No. 200	94
Sand content % (0.075 to 4.75 mm)	6
Silt content % (0.005 to 0.075 mm)	48
Clay content % (< 0.005 mm)	46
Maximum dry unit weight (kN/m^3)	18.24
Optimum moisture content (%)	13
Soil symbol according to USCS	CL
Total soluble salts (%)	6.13
SO_3 (%)	0.6
Organic matter (%)	1.09
Gypsum content (%)	1.17
pH	8.34

Table 2: Physical properties of the crushed stone.

Property	Value
Maximum dry unit weight (kN/m^3)	15.7
Minimum dry unit weight (kN/m^3)	13
Dry unit weight (kN/m^3) at	
Dr =55%	14.4
D_{10} (mm)	3.8
D_{30} (mm)	6
D_{60} (mm)	7.5
Coefficient of uniformity (C_u)	1.97
Coefficient of curvature (C_c)	1.26
Angle of internal friction ($Ø^o$)	41.5
Specific gravity (G_s)	2.65

Table 3: Physical and chemical properties of the sub-base material used.

Property	Value
CBR (%)	51
Maximum dry unit weight (kN/m^3)	21.84
Optimum moisture content (%)	6.3
D_{10} (mm)	0.15
D_{30} (mm)	1.5
D_{60} (mm)	12
Coefficient of uniformity (C_u)	80
Coefficient of curvature (C_c)	1.25
Angle of internal friction ($Ø^o$)	40
SO_3 (%)	0.23
Total soluble salts (%)	2.93
Gypsum content (%)	0.494
Organic matter (%)	0.057

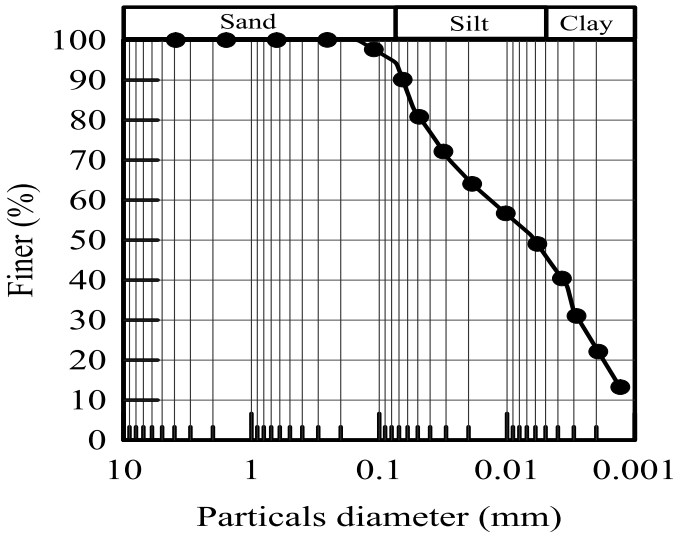

Figure 1. Grain size distribution of clayey soil used.

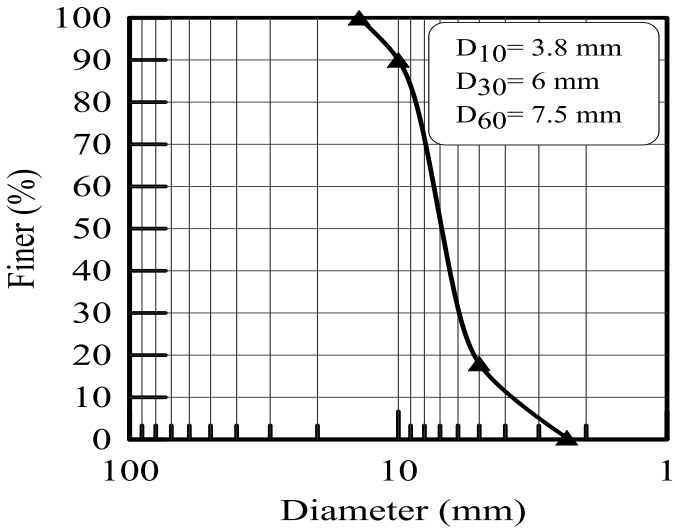

Figure 2. Grain size distribution of stone used.

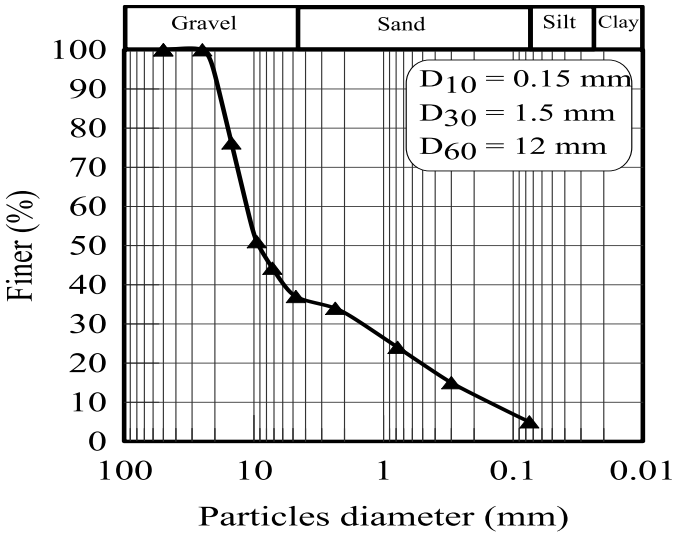

Figure 3. Grain size distribution sub-base material used.

Plate 1. Experimental test container and loading system.

Plate 2. Load cell and load readout.

Plate 3. Earth pressure cell model 4800.

Plate 4. Readout of pressure cell.

Plate 5. Portable vane shear device.

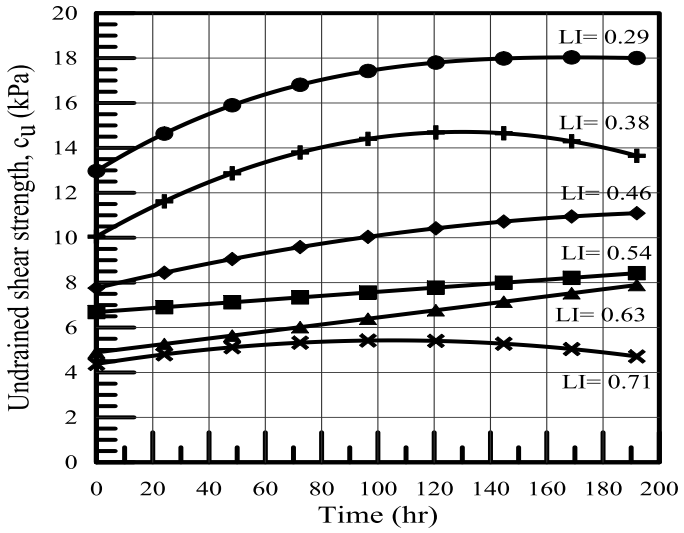

Figure 4. Variation of undrained shear strength with time after mixing.

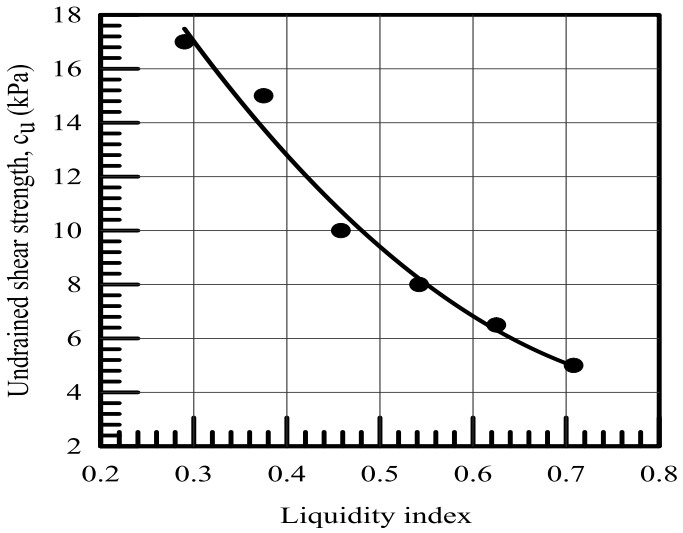

Figure 5. Variation of the undraied shear strength with liquidity index.

Plate 6. Soil preparation inside the manufactured container.

Plate 7. The process of stone column installation.

Plate 8. Configuration of patterns of stone columns, S= 3d.

Plate 9. Installation of embankment fill.

Plate 10. Model testing procedure.

Plate 11. Stone columns failure (S=3d, L/d=8).

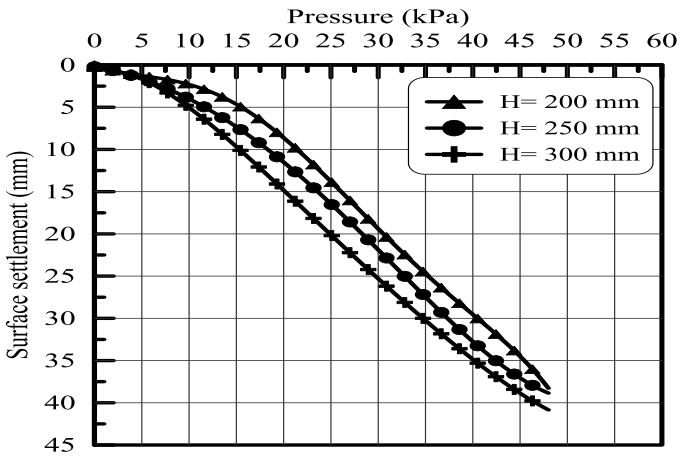

Figure 6. Bearing pressure versus surface settlement for untreated embankment model.

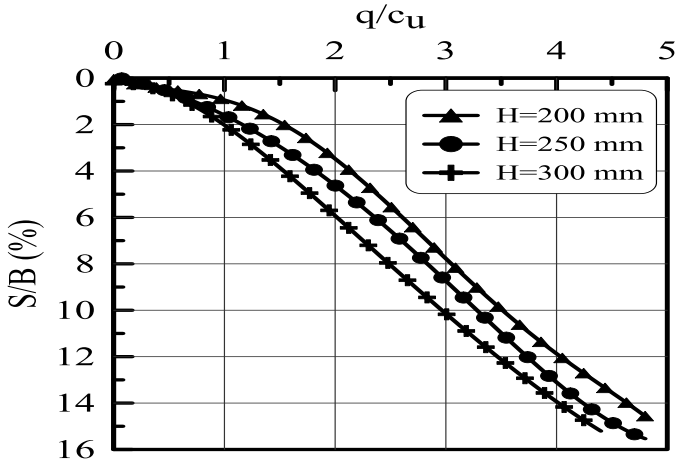

Figure 7. Bearing ratio versus settlement ratio for untreated embankment model.

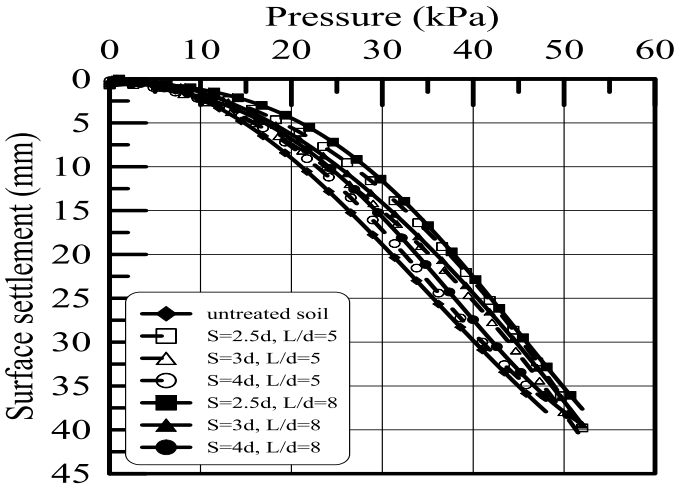

Figure 8. Bearing pressure versus settlement for embankment model 200 mm high resting on soft soil treated by stone columns.

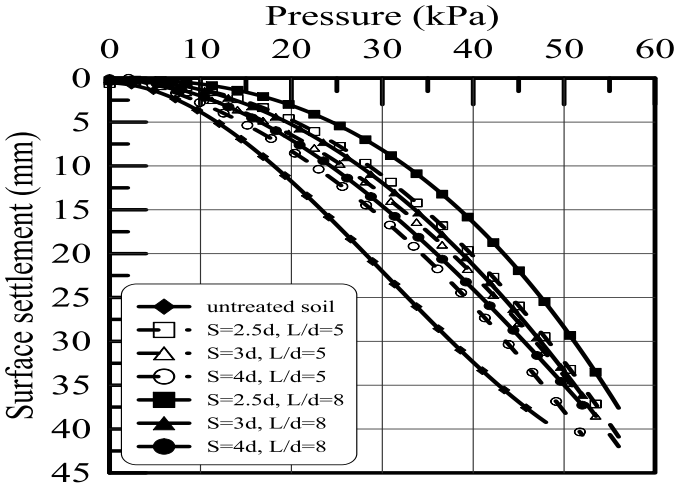

Figure 9. Bearing pressure versus settlement for embankment model 250 mm high resting on soft soil treated by stone columns.

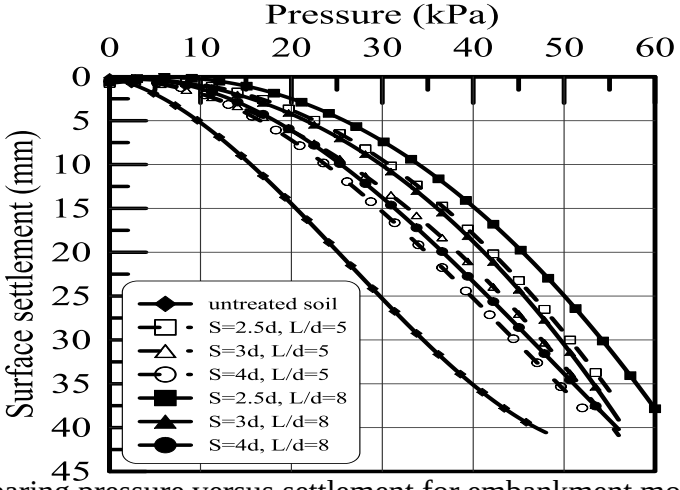

Figure 10: Bearing pressure versus settlement for embankment model 300 mm high resting on soft soil treated by stone columns.

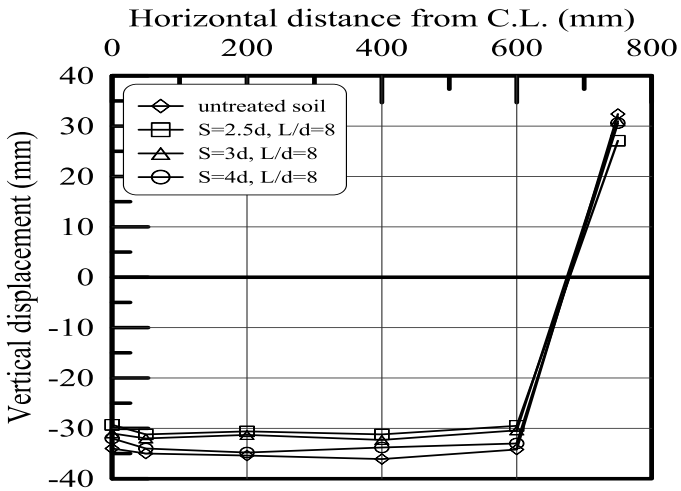

Figure 11. Settlement distribution at the base of embankment model 200 mm high constructed on soft soil treated by stone columns and L/d = 8.

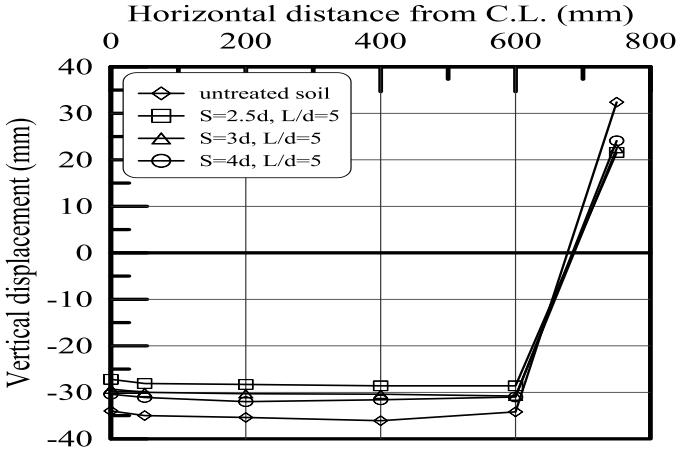

Figures 12. Settlement distribution at the base of embankment model 200 mm high constructed on soft soil treated by stone columns and L/d = 5.

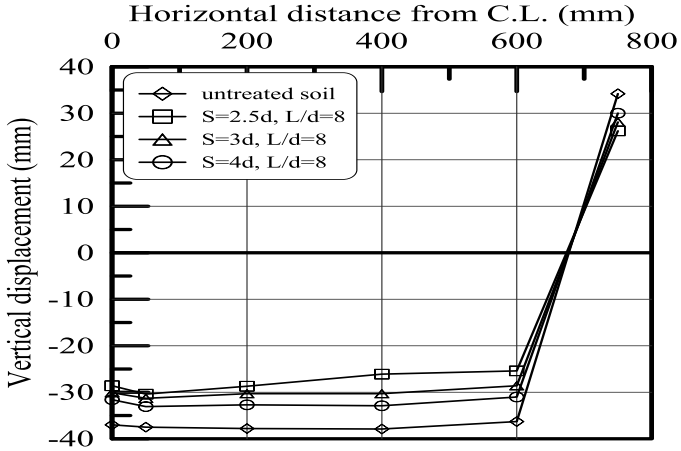

Figures 13. Settlement distribution at the base of embankment model 300 mm high constructed on soft soil treated by stone columns and L/d = 8.

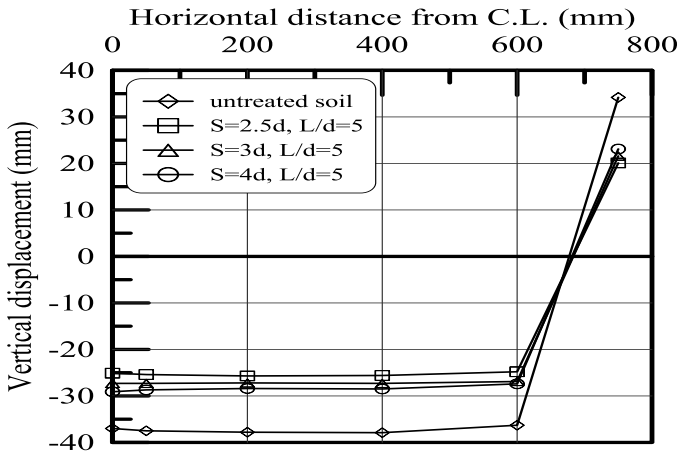

Figures 14. Settlement distribution at the base of embankment model 300 mm high constructed on soft soil treated by stone columns (OSC) and L/d = 5.

Table 4. Bearing ratio at failure for embankment model constructed on soft clay treated by stone columns.

Spacing	Bearing ratio, q/c_u					
	H=200 mm		H=250 mm		H=300 mm	
L/d ratio	5	8	5	8	5	8
Untreated soil	3.5		3.3		3.0	
S= 2.5d	4.1	4.2	4.3	4.7	4.6	5.0
S= 3d	3.9	4.0	4.2	4.3	4.3	4.5
S= 4d	3.65	3.8	3.8	4.05	4.0	4.1

Table 5. Bearing improvement ratio at failure for embankment models constructed on soft clay treated by stone columns.

Spacing	Bearing improvement ratio, q_t/q_{unt}					
	H=200 mm		H=250 mm		H=300 mm	
L/d ratio	5	8	5	8	5	8
S= 2.5d	1.2	1.21	1.38	1.43	1.63	1.7
S= 3d	1.11	1.15	1.30	1.36	1.42	1.55
S= 4d	1.06	1.09	1.20	1.23	1.35	1.43

Table 6. Settlement improvement ratio at failure for embankment models constructed on soft clay treated by stone columns.

Spacing	Settlement improvement ratio, S_t/S_{unt}					
	H=200 mm		H=250 mm		H=300 mm	
L/d ratio	5	8	5	8	5	8
S= 2.5d	0.88	0.78	0.72	0.67	0.61	0.56
S= 3d	0.89	0.81	0.78	0.70	0.70	0.62
S= 4d	0.96	0.91	0.88	0.72	0.74	0.70

Table 7. Vertical effective stress on stone column at failure for embankment models constructed on soft clay treated by 7stone columns.

Spacing	Stress on column (kPa)					
	H=200 mm		H=250 mm		H=300 mm	
L/d	5	8	5	8	5	8
S= 2.5d	16	18.8	23.6	31	25	36
S= 3d	15	17	19.8	23.6	22.8	31
S= 4d	11.6	13.3	14.5	19.8	17.5	21

Table 8. Vertical effective stress in soil at failure for embankment models constructed on soft clay treated by stone columns.

Spacing	Stress in soil (kPa)					
	H=200 mm		H=250 mm		H=300 mm	
L/d	5	8	5	8	5	8
S= 2.5d	23	22.5	19.8	18	18.3	16.2
S= 3d	27.2	26.5	24.8	23.9	22	20.5
S= 4d	30.5	27.5	27	25.8	24.6	23

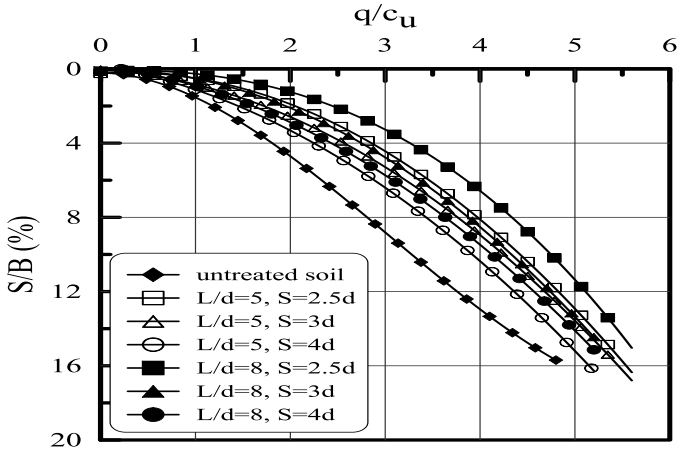

Figure 15. Bearing ratio versus settlement ratio for embankment model 200 mm high resting on soft soil treated by stone columns.

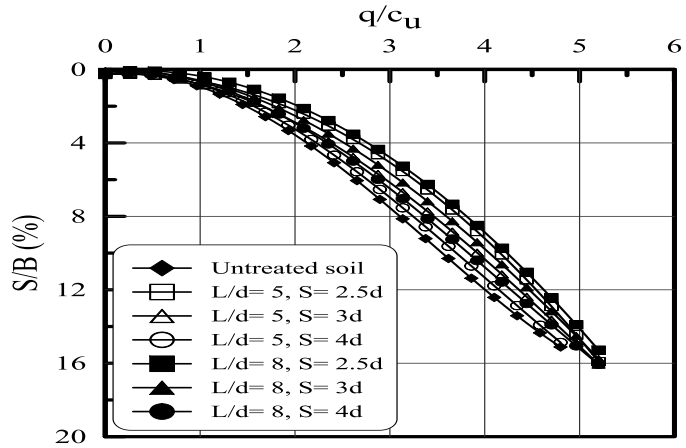

Figure 16. Bearing ratio versus settlement ratio for embankment model 250 mm high resting on soft soil treated by stone columns.

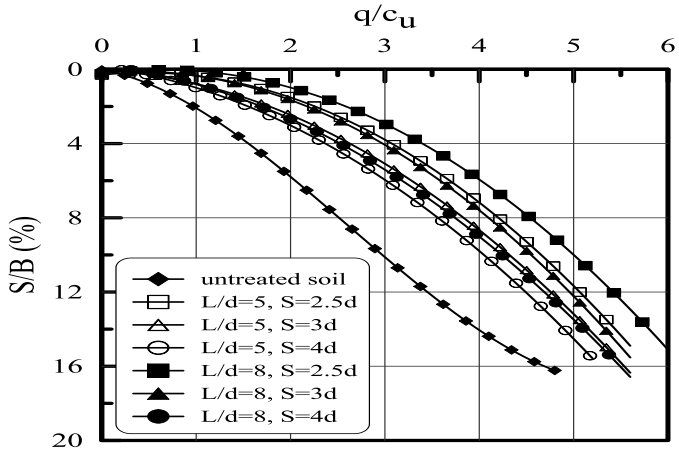

Figure 17. Bearing ratio versus settlement ratio for embankment model 300 mm high resting on soft soil treated by stone columns.

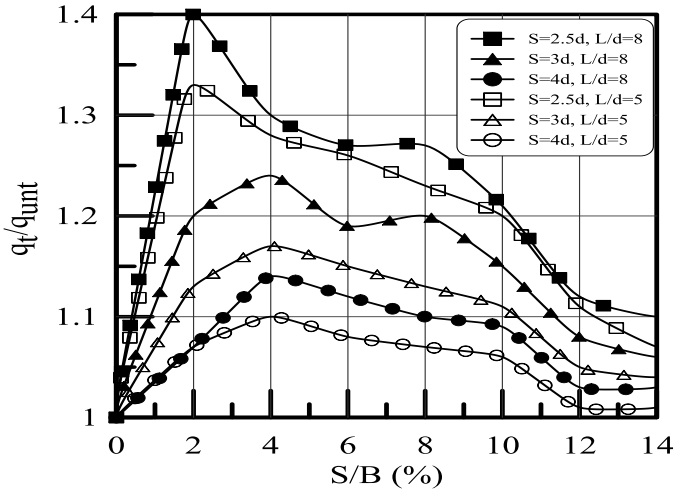

Figure 18. Bearing improvement ratio versus settlement ratio for embankment 200 mm high resting on soft soil treated by stone columns.

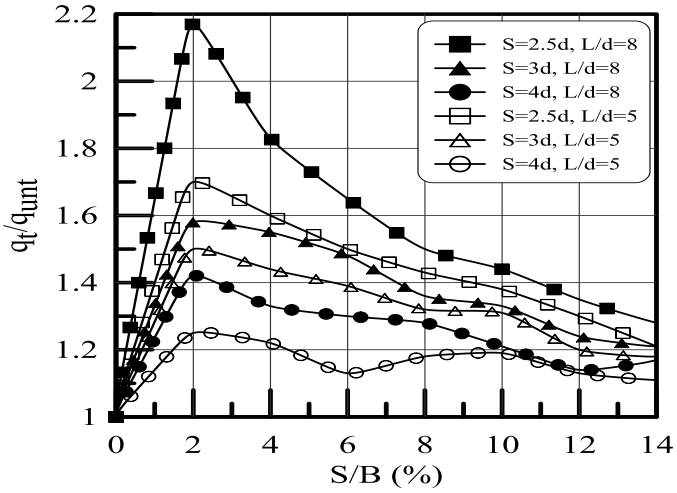

Figure 19. Bearing improvement ratio versus settlement ratio for embankment 250 mm high resting on soft soil treated by stone columns.

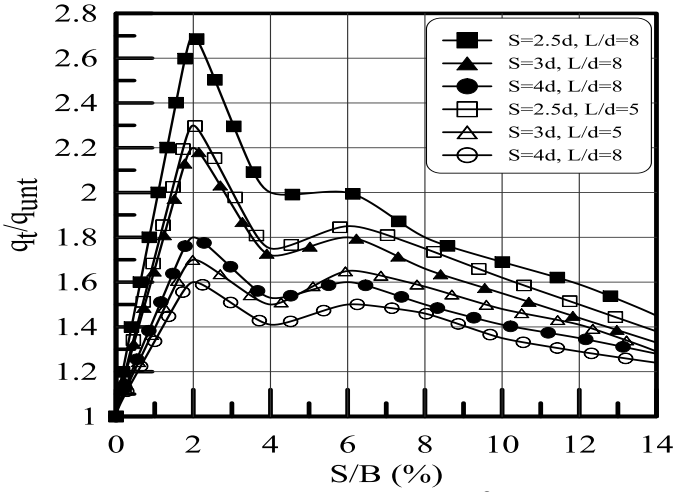

Figure 20. Bearing improvement ratio versus settlement ratio for embankment 300 mm high resting on soft soil treated by stone columns.

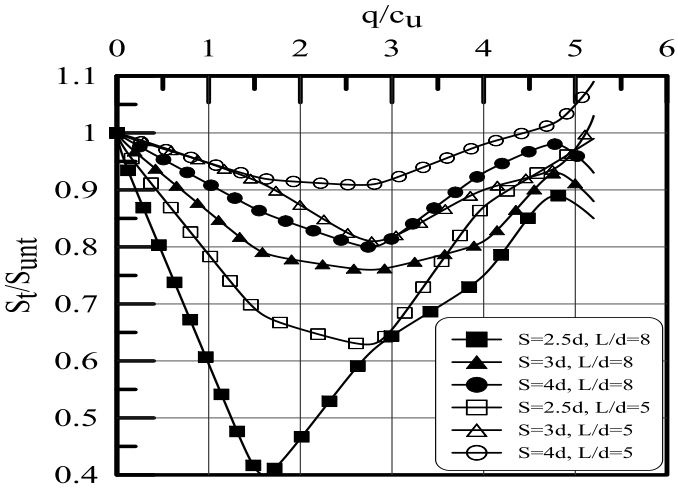

Figure 21. Settlement improvement ratio versus bearing ratio for embankment 200 mm high resting on soft soil treated by stone columns.

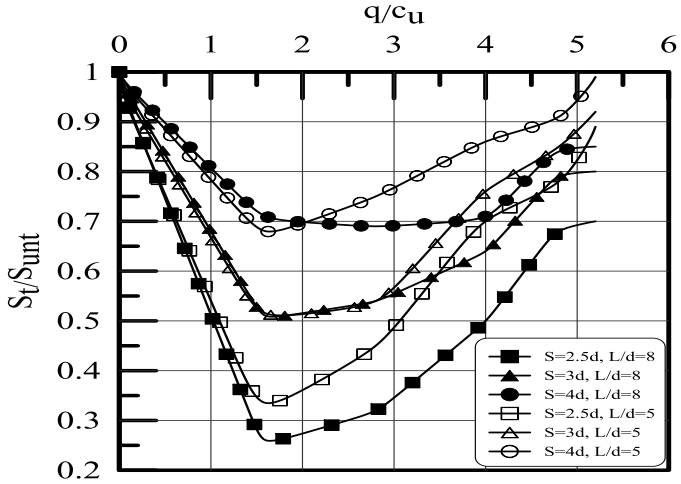

Figure 22. Settlement improvement ratio versus bearing ratio for embankment 250 mm high resting on soft soil treated by stone columns.

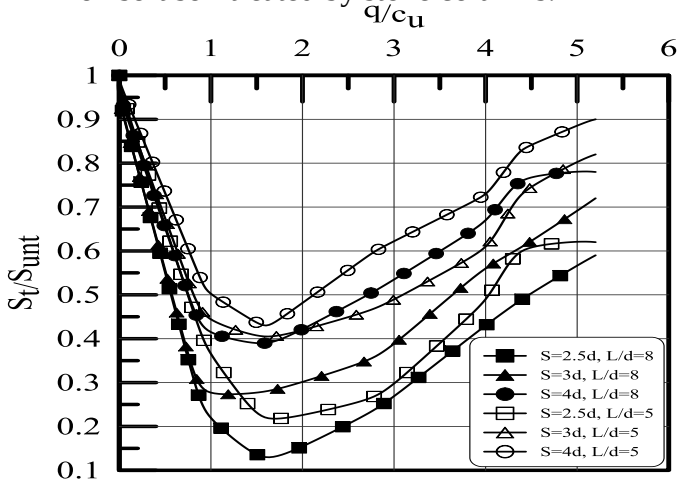

Figure 23. Settlement improvement ratio versus bearing ratio for embankment 300 mm high resting on soft soil treated by stone columns.

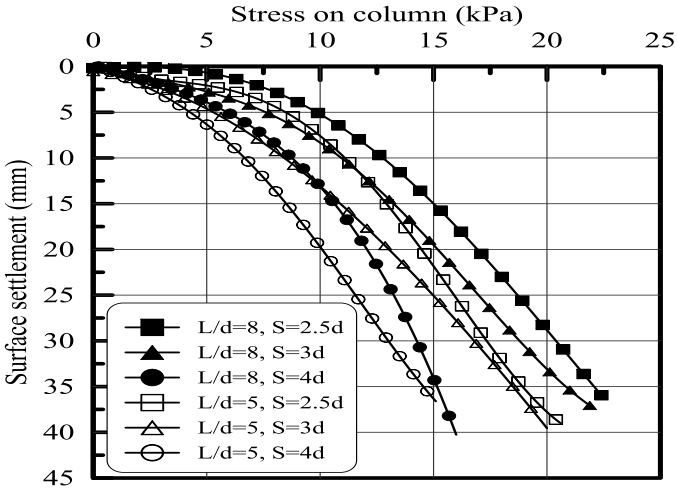

Figure 24. Vertical effective stress on column at failure versus surface settlement for embankment model of 200 mm height constructed on soft soil treated by stone columns.

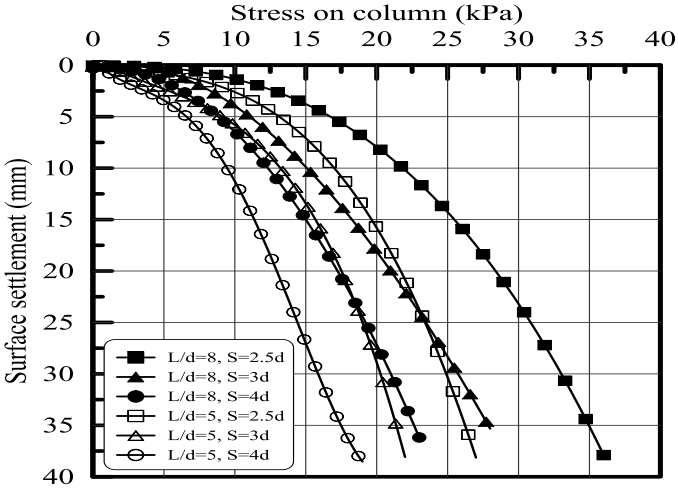

Figure 25. Vertical effective stress on column at failure versus surface settlement for embankment model of 250 mm height constructed on soft soil treated by stone columns.

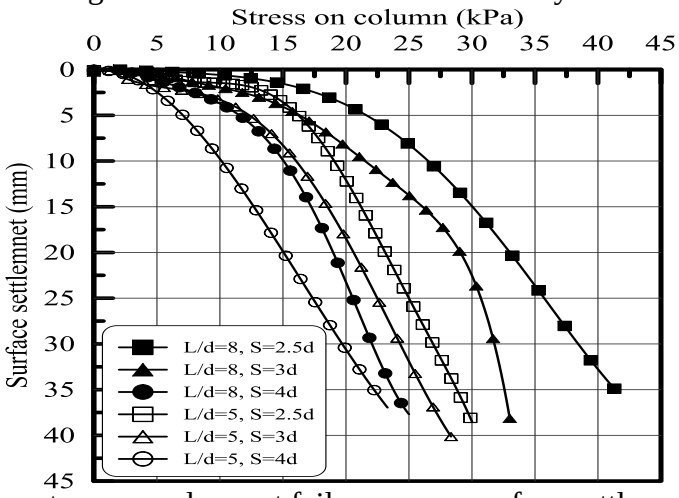

Figure 26. Vertical effective stress on column at failure versus surface settlement for embankment model of 300 mm height constructed on soft soil treated by stone columns.

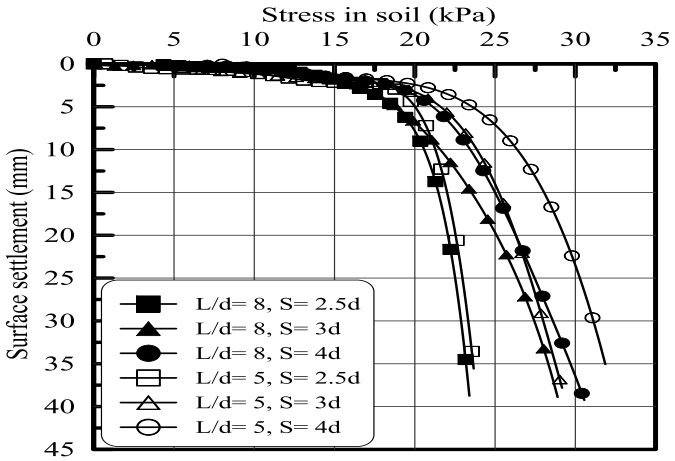

Figure 27. Vertical effective stress in soil at failure versus surface settlement for embankment model of 200 mm height constructed on soft soil treated by stone columns.

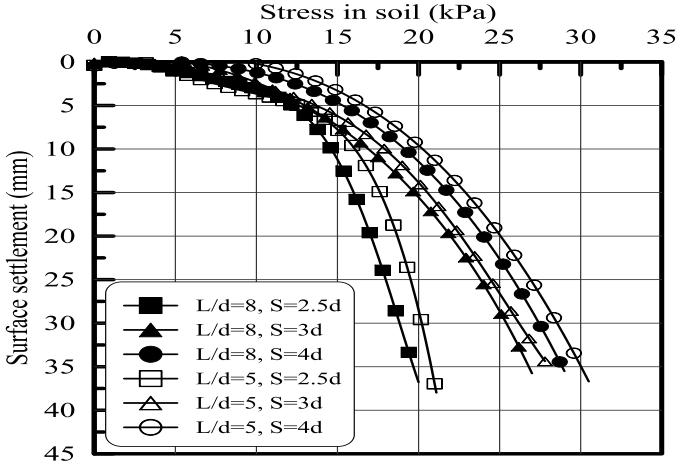

Figure 28. Vertical effective stress in soil at failure versus surface settlement for embankment model of 250 mm height constructed on soft soil treated by stone columns.

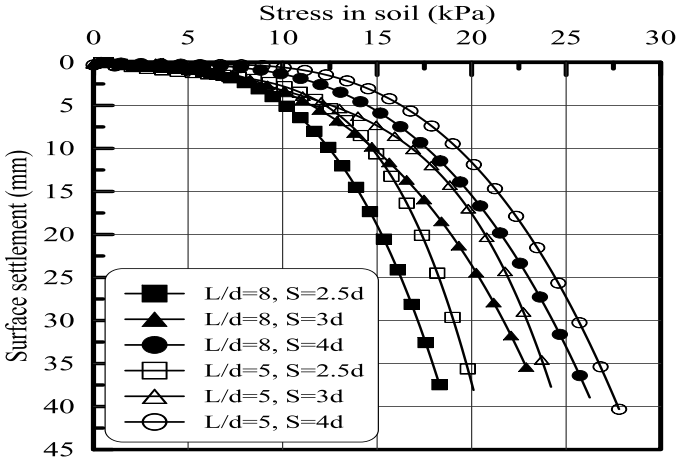

Figure 29. Vertical effective stress in soil at failure versus surface settlement for embankment model of 300 mm height constructed on soft soil treated by stone columns.

A Multi-variables Multi -sites Model for Forecasting Hydrological Data Series

Rafa H. Al-Suhili
Prof. ,Civil Engineering Dept., College of Engineering, University of Baghdad, Iraq.
A visiting Professor to the City College of New York, New York, USA.
Email: rafiishaker@yahoo.co.in

Nawbahar F. Mustafa
Lecturer, Dams and Water resources Eng., College of Engineering, University of Sulaimania.

ABSTRACT

A multivariate multisite hydrological data forecasting model was derived and checked using a case study. The philosophy is to use simultaneously the cross-variable correlations, cross-site correlations and the time lag correlations. The case study is of two variables, three sites, the variables are the monthly rainfall and evaporation; the sites are Sulaimania, Dokan, and Darbandikhan.. The model form is similar to the first order auto regressive model, but in matrices form. A matrix for the different relative correlations mentioned above and another for their relative residuals were derived and used as the model parameters. A mathematical filter was used for both matrices to obtain the elements. The application of this model indicates it's capability of preserving the statistical characteristics of the observed series. The preservation was checked by using (t-test) and (F-test) for the monthly means and variances which gives 98.6% success for means and 81% success for variances. Moreover for the same data two well-known models were used for the sake of comparison with the developed model. The single-site single-variable auto regressive first order and the multi-variable single-site models. The results of the three models were compared using (Akike test) which indicates that the developed model is more successful ,since it gave minimum (AIC) value for Sulaimania rainfall, Darbandikhan rainfall, and Darbandikhan evaporation, while Matalas model gave minimum (AIC) value for Sulaimania evaporation and Dokan rainfall, and Markov AR (1) model gave minimum (AIC) value for only Dokan evaporation).However, for these last cases the (AIC) given by the developed model is slightly greater than the minimum corresponding value.

Key words: forecasting, multi-sites, multi-variables, cross sites correlation, serial correlation, cross variables correlations, hydrology.

الخلاصة

تم اشتقاق نموذج تنبأ بالبيانات الهيدرولوجية لمتغيرات مختلفة وفي مواقع متعددة وتحقيقه باستخدام حالة دراسية. تعتمد فلسفة النموذج على الاستخدام الاني لمعاملات الارتباط المكانية وتلك التي توجد بين المتغيرات في الموقع الواحد بالإضافة الى الارتباط التسلسلي الزمني. الحالة الدراسية هي لمتغيرين في ثلاثة مواقع, المطر والتبخر في السليمانية, دوكان و دربندخان. ان النموذج شبيه بنموذج الارتباط التسلسلي ولكن معاملاته بصيغة المصفوفات . للنموذج مصفوفتي معاملات الاولى ذات عناصر تمثل معاملات الارتباطات النسبية والثانية تمثل معاملات بقايا الارتباط النسبية. بينت النتائج قدرة النموذج على التنبؤ بالمعلومات بصورة صحيحة حيث تم استخدام اختباري فحص الفرق بالأوساط الحسابية والتباين, وكانت نسب النجاح (81,98) على التوالي. ولغرض المقارنة بين النموذج المشتق والنماذج المعروفة في ادبيات الموضوع, تم بناء نموذج ذو المتغير الواحد لكل متغير من المتغيرات المستخدمة(ستة نماذج)و ثلاث نماذج من نوع النماذج المتعددة المتغيرات نموذج لكل

موقع . تم مقارنة نتائج هذه النماذج مع النموذج المشتق باستخدام اختبار (اكايكي) الذي يستخدم لهذا الغرض. بينت النتائج بان النموذج اعطى اقل القيم للاختبار بالنسبة للمطر في السليمانية و دربندخان والتبخر لدوكان اما فيما يخص نتائج بقية المتغيرات كانت قيم الاختبار اعلى بقليل عن القيم الصغرى المناظرة.

1. INTRODUCTION

Weather generation models have been used successfully for a wide array of applications. They became increasingly used in various research topics, including more recently, climate change studies. They can generate series of climatic data with the same statistical properties as the observed ones. Furthermore, weather generators are able to produce series for any length of time. This allows developing various applications linked to extreme events, such as flood analyses, and draught analysis, and hence putting proper long term water resources management to face the expected draught or flood events. There exist in the literature many types of stochastic models that simulate weather data required for various water resources applications in hydrology, agriculture, ecosystem, climate change studies and long term water resource management.

Single site models of weather generators are used for forecasting a hydrological variable at a single site independent of the same variable at the near sites, and thus ignoring the spatial dependence exhibited by the observed data. On the other hand single variable forecasting models are used for forecasting a hydrological variable in a site independent of the other related variables at the same site, thus ignoring the cross variables relations that physically exist between these variables. **Tobler, 1970,** mentioned in the first law of geography that "everything is related to everything else, but near things are more related than distant things." The most commonly used multi-sites stochastic weather models are of the form proposed by **Richardson, 1981**. for daily precipitation, maximum temperature, minimum temperature, and solar radiation , **Wilks, 1999.**These models forecast a hydrological variable at multiple sites simultaneously, hence simulate the cross sites dependency between these sites. The Multi-variables models are similar to the multi-sites model but simulate the cross variables dependency that exists between some variables at a certain site. The two models forms are similar but using cross sites correlations in the first one , while the second one uses the cross variables correlations. Much progress had been made principally in the last 20 years to come up with theoretical frameworks for spatial analysis **Khalili , 2007.**Some models, such as space–time models have been developed to regionalize the weather generators. In these models, the precipitation is linked to the atmospheric circulation patterns using conditional distributions and conditional spatial covariance functions **Lee et al., 2010.** The multi-site weather generators presented above are designed using relevant statistic information. Most of these models are either complicated or some are applicable with a certain conditions. In real situation both cross variables and cross sites correlation may exist between different hydrological variables at different sites. There exist in the literature some relatively recent some trials to account for the spatial variation in multi-sites. **Calder, 2007,** had proposed a Bayesian dynamic factor process convolution model for multivariate spatial temporal processes and illustrated the utility of the approach in modeling large air quality monitoring data. The underlying latent components are constructed by convolving temporally-evolving processes defined on a grid covering the spatial domain and include both trend and cyclical components. As a result, by summarizing the factors on a regular spatial grid, the variation in information about the pollutant levels over space can be explored. **Al-Suhili et al., 2010,** had presented a multisite multivariate model for forecasting different water demand typesat different areas in the city of Karkouk, north Iraq. This model first relate the each demand type with explanatory variables that affect its type, using regression models, then obtaining the residual series of each variable at each site. These residual are then modeled using multisite Matalas models for each type of demand. These models were coupled with the regression equation to form the multisite

multivariate variation. The last two cited research are those among the little work done on forecasting models of multi-sites multivariate types. However these model are rather complicated, and/or do not model the process of cross site and cross variables correlation simultaneously, which as mentioned above the real physical case that may exist. Hence researches are further required to develop a simplified multisite multivariate model. In this research a new straightforward multisite-multivariate approach is proposed to develop such a model that describe the cross variables and cross sites correlation structure in the forecasting of multi variables at multi sites simultaneously. This model was applied to a case study of monthly data of two hydrological variables, rainfall and evaporation at three sites located north Iraq, Sulaimania, Dokan, and Darbandikhan.

2. THE MODEL DEVELOPMENT

The multivariate multisite model developed herein, utilizes single variable lag correlations, cross variables lag-correlations, and cross sites correlations.

In order to illustrate the model derivation consider **Fig.1** shown. This figure illustrates the concept of two variables, two sites and first order model. This simple form is used to simplify the derivation of the model. However, then the model could be easily generalized using the same concept. For instant, **Fig. 2** is a schematic diagram for a multivariate multisite model of two variables, three sites and first order time. The concept is that if there will be two-variables, two sites, and one time step (first order), then there will exist (8) nodal points. Four of these represent the known variable, i.e. values at time (t-1); the other four are the dependent variables, i.e. the values at time (t). As mentioned before **Fig. 1** shows a schematic representation of the developed multisite multivariate model and will be abbreviated hereafter as MVMS (V, S ,O),where V: stands for number of variables in each site , S: number of sites , and O : time order, hence figure (1) can be designated as MSMV (2,2,1), while **Fig. 2** MVMS (2,3,1).

This model can be extended further to (v-variables) and / or (s-sites) and / or (o- time) orders as will be shown later .The model concept assume that each variable dependent stochastic component at time t can be expressed as a function of the independent stochastic component for all other variables at time (t), and those dependent component for all variables at time (t-1) at all sites. The expression is weighted by serial correlation coefficient, cross-site cross-correlation coefficient, cross-variable cross coefficient and cross-site, cross-variable correlation coefficient. In addition to that; the independent stochastic components are weighted by the residuals of all types of correlations. These residual correlations are expressed using the same concept of autoregressive first order model (Markov chain). Further modification of this model is to use relative correlation matrix parameters by using correlation values relative to total sum of correlation for each variable, and the total sum of residuals as a mathematical filter ,as will be shown later.

A model matrix equation for first order time lag, O=1, number of variables=V, and number of sites=S, could be put in the following form:

$$[\epsilon_t]_{v*s,1} = [\rho]_{v*s,v*s} * [\epsilon_{t-1}]_{v*s,1} + [\sigma]_{v*s,v*s} * [\xi_t]_{v*s,1} \quad (1)$$

Which for v=2,s=3,and =1

$$[\epsilon_t]_{6,1} = [\rho]_{6,6} * [\epsilon_{t-1}]_{6,1} + [\sigma]_{6,6} * [\xi_t]_{6,1} \quad (2)$$

Where :

$$\begin{pmatrix} \epsilon_{(v1,s1)} \\ \epsilon_{(v2,s1)} \\ - - - \\ \epsilon_{(v1,s2)} \\ \epsilon_{(v2,s2)} \\ - - - \\ \epsilon_{(v1,s3)} \\ \epsilon_{(v2,s3)} \end{pmatrix}_{t} = [\epsilon_t]_{6,1} \quad (3)$$

$$\begin{pmatrix} \epsilon_{(v1,s1)} \\ \epsilon_{(v2,s1)} \\ - - - \\ \epsilon_{(v1,s2)} \\ \epsilon_{(v2,s2)} \\ - - - \\ \epsilon_{(v1,s3)} \\ \epsilon_{(v2,s3)} \end{pmatrix}_{t-1} = [\epsilon_{t-1}]_{6,1} \quad (4)$$

$$\begin{pmatrix} \xi_{(v1,s1)} \\ \xi\epsilon_{(v2,s1)} \\ - - - \\ \xi_{(v1,s2)} \\ \xi\epsilon_{(v2,s2)} \\ - - - \\ \xi_{(v1,s3)} \\ \xi\epsilon_{(v2,s3)} \end{pmatrix}_{t} = [\xi_t]_{6,1} \quad (5)$$

$$\begin{pmatrix} \rho_{1,1} & \rho_{1,2} & \rho_{1,3} & \rho_{1,4} & \rho_{1,5} & \rho_{1,6} \\ \rho_{2,1} & \rho_{2,2} & \rho_{2,3} & \rho_{2,4} & \rho_{2,5} & \rho_{2,6} \\ \rho_{3,1} & \rho_{3,2} & \rho_{3,3} & \rho_{3,4} & \rho_{3,5} & \rho_{3,6} \\ \rho_{4,1} & \rho_{4,2} & \rho_{4,3} & \rho_{4,4} & \rho_{4,5} & \rho_{4,6} \\ \rho_{5,1} & \rho_{5,2} & \rho_{5,3} & \rho_{5,4} & \rho_{5,5} & \rho_{5,6} \\ \rho_{6,1} & \rho_{6,2} & \rho_{6,3} & \rho_{6,4} & \rho_{6,5} & \rho_{6,6} \end{pmatrix} = [\rho]_{6,6} \quad (6)$$

$$\begin{pmatrix} \sigma_{1,1} & \sigma_{1,2} & \sigma_{1,3} & \sigma_{1,4} & \sigma_{1,5} & \sigma_{1,6} \\ \sigma_{2,1} & \sigma_{2,2} & \sigma_{2,3} & \sigma_{2,4} & \sigma_{2,5} & \sigma_{2,6} \\ \sigma_{3,1} & \sigma_{3,2} & \sigma_{3,3} & \sigma_{3,4} & \sigma_{3,5} & \sigma_{3,6} \\ \sigma_{4,1} & \sigma_{4,2} & \sigma_{4,3} & \sigma_{4,4} & \sigma_{4,5} & \sigma_{4,6} \\ \sigma_{5,1} & \sigma_{5,2} & \sigma_{5,3} & \sigma_{5,4} & \sigma_{5,5} & \sigma_{5,6} \\ \sigma_{6,1} & \sigma_{6,2} & \sigma_{6,3} & \sigma_{6,4} & \sigma_{6,5} & \sigma_{6,6} \end{pmatrix} = [\sigma]_{6,6} \quad (7)$$

where:
$\rho_{1,1}$ = ρ [(x1, x1), (s1, s1), (t, t-1)]= population serial correlation coefficient of variable 1 with itself at site 1 at site 1, for time lagged 1

$\rho_{1,2}$= ρ [(x1, x2), (s1, s1), (t, t-1)]= population cross correlation coefficient of variable 1 at site 1 with variable 2 at site 1, for time lagged 1

$\rho_{1,3}$= ρ [(x1, x1), (s1, s2), (t, t-1)]= population cross correlation coefficient of variable 1 at site 1 with variable 1 at site 2, for time lagged 1

$\rho_{1,4}$= ρ [(x1, x2), (s1, s2), (t, t-1)]= population cross correlation coefficient of variable 1 at site 1 with variable 2 at site 2, for time lagged 1

$\rho_{1,5}$= ρ [(x1, x1), (s1, s3), (t, t-1)]= population cross correlation coefficient of variable 1 at site 1 with variable 1 at site 3, for time lagged 1

$\rho_{1,6}$= ρ [(x1, x2), (s1, s3),(t,t-1)]= population cross correlation coefficient of variable 1 at site 1 with variable 2 at site 3, for time lagged 1,the definition continues… , finally

$\rho_{6,6}$= ρ [(x2, x2), (s3, s3), (t, t-1)]= population serial correlation coefficient of variable 2 at site 3 with variable 2 at site 3, for time lagged 1.

The designated ($\rho_{i,j}$) is used for simplifying .That is variables at site 1 ,as 1, and 2,for this model (in general to 1,2,…v),then for variables at site 2,as 3 ,and 4 (in general from v+1 to 2v and so on) hence (r1,v+1) stands for the correlation between variable 1 at site 1,and variable 1 at site 2 and so on.
ϵ: is the Stochastic dependent component.

ξ: is the Stochastic independent component.

$\sigma_{i,j}$: are the residual of the correlation coefficient $\rho_{i,j}$.

The matrix, Eq. (2) can be written for each term, for example, for the first term:

$$\epsilon_{(1,s1,t)} = \rho_{1,1} * \epsilon_{(1,s1,t-1)} + \rho_{1,2} * \epsilon_{(2,s1,t-1)} + \rho_{1,3} * \epsilon_{(1,s2,t-1)} + \rho_{1,4} * \epsilon_{(2,s2,t-1)} +$$

$$\rho_{1,5} * \epsilon_{(1,s3,t-1)} + \rho_{1,6} * \epsilon_{(2,s3,t-1)} + \sigma_{1,1} * \xi_{(1,s1,t)} + \sigma_{1,2} * \xi_{(2,s1,t)} + \sigma_{1,3} * \xi_{(1,s2,t)} + \sigma_{1,4} *$$

$$\xi_{(2,s2,t)} + \sigma_{1,5} * \xi_{(1,s3,t)} + \sigma_{1,6} * \xi_{(2,s3,t)} \quad (8)$$

Similar equations could be written for the other variables. The correlation coefficient in each equation is filtered by a division summation filter, as in the following equation:

$$\rho r_{i,j} = \frac{\rho_{i,j}}{\sum_{j=1}^{n=v*s} abs\rho_{i,j}}. \quad (9)$$

Where $\rho r_{i,j}$ is the relative correlation coefficient of row i and column j of the matrix in eq.(6). The corresponding σ values are estimated using the following equation:

$$\sigma_{i,j} = \sqrt{1 - \rho_{i,j}^2} \quad (10)$$

Then these $\sigma_{i,j}$ are also filtered using equation similar to eq.(9) as follows:

$$\sigma r_{\mathbf{i,j}} = \frac{\sigma_{i,j}}{\sum_{j=1}^{n=v*s} abs\sigma_{i,j}} \quad (11)$$

Then the model matrix equation is the same as that appear in Eq.(2), replacing $\rho_{\mathbf{i,j}}$ values by the corresponding relative values $\rho r_{\mathbf{i,j}}$in the matrix Eq.(6), and $\sigma_{i,j}$ with the corresponding relative values $\sigma r_{i,j}$ in the matrix Eq.(7) . The model can be generalized to any number of variables and number of sites.

3. THE CASE STUDY AND APPLICATION OF THE MODEL.

In order to apply the new developed (MVMS) model explained above the Sulaimania Governorate was selected as a case study. Sulaimania Governorate is located north of Iraq with total area of (17,023 km2) and **population, 2009.** 1,350,000. The city of Sulaimania is located (198) km north east from Kurdistan Regional capital (Erbil) and (385) km north from the Federal Iraqi capital (Baghdad). It is located between (33/43- 20/46) longitudinal parallels, eastwards and 31/36-32/44 latitudinal parallels, westwards. Sulaimania is surrounded by the Azmar Range, Goizja Range and the Qaiwan Range from the north east, Baranan Mountain from the south and the Tasluje Hills from the west. The area has a semi-arid climate with very hot and dry summers and very cold winters. **Barzanji, 2003**.

The variables used in the model among other meteorological recoded data are (rainfall and evaporation) for monthly model as a two main variables that are expected to be useful for catchment management and runoff calculation. Data were taken from three meteorological stations (sites) inside and around Sulaimania city, which are Sulimania, Dokan dam, and Darbandikhan dam meteorological stations. Dokan dam metrological station is located (61 km) north east, and Darbandikhan dam metrological station is located (55 km) south east of Sulaimania city. While Dokan dam meteorological station is located (114 km) north east of Darbandikhan dam metrological station .The sites coordinates are given in **Table 1**, **Barzinji ,2003**.The Satellite image of the locations of the three stations showed in **Fig.3.**

The model was applied to the data of the case study described above. The length of record for the two variables and the three stations is (27) years, (1984-2010). The data for the first (22), (1984-2005) years were used for model building, while the left last 5 years data were used for verification,(2006-2010). It is worth to mention that the data are on monthly basis. Moreover since the analysis includes the rainfall as a variable which has zero values for June, July, August and September, in the selected area of the case study, these months are excluded from the analysis. Hence the model was built for the continuous period from October to May.

In order to give a general view for the data used the descriptive statistics (Mean, Standard deviation Sd, Coefficient of Skewness Cs, Coefficient of kurtosis Ck, Maximum Max, Minimum Min) were calculated for rainfall and evaporation of Sulaimania, Dokan dam, and Darbandikhan dam meteorological stations and are shown in **Table 2.**

Before proceeding with the modeling process the data series should be checked for their homogeneity . The split sample test suggested by **Yevjevich, 1972,** was applied for this purpose for each data series to test the homogeneity both in mean and standard deviation values. Different sizes of the subsamples were used for dividing the data sample into two subsamples with (n1,and n2) as number of years for subsample one and subsample 2 respectively. That is

(n1:n2) as (1,26),(2,25),(3,24), and so on. The split sample test result on estimated t-values that was compared with the critical t-value. If the t-value estimated is greater than the critical t-value then the data series is considered as non-homogeneous, **Yeijevich, 1972 ,** and thus this non-homogeneity should be removed. The results of this test had showed that there are some different subsamples splitting (n1:n2) values that exhibit non- homogeneity exist, however these cases that gives the maximum t-test values were considered for each of the 6- data series.**Table.3** shows these results, which indicates that non-homogeneity is exist in Sulaimania evaporation, Dokan rainfall, and Derbendikhan evaporation data series, while the series of the other variables are homogeneous. To remove this non-homogeneity the method suggested by **Yeijevich,1972** was used that using the following equation:

$$H_{i,j} = Mean2 + \frac{X_{i,j} - (A1 - B1 * i)}{A2 - B2 * i} * Sd2 \quad (12)$$

Where,
$H_{i,j}$: is the homogenized series at year i,month j of the first sub-sample (old).
$X_{i,j}$: is the original series at year i, month j, of the first sub-sample .
A1, B1: are the linear regression coefficients of the annual means.
A2,B2 : are the linear regression coefficients of the annual standard Deviations.
Mean2,Sd2 : are the overall mean and standard deviation of the second sub-sample.
This implies that the data is normalized according to the second sub-sample, i.e., the most recent one which is the correct way for forecasting. **Table.4** shows the values of the of Mean2,Sd2,A1,B1,A2,and B2, for the three non-homogeneous series.
The homogenized data were then retested to make sure that the transformation applied in Eq.(12), had removed the non-homogeneity. **Table.5** shows these results which ensure that the data series are all now homogeneous.
The next step in the modeling process is to check and remove the trend component in the data if exist. This was done by finding the linear correlation coefficient(r) of the annual means of the homogenized series, and the t-value related to it. If the t-value estimated is located in the r=0 hypothesis rejecting area t> + or - critical t-value of 2.83 then trend exist otherwise it is not. The following equation is used to estimate the T-values.

$$T=\frac{r\sqrt{n-2}}{\sqrt{1-r^2}} \quad (13)$$

Where
Table 6 shows these results, which indicate the absence of the trend component in all of the data series of the six variables.
Before proceeding into the modeling process the data should be normalized to reduce the skewness coefficient to zero. The well-known Box-Cox transformation Box and **Jenkin , 1976** was used for this purpose as presented in the following equation:

$$XN = \frac{(H+\alpha)^{\mu}-1}{\mu} \quad (14)$$

Where:
μ : is the power
α : is the shifting parameter.
XN : is the normalized series.
Table.7 shows the coefficients of the normalization transformation of all of the six series. The shifting parameter is selected to ensure avoiding any mathematical problem that may occur due

to the fraction value of the power μ. The power value is found by trial and error so as to select its value that reduce the skewness to almost zero value. **Table 8** shows the statistical properties of the series before and after normalization, which indicate that the skewness coefficients are reduced to almost zero a property of the normal data.
The next step in the modeling process is to remove the periodic component to obtain the stochastic dependent component of the series, which is done by using Eq.(15), as follows:

$$\epsilon_{i,j}=\frac{XN_{i,j}-Xb_j}{Sd_j} \quad (15)$$

Where:
$\epsilon_{i,j}$: is the obtained dependent stochastic component for year i, month j.
Xb_j : is the monthly mean of month j of the normalized series XN.
Sd_j : is the monthly standard Deviation of month j of the normalized series XN.
Table 9 shows the monthly means and monthly standard deviations of the normalized data series XN. The $\epsilon_{i,j}$ obtained series are then used to estimate the Lag-1 serial and cross correlation coefficients $\rho_{i,j}$, and $\sigma_{i,j}$of matrix Eqs.(6) and (7) respectively, which then used to estimate $\rho r_{i,j}$ and $\sigma r_{i,j}$ using Eqs.(9), and (11), respectively..

4. RESULTS AND DISCUSSION

The developed model above is used for data forecasting, recalling that the estimated parameters above are observed using the 22 years data series (1984-2005). This model will be used to forecast data for the next 5- years (2006-2010) since the data available are up to 2010, that could be compared with the observed series available for these years, for the purpose of model validation.
The forecasting process was conducted using the following steps:

1. Generation of an independent stochastic component (ξ) using normally distributed generator, for 5 years,i.e., (5*12) values.

2. Calculating the dependent stochastic component ($\epsilon_{i,j}$) using Eq. (2) and the matrices of $\rho r_{i,j}$ and $\sigma r_{i,j}$ as shown in Eqs. (9) and (11), respectively.

3. Reversing the standardization process by using the same monthly means and monthly standard deviations which were used for each variable to remove periodicity using Eq. (15) after rearranging.

4. Applying the inverse power normalization transformation (Box and Cox) for calculating un-normalized variables using normalization parameters for each variable and Eq.(14).

In most forecasting situation, accuracy is treated as the overriding criterion for selecting a model. In many instance the word "accuracy" refers to "goodness of fit," which in turn refers to how well the forecasting model is able to reproduce the data that are already known. The model validation is done by using the following steps:
1. Checking if the developed monthly model resembles the general overall statistical characteristics of the observed series.

2. Checking if the developed monthly model resembles monthly means, monthly standard deviations using t-test for the means and F-test for the standard deviation.

Furthermore the performance of the new multi-variables multi-sites model developed herein was compared with the well-known single variable single site model, and multi-variables single site model (MATALS model). This performance was made to investigate whether the new model can produce better forecasted data series. For purpose of comparison of different forecasting models performance, the Akaike (AIC), test given by the following equation:

$$AIC = 2K + nLn\frac{Rss}{n} \quad (16)$$

Where:
n: is the number of the total forecasted values .
K: number of parameters of the model plus 1.
Rss: is the sum of square error between the forecasted value and the corresponding observed value.
For each site and variable three sets of data are generated. The overall statistical characteristics are compared with those observed, for each of the generated series. **Table 10** shows these comparisons. For all variables and sites the generated sets resemble the statistical characteristics not exactly with the same values of the observed series but sometimes larger or smaller but within an acceptable range. **Table 11** shows the t-test and F-test summary for all of the variables and sites. As it is obvious from the results of these tables, that the generated series succeed in (t-test) for all of the monthly means, except for two months for Sulaimania rainfall, i.e. overall succeed percent of (98.6%). This indicates that the model is successfully resembled the monthly means values, with excellent accuracy.
Based on (F-test) which seek the variance differences between the observed and generated series; the success percentage ranking of the generated series was: the best being for Sulaimania rainfall (96%), followed by Darbandikhan evaporation (88%), Darbandikhan rainfall (83%), Dokan evaporation (83%), Dokan rainfall (71%), and finally Sulaimania evaporation (67%). The overall success percentage was (81%). These results of the F-test indicate that the model was successfully resembled the monthly standard deviations, with a very good accuracy. As mentioned above for purpose of the comparison of the model performance with the available forecasting models, the **Akaike , 1974** test was used. Before that six single variable single site models were developed, one for each variable, and three single variable multi-site models, **Matalas ,1967** one for each site. These models were then used for forecasting monthly data for the same period (2006-2010), forecasted by the developed model.
Table.12 shows the Akaike test results for all of the forecasted variables, in each sites, obtained using these model and those obtained by the developed model. It is obvious that the developed model had produced for most of the cases the lowest test value, i.e, the better performance. Even though for some cases it has higher test value than the other models, but for these cases it is observed that a very little differences are exist between these test values and the minimum obtained one.

5. CONCLUSIONS

From the analysis done in this research, the following conclusion could be deduced:

1- The model parameters can be easily estimated and do not require any extensive mathematical manipulation.
2- The model can preserve the overall statistical properties of the observed series with high accuracy.

3- The model can preserve the monthly means of the observed series with excellent accuracy, evaluated using the t-test with overall success (98.6%).
4- The model can preserve the monthly standard deviations of the observed series with a very good accuracy, evaluated using the F-test with overall success (81%).
5- The comparison of the model performance with the single variable single site and the multi-site single variable models, using the Akaike tset had proved that the developed model had proved better performance in the most cases. Moreover for those less cases where other models had the better performance; the test value of the developed model is slightly higher than the minimum value.

REFERENCES

Al-Suhili R.H., Al-Kazwini, M. J., and Arselan, C. A., *Multivariate Multisite Model MV.MS. Reg. for Water Demand Forecasting* , Eng. and Tech. Journal Vol. 28, No. 13 ,2010, pp 2516-2529.

Akaike, H., 1974, *A New Look at the Statistical Model Identification* , IEEE T. Automat. Contr., 19(6), 716–723.

Barzinji K. T., 2003, *Hydrogic Studies for Goizha Dabashan and Other Watersheds in Sulimani Governorate* , M.Sc. thesis submitted to the college of Agriculture, University of Sulaimani

Box, G.E., and Jenkins, G. M. (1976), *Time Series Analysis and Control*, San Francisco, California: Holden-Day,Inc.

Calder C.A., 2007, *Dynamic Factor Process Convolution Models for Multivariate Space-Time Data with Application to Air Quality Assessment*, J. Environ.Ecol. Stat. Vol.14: 229-247.

Khalili M, Leconte R. and Brissette F., 2007, *Stochastic Multisite Generation of Daily Precipitation Data Using Spatial Autocorrelation*, J Hydrometeorology, Vol.8, P 396-412

Lee Seung-Jae and Wents E. A., 2010, *Space-Time Forecasting Using Soft Geostatitiscs: A Case Study in Forecasting Municipal Water Demand for Phhonex, Arizona* , Stoch Environ Risk Assess 24: pp 283- 295

.

Matalas N.C., 1967, *Mathematical Assessment of Synthetic Hydrology*, Water Resoures 3: 937-945.

Richardson C. W. and Wright D. A., 1984, *WGEN: A Model for Generating Daily Weather Variables*, United States Department of Agriculture, Agriculture Research Service ARS-8

Tobler W., (1970) , *A Computer Movie Simulating Urban Growth in the Detroit Region*, Economic Geography, 46(2): 234-240.

Wilks D. S., 1999, *Simultaneous Stochastic Simulation of Daily Precipitation, Temperature and Solar Radiation at Multiple Sites in Complex Terrain*, Elsevier, agricultural and forest meteorology 96:85-101.

Yevjevich, V. M., *The Structure of Hydrologic Time Series*, Fort Collins, Colorado State University, 1972.

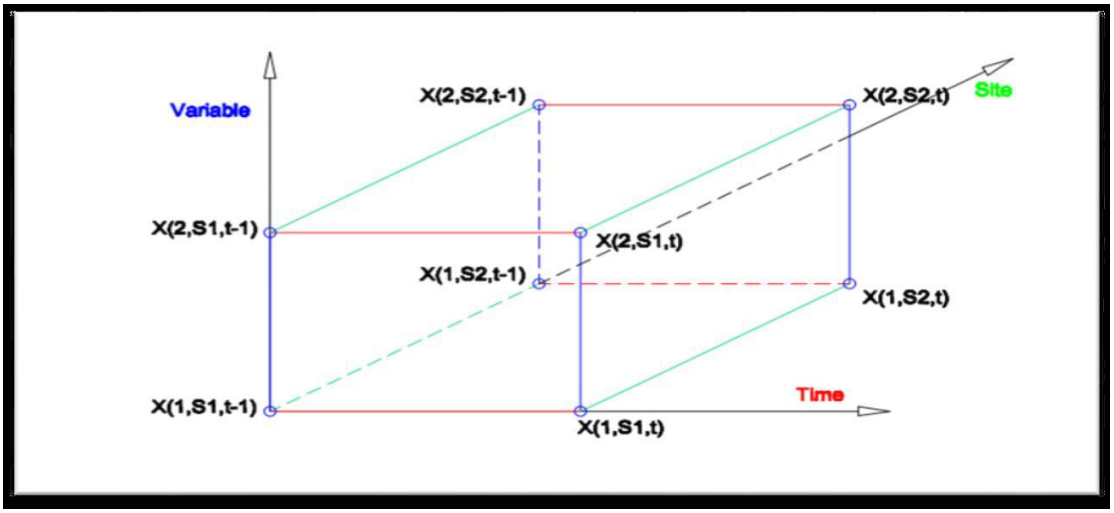

Figure 1. Schematic representation of the two variables two sites multi variables multisite model.

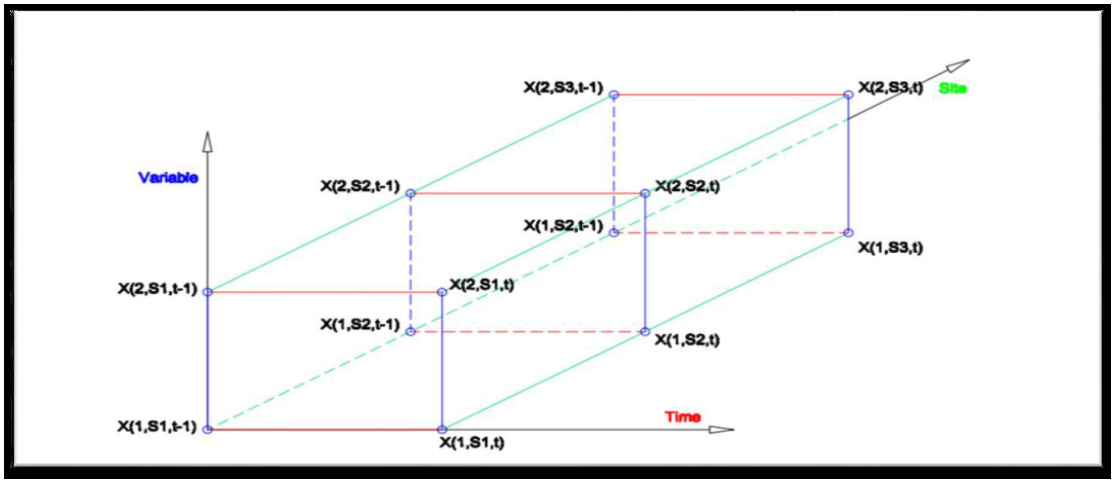

Figure 2. Schematic representation of the two variables three sites multi variables multisite model.

Table 1. North and east coordinates of the metrological stations selected for analysis.

Metrological station	N	E
Sulaimania	35° 33' 18"	45° 27' 06"
Dokan	35° 57' 15"	44° 57' 10"
Derbenikhan	35° 06' 46"	45° 42' 23"

Table 2. Descriptive statistics of the original data series.

Variable	1984-2005						2006-2010					
	Mean	S.D.	Skewness	Kurtosis	Max	Min	Mean	S.D.	SkewnessCs	Kurtosis	Max	Min
Sulaimania Rainfall(mm)	91	69	0.9	0.7	354	0.1	73	63	1	3	310	0.1
Sulaimania Evapor.(mm)	120	70	1	1	415	36	106	51	1	-1	220	40
Dokan Rainfall(mm)	93	80	1	0.7	416	0.1	64	56	1	2	262	1
Dokan Evapor.(mm)	116	68	0.9	-0.1	322	24.9	101	60	1	1	284	35
Derbendkan Rainfall(mm)	78	67	1.2	1.3	326	0.4	69	59	1	1	247	0
Derbendkan Evapor.(mm)	134	69	0.7	-0.3	341	34.1	111	62	1	0.1	276	37

Table 3. Test of homogeneity results, with tc=2.38, at 95% significant level.

Variable	Test for Means				Test for S. D.			
	t-statistic	N1	N2	Homo.	t-statistic	N1	N2	Homo.
Sulaimania Rainfall(mm)	2.08	15	12	Yes	1.7	23	5	Yes
Sulaimania Evapor.(mm)	2.56	21	6	No	2.91	22	5	No
Dokan Rainfall(mm)	2.76	15	12	No	2.77	24	3	No
Dokan Evapor.(mm)	2.31	25	2	Yes	1.77	23	4	Yes
Derbendkan Rainfall(mm)	2.3	5	22	Yes	2.05	6	21	Yes
Derbendkan Evapor.mm)	3.25	18	9	No	0.93	17	10	Yes

Table 4. Coefficients of non-homogeneity removal.

Variable	Mean2	S.D.2	A1	B1	A2	B2
Sulaimania Evapor.(mm)	106.3	50.62	127.297	-0.602	62.958	0.7065
Dokan Rainfall(mm)	55.96	41.33	101.91	-0.815	79.314	-0.319
Derbendkan Evapor.mm)	117.5	70.45	131.18	0.4	69.93	-0.229

Table 5. Re- test of homogeneity, with tc=2.38, at 95% significant level.

Variable	Test for Means				Test for S. D.			
	t-statistic	N1	N2	Homo.	t-statistic	N1	N2	Homo.
Sulaimania Rainfall(mm)	2.08	15	12	Yes	1.7	23	5	Yes
Sulaimania Evapor.(mm)	1.69	26	1	Yes	1.17	9	18	Yes
Dokan Rainfall(mm)	1.92	1	26	Yes	1.61	2	25	Yes
Dokan Evapor.(mm)	2.31	25	2	Yes	1.77	23	4	Yes
Derbendkan Rainfall(mm)	2.3	5	22	Yes	2.05	6	21	Yes
Derbendkan Evapor.mm)	1.08	26	1	Yes	1.33	8	19	Yes

Table 6.Test of trend results, with tc=2.38, at 95% significant level.

Variable	T for means	T for S.D.
Sulaimania Rainfall(mm)	0.16	0.023
Sulaimania Evapor.(mm)	0.21	1.06
Dokan Rainfall(mm)	0.2	0.4
Dokan Evapor.(mm)	0.04	0.13
Derbendkan Rainfall(mm)	1.04	0.04
Derbendkan Evapor.mm)	0.28	0.41

Table 7. Coefficients of the normalization transformation.

Variable	Power μ	Shifting α
Sulaimania Rainfall(mm)	0.47	1
Sulaimania Evapor.(mm)	-0.52	0
Dokan Rainfall(mm)	0.27	0
Dokan Evapor.(mm)	-0.054	0
Derbendkan Rainfall(mm)	0.359	0
Derbendkan Evapor.mm)	0.232	0

Table 8. Statistical properties before and after the normalization transformation.

Variable	Before Norm.				After Norm.			
	Mean	S.D.	Skewness	Kurtosis	Mean	S.D.	Skewness	Kurtosis
Sulaimania Rainfall(mm)	91	69	0.9	0.7	14.36	6.84	-0.15	-0.49
Sulaimania Evapor.(mm)	106	49	1	0.7	1.8	1.32	0.1	-1.1
Dokan Rainfall(mm)	54.8	42.9	0.9	0.5	6.5	2.5	-0.1	-1.0
Dokan Evapor.(mm)	116	68	0.9	-0.1	4.1	0.5	0.0	-0.9
Derbendkan Rainfall(mm)	93	80	1	0.7	9.2	4.5	-0.12	-0.61
Derbendkan Evapor.(mm)	118.3	71.3	0.75	-0.27	8.3	1.8	-0.04	-0.79

Table 9. Monthly means and standard deviations for the dependent stochastic component.

Variable	Oct.	Nov.	Dec.	Jan.	Feb.	Mar.	Apr.	May
Sulaimania Rainfall Means	6.923738	15.95873	18.27623	17.95162	16.6502	17.02956	15.15592	8.927809
Sulaimania Rainfall S.D	5.851398	7.895653	6.532181	5.975568	5.221715	5.869138	5.521562	5.782993
Sulaimania Evapor. Mean	1.790015	1.750803	1.715869	1.707902	1.715362	1.756555	1.779253	1.810782
Sulaimania Evapor. S.D.	0.010111	0.016859	0.019150	0.022393	0.013306	0.017357	0.016122	0.010803
Dokan Rainfall Mean	3.908560	1.816542	3.908560	1.816542	3.908560	1.816542	3.908560	1.816542
Dokan Rainfall S.D.	6.718586	2.294015	6.718586	2.294015	6.718586	2.294015	6.718586	2.294015
Dokan Evapor Mean	4.56241	0.091936	4.56241	0.091936	4.56241	0.091936	4.56241	0.091936
Dokan Evapor. S.D.	4.006939	0.176918	4.006939	0.176918	4.006939	0.176918	4.006939	0.176918
Derbendkan Rainfall Mean	4.932498	9.747093	11.70001	11.72048	11.67984	11.31086	7.90416	4.803818
Derbendkan Rainfall S.D.	3.35148	4.540729	4.442926	3.669128	2.898333	3.798071	2.871659	2.83866
Derbendkan Evapor. Mean	10.02914	7.414099	6.914041	6.468882	6.859431	8.805194	9.050721	10.86809
Derbendkan Evapor. S.D.	0.599518	0.585723	2.012912	1.68868	0.775737	1.093621	0.677337	0.609332

Table 10. Statistical properties of observed and forecasted rainfall series (2006-2010).

Variable	Min	Max	Kurtosis	Skewness	S.D.	Mean
Sul. Obs. R	0.1	310	3	1	63	73
Sul. Gen 1 R	2.3	360.1	-0.6	0.4	66.1	75.1
Sul. Gen 2 R	2.5	282.1	0.1	0.7	64.2	72.7
Sul. Gen 3 R	6.8	248.3	-0.2	0.5	65.5	75.3
Dok. Obs. R	1	262	2	1	56	64
Dok. Gen 1 R	3	261	0.5	0.7	54	68
Dok. Gen 2 R	3	246	-0.1	0.7	52	58
Dok. Gen 3 R	6	266	0.2	0.7	49	65
Der. Obs. R	0.1	247	1	1	59	69
Der. Gen 1 R	0.9	375	-0.4	0.7	55	71
Der. Gen 1 R	1.4	243	0.1	0.9	51	66
Der. Gen 1 R	6.0	241	-0.1	0.7	53	78
Sul. Obs. E	40	220	-1	1	50	105
Sul. Gen 1 E	43	220	0.1	1.0	52	94
Sul. Gen 2 E	49	255	-0.1	1.0	53	101
Sul. Gen 3 E	53	227	0.0	0.9	48	109
Dok. Obs. E	35	262	1	1	60	101
Dok. Gen 1 E	27	276	-0.2	0.9	61	100
Dok. Gen 2 E	35	318	-0.1	0.9	68	105
Dok. Gen 3 E	37	279	-0.3	0.9	62	109
Der. Obs. E	37	276	0	1	62	111
Der. Gen 1 E	10	270	-0.4	0.7	62	95
Der. Gen 1 E	19	303	-0.5	0.6	67	123
Der. Gen 1 E	16	262	-0.5	0.7	60	108

R: Rainfall, E: Evaporation.

Table 11. Percentage success of T-test for monthly means and F-test for monthly standard deviations for three generated series for each variable, for years (2006-2010).

Variable	% Success in T-test	% Success in F-test
Sulaimania Rainfall(mm)	97.22	96
Sulaimania Evapor.(mm)	100	67
Dokan Rainfall(mm)	100	71
Dokan Evapor.(mm)	100	83
Derbendkan Rainfall(mm)	100	83
Derbendkan Evapor.mm)	100	88
Over all	98.60	81

Table 12. Comparison between the minimum Akaike test values obtained by the developed model, the multi-variable single site model, and the single variable single site model, for three generated series for each variable, by each model, for years (2006-2010).

variable	Sulaim. Rainfall	Sulaim. Evap.	Dokan Rainfall	Dokan Evap.	Derbend. Rainfall	Derbend. Evap.
The Developed Model	1,544	1,189	1,438	1,264	1,535	1,404
Multi Variable Multi Sites Model	1,600	1,179	1,421	1,253	1,628	1,423
Single Variable Single Site Model	1,606	1,191	1,463	1,214	1,550	1,420

Removal of Water Turbidity by using Aluminum Filings as a Filter Media

Dr. Abeer Ibrahim Alwared
Instructor
College of l Engineering / University of Baghdad
abeerwared@yahoo.com

Suhair Luay Zeki
Ministry of Water Resources
suhairluay@yahoo.com

ABSTRACT

The ability of using aluminum filings which is locally solid waste was tested as a mono media in gravity rapid filter. The present study was conducted to evaluate the effect of variation of influent water turbidity (10, 20and 30 NTU); flow rate(30, 40, and 60 l/hr) and bed height (30and60)cm on the performance of aluminum filings filter media for 5 hours run time and compare it with the conventional sand filter. The results indicated that aluminum filings filter showed better performance than sand filter in the removal of turbidity and in the reduction of head loss. Results showed that the statistical model developed by the multiple linear regression was proved to be valid, and it could be used to predict head loss in aluminum filings filter and sand filter with R^2equal to 0.94 and 0.968 respectively.

Key words: water treatment turbidity, filtration, aluminum filings, sand .

ازالة عكورة المياه باستعمال برادة الالمنيوم كوسط ترشيح

د. عبير ابراهيم موسى
مدرس
كلية الهندسة – جامعة بغداد

سهير لؤي زكي
وزارة الموارد المائية

الخلاصة

تضمن البحث دراسة امكانية استخدام برادة الالمنيوم كماده مرشحه احادية لازالة عكورة الماء من خلال اختبار كفاءة المرشح لتاثير التغير في عكورة الماء الداخل(10، 20 ،30 وحدة عكورة) ومعدل الجريان (30، 40، 60) لتر/ساعة و ارتفاع الوسط(30 ، 60) سم على مقدار العكورة الخارجة وارتفاع عمود الماء ومقارنتها مع مرشح الرمل التقليدي ولمدة تراوحت بين (0.5 و5 ساعات) . ولقد بينت النتائج ان كفاءة مرشح برادة الالمنيوم كانت اعلى من كفاءة المرشح الرملي كما اظهرت النتائج ان ارتفاع عمود الماء لبرادة الالمنيوم كان اقل مماهو عليه في حالة المرشح الرملي بحوالي (8-32%). كما استخدمت البيانات من اختبارات الترشيح لبناء نموذج إحصائي لدراسة تاثير المتغيرات المدروسة على ارتفاع عمود المياه باستخدام الانحدار الخطي المتعدد ومن خلال مقارنة النتائج الحقلية مع تلك التي تم الحصول عليها باستخدام النموذج الاحصائي تم التوصل الى كفاءة النموذج الاحصائي بحيث يمكن استخدامه للتنبؤ باتفاع عمود المياه في مرشح الألمنيوم ومرشح الرمل حيث كانت R^2 تساوي 0.94 و 0.968 على التوالي.

الكلمات الرئيسة : معالجة المياه ،عكورة، ترشيح ، برادة الالمنيوم، رمل.

1. INTRODUCTION

One of the many challenges faced in developing world is the issue of waste management. According to the US Army Corps. of Engineers, **USACE, 1995.** "Aluminum has excellent corrosion resistance in a wide range of water and soil conditions because of the tough oxide film that forms on its surface.

The Aluminum Association, 2005. states, "Unless exposed to some substance or condition which destroys this protective oxide coating, the metal remains resistant to corrosion. Aluminum is highly resistant to weathering, even in many industrial atmospheres, which often corrode other metals. It is also resistant to many acids."

The surface water is the main source for water supply in most developing countries and in many parts of the world, river water that can be highly turbid, is used for drinking purposes. Access to improved drinking water is unavailable to an estimated 884 million people in the world most of who live in rural dispersed and often remote communities in developing countries **WHO/UNICEF, 2010**. As identified by the United States Environmental Protection Agency (USEPA), turbidity is a measure of the cloudiness of water; it is used to indicate water quality. The main problem in using surface water as a source of water supply is high concentration of clay and suspended solids, organic compounds and disease-causing microorganisms (such as viruses, parasites and some bacteria) which can cause symptoms such as nausea, cramps, diarrhea, and provide food and shelter for pathogens **,WHO, 2007**. The permissible limit for treated water in Iraq is 5 NTU **, according to Iraqi standards, 2001.**

Filtration is the most common method to remove clay and suspended solids, in filtration process, water is purified by passing through a bed of porous media which cause the retention of suspended matters within it. Although the existing granular filter media such as sand is sufficient to treat turbid water, discovering an alternative filter media from local source is also highly essential and are becoming popular since it will help to reduce the cost of treatment, as it can be processed and produced locally, and of their better removal efficiency as compared to conventionally used media **Jusoh et al., 2006** .

Jasim ,1977 examined the efficiency of rice shell and crushed date stone as an alternative materials due to their availability in large quantities in Iraq, and concluded that these materials can be utilized as a filtering media rather than as animal feed.

Al-Anbari,1997 selected suitable and durable locally filter media. The author tested the lightweight material like (porcelanite rocks and brunt kaolinite), and a heavy weight media like (goethite rock). For single media filter, porcelanite and kaolinite gave better results in turbidity removal efficiency and net water product value than sand medium.

Tang et al., 2006 evaluated the performance of crumb rubber as filtering material for ballast water treatment. It was found that crumb rubber is an excellent filter media for downward granular media filters in comparison to traditional granular media filters, a substantial reduction in turbidity was achieved, no clear relationship between filter depth and turbidity removal efficiency was found, higher filtration rate resulted in a lower turbidity removal efficiency.

Juosh et al.,2006 used palm shell as single and dual media filter. Palm shell is one of the industrial wastes that are abundantly available. Result suggests that all the filters are capable of producing water with acceptable turbidity unit (<1 NTU).

Nasser, 2010 investigated the ability of using crushed glass solid wastes as mono media with sand in the filtration process. The results indicated that the glass filters had better turbidity removal

efficiencies with a reduction of about 50% in washing water was required to wash the glass filters. Also glass filters were slower in the development of head losses.

Shubir, 2011 investigated the ability of using crushed plastic solid wastes, whose density less than that of water, in water filtration. The results indicated that the single plastic filters and the dual filters produced water of the same (high) quality as the sand filter. Also, it showed that plastic filters were slower in development of head losses and they have longer running time than the sand filters. The main objective of this work is to evaluate the performance and effectiveness of sand filters by utilizing aluminum filings as filter media which is a locally available solid waste material .

2. EXPERIMENTAL WORK

The experimental work of this study was based upon the use of packed bed filtration pilot plant for the removal of water turbidity by using different types of solid wastes as a filter media (aluminum filings and sand) at different flow rate , initial turbidity and bed height The experimental apparatus is shown in **Fig. 1.** It consisted of two galvanized cylindrical tanks of capacity 70 L; Perspex filter column of 7.5 cm inner diameter and 150 cm height designed and built to run with down flow direction according to **,AWWA Manual, 2000**. Calibrated flow meter was used to control the flow, with flow range of (10-100 l/hr). Four glass tubes fitted on a board was used to record the height of water at different depths for each filter. Two types of filter media were used aluminum filings as a locally available solid waste and conventional sand filter media, **Table 1.** show the characteristics of these filter media.

The aluminum filings used is flat shaped, 100% recycled from solid wastes. It is washed and sieved to obtain grain sizes of (0.6-1) mm in diameter

The filter was operated on the principle of constant flow rate and variable head loss mode. 70 liter of turbid water (10, 20, or 30 NTU) was pumped through the flow meter at different flow rates (30, 40, or 60 l/hr). This flow range was chosen to simulate the rapid filter flow rate in most water treatment plants. Two different bed heights were studied 30 and 60 cm for each experiment. Samples of the filtered water were taken every (30 minutes) during the run of 5 hours. The water level in the piezometers was recorded at the starting of each run and at fixed time intervals (each 30 minutes) to determine the head loss along the filter depth.

Turbidity was measured by a portable turbidity meter (Hanna instruments, HI 93703). The recorded level had accuracy of (0.5) NTU. The values of the available head were read by using the piezometers at fixed time intervals. PH value was measured for every sample and it was found that it was within the PH value for tap water.

Large quantity of kaolin was added to 10 liter preparation tank, shaken well, and left for 15 min in order to let larger suspended solids settle under the influence of gravity, and to obtain turbidities of (10, 20 , 30) NTU , then it is transferred to the storage tank. Turbid water (10, 20, 30) NTU from the storage tank was pumped through flow meter at different flow rates (30, 40, 60) l/hr, this flow range was chosen to simulate the rapid filter flow rate to the filter column. The water level in the piezometers were recorded at the starting of each run and at fixed time intervals (each 30 minutes) to determine the head loss along the filter depth. Samples of the filtered water were taken every (30 minutes) during the run of 5 hours. The experimental work was achieved in the Environmental Engineering Department/ Baghdad University.

3. RESULTS AND DISCUSSION

3.1 Effect of Influent Turbidity

Three different influent turbidities were tested in this study (10, 20, and 30 NTU), during each run the flow rate and bed depth were kept constant. **Fig.2** illustrates the effect of influent turbidity on the turbidity removal efficiency. It can be seen from this figure that sand has lower turbidity removal efficiency compared with aluminum filings filter. It is obvious that greater porosity value yield poorer filtrate quality due to smaller available surface area for deposition **, Gronow, 1986**. In this experimental work, best filtrate results were for aluminum filings filter though they had a higher porosity than sand filter. The flat shape for the aluminum filings gave better results due to stability of deposits onto flat surfaces, and not critical deposits onto rounded surfaces as in the case of sand. These results are in good agreement with **Jasim, 1977**; who found that flat shaped grains usually perform better than do rounded or worn grains due to their higher stability of sediments.

3.3 Effect of Flow Rate

The flow rate affects the filtrate quality; it is believed to be due to the increase of interstitial velocity. The interstitial velocity depends on the incoming approach velocity above the filter bed as well as the porosity **, Holdich, 2002**.

Three different flow rates were tested in this study (30, 40 and 60) l/hr. During each run influent turbidity and bed depth were kept constant. **Fig.3** shows the effect of flow rate on turbidity removal efficiency at 10 NTU influent turbidity of each filter type. It can be seen from these figures that when the flow rate increased removal efficiency decreased, and this is in a good agreement with the results of **Mohammed, 1989** and **Degremont, 1991**. At high filtration velocity the retained suspended solids are sheared off from the bed due to the high velocity force **Sundarakumar, 1996**.

3.4 Head Loss Variation with Time

In order to study the head loss across the bed. Piezometers were installed at different depths across the bed. During the filtration process, head loss built up because particles began to fill the void space in the filter media. The head loss development was increased with increase in influent turbidity for all filter media types. **Figs. 4, 5 and 6** illustrate the relation between the head loss with time at different depths for each type of filter media and at10 NTU influent turbidity and 60 cm bed depth. The head loss development for different influent turbidities is shown in **Fig.7**.

At low filtration velocity, the amount of suspended solids captured within the media is lower than the high filtration velocity. So in the case of low filtration velocity, the head loss development is very slow. This phenomenon is common for all media types as can be seen in **Fig. 8**.

For the same operational conditions and for all media types, sand filter showed the higher head loss at different depths than aluminum filings filter. This phenomenon is due to the high porosity of aluminum compared with sand, sustaining a greater load of sediments with lower head losses.

The head loss after five hours of filtration is presented in **Table 2** it can be seen from this table that aluminum filings filter shows less head losses than the sand filter during all runs, filtration rate impacted head loss substantially. Generally, a deeper filter depth and higher filtration rate resulted in a higher head loss.

4. EFFECT OF BED HEIGHT

Two different bed heights were tested in this study (30, and 60) cm, during each run influent turbidity and flow rate were kept constant. Filter depth appeared to have fairly significant influence on turbidity removal efficiency for different initial water turbidity. **Fig.9** shows the effect of depth on the removal efficiency. This can be attributed to the availability of more opportunity for particles to accumulate in higher depth. These accumulated particles act as new collectors until a saturation state is reached.

5. STATISTICAL ANALYSIS

A total filtration data sets (two types of filter media (aluminum filings and sand), two media depth (30 and 60cm) ,three different flow rates (30 , 40 and 60 l/hr), and three different initial turbidities (10 , 20, and 30 NTU) were collected and a analysis by using Multiple regression was performed using excel program for the examination the effects of each parameter on the head loss at the end of five hours run time.

A mathematical equation was introduced to correlate all of the data obtained using a multiple regression technique for aluminum filings filter and for and filter is as follows

For aluminum filings:

$$Head\ loss(X_1) = -28.188+0.0.504\ X_2 +0.0.472\ X_3 + 0.723X_4 \quad (1)$$

For sand:

$$Head\ loss(X_1)= -19.067+0.568\ X_2+0.344\ X_3+ 0.9083\ X_4 \quad (2)$$

Where: X_1= head loss

X_2 = flow rate

X_3 = bed height and

X_4 = influent turbidity

The equations fits the experimental data very well with R^2 = 0.94 and 0.968 for aluminum filings and sand filter respectively, as shown in **Fig.10**

6. CONCLUSIONS

1. Aluminum filings filter was efficient in turbidity removal as in sand filters. The maximum turbidity removal efficiency for sand filter was 86% at 40 l/hr filtration rate, while for aluminum filters as 89% at 30 l/hr filtration rate, 10 NTU influent turbidity, and 60m depth.
2. The maximum head loss for sand was 64.7cm,and aluminum filings was 55.7cm respectively at 60l/hr filtration rate, 30 NTU influent turbidity, and 60cm depth at the end of five hours run time.
3. Stability of the sediments in filtration contributed to the shape of the grains forming the filter bed.
4. Filter depth have fairly significant influence on turbidity removal efficiency, a deeper filter depth resulted in a higher head loss.
5. The statistical model developed by the multiple linear regression can be used in predicting head loss in aluminum filings filter and sand filter.

REFERENCES

- Al-Anbari, R. H.,1997, *Selected Alternatives for up Grading Existing Water Treatment Plants*, a Quantitative and Qualitative Improvement, Ph. D. Thesis, University of Technology, Iraq.
- AWWA, 2000, *Operational Control of Coagulation and Filtration Processes*, Manual of Water Supply Practices-M37, 2nd edition.
- Degremont, 1999, *Water Treatment Handbook*, vol. 1, 6th edition, Lavoisier Publishing, Paris.
- Gronow, J. R., 1986, *Mechanisims of Particle Movement in Porous Media*, Clay Minerals (1986) 21, 753-767.
- Holdich R., 2002, *Fundamentals of Particle Technology*, Midland Information Technology and Publishing, Leicestershire, UK.
- Iraqi Central Organization for Standardization and Quality Control, 2001, *Drinking Water Standards.*
- Jasim, L.M., 1977, *The Kinetics of Turbid Water Filtration through New Filtering Media for Rural Treatment*', M.Sc. Thesis, University of Baghdad, Iraq.
- Jusoh, A., Giap G., Aini, A., Halim, A., Noor, M. and Zakaria, M., 2006, *Comparative Performance of Single and Dual Media Filters of Sand and Burnt Oil Palm Shell*, Journal Teknologi, vol.45 (F) University Teknologi Malaysia, Pp.43-52.
- Mohammed, O. I., 1989,*A Comparison between the Performance of the Conventional and the Dual-media Filters*, M. Sc. Thesis, University of Basrah , Iraq.
- Nasser, N. O. A., 2010, *Investigating the Ability of using Crushed Glass Solid Wastes in Water Filtration*, ph. D. Thesis, University of Baghdad, Iraq.
- Shubir, M.D., 2011, *Study the Ability of using Crushed Plastic Solid Wastes in Water Filtration*, M. Sc. Thesis, University of Babylon, Iraq.
- Sundarakumar, R., 1996, *Pilot Scale Study on Floating Media Filtration for Surface Water Treatment*, M.Sc. Thesis, Asian Institute of Technology School of Environmental and Resources Development Bankok, Thailand.
- Tang, Z., *Butkus, M.A. ,and Xie, Y., F. ,2006, Enhanced Performance of Crumb Rubber Filtration for Ballast Water Treatment*, Chemosphere, 74, Pp.1396-1399.
- The Aluminum Association, 2005, *Specifications and Guidelines for Aluminum Structures*, 8th ed., Arlington, VA.
- United States Army Corps of Engineers (USACE), 1995, *Design of Seawalls and Bulkheads*, Washington , Pp.1110-2-1614.
- WHO, 2007, *Combating Waterborne Disease at the Household Level*, World Health Organization, 729 Geneva.
- WHO/UNICEF, 2010, *Progress on Sanitation and Drinking-Water*: 2010 Update, WHO/UNICEF 732 Joint Monitoring Programme *for Water Supply and Sanitation*, World Health Organization, 733 Geneva.

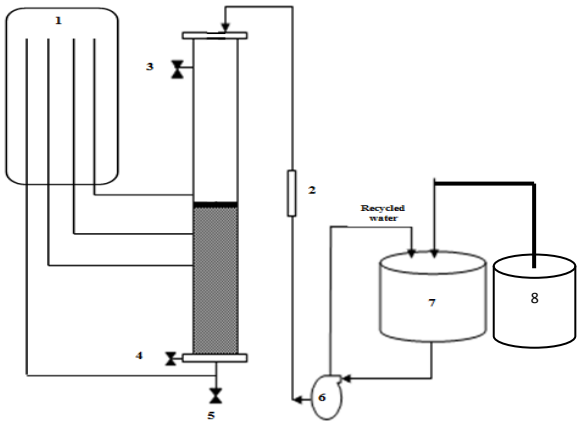

1.Manometer board 2.Flow meter 3.Wash water valve 4.Air valve 5 . Filtered water valve 6.Pump 7.Water tank 8.Preparation tank

Figure1. Schematic diagram of experimental apparatus.

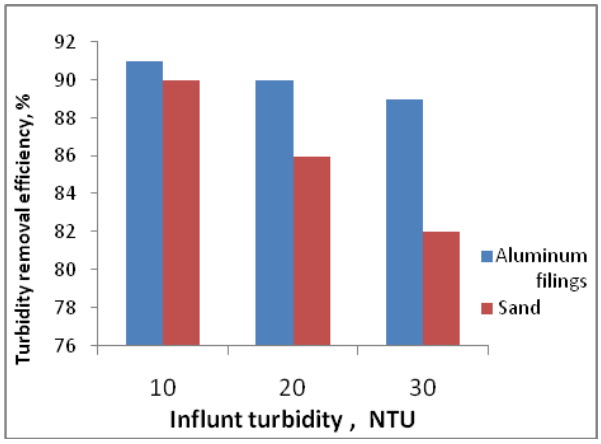

Figure 2. Effect of influent turbidity on the turbidity removal efficiency at bed deptht=30, flow rate 30 lit/hr.

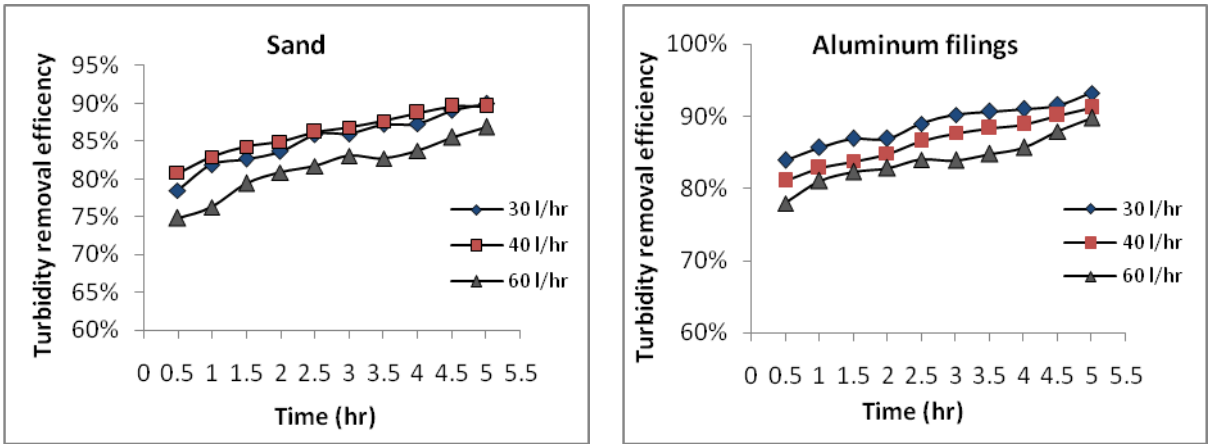

(a) (b)

Figure3. Effect of flow rate variation on turbidity removal efficiency, influent turbidity =10NTU, bed depth=60 cm.

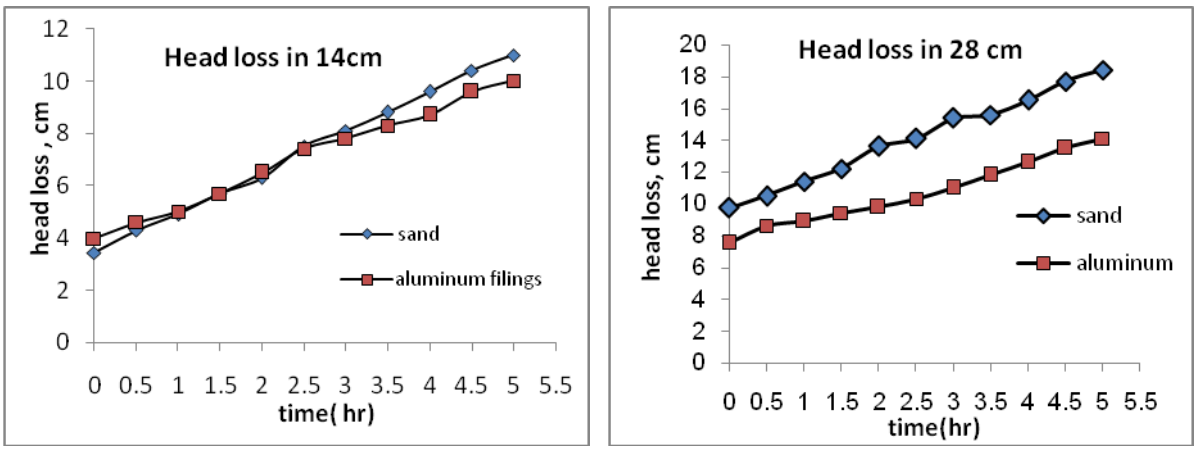

(a) (b)

Figure4. Head loss versus time at different heights of the filter at bed depth 60 cm, flow rate = 30 l/hr, turbidity =10 NTU.

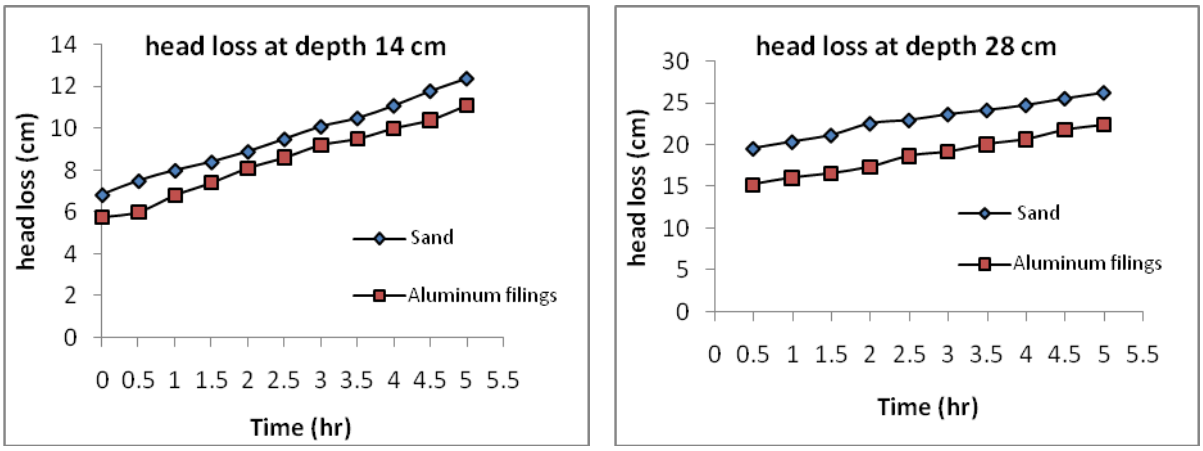

(a) (b)

Figure5. Head loss versus time at different heights of the filters at bed depth 60 cm, flow rate = 40 l/hr, turbidity =10 NTU.

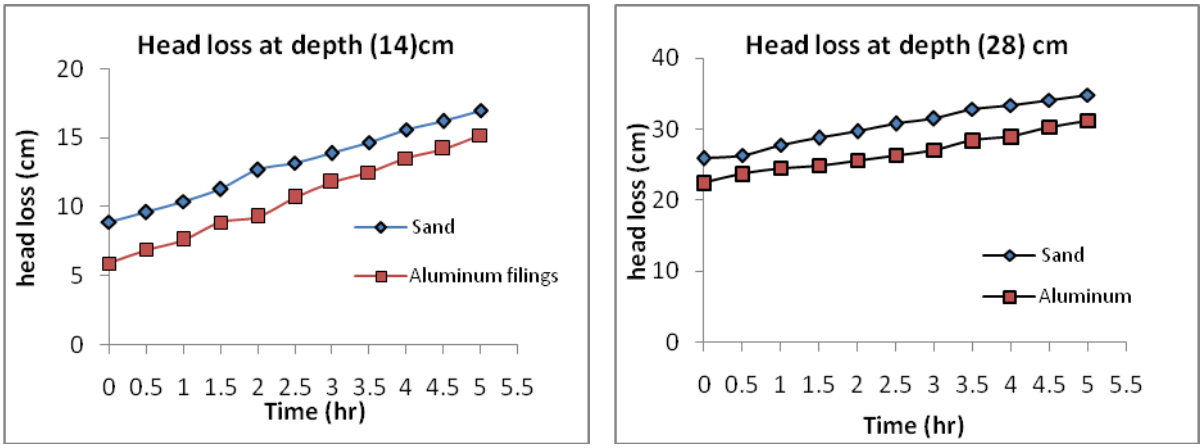

(a) (b)

Figure6. Head loss versus time at different heights of the filters at bed depth60 cm, flow rate=60 l/hr, turbidity=10 NTU.

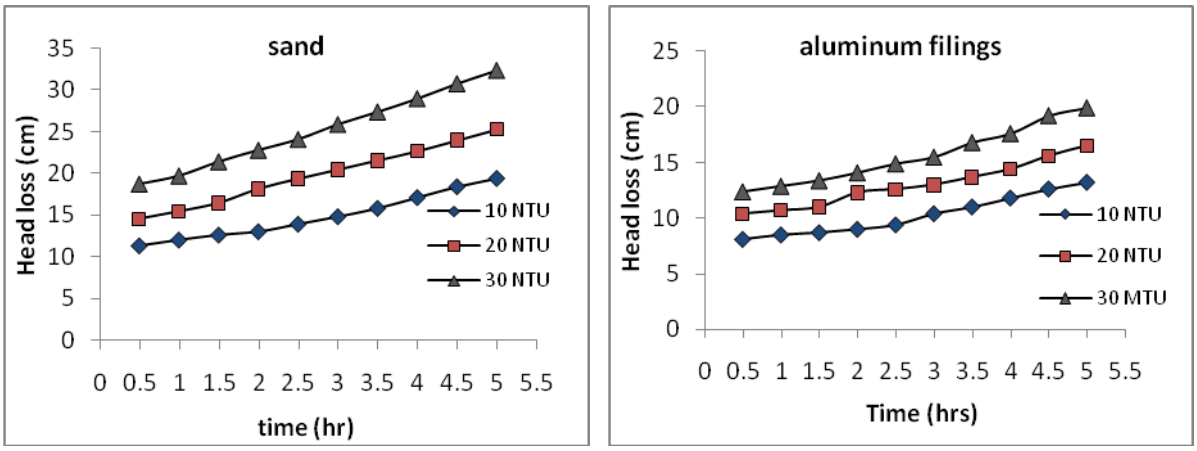

(a) (b)

Figure 7. Head loss versus time at different influent turbidity, flow rate=30 l/hr, filter depth =30 l/hr.

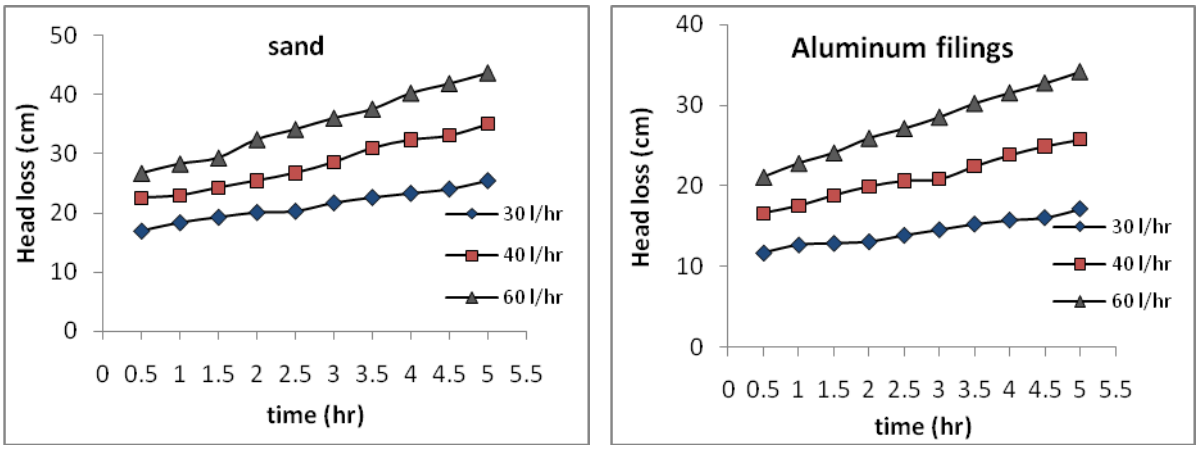

(a) (b)

Figure 8. Head loss versus time at influent turbidity = 10 NTU , bed depth = 60cm and different filtration rates.

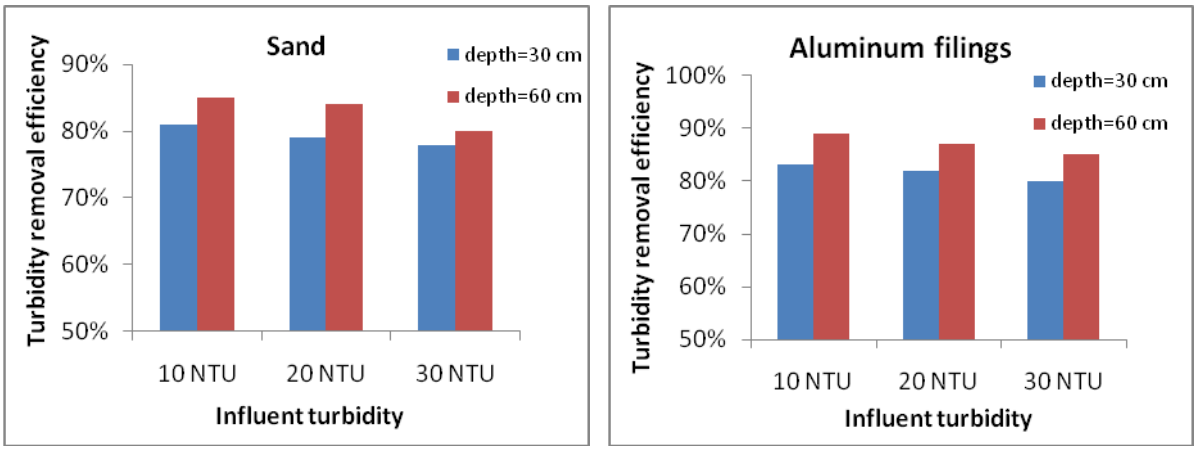

(a) (b)

Figure. 9 Impact of bed height on the removal efficiency at different influent and flow rate = 30 l/hr.

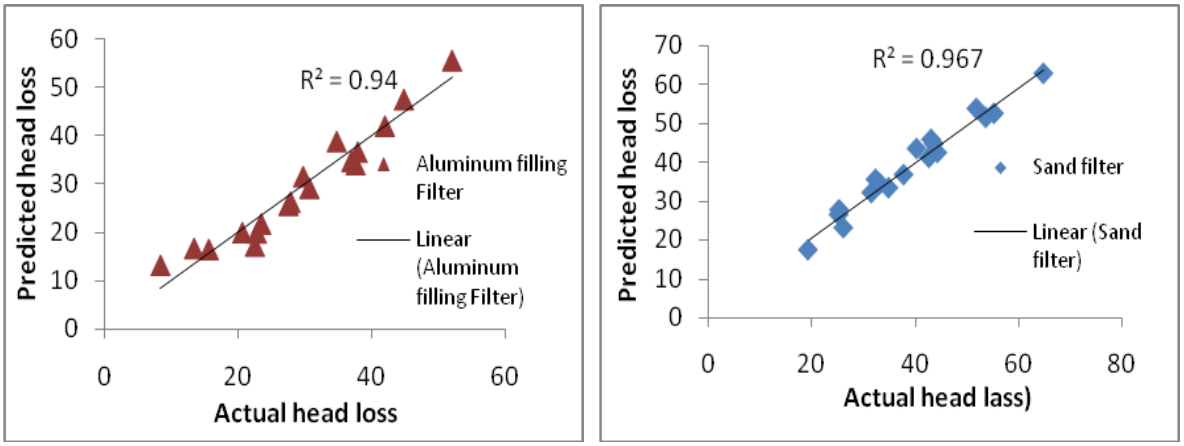

(a) (b)

Figure10. Comparison between actual and predicted head loss.

Table 1.Characteristics of filter media.

Media	Specific gravity	porosity	Effective size	Uniform coefficient
Aluminum filings	3.08	80%	0.62mm	1.35
Sand	2.66	37%	0.62mm	1.4

Table 2. Head loss for the two filters.

Flow rate (l/hr)	**Influent Turbidity, NTU**	**Head loss (cm), bed height 30cm**		**Head loss (cm), bed height 60cm**	
		Sand filter	**Aluminum filings filter**	**Sand filter**	**Aluminum filings filter**
30	10	19.4	13.2	25.4	17.2
	20	25.3	16.5	37.8	31.6
	30	32.4	19.9	43.1	34.8
40	10	26.2	16.7	34.9	25.7
	20	31.6	20	44.3	38.9
	30	42.7	26.3	53.6	42.1
60	10	33.2	21.8	43.6	34.1
	20	40.3	29.2	51.8	47.6

The Effect of Dynamic Loading on Stresses Induced in Charnley Hip Prosthesis

Ahmed Abdul Hussain
Assistant professor
Engineering College – Baghdad University
Email: ahmedrobot65@yahoo.com

Mahmood Wael Saeed
MS.C. Student (Mechanical Department)
Engineering College – Baghdad University
Email:mahmoodwael@rocketmail.com

ABSTRACT

This study produces an image of theoretical and experimental case of high loading stumbling condition for hip prosthesis. Model had been studied namely Charnley. This model was modeled with finite element method by using ANSYS software, the effect of changing the design parameters (head diameter, neck length, neck ratio, stem length) on Charnley design, for stumbling case as impact load where the load reach to (8.7* body weight) for impact duration of 0.005sec.An experimental rig had been constructed to test the hip model, this rig consist of a wood box with a smooth sliding shaft where a load of 1 pound is dropped from three heights. The strain produced by this impact is measured by using rosette strain gauge connected to Wheatstone bridge for the model .The signal is amplified and sent forward to a data acquisition and then saved in the connected laptop. From this study it is found that the changing in stem length had large effect on effective stress where the change in effective stress while stem length increased from (110mm to 140mm) was not more than (209MPa).

Keywords: hip prosthesis; charnley design; finite element method; design parameters; data acquisition

تأثير الحمل الديناميكي على الاجهادات المتولدة في مفصل الورك الصناعي من نوع جارلي

أحمد عبدالحسين علي
استاذ مساعد
كلية الهندسة – جامعة بغداد

محمود وائل سعيد
طالب ماجستير (قسم الميكانيك)
كلية الهندسة – جامعة بغداد

الخلاصه

هذه الدراسه قدمت تصور نظري وعملي عن حاله حمل عاليه جدا هي حالة التعثرعلى بديل مفصل الورك الصناعي وقد تم دراسة موديل من نوع جارلي.تم تمثيل النموذج بطريقه العناصر المحدده وذلك بواسطة برنامج الانسز للموديل جارلي ودراسه تأثير تغيير المتغيرات التصميميه للموديل جارلي (نصف قطر الكره , طول العنق , نسبة تغيير العنق , طول الجذع) لحالة الحمل الصدمي في حالة التعثر حيث يصل الحمل الى (8.7* وزن الجسم) ولمدة صدمه مقدارها 5 مللي ثانيه.الطريقة العمليه التي تم العمل بها هي صناعة هيكل مستطيل مجوف بداخله ذراع املس ينزلق عليه الحمل من ثلاث ارتفاعات .وتم تحسس الانفعال الناتج من الصدمه بواسطة مقياس انفعال ثلاثي للموديل جارلي حيث تم استخدام قنطرة وتستن ومضخم فولتيه لتتجه الاشاره نحوجهاز حيازة البيانات ومحولها ثم الى الكومبيوتر.وجد ان اكثر المتغيرات التصميميه تأثيرا على الاجهاد المحصل في الجزء الاضعف في موديل جارلي هو طول الجذع حيث ان مقدار التغير في الاجهاد الاعظم عند تغيير طول البديل من (110ملم الى 140ملم) لم يتجاوز (209 ميجاباسكال).

الكلمات الرئيسيه: مفصل الورك الصناعي, تصميم جارلي, طريقة العناصر المحدده، المتغيرات التصميمية، جهازحيازة البيانات.

1. INTRODUCTION

This work presents an overview about the hip joint, the causes of its failure and the historical attempts to overcome this problem as well as the most important stem types used in this field enhanced by some definitions and concepts related to the shape variables and materials. Total hip replacement is most commonly used to treat joint failure caused by osteoarthritis or other diseases. The aims of the procedure are pain relief and improvement in hip function. Hip replacement is usually considered only once other therapies, such as physical therapy and pain medications, have failed. In order to design a successful stem implant some important things must take in account such human activities, weight and age. Some of researchers such as ,H.F. **El'Sheikh, et.al., 2003**, studied a component (hip prosthesis) had been subjected to a dynamic load due to stumbling and the peak static load of the same patient load activity. Two quantitative measures are calculated: peak stress and stressed volume. It has been shown that each measure may lead to differing conclusions. It is concluded that from a thorough analysis of the hip prosthesis components (prosthesis, cement mantle and bone) it is not the peak stress but rather the proportion of the stressed elements (or stressed volume) which should be the indicator if a precise analysis of the load transfer mechanism is required. In static analysis the material was assumed to be linear elastic continuum with isotropic properties, whereas in dynamic analysis it was assumed to be bi-linear elastoplastic, and studied the effect of some design parameter such as stem thickness, the effect of changing the material, the effect of changing the stem length, the effect of collar of hip prosthesis and the effect of damper on stresses induced in prosthesis.

2. FINITE ELEMENT MODEL

The concept of piecewise discretization or dividing a complex object into simpler pieces is one of the oldest logical concepts known to man, when trying either to construct a complex shape or to understand an enigmatic phenomenon. More recently, structural engineers had developed matrix methods for the analysis of framed structures, which can easily be recognized as assemblages of members or, element, connected by joints, or nodes. The finite element (FEM) can now be considered as the most popular theoretical technique ever known to man, and it has been applied successfully to many engineering disciplines, such as structural mechanics, computational fluid dynamics, tribology, heat transfer , electromagnetism, biomechanics,… etc.
The Charnley model which was used should be discretized to small elements for finite element analysis; the element type that used in this discrediting was SOLID45, 10-node tetrahedral. SOLID 45 has a quadratic displacement behavior and is well suited to modeling irregular meshes; the element is defined by 10 nodes having three degrees of freedom at each node: translations in the nodal x, y, and z directions as shown in **Fig. 1** , the element has plasticity, , creep, stress stiffening, large deflection, and large strain capabilities with respect to contact region between cup and femoral head the element contact 174 had been used where this is a three- dimensional, eight-node , higher order quadrilateral element that can be located on the surfaces of three- dimensional solid or shell element with mid side nodes, It can be degenerated to 3-7 node quadrilateral triangular shapes, and also element target where it is a three-dimensional element and shape is described by a sequence of triangles, quadrilaterals, straight lines , parabolas, cylinders, cones, (Release 14.0 Documentation for ANSYS 2012).With changing the coarser of this element in order to investigate the right element number. The result of the convergence test show that the best element number that can 253481elements as in **Fig. 2** .

3. MATERIAL PROPERTIES

The material properties of each types of hip prosthesis that are used in present work are illustrated in **Table1, Zafer Senalp , et.al., 2007,** below where the Charnley hip prosthesis is made from (stainless steel alloy 316L)..And acetabulum cup made from ultra-high molecular weight polyethylene (UHMWPE)**, Mamdouh, 2012**.

4. LOADING AND BOUNDARY CONDITION

For dynamic analysis, the load time curve during walking that applied as time history of the dynamic load components for 5 s show that the maximum load applied on hip prosthesis reached to 8.7 times the body weight during stumbling case so the case with this excessive load should be studied, In our study we take stumbling case as impact load with time of impact (impact duration) of (0.005sec), **El'Sheikh, et.al., 2003,**. The boundary condition which had been applied in this work is according to (ISO-7206 standard, modified in 2002) .Where 60% of stem length (which is the distance from stem distal point to center of head ball) was fixed**, Chan-tsungyang, et. al., 2009.** The design parameters that studied is shown in the **Fig. 3** Charnley model.

5. EXPERIMENTAL

5.1 Model to be Tested

In this study real models of total hip prosthesis which had been bought it from market deal with prosthesis (DePuy-Synthes device market).We used Charnly hip prosthesis for this type of total .The dimensions of Charnley hip prosthesis is shown in **Table 2. . Fig. 4** shows the real Charnley model that had been studied.

5.2 Experimental Circuit

The interface circuit which has been used consists of rosette strain gage and whetstone bridge with signal amplifier and this circuit is connected to data acquisition of 16 Flexible I/O (Digital Input, Digital Output, or Analog Input) (LabJack–U3-LV,Colorado,USA) and it is able to read and write the signal in millisecond . This system was linked to a computer for storage and analysis of data using software LabJack UDV3.25computer to record the results with time, the circuit is shown in **Fig. 5**.Where this figure showed the method of circuit connections and its parts.

5.3 Testing Device

The test rig has been designed to simulate the environments of loading case of reference, **Farhad N. et. al., 2008,** where a frame work consists of smooth steel sliding shaft that allows weights to be dropped on the hip prosthesis from different height up to 30 cm ,as shown in **Fig. 6** which shows the test rig and the assisting measuring devices . In the different impact loads had been applied by falling weight of (1pound=453.59g) from 30cm then from 20cm and then from 10cm. A rosette strain gauge (Tokoyo Sokki Kenkyujo co.,LTD. –Japan) attached on the hip prosthesis (Charnley) connected to a Wheatstone bridge with signal amplifier measures the strain and gives the amplified signal from(0 to 4.8 volt) to LabJack data acquisition where a stream UD software gives the final values of strain with the aid of scaled equation of voltage. The final results are compared with those obtained by ANSYS. One of the most important case in experimental part is the fixation of the model during the test because the bad fixation may lead to wrong results and also became a far from reality, the (ISO7206-4 standard, Modified in 2002) solved this problem where by this standard we can become near to the reality case. In this

study according to modified ISO7206-4 standard 60% of stem length of hip prosthesis is fixed by using gypsum type 4(elite stone ,thixotropic,zermak-italy) which is used for fixation of master models in removable prosthesis. The fixing stone holds the distal end of the stem starting at 40% from center of the femoral head with stone thickness of 70mm.In addition, the stem is aligned at 10◦ in adduction and 9◦ in flexion, **Chan-tsungyang, et. al.2009,** as shown in **Fig.7** showed the fixation of Charnley type **Tables 4, 5** shows comparison between numerical and experimental results

6. RESULTS

In **Figs. 8, 9** different head and diameter (22mm,26mm) respectively were shown and it is clear from this figure that the position of maximum effective stress for both sizes was the same , where increasing head diameter lead to increase maximum effective stress by (16%), this is due to the shifting of load position which increases the moment on the weakest part. The effective stress for Charnley design with (a) 32mm neck length and (b) 40mm neck length, shown in **Fig. 10,11.** certainly increasing neck length will lead to increase maximum effective stress and that is clear from this figure. Increasing neck length from 32mm to 40mm lead to increase the maximum effective stress by (1.5%) it is small value compared with increasing head diameter or increasing stem length. It should be noted that increasing neck length lead to increase the effective stress at necking section by (32%). The effect of varying two neck ratio ((a) 0.5, (b) 0.8) is shown in **Figs. 12, 13,** respectively, it's clear to be noted that increasing neck ratio is not effected with large amount on maximum effective stress where increasing neck ratio from (0.5 to 0.8) didn't change the maximum effective stress at stem more than (3%), but decreases the effective stress at neck by (28%), this is due to reduction in stress concentration at necking section.

Figs. 14, 15. show the effective stress for Charnley design with stem length (a) 110mm (b) 140 mm, from figure the maximum effective stress is at the same position for both stem sizes with different values where maximum effective stress increased by (16%) with increasing stem length. This is due to the reduction in cross sectional area of the loaded section with increasing stem length.

7. DISCUSSION

Fig. 16 shows the variation of effective stress with respect to changing the head diameter , the relation theme gives indication that with increasing the head diameter the effective stress in weaken part of hip prosthesis will increase and this relation may be caused by the sweeping of load position in vertical direction due to increase the head diameter, this sweeping of load position lead to increase moment at weaken part and thus will increase the stress. The change in effective stress values while head diameter increased from(20mm to 26mm) with step of 2mm was not more than (73Mpa) except head diameter of 22mm where change in effective stress reached to (121Mpa).

Fig. 17 shows the variation of effective stress with changing of neck ratio(neck ratio: represent the position of necking part with respect to total neck length),the chart theme shows that it should take into account while designing to make the neck ratio more than 0.5 as possible to decrease the force arm on neck where this may prevent the fracture at neck and lead to decrease the stress at weaken region of hip prosthesis so it should take into consideration to make balancing of changing this factor and it is clear that changing of stress is not more than (42Mpa)

for changing this parameter from (0.5 to 0.8).Except neck ratio of (0.6) where change in effective stress reached to (97MPa).

Fig. 18 shows the variation of effective stress with respect to changing the third design parameter that is the stem length and so due to this point it is clear to most biomedical researchers and (Depuy-synthes) manufacturing companies, that produced medical orthotropic products, to reduce the stem length as possible to prevent the increasing in stress where this increasing in stress may be caused by three reasons the first one is by increasing stem length the overall mass of system with axial axis of hip prosthesis will increase, the second reason is increasing the stem length lead to increase the free part of the fixed hip prosthesis according to (ISO_7204 standard modified in 2002) and that lead to increase the bending stress in weaken part. Second thing is increasing the weight of free part of fixed hip prosthesis. The third reason is increasing stem length lead to decrease the stem cross sectional area to be loaded; this decreasing in stem cross sectional area is due to curvature shape of stem. The change in effective stress while stem length increased from (110mm to 140mm) was not more than (209Mpa) except stem length of (130mm) where change of effective stress reached to nearly (245Mpa)so the stem length of (130mm) and what is nearest to this value should be averted while designing stem.

Fig. 19 shows the variation of effective stress in weaken part of hip prosthesis (at stem) with changing the neck length and it is clear that increasing neck length lead to increase the effective stress due to increase the arm of force where that leads to increase the stress. In this study five sizes of neck length had been used, and it turned out that changing of neck length from(110mm to 140mm) lead to change the effective stress with value more than (53Mpa) except neck length of (36mm),(32mm) where change jumped to (73Mpa).

8. CONCLUSIONS

1. It is found that changing in stem length lead to increase the effective stress with values higher than the other designs parameters so it should be taken in account this parameter because of its heavy influence on effective stress so for Charnley design the stem length should be decreased as possible, under cases of impact load. Changing in effective stress not exceeded (22%).
2. It is found that the changing in head diameter had an influence on effective stress values but with small amount as compared with stem length, where changing in effective stress not exceeded (16%).
3. It is found that the increasing of the neck length for Charnley design lead to increases effective stress with values less than stem length where changing in effective stress not exceeded (5.5%). So that it must be decreased as possible, where increasing neck length lead to increase maximum effective stress.
4. The effect of the ball radius on both contact pressure and total contact stress is larger than that on the effective stress. Where changing in contact pressure not exceeded (41%), and changing in total contact stress not exceeded (32%).
5. It is found that increasing the neck ratio had an effect on the effective stress, where changing in effective stress not exceeded (7%).

6. It is found that the best sizes of low effective stress with these dimensions (head diameter of 22mm, 0.6 neck ratio, stem length of 110mm, neck length of 24mm) can be considered as safest sizes.

REFERENCES

- A. Zafer Senalp , Oguz Kayabasi, Hasan Kurtaran, 2007, *Static and Dynamic and Fatigue Behavior of Newly Designed Stem Shapes for Hip Prosthesis Using Finite Element Analysis*, Materials and Design, vol.28, No.4 pp. 1577–1583.

- Chan-tsungyang, hung-wen wei,hung-and chankao,cheng-kung cheng, 2009, *Design and Test of Hip Stem or Medullary Revascularization*, Medical Engineering and Physics, vol.21, No.3 ,pp.994-1001.

- H.F. El'Sheikh, B.J. MacDonald, M.S.J. Hashmi, 2003, *Finite Element Simulation of The Hip Joint During Stumbling: a Comparison Between Static and Dynamic Loading*, Journal of Materials Processing Technology vol.144, No. 2, pp. 249–255.

- Mamdouh M. Monif, 2012, *Finite Element Study on The Predicted Equivalent Stresses in The Artificial Hip Joint* , IVSL/ J. Biomedical Science and Engineering, vol.5, No.2, pp.43-51.

- Release 14.0 Documentation for ANSYS, Elements Reference, Part I, Element Library.

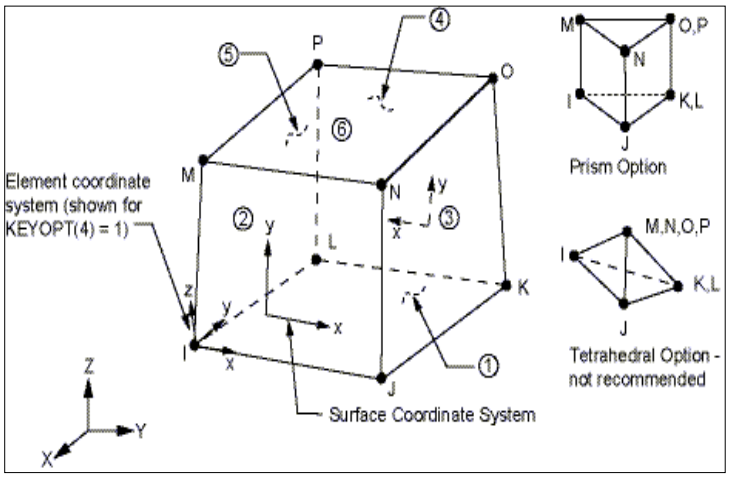

Figure 1. Solid45 geometry.

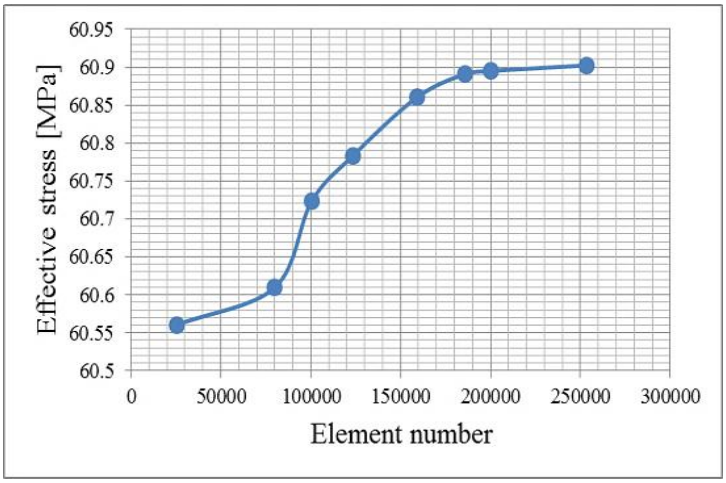

Figure 2. Convergence test.

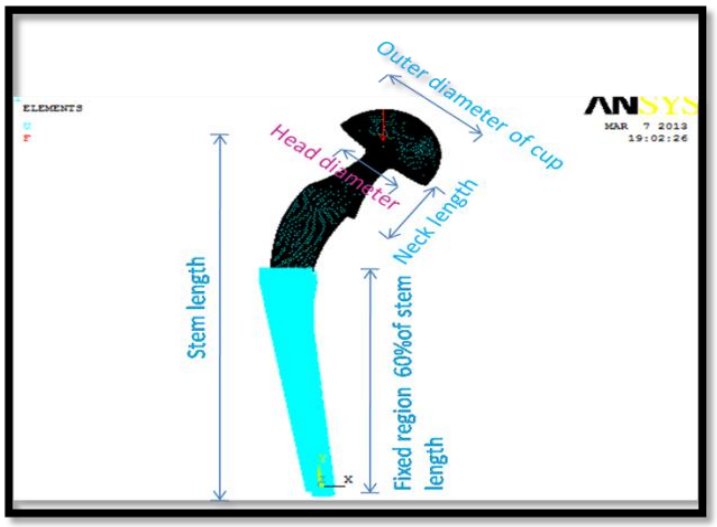

Figure 3. Design parameters and boundary condition, Charnley.

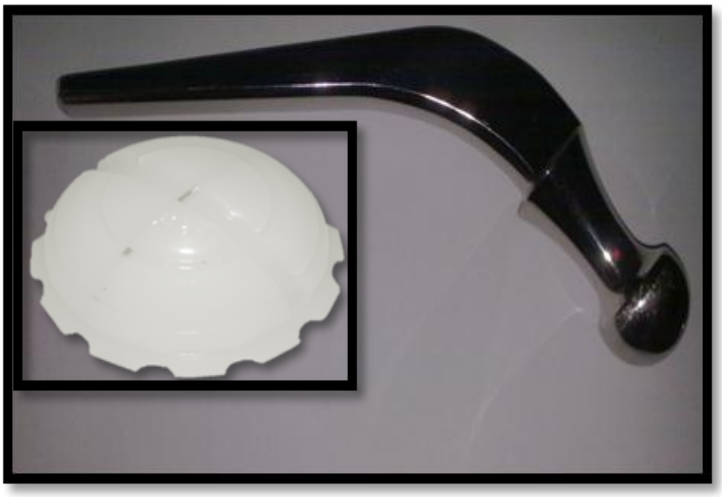

Figure 4. Charmly hip prosthesis, upper view of white acetabulum part (cup), femoral part(stem).

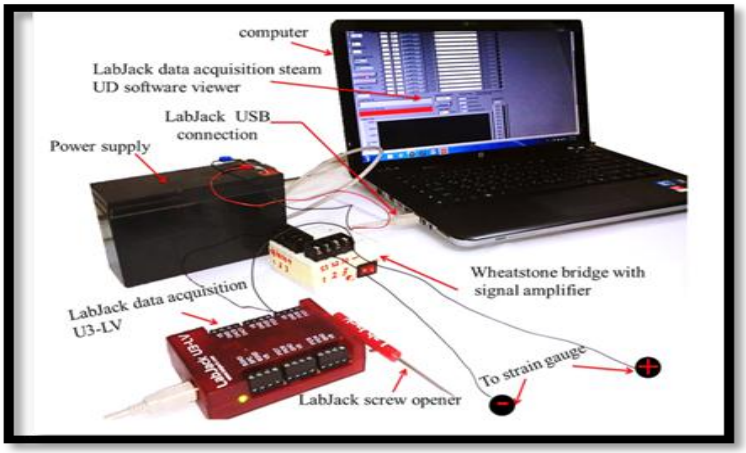

Figure 5. Interface circuit .

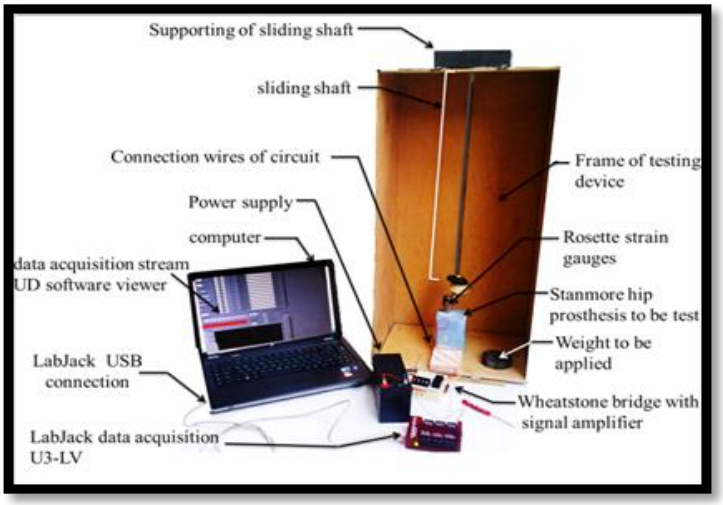

Figure 7. Structure of testing device.

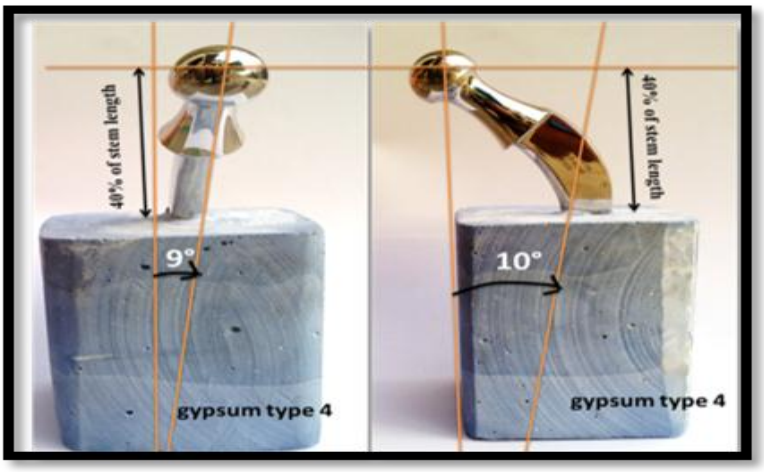

Figure 7. Fixation of hip prosthesis according to ISO-7206 standard where: a- fixation of Charnley hip prosthesis.

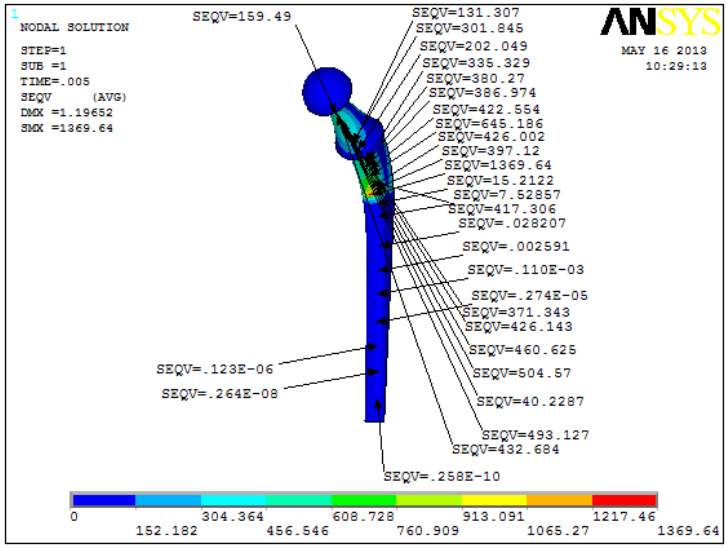

Figure 8. Charnley model effective stress 22mm head diameter.

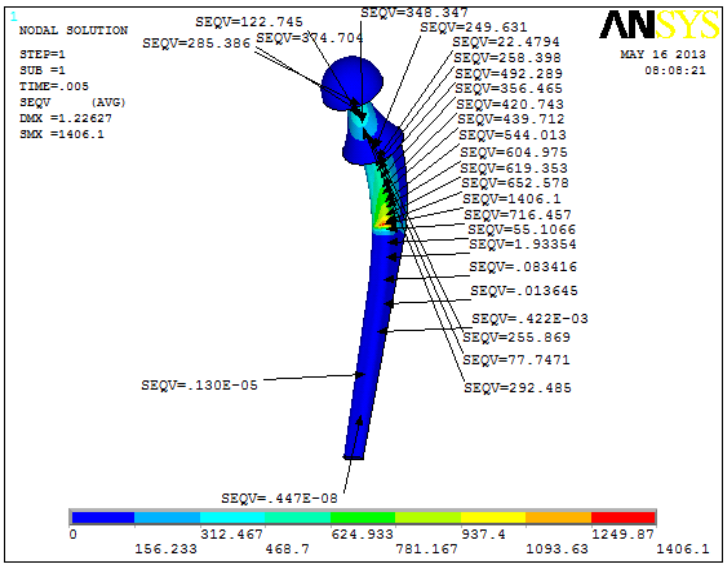

Figure 9. Charnley model effective stress 26mm head diameter.

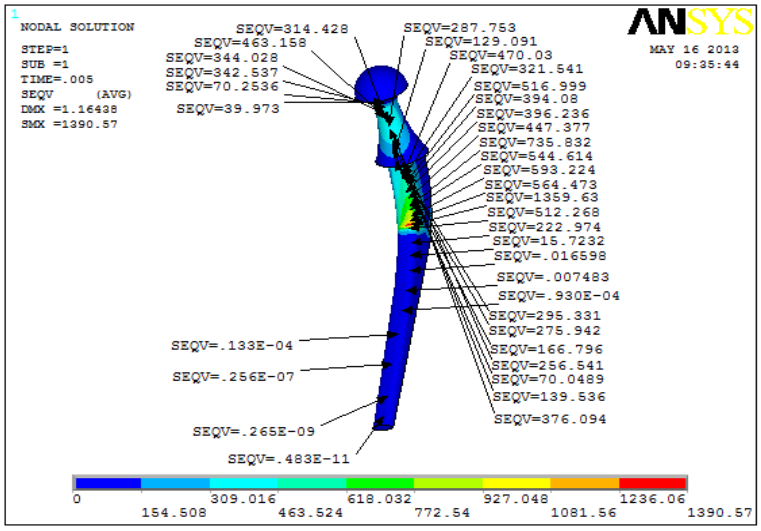

Figure 10. Charnley model effective stress 32 mm neck .lengths.

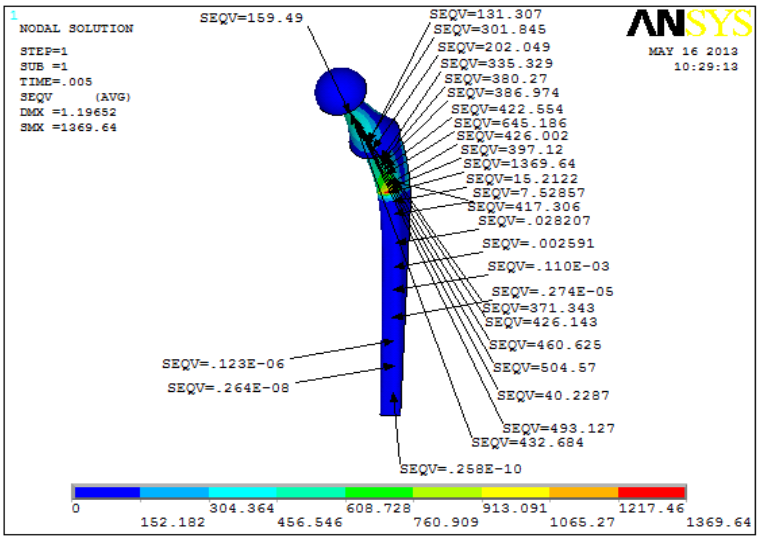

Figure 11. Charnley model effective stress 40 mm neck length.

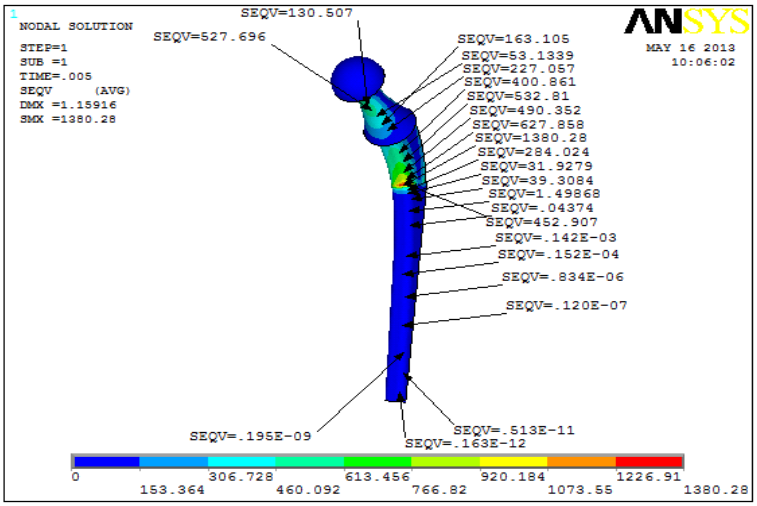

Figure 12. Charnley model effective stress 0.5 neck ratio.

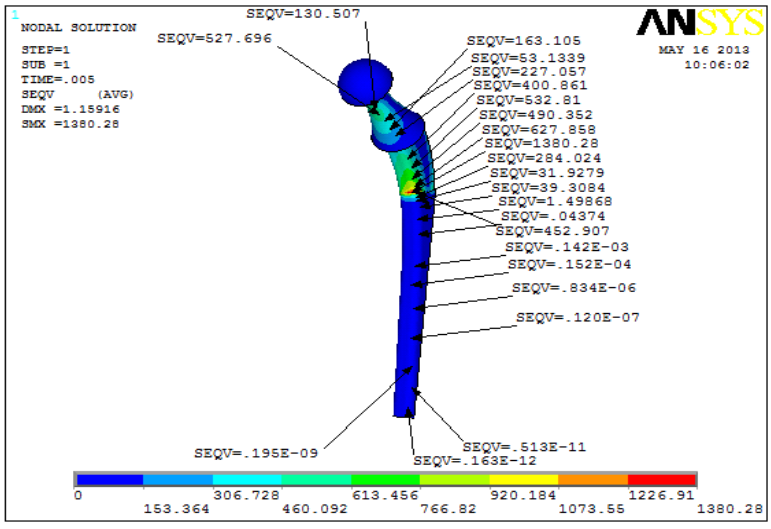

Figure 13. Charnley model effective stress 0.8 neck ratio.

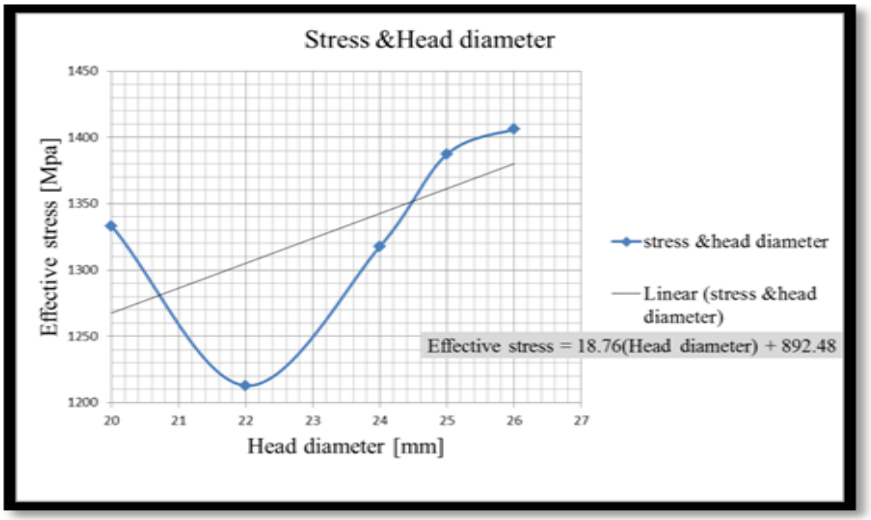

Figure 14. Charnley model effective stress 110 stem length.

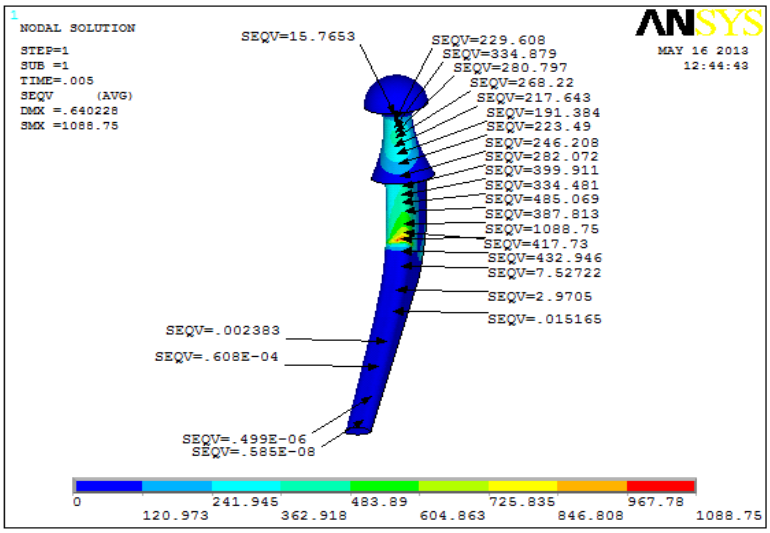

Figure 15. Charnley model effective stress 140 stem length.

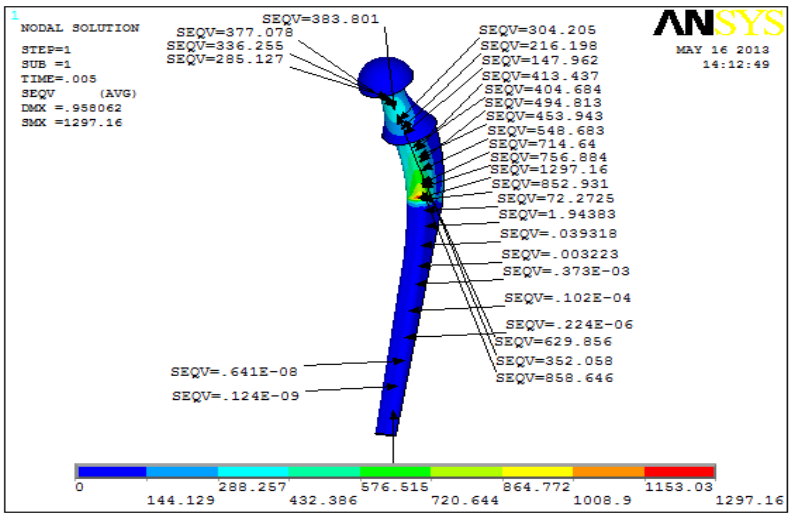

Figure 16. Variation of effective stress of Charnley model with changing head diameter.

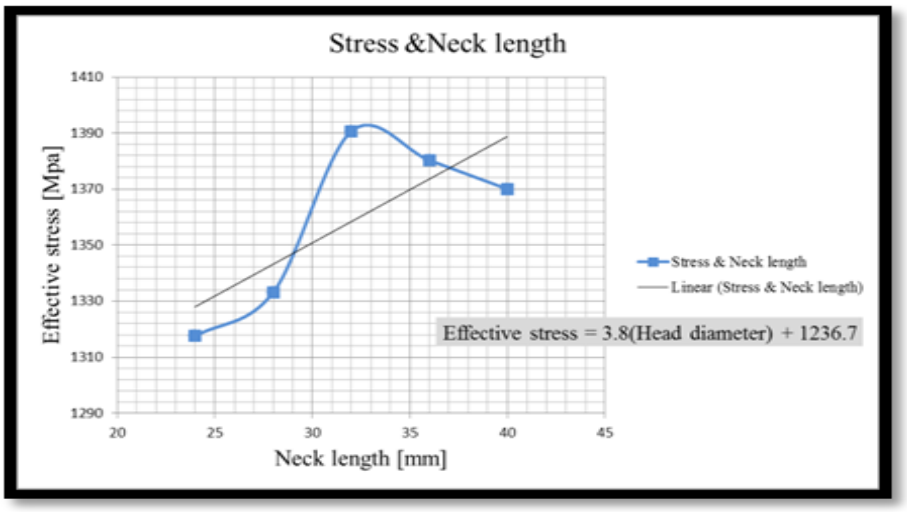

Figure 17. Variation of effective stress of Charnley model with changing neck

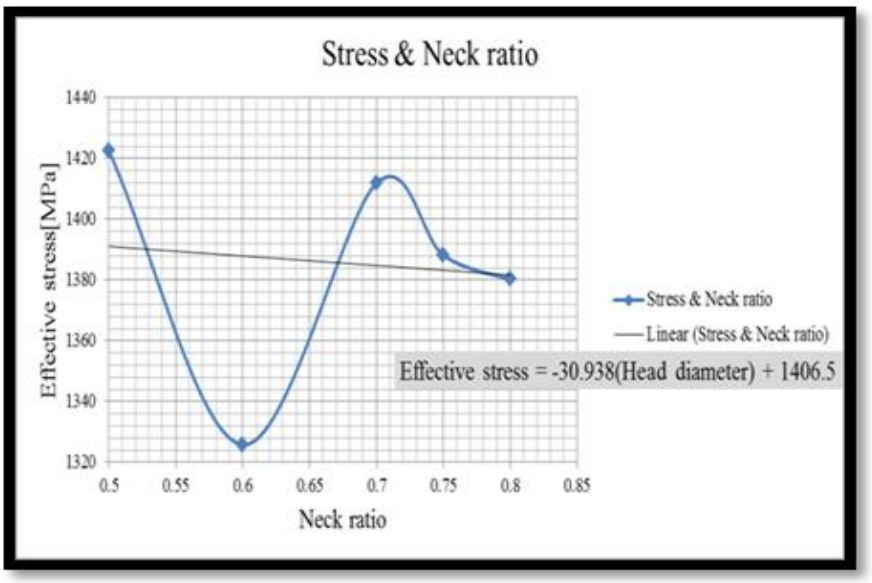

Figure 18. Variation of effective stress of Charnley model with changing stem length.

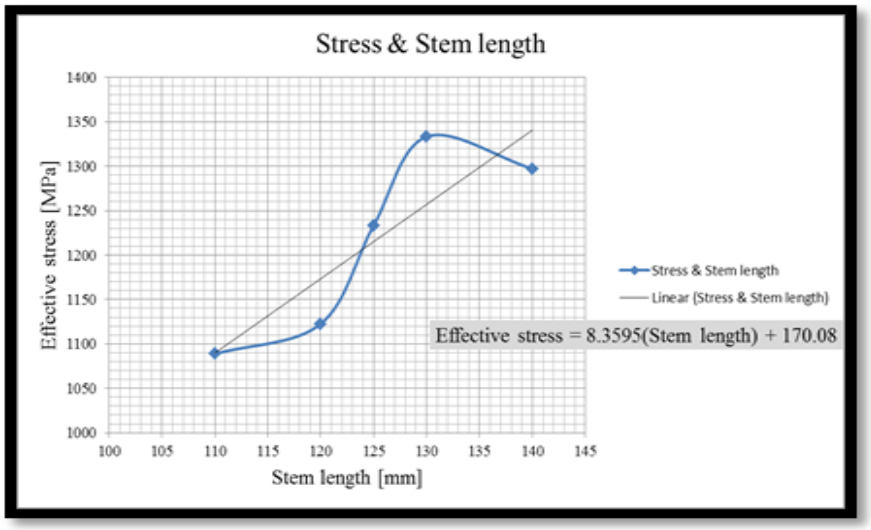

Figure 19. Variation of effective stress of Charnley model with changing neck length.

Table 1. Material properties.

Material	Young's Modulus (GPa)	Poisson's Ratio (v)	Density (g/ cm^3)
Stainless steel	193	0.32	8
UHMWPE	1.2	0.4	0.945

Table 2. Dimensions of Charnley model.

Head Diameter (mm)	Neck Length (mm)	Neck Ratio (mm)	Stem Length (mm)
20	24	0.5	110
22	29	0.6	120
24	32	0.7	125
25	34	0.75	130
26	40	0.8	140

Table 3. Comparison between experimental and numerical results for Charnley design .

Height of Load Dropping (cm)	ANSYS Effective Stress (MPa)	Experimental Effective Stress(MPa)	Error Percent (%)
10	12.15	11.056	9
20	17.183	15.842	7.8
30	21.8131	20.046	8.1

Structural Behavior of Reinforced Concrete Hollow Beams under Partial Uniformly Distributed Load

Ahmad Jabbar Hussain Alshimmeri
Instructor
Engineering College - Baghdad University
E-mail: dr.ahmadalshimmeri@yahoo.com

Hadi Nasir Ghadhban Al-Maliki
Instructor
Engineering College - Mustansiriya University
E-mail: hadi_gahdban@yahoo.com

ABSTRACT

A Longitudinal opening is used to construct hollow core beam is a cast in site or precast or pre stressed concrete member with continuous voids provided to reduce weight, cost and, as a side benefit, to use for concealed electrical or mechanical runs. Primarily is used as floor beams or roof deck systems. This study investigate the behavior of six beams (solid or with opening) of dimension (length 1000 x height 180 x width120mm) simply support under partial uniformly distributed load, four of these beam contain long opening of varied section (40x40mm) or (80x40mm). The effect of vertical steel reinforcing, opening size and orientations are investigated to evaluate the response of beams. The experimental behavior based on load-deflection measured at central and quarter of tension zones. The experimental test result shows the presence of Hollow decrease the load carrying capacity by about (37.14% to 58.33%) and increased the deflections by about (71.6% for (Hollow ratio 7.4%) to 75.5% for (Hollow ratio 14.8%)) for same applied load compared with solid beams with the same properties. The increase shear steel reinforcing will decrease all the deformations at all stages of loading, but particularly after initial cracking and give enhancement in ultimate load capacity of beams by about 31.5% with increasing the amount of shear steel reinforcing by about 50%. Finally, ductility is increased in all cases under partial uniformly distributed load when hollow ratio decreased by about 50% or increased in shear steel reinforcing by about 50%.

Key words: longitudinal opening, shear reinforcing, first crack, deflection, hollow ratio.

السلوك الإنشائي للعتبات الخرسانية المسلحة المجوفة تحت حمل موزع بانتظام جزئياً

احمد جبار حسين الشمري
مدرس
كلية الهندسة - جامعة بغداد

هادي ناصر غضبان المالكي
مدرس
كلية الهندسة - الجامعة المستنصرية

الخلاصة

الفتحات الطولية تستعمل لتكوين عتبة مجوفة مصبوبة موقعيا" أو مسبقة الصب أو مسبقة الإجهاد ومستمرة الفراغات مع العضو الخرساني وذلك لتخفيف الوزن وكذلك الكلفة والفائدة الرئيسية هو لتمرير الخدمات الكهربائية والميكانيكية . الاستعمال الرئيسي هو كعتبات الطوابق او أنظمة السقوف. هذه الدراسة تحرت سلوك ست عتبات خرسانية مسلحة (صلدة او مجوفة) وبأبعاد (الطول 1000 ملم والارتفاع 180ملم وعرض 120 ملم) بسيطة الإسناد تحت تأثير الحمل الجزئي الموزع بانتظام، أربعة من النماذج مجوفة وبأبعاد تجويف مختلفة (40*40 ملم او 40*80 ملم). تم دراسة تأثير نسبة التسليح العمودي ونسبة الفتحة واتجاهها لتقييم استجابة العتبات من الناحية العملية بالاعتماد على علاقة الهطول - الحمل المقاس في مركز وربع الطول تحت منطقة الشد. نتائج الفحص العملي بينت ان وجود التجاويف (الفتحات الطولية) في العتبات

الخرسانية تقلل قابلية التحمل لها بمقدار حوالي (37.14% إلى 58.33%) وتزيد في الهطول بمقدار (71.6% الى 75.5% لنسبة تجويف مقدارها 7.4% و 14.8%على التوالي) لنفس الحمل المسلط وبالمقارنة مع العتبات الصلدة ولنفس الخصائص الأخرى, كذلك زيادة حديد القص يقلل كل التشوهات في كل مراحل التحميل ولكن عملياً بعد التشقق الأولي وتعطي تحسين في قابلية التحمل للعتبات بمقدار 31.5% مع زيادة حديد القص بمقدار 50%. أخيرا" المطاوعة تزداد في كل الحالات تحت تأثير الحمل الموزع بانتظام عند نقصان نسبة التجويف بمقدار 50% أو زيادة حديد القص بمقدار 50 %.

1. INTRODUCTION

Many parameters may influence the overall hollow girder response such as: the shape of the section, the amount of the longitudinal and transverse reinforcement, the cross section thickness, load ratio and finally the material strength of concrete and reinforcement, **Alnuaimi, 2003** and **Mander, 1984**. This study focuses on rectangular hollow cross sections and investigates the beams behavior under a state of uniformly distributed loading

2. ADVANTAGE OF HOLLOW CROSS SECTION

The advantages of hollow cross section , **Nimnim, 1993**.

1. Reduced the weight, which affects especially the cost of transport, handling and erection for pre-cast cross sections.
2. Substantial reduction of material quantities, the materials required are usually much less than those needed for other conventional systems and they are little more than those required for continuously curved shells, with the advantage of utilizing relatively simple formwork.

3. OBJECTIVE OF THE RESEARCH

The main target of this research is studying the effect of different amount of shear reinforcement (stirrup) and hollow ratio of cross section on the strength and behavior of hollow cross section beams subject to partial distributed load and also studying load deflection behavior which occurs at the center and quarter of span length of beams.

The variables which taken in this research are: stirrups (shear reinforcement, hollow and solid section with thickness of walls for hollow section.

It's expected in this research to state the influence of distributed load on the strength and behavior of hollow cross section beam and comparison between experimental tests result of specimens and confirm the best specimens with hollow section which result the nearest value to the solid section result.

Finally studying the factors that affect the behavior of reinforced concrete beams under partial uniformly distributed load which have directly relation with the (stirrup reinforcement and dimension of sections).

4. EXPERIMENTAL WORK

4.1 Scope of Work

In order to study the structural behavior and ultimate strength of reinforced concrete beam under partial uniformly distributed load, which can be used as rectangular hollow cross section. A total of six specimens in four groups, detailed as shown in **Table 1**, were cast in plywood forms. All the beams were made from a single mix proportion (Cement: Sand: Gravel) of 1:1.5:3 by weight with a water/cement ratio 0.45 and also all beams were designed to have the same longitudinal and varied stirrup reinforcing. Each of the mixtures was thoroughly mixed prior to casting. The beams details, mix proportion, materials properties and formwork given in **Tables 1,**

2, 3 and 4, and **Figs. 1,2** and **3** respectively.

4.2 Considered Parameters

In the present investigation, four group parameters were adopted to study the behavior and ultimate load of beams and to investigate the influence of hollow ratio, shear reinforcing in concrete beams when subjected to uniformly distributed load. All beam details are shown in Table 1.

Group 1: Consists of one solid specimen with dimension (120, 180) mm, length (1000 mm), longitudinal bars (3-Ø12mm) with stirrups of (Ø10mm @ 100 mm c/c).

Group 2: Consists of one solid specimen with dimension (120, 180) mm, length (1000 mm), longitudinal bars (3Ø10 mm) with stirrups of (Ø10 mm @ 50 mm c/c).

Group 3: Consists of two hollow specimens, all properties as same in group 1, but with different hollow section (40x40 mm and 40x80 mm). Group 4: Consists of two hollow specimens, all properties as same in group 2, but with different hollow section (40x40 mm and 40x80 mm).

5. TEST RESULTS OF REINFORCED CONCRETE BEAMS

A partial uniformly distributed load (i.e. loaded length 120mm which equal to 13.34% of span length) was provided using universal testing machine of capacity (3000 kN) applied at the center of the beam gradually at increments of (5 kN) up to failure. Test results for each case, including deflections and cracking are highlighted. Load versus deflection was recorded at point of (central and quarter of span length) at distances about (500 and 250 mm) from the edges of the beam. Arrangement specimens of partial uniformly distributed loading and instrumentation as shown in **Figs. 4 and 5**. Crack patterns, first crack load and propagation of cracks are also studied. Ultimate load capacity and failure modes are recorded as shown in **Table 5**. A study of the effect of vertical shear reinforcement and section type (solid or hollow), was carried out. Deflections, crack patterns at all stages of loading of the reinforced concrete beam were also discussed.

6. CRACK PATTERNS

The first crack was found to develop around the sides of the loading area of ($120mm^2$) on the tension fiber of the beam center. These cracks were formed at about (8.0 – 11.5%) of the ultimate failure load, as shown in **Table 5**. In the case of beams with hollow section cracks appear in the tension zone of the beam near one or more of the corners as shown in Table 5. The ultimate load, maximum central deflection were recorded and given in **Table 5**. As the load is increased after formation of the first crack, more cracks begin to appear and, propagated diagonally towards the corners of applied load (i.e. under position of applied load). At high loads, these cracks extended with the formation of new cracks at different orientations. Meanwhile, cracks start to appear around the edge of the applied load at tension zone.

Failure was distinguished by the successive deflections at the center of the beam at higher load levels through shear and wide flexural cracks at the tension zone, then, yielding of the tensile reinforcing steel. All beams were tested up to failure. The crack pattern zone of each reinforced concrete beam was painted with concrete color this allows the cracks to be visible and the failure can be pointed as shown in **Figs. 6 to 11**.

7. DEFLECTION MEASUREMENT

For all tested beams, deflections were measured at a distance of (500mm and 250 mm) from the ends of beams at the bottom surface. The deflections occur at these locations were measured to compare response.

Deflection measures may give a reasonable interpretation of the load carrying capacity of the beams. The load-deflection curves for six tested beams under applied loads are shown in **Figs. 12 to 16**, While the comparison of deflection for all beams at quarter and central location as show in **Figs. 17 and 18** for the cases of beam solid or hollow section. While, these curves demonstrate a certain tendency in which, at early stages of loading (elastic stage), the deflection-load relation is linear up to the first cracking load. After this, new cracking start and continuous up to the first yielding; these are flexural cracking. Beyond first yielding plastic deformations continuous and yielding up to failure at a stress near the ultimate flexural strength, as calculated by the yield line theory. In this stage, yielding of the tension reinforcement spreads from the loaded area towards the beam edges. Finally (stage of failure) a plastic stage of rapidly increasing deflection at no additional load application.

Tests of all beams demonstrated that the ultimate load becomes smaller as the beam varied from solid to Hollow by about (37.14% to 58.33%). Also ultimate load increases as shear reinforcement ratio increases. The deflections of the beams at both points (A and B) increase when the beam varied from solid to hollow section (71.6% (hollow ratio of 7.4%) to 75.5% (hollow ratio of 14.8%)) for the same applied load compared with solid beams with the same properties and noticed smaller values when increased shear reinforcing as shown in Table 5. In general R.C. beams those are solid or hollow with more shear reinforcing show higher load carrying capacity with reduction in deflection values. Finally the deflection varied along of all tested specimens at loading stages are shown in **Figs. 19 to 24**.

8. CONCLUSION

In this study it has become to study the behavior and strength of hollow concrete beams under partial uniformly distributed load was investigated. From an experimental program the following conclusion were drawn:

1- It has been observed from the tests carried out that the slope of main cracks under partial uniformly distributed load for reinforced concrete beam is about 45^{o}.

2- As per the result of tested, some of concrete beams fails under flexural failure and other compound failure (i.e. shear and flexural failures) when the crack constructed at flexural zone or flexural and near support under load.

3- The presence of hollow recess in reinforced concrete beams was found to decrease the load carrying capacity by about (37.14% to 58.33%) and increase the deflections by about (71.6% (hollow ratio 7.4%) to 75.5% hollow ratio (14.8%)) for same applied load compared with solid beams for same properties.

4- When increasing the hollow ratio from (7.4% to 14.8%) the load carrying capacity is decreased and deflection is increased by about (28.5% and 14%) respectively for same other properties.

5- Shear steel reinforcement decreased all the deformations at all stages of loading, particularly after initial cracking.

6- Ductility is increased in all cases for partial uniformly distributed load when decreased Hollow ratio by about 50% or increased in steel reinforcing.

7- The phenomenon of crushing concrete cover (Spalling down) was avoided when increased the shear steel reinforcing by about 50% in the reinforced concrete beam under partial uniformly distributed load.

9. REFERENCES

Abbas, N. J., 2000 , *Structural Behavior of Ferrocement Box-Beam,* Deploma, Research, University of Technology.

ACI 318M – 11, 2011, *Building Code Requirements for Reinforced Concrete,* ACI Committee 318M.

Alnuaimi, A.S., 2003, *Parametric Study on the Computational Behaviour of Hollow Beams Designed Using the Direct Design Method - Numerical Factors,* Proceedings of International Conference on Advances in Structures, ASSCCA'03, Sydney, Australia, A.A., 22-25 June, Balkema Publishers, Vol. 2, pp. 1017 - 1021.

Alnuaimi, A.S., 2002, *Parametric Study on the Computational Behaviour of Hollow Beams Designed Using the Direct Design Method - Material Factors,* Proceedings of High Performance Structures and Composites, Seville, Spain, WIT Press Publishers, March, pp. 605-614.

British Standard Institution (BS 8110), 1997, *Code of Practice for Design and Construction,* British Standard Institution Part 1, London.

Mander J.B. ,1984, *Experimental Behavior of Ductile Hollow Reinforced Columns*, In Proceedings, 8th World Conference on Earthquake Engineering, Vol. 6, pp. 529-536.

Nilson, A. H. , Darwin, D. and Dolan, C. W., 2006, *Design of Concrete Structure* McGraw-Hill Book Company.

Nimnim, H. T., 1993, *Structural Behavior of Ferrocement Box-Beams,* M.Sc., thesis, University of Technology.

Oehlers, D. J., and Bradford, M. A., 1995, *Composite Steel and Concrete Structural Members*, Kidlington, Oxford, U.K.: Elsevier Science, Ltd.

Takahashi Y., Iemura H., 2000 *Inelastic Seismic Performance of RC Tall Piers with Hollow Section*, In Proceedings, 12th World Conference on Earthquake Engineering, ref. 1353.

Table 1. Details of reinforced concrete beams specimens.

Specimen Symbol	Bottom Reinforcing	Top Reinforcing	Stirrups Reinforcing	Hollow Ratio	Section Property
B1	3 Ø 12 mm	2 Ø 12 mm	Ø10@100 mm	---	Solid
B2	3 Ø 12 mm	2 Ø 12 mm	Ø10@ 50 mm	---	Solid
B3	3 Ø 12 mm	2 Ø 12 mm	Ø10@100 mm	7.4%	Hollow
B4	3 Ø 12 mm	2 Ø 12 mm	Ø10@ 50 mm	7.4%	Hollow
B5	3 Ø 12 mm	2 Ø 12 mm	Ø10@ 50 mm	14.8%	Hollow
B6	3 Ø 12 mm	2 Ø 12 mm	Ø10@100 mm	14.8%	Hollow

Table 2. Mix proportions for (1 m^3) of concrete (1: 1.5: 3) by weight.

Cement (kg/m^3)	Sand (kg/m^3)	Gravel (kg/m^3)	Water/Cement Ratio	Water (kg/m^3)
400	590	1180	0.45	180

Table 3. Properties of steel reinforcement.

Nominal Diameter (mm)	Measured Diameter (mm)	A_s (mm^2)	Yield Stress f_y (MPa)	Tensile Strength f_u (MPa)
10	9.88	76.67	421	520
12	12.2	116.89	480	570

Table 4. Compressive strength of concrete cylinder (150 x 300 mm) (28 days).

Sample No.	Strength (MPa)	Average Strength (MPa)
1	29.43	
2	28.41	
3	27.73	28.52

Figure 1. Moulds of reinforced concrete solid and hollow reinforced concrete beams.

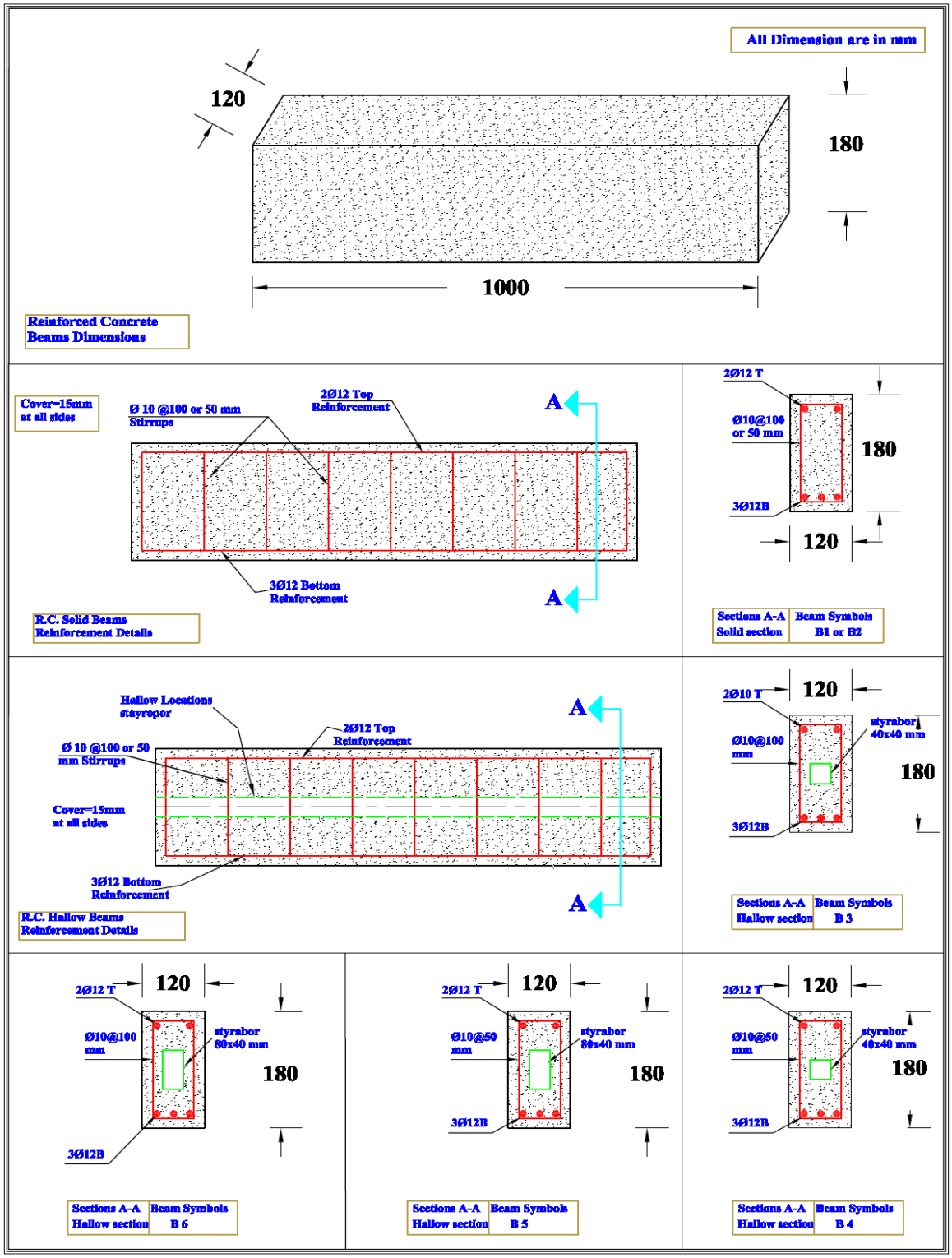

Figure 2. Cross-section & longitudinal shape of the beam.

Figure 3. Recess through section of hollow beams.

Figure 4. Beams under partial uniformly distributed loading.

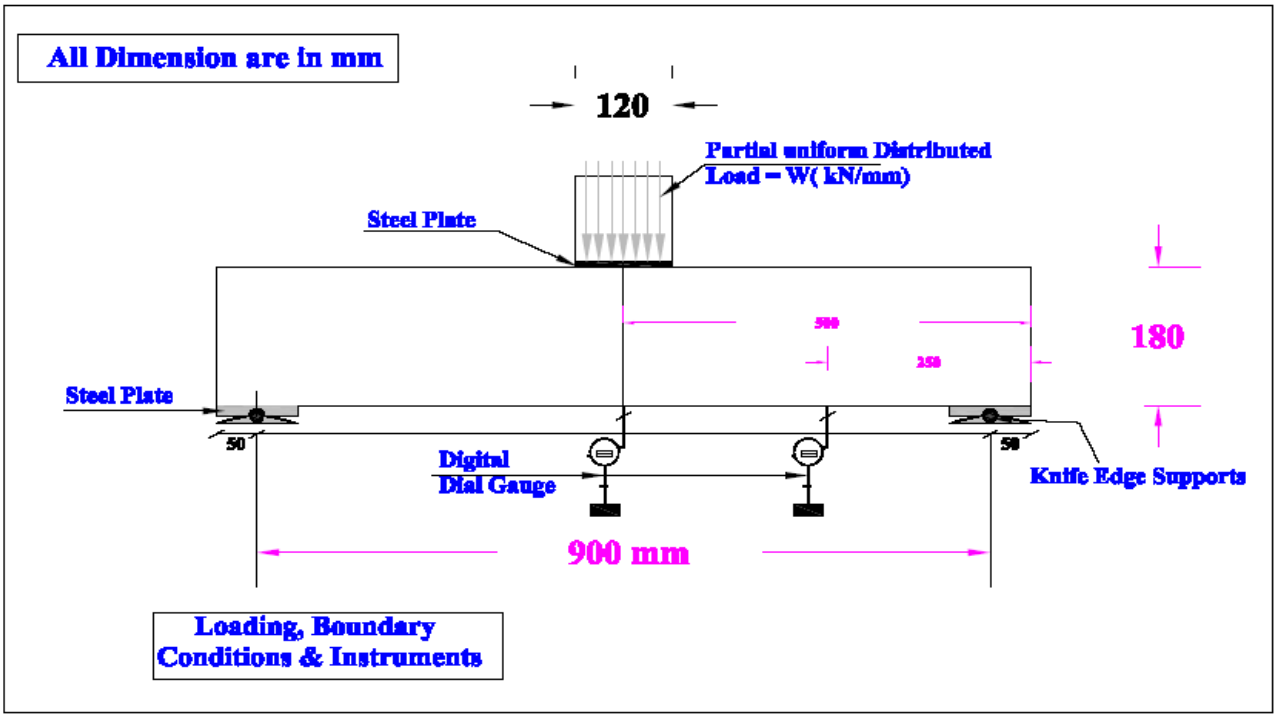

Figure 5. Arrangement specimens of partial uniformly distributed loading and instrumentation**.**

Table 5. First crack, ultimate load and deflections.

Beam No.	Beam Section	Shear Reinforcing	Hollow Ratio %	First Crack Load (Wcr) (kN/m)	Ultimate Load (Wu) kN/m	Central Deflection (mm)	Wcr / Wu %
B1	Solid	Ø10@100 mm	---	5.0	60.0	3.32	8.3
B2	Solid	Ø10@50 mm	---	10.0	87.5	3.72	11.5
B3	Hollow	Ø10@100 mm	7.4	4.0	40.0	5.70	10.0
B4	Hollow	Ø10@50 mm	7.4	5.0	55.0	8.08	9.0
B5	Hollow	Ø10@50 mm	14.8	3.0	35.0	5.69	8.5
B6	Hollow	Ø10@100 mm	14.8	2.5	27.0	4.3	9.2

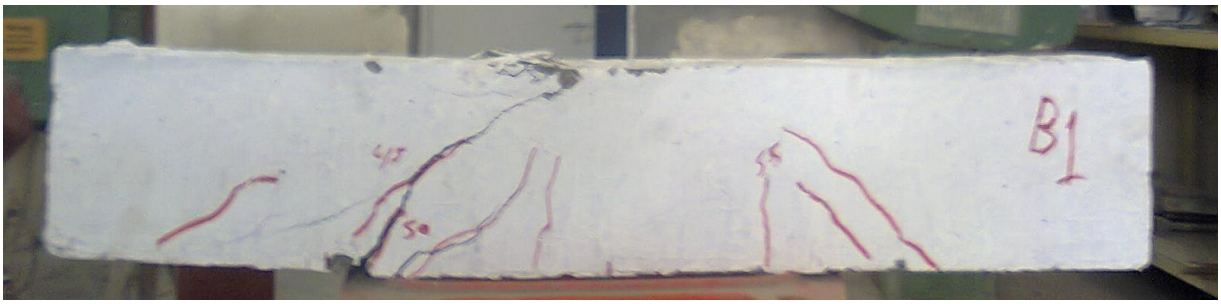

Figure 6. Crack patterns of beam (Solid) B1.

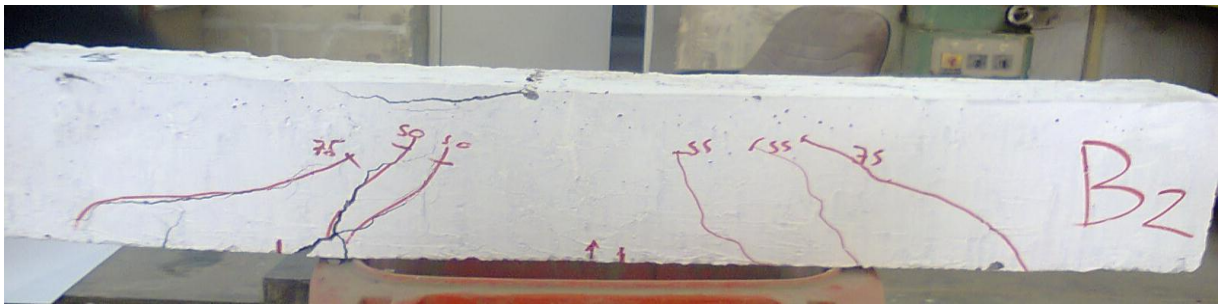

Figure 7. Crack patterns of beam (Solid) B2.

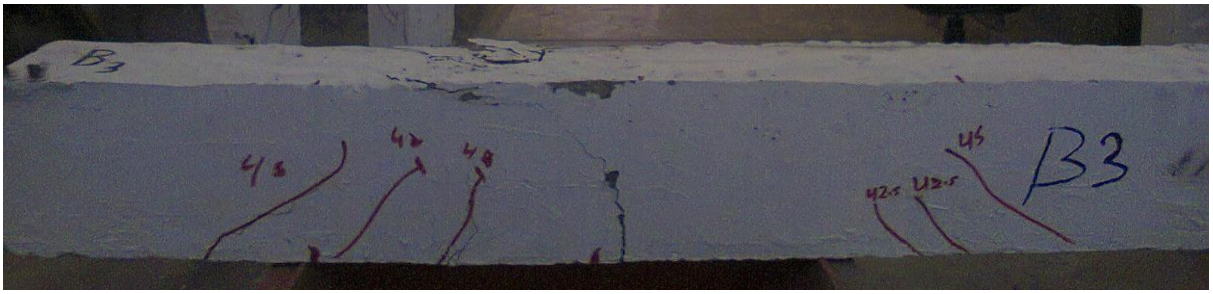

Figure 8. Crack patterns of beam (Hollow) B3.

Figure 9. Crack patterns of beam (Hollow) B4.

Figure 10. Crack patterns of beam (Hollow) B5.

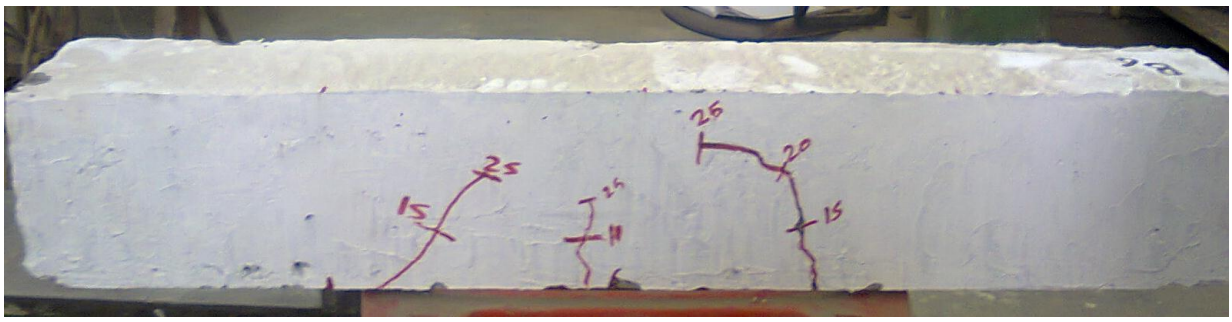

Figure 11. Crack patterns of beam (Hollow) B6.

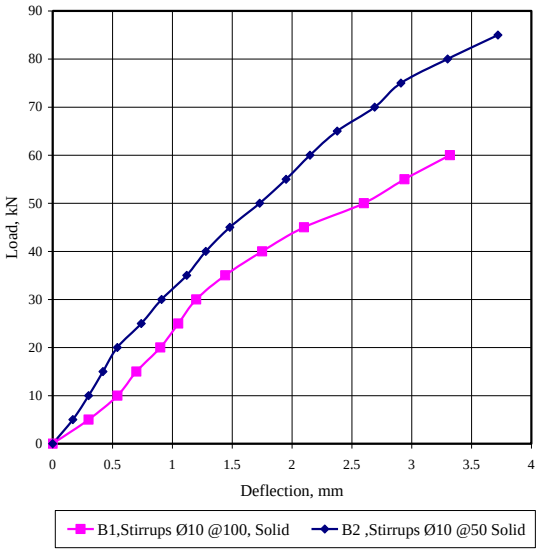

Figure 12. Comparison of central deflection of beams B1 & B2.

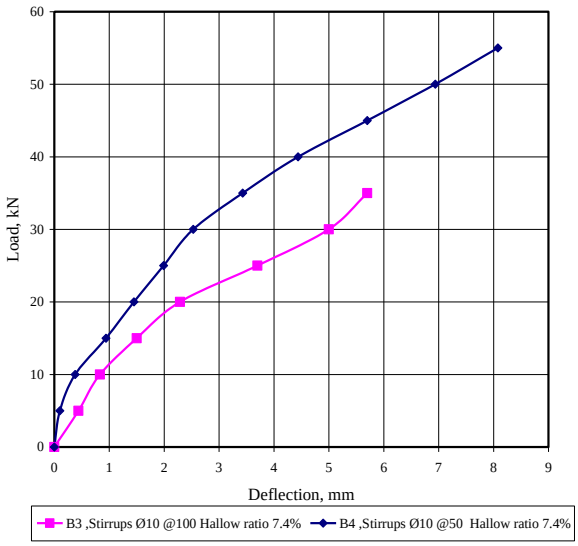

Figure 13. Comparison of central deflection of beams B3 & B4.

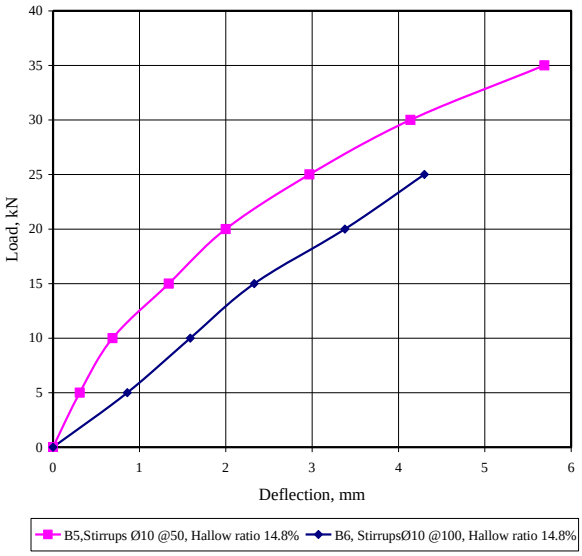

Figure 14. Comparison of central deflection of beams B5 & B6.

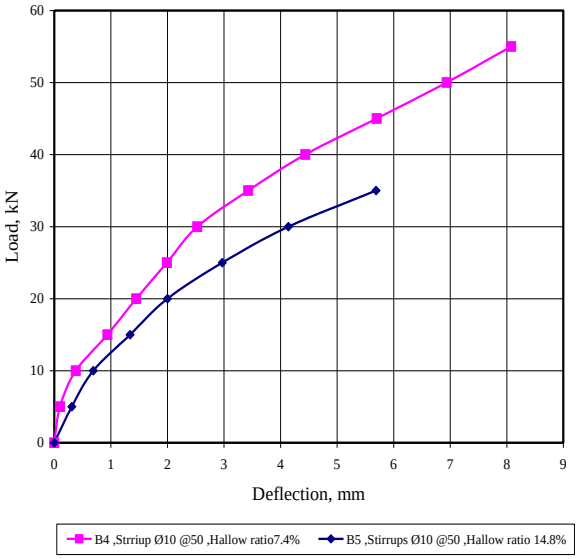

Figure 15. Comparison of Central Deflection of Beams B4 & B5.

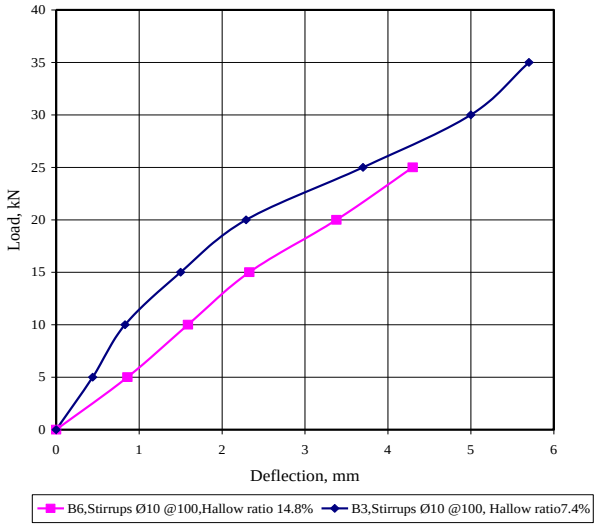

Figure 16. Comparison of central deflection of beams B6 & B3.

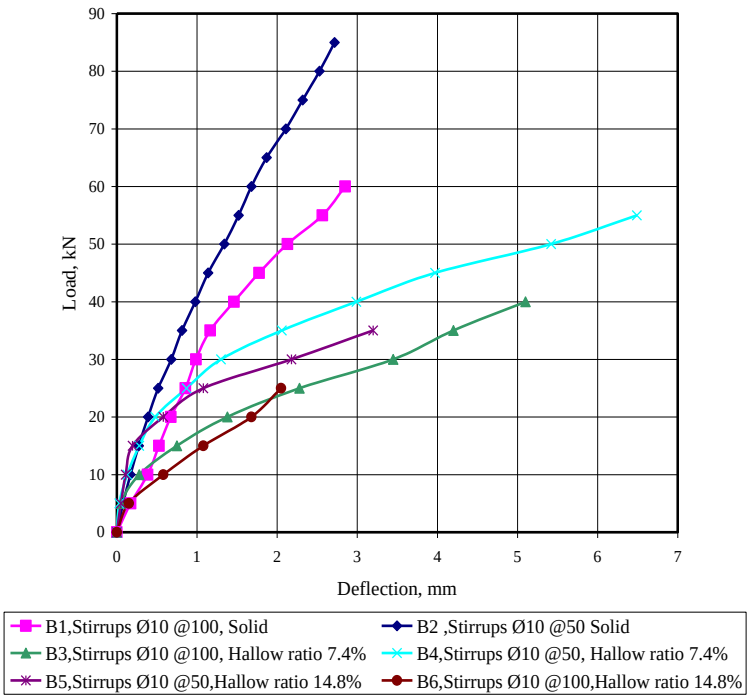

Figure 17. Comparison of quarter deflection of all beams.

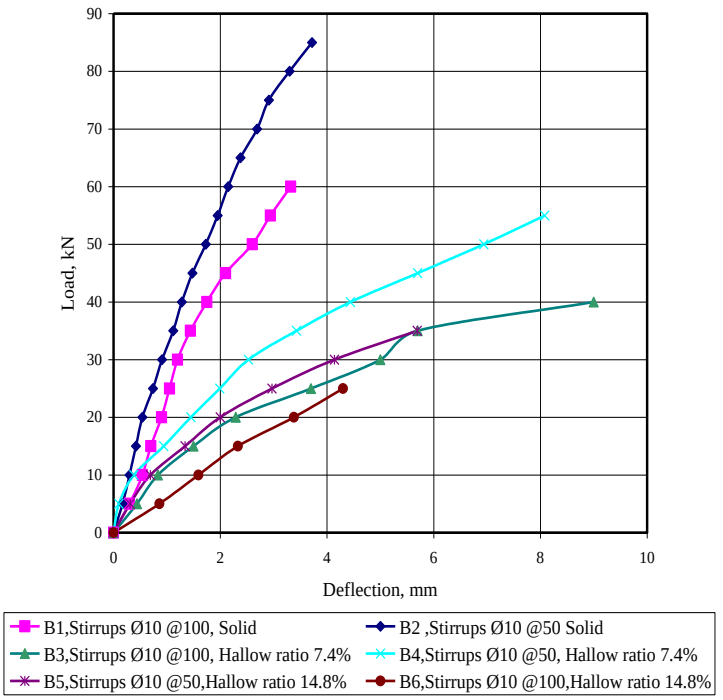

Figure 18. Comparison of central deflection of all beams.

Note: The deflection of all beams at left quarter side are assumed to be the same values on right quarter side as shown in Figs. 19 to 24.

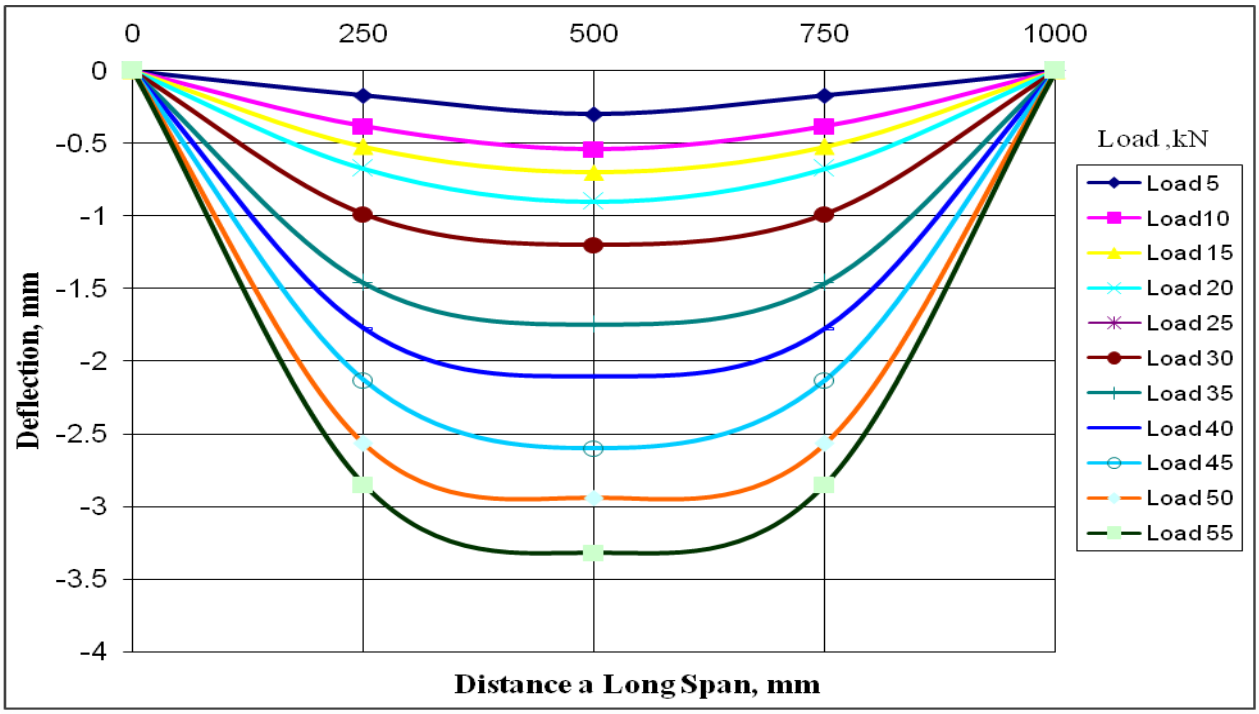

Figure 19. Deflection through a long of reinforced concrete beam, B1.

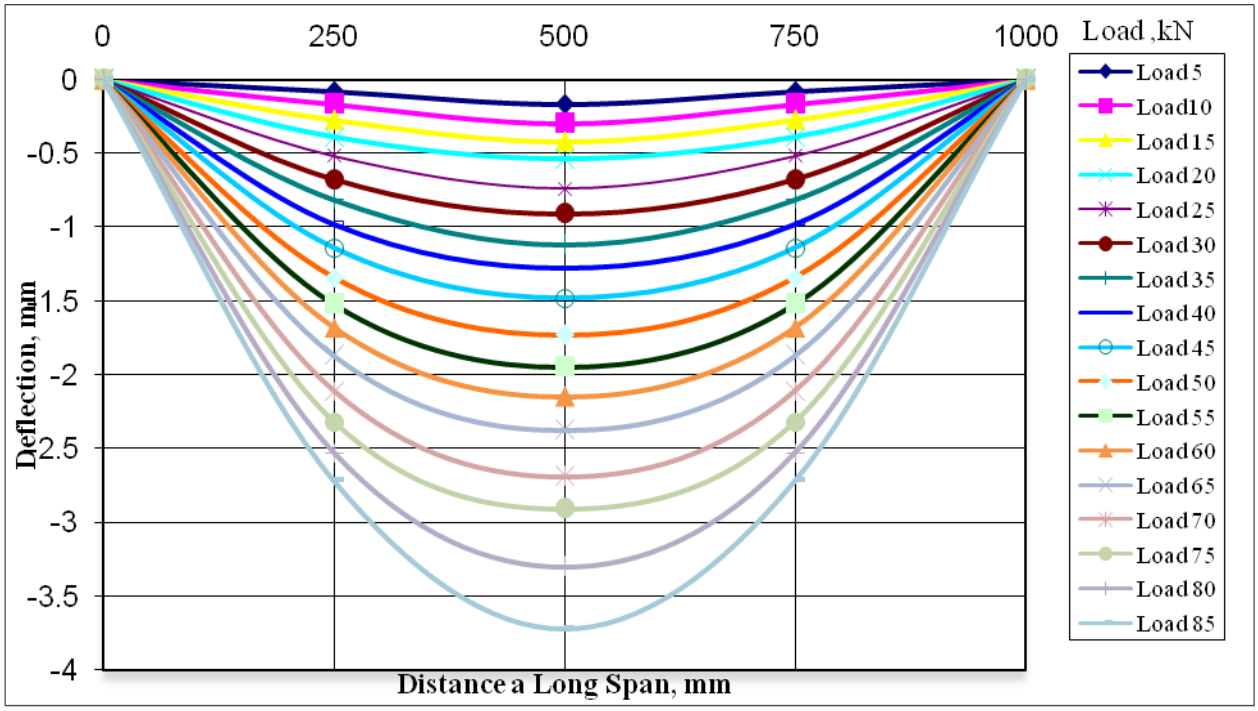

Figure 20. Deflection through a long of reinforced concrete beam, B2.

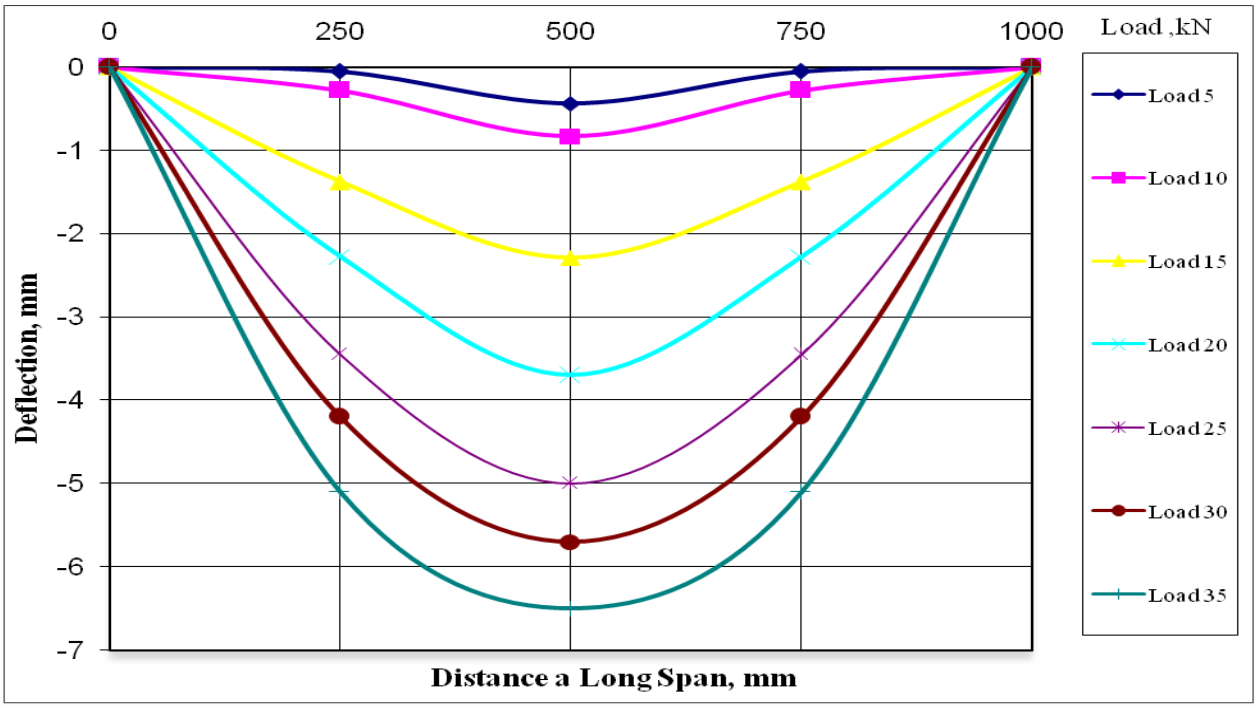

Figure 21. Deflection through a long of reinforced concrete beam, B3.

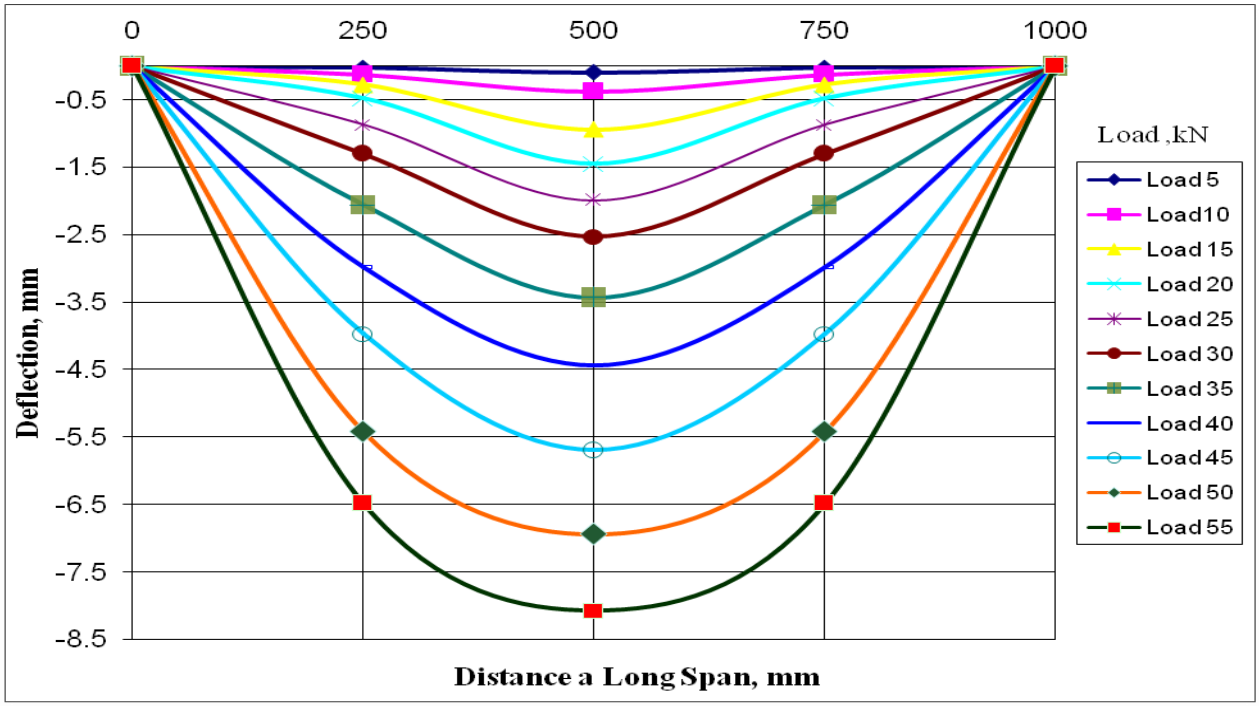

Figure 22. Deflection through a long of reinforced concrete beam, B4.

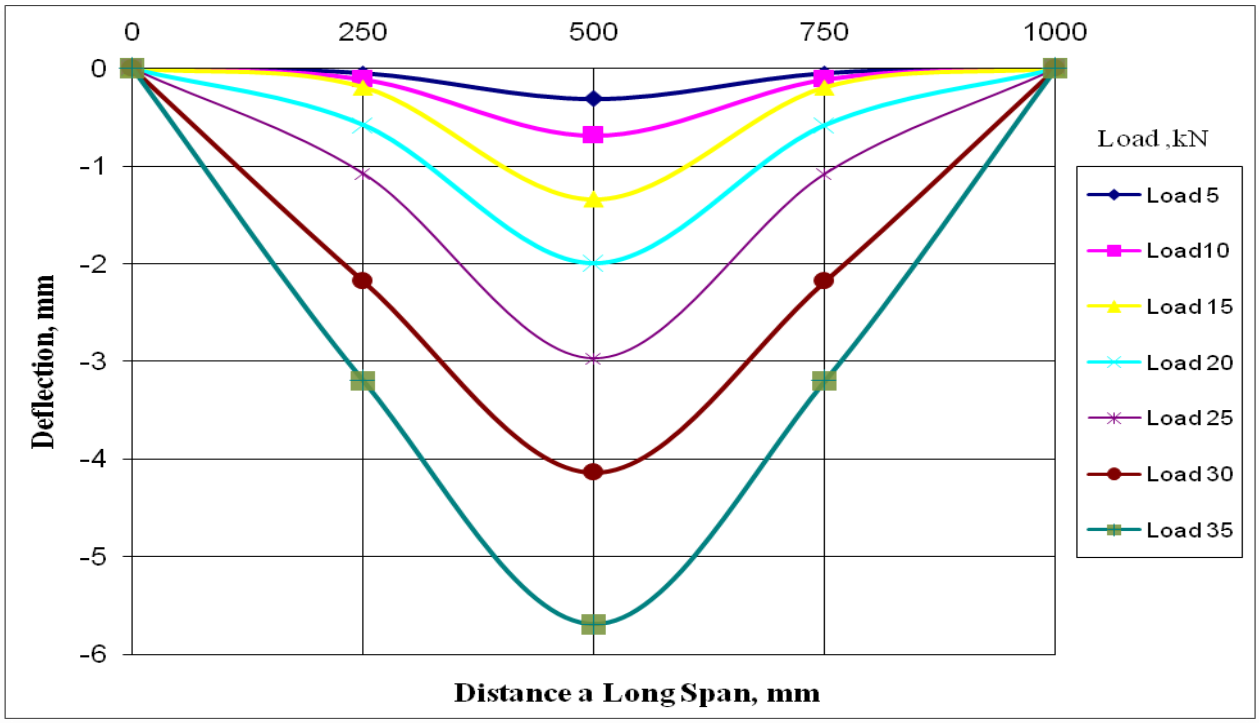

Figure 23. Deflection through a long of reinforced concrete beam, B5.

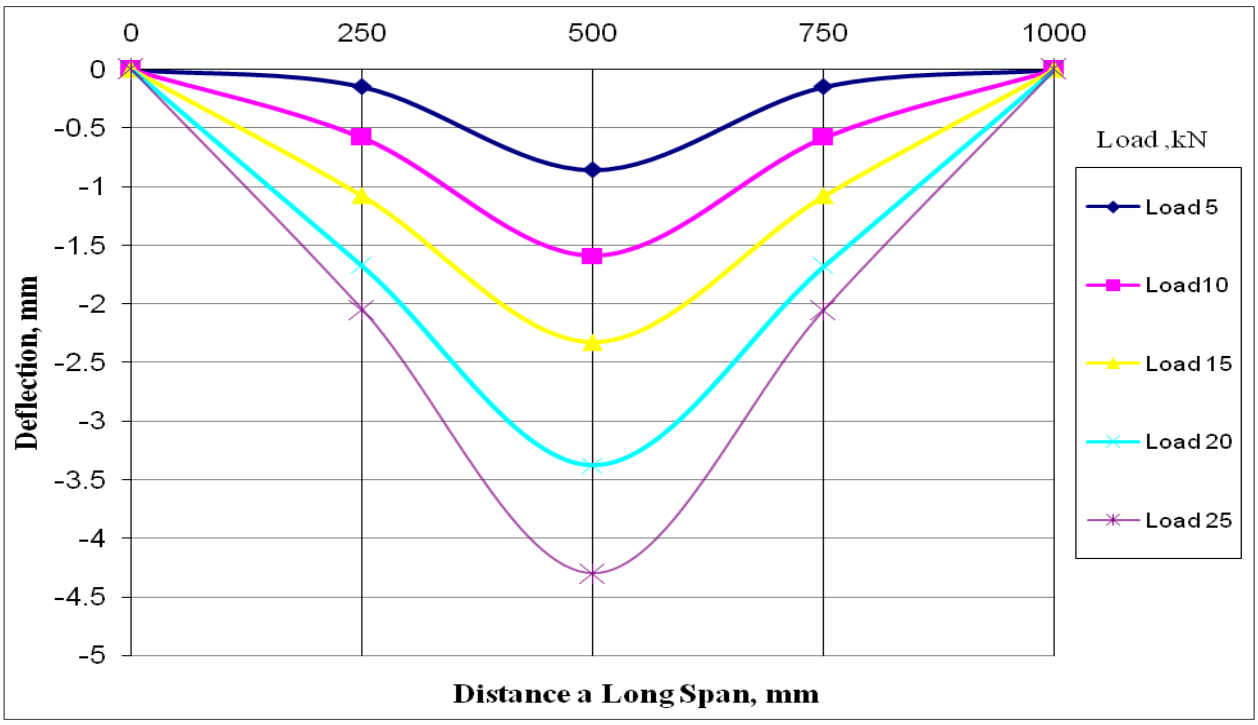

Figure 24. Deflection through a long of reinforced concrete beam, B6.

An Analysis of Stress Distribution in a Spline Shaft Subjected to Cycilc Impulsive Load

Ass. Prof. Dr. Fathi A. AL- Shammaa
Department of Mechanical Engineering
University of Baghdad
E-Mail: Fathi_alshammaa@yahoo.com

Hawaa F. Kadhim
Department of Mechanical Engineering
University of Baghdad
E-Mail: Hawaa_Falih@yahoo.com

ABSTRACT

In this paper the effect of engagement length, number of teeth, amount of applied load, wave propagation time, number of cycles, and initial crack length on the principal stress distribution, velocity of crack propagation, and cyclic crack growth rate in a spline coupling subjected to cyclic torsional impact have been investigated analytically and experimentally. It was found that the stresses induced due to cyclic impact loading are higher than the stresses induced due to impact loading with high percentage depends on the number of cycles and total loading time. Also increasing the engagement length and the number of teeth reduces the principal stresses (40%) and (25%) respectively for increasing the engagement length from (0.15 to 0.23) and the number of teeth from (8 to 10). while increasing the other parameters (amount of applied load, wave propagation time, number of cycles, and initial crack length) increase the principal stresses at the root of the tooth (37% when the applied load rises from (8 KN to 11KN) and (62% when the wave propagation time rises from (0.5 to 1).

Key words: spline coupling, cyclic impact, stress distribution, velocity of crack propagation, cyclic crack growth rate.

الخلاصة

في هذا البحث تم اجراء دراسة عملية ونظرية لتأثير طول التعشيق, عدد الاسنان, مقدار الحمل المسلط, زمن انتقال الموجة, عدد الدورات, والطول الابتدائي للشق على كل من توزيع الاجهادات الرئيسية, سرعة امتداد الشق, و معدل نمو الشق الدوري في وصلة اللربط المسننة المعرضة لصدمة دورية التوائية. وقد وجد ان الاجهادات الرئيسية الناتجة عن الصدمة الدورية اعلى من الاجهادات الرئيسية الناتجة عن صدمة منفردة بنسبة عالية تعتمد على عدد الدورات و زمن التحميل. وان زيادة طول التعشيق وعدد الاسنان يقلل الاجهادات المتولدة بنسبة(40% 25%)على التوالي عند زيادة طول التعشيق من (0.15m الى 0.23m)وعدد الاسنان من(8 الى10)في حين زيادة العوامل الاخرى (مقدار الحمل المسلط, زمن انتقال الموجة, عدد الدورات, والطول الابتدائي للشق) تؤدي الى زيادة الاجهادات الرئيسية المتولدة في وصلة الربط المسننة.حيث يزداد(37%)عند زيادة الحمل المسلط من(8 الى 11KN) و(62%)عند زيادة زمن انتقال الموجة من (0.5 الى 1).

1.INTRODUCTION

A spline coupling is an effective mode of torque transfer between two rotating parts. It transmits torque, but permits axial sliding. The spline coupling is used in high torque transmission engines like vehicles, turbines, and jet engines. The literature that deals with spline coupling has been investigated experimentally and theoretically in several studies which considered the spline tooth profile like ; **Yeung 1999, Baker 1999, Chitkara et al 2001,** and **Yang et al 2007**, failure analysis of the spline coupling like: **Li et al 2007, Ding et al 2007, Ding et al 2008,** and **Lin et al2008**, and the stress distribution along the axial direction of a spline coupling under static load like; **Taylor 2001, Tjernberg 2001, Barrot et al 2009, and Grath 2009**. In the present work the stress distribution, velocity of crack propagation, and cyclic crack growth rate in a spline coupling

subjected to cyclic torsional impact load have been investigated analytically and experimentally for two different boundary conditions.

2.ANALYTICAL ANALYSIS

The torque distribution along the pressure face of the spline coupling tooth was assumed to be unevenly distributed due to the deformation occurs in the spline teeth which caused during torque transmitting ,**Baker 1999**, see **Fig. 1.**

For a spline coupling subjected to impact load the torque distribution along the axial direction can be described as; **Barrot 2009**.

$$m(x) = N\,R\,C\,P(x) = c_\theta[\theta_1(x) - \theta_2(x)] \quad (1)$$

Where;

$$\alpha = \sqrt{[\frac{C_{\theta 2}}{G_2 J_2} + \frac{C_{\theta 1}}{G_1 J_1}]} \quad (2)$$

$$J_1 = \frac{\pi\,(D_0^4 - D_i^4)}{32} - \left(N\frac{C\,w^3}{12} + N\frac{w\,C^3}{12}\right) \quad (3)$$

$$J_2 = \frac{\pi\,D_i^{\,4}}{32} + \left(N\frac{C\,w^3}{12} + N\frac{w\,C^3}{12}\right) \quad (4)$$

$$C_\theta = \frac{T\,J}{L\,R} \quad (5)$$

The coefficients A and B depend on the boundary condition of the spline coupling. Two types of boundary conditions were studied, in the first type the spline shaft was fixed (built in) at one end and free at the other and the sleeve was engaged at the free end, so it called (Built in-Free spline coupling BFSC). In the second type the spline shaft was fixed at both ends and the sleeve was engaged at the middle of the shaft and it was called (Built in-Built in spline coupling BBSC).

For (BFSC); m (0, t) =0 , m (L, t) =T

$$A = \left[\frac{T}{e^{\alpha L} - e^{-\alpha L}}\right] \quad (6)$$

$$B = \left[\frac{-T}{e^{\alpha L} - e^{-\alpha L}}\right] \quad (7)$$

For (BBSC); m (0, t) =T , m (L, t) =T

$$A = T\left[\frac{e^{\alpha L} - 1}{e^{2\alpha L} - 1}\right] \quad (8)$$

$$B = T\left[\frac{e^{2\alpha L} - e^{\alpha L}}{e^{2\alpha L} - 1}\right] \quad (9)$$

The torque transmitted due to cyclic impact load was described as follows;

$$m(x,t)_{cyclic} = [Ae^{\alpha x} + Be^{-\alpha x}]\left[e^{\frac{t}{t_o}} - 1\right]\left[f\frac{t}{t_o}\right] \qquad (10)$$

3. PRINCIPAL STRESS DISTRIBUTION

The principal stress distribution was calculated using the equation ; **Mancuso, J.R.,2001**

$$\sigma_1(x,t) = \frac{m(x,t)}{N\,R\,C\,L} \qquad (11)$$

$$\sigma_1(x,t)_{cyclic} = \frac{m(x,t)_{cyclic}}{NR\,C\,L} \qquad (12)$$

4. VELOCITY OF CRACK PROPAGATION

As the crack propagates the displacement V will change with time. Denoting the rate of change dV/dt as V'; **Ewalds, 1989**.

$$V' = \frac{Z_1}{E^{\circ}}[\,\sigma\,a' + \sigma' a] \qquad (13)$$

$$V' = \frac{Z_1}{E^{\circ}NCRL}\left[\left[[Ae^{\alpha x} + Be^{-\alpha x}]\left[e^{\frac{t}{t_o}} - 1\right][f\frac{t}{t_o}]\sqrt{\frac{\pi}{k}}\sqrt{\frac{E^{\circ}}{\rho}}\left(1 - \frac{a_o}{a_i}\right)\right] + [[Ae^{\alpha x} + Be^{-\alpha x}][\left[\left[e^{\frac{t}{t_o}} - 1\right]\frac{f}{t_o}\right] + \left[\left[\frac{1}{t_o}e^{\frac{t}{t_o}}\right]f\frac{t}{t_o}\right]]a\right] \qquad (14)$$

Where;

$$a' = \sqrt{\frac{\pi}{k}}\sqrt{\frac{E^{\circ}}{\rho}}\left(1 - \frac{a_o}{a_i}\right) \qquad (15)$$

$$E^{\circ} = E/(1 - v^2)$$

$$Z_1 = 2\sqrt{a^2(1 - z^2)} \qquad (16)$$

$0 < z < 1$

For steel $\sqrt{\frac{\pi}{k}} = 0.8$

5. CYCLIC CRACK GROWTH RATE

Paris' law relates the stress intensity factor rang to sub-critical crack growth rate. The basic formula reads;

$$\frac{da}{dn} = C_2 \Delta K^m \qquad (17)$$

The term in the left hand side known as the crack growth rate under cyclic loading regime is called cyclic crack growth rate. On the right hand side C_2 and **m** are material constants, and **ΔK** is the range of the stress intensity factor.

$$\Delta K = K_{max} - K_{min} \quad (18)$$

$$\Delta K = \Delta\sigma Y\sqrt{\pi a} \quad (19)$$

For an edge crack in an infinite sheet **Y=1.12, Ewalds, 1989.**

For steel **m=3** and C_2**is** 10^{-11}, **David R., 2001**, see **Fig.2.**

6. EXPERIMENTAL WORK

A spline coupling models of ST-45 simulate the spline coupling of a Power Take-Off engine have been manufactured at the manufactory of "THE STATE COMPANY OF MECHANICAL INDUSTRES" with two number of teeth (8 and 10) and three engagement lengths (0.08m,0.15m,0.23m). The spline coupling samples were manufactured in two groups the first group suitable to set as (BBSC) and the second group suitable to set as (BFSC). The test rig consisted of fixing plate which is a heavy rectangular base with two vertical plates. At the upper end of each vertical plate there is a circular hole to carry and fix the spline coupling samples. The impactor which consisted of two arms connected to a disc. The disc had a several holes around its circumference each hole represented a different winding angle which causes a different amount of load. The disc was connected to a helical spring, see **Fig. 3**. The strain induced at the root of the spline coupling tooth was measured using strain gauges connected to a sensor circuit to convert the change in resistance into change in voltage and amplify the strain gauge output signal. The output signal of the sensor circuit goes to a digital data logger, (ORDEL UNIVERSAL DATA LOGGER (UDL 100)), to record the data and the display and save them on a computer, see **Fig. 4**.

7. ANALYTICAL RESULTS

Theoretical investigation is done for two loading cases (impact load and cyclic impact load), two boundary conditions (BBSC and BFSC), three engagement lengths (0.08m,0.15m,0.23m), and three amounts of applied load (5 kN, 8 kN, 11 kN). **Fig. 5** shows that the principal stress distributes exponentially along the axial direction of the BFSC tooth and that the principal stresses induced in the spline shaft are higher than the principal stresses induced in the sleeve because of the difference between their geometry especially their root radiuses. **Fig. 6** shows that the principal stress distributes exponentially along the axial direction of the BBSC tooth and it distributes evenly due to the symmetric boundary conditions at its both ends. **Fig. 7** shows that the principal stresses induced due to applying cyclic impact load are higher than the principal stresses induced due to applying impact load with high different percentage depends on the number of cycles per unit time and the total loading time. The increasing in stresses results from accumulating the stresses induced at each cycle. **Fig. 8** shows that increasing the amount of the applied load increases the induced principal stresses and the increasing is linear because the stresses are linearly related to the amount of applied load. **Fig. 9** shows the significant effect of the engagement length on the principal stresses where it shows that increasing the engagement length reduces the principal stresses with a high ratio due to increasing the area that carries the load. **Fig. 10** shows that increasing the number of teeth reduces the induced principal stresses due to dividing the applied load on a higher number of teeth and hence each tooth carries fewer load. **Fig. 11** shows that the principal stresses increases exponentially with the wave propagation time and 62% of this increasing occurs between (t/to =0.5 to t/to =1). **Fig. 12** shows that the behavior of the velocity of crack propagation is similar to the behavior of the principal stresses with respect to time. That is because the velocity of crack propagation depends on the principal stress values. Also **Fig.12** shows that increasing the number of cycles increases the velocity of crack propagation due to increasing the accumulated stresses. **Fig. 13** shows that the cyclic crack growth rate increases with increasing the number of cycles, this

increasing occurs due to increasing the accumulative stresses from each cycle. **Fig. 14** shows that the cyclic crack growth rate increases with high percentage with increasing the initial crack length because of increasing the energy released from the tooth. The energy released causes energy concentration at the tip of the crack which results in increasing the principal stresses at the tip of the crack that's results in increasing the cyclic crack growth rate.

8. EXPERIMENTAL RESULTS

Fig. 15 shows that increasing the amount of the applied load increases the induced principal stresses and this increasing is linear. **Fig. 16** shows that at the fixed end of the spline coupling the effect of the amount of the applied load on the induced principal stresses is the same for (BBSC) and (BFSC). **Fig. 17** shows that increasing the number of the spline coupling teeth reduces the induced principal stresses due to distribute the load over a higher number of teeth hence each tooth carries less load. **Fig. 18** shows that increasing the engagement length have a significant effect in reducing the induced principal stress because of increasing the area carries the load. **Fig. 19** shows that the stresses induced due to cyclic impact load are higher than the stresses induced due to impact load with a high percentage depends on the number of cycles per unit time and the total loading time. **Fig. 20** shows that increasing the number of cycles results in increasing the velocity of crack propagation due to increasing the accumulative stresses that accumulates from each cycle. **Fig. 21** shows that the cyclic crack growth rate increases exponentially with the increasing of the number of cycles, this increasing occurs due to the increasing of the accumulative stresses.

9. VERIFACATION

The experimental results verified the theoretical results and showed a good agreement with reasonable error percentage comes from the delay time of the response of the measuring instruments therefore this error percentages increase as the impact wave propagates faster due to increasing the delay time. **Fig. 22** shows that the experimental results of the principal stress variation with the amount of applied load coincides with the theoretical results with an error percentage equals to (9%). **Fig. 23** shows that the experimental results of the velocity of crack propagation variation with the wave propagation time coincides with the theoretical results with an error percentage equals to (9%). **Fig. 24** shows that the experimental results of the cyclic crack growth rate variation with the number of cycles coincides with the theoretical results with an error percentage equals to (10%).

10. CONCULUSIONS

1. The principal stresses induced in the spline shaft are different from the principal stresses induced in the sleeve with a percentage depends on their geometry.
2. The end of the engagement length endures the maximum stress and it's the most susceptible point to failure.
3. In the BBSC both ends endures the maximum stresses while in the BFSC only one end endures the maximum stresses.
4. The engagement length has a significant effect on reducing the stresses**.**
5. The time of wave propagation of the cycling impact loads wave have a very significant effect on the stresses induced in the spline shaft then the impact loads**.**
6. Appling cyclic impact load on the spline coupling highly raises the velocity of crack propagation.
7. The cyclic growth rate obeys Paris law.

NOMENCLUTURE

Symbol	meaning	Unit
A:	coefficient	#
B:	coefficient	#
C :	spline tooth height	Mm
N :	number of teeth	#
L:	engagement lengt	mm
W:	spline tooth width	mm
w :	applied load	applied load
X:	axial posision	mm
m:	material coefficient	#
.n:	number of cycles	Cpm
Z :	half crack length	mm
k:	integral constant	#
K:	stress intensity factor	Mpa
T:	applied torque	KN.m
t:	instantaneous wave propagation time	Sec
t_o:	total wave propagation time	Sec
E :	modulus of elasticity	Kn.m
Cpm:	cycle per minute	cycle/min
G:	modulus of rigidity	KN.m
a:	crack length	mm
a_o:	Initial crack length	mm
a_i :	instantaneous crack length	mm
C_2:	material coefficient	#
R_1:	sleeve root radius	mm
R_2:	shaft root radius	mm
R_o :	sleeve outer radius	mm
R_p:	spline coupling pitch radius	mm
J_1:	sleeve polar moment of inertia	mm^4
J_2:	shaft polar moment of inertia	mm^4
P(x):	static presser	Kpa
$M_1(x,t)$:	torque transmitted by sleeve	Kn.m
$M_2(x,t)$:	Torque transmitted by shaft	Kn.m
m(x,t):	torque transmitted by	Kn.m
$m(x,t)_{cyclic}$	transmitted torque	Kn.m
Kn.m:	Spline coupling	due to cyclic impact load
V:	velocity of crack propagation	m/sec
V'_i:	impact velocity of crack	m/sec`
α:	coefficient	N/rad
ρ:	material density	Kg/m^3
v:	poison's ratio	#
$\sigma_1(x,t)$:	principal stress	KN/m^2
C_θ:	torsional rigidity	KN/rad

$\sigma_1(x,t)_{cyclic}$	principal stress due to	cyclic impact load
θ_1:	sleeve angle of twist	rad
θ_2:	shaft angle of twist	rad

REFERANCES

Ali, M.A., 2009,*A Study of a Delimitation Problem in a Leaf Spring Made of Composite Material under Impact Load*, M.Sc. Thesis, University of Baghdad, Baghdad.

Baker, D.A, 1999, *A Finite Element Study of Stresses in Stepped Spline Shafts and Partially Splined Shafts under Bending, Torsion And Combined Loadings*", M.Sc. Thesis, Virginia Polytechnic Institute , State University, Virginia.

Barrot, A., Paredes, M., and Sartor. 2009, *Extended Equations of Load Distribution in the Axial Direction in a Spline Coupling*, Journal of Engineering Failure Analysis, Vol. 16, P.P. 200-211.

Darrell, F.S., and Gary, B.M., 2000,*Multiaxial Fatigue*, SAE,Inc.

David, Roylance, 2001,, *Fatigu*e, Department of Materials Science and Engineering, Massachusetts Institute of Technology, Cambridge, MA 02139.

Ding, J., Leen, S.B., Williams, E.J., and Shipway, P.H., 2008, *Finite Element Simulation of Fretting Wear-Fatigue Interaction in Spline Couplings*, Journal of Tribology, Vol.2, No. (1).

Ding, J., McColl, I.R., Leen, and S.B., 2007, *The Application of Fretting Wear Modeling To a Spline Coupling*, Journal of Wear,Vol.262, P.P.1205-1216.

Ewalds, H.L., and Wanhill, R.J.H. 1989, *Fracture Mechanics*, Edward Arnold.

Grath, J.P., 2009, *Analysis of Axial Load Distribution in a Jet Engine Disk-Shaft Spline Coupling*, M.Sc. Thesis, Faculty of Rensselaer Polytechnic Institute.

Hall, A.S., Holowenko, A.R., and Laughlin, H.G., 1961, *Theory and Problems of Machine Design*, Schaum's outline, Mc-Graw Hill, Inc.

Hearn, E.J., 2000, *Mechanics of Materials1*, Butterworth Heinemann.

Johanson, W. 1972, *Impact Strength of Materials*, Edward Arnold.

Jonas, A.Z., Theodore, N., Hallock, F.S., Longin, B.G., and Donald, R.C., 1982, *Impact Dynamics*, John Wiley &Sons.

Li, Y.J., Zhang, W.F., and Tao, C.H., 2007, *Fracture Analysis of Castellated Shaft* Journal of Engineering Failure Analysis, Vol.14, P.P.573-578.

Lin, C., Hung, J., and Hsu, T., 2008, *Failure Analysis of Reverse Shaft in the Transmission System of All-Terrain Vehicles*, Journal of Fail. Anal. and Prevent. , Vol. 8, P.P. 75-80.

Mancuso, J.R., and Jones, R., 2001, *Coupling Interface Connection*

Naser Shabakhty, 2004, *Durable Reliability of Jack-up Platforms*, Ph.D. Thesis, Delft University of Technology, Netherlands.

Sowrappa, L.R., 2005, *Laminated Architecture Glass Subjected to Blast, Impact loading,*

Patricio, M., and Mattheji, R.M.M., 2002, *Crack Propagation Analysis*.

Shigly, 2006,*Mechanical Engineering Design,* Mc-Grow Hill Inc., eighth edition.

Tariq, M.H., 2008,*The Effect of Low Velocity Impact with Fatigue Loading on Cracked Rectangular Plate* M.Sc. Thesis, University of Baghdad, Baghdad.

Taylor, J.W., 2001, *Modeling and Simulation of Spline Couplings*, United Kingdom.

Tjernberg, A., 2001, *Load Distribution and Pitch Errors in a Spline Coupling*, Journal of Materials and Design, Vol.22, P.P.259-266.

Varin, J.D., 2002,*Fracture Characteristic of Steering Gear Sector Shaft*, Journal of Practical Failure Analysis, Vol.2, No.(4), P.P.65-69.

Yang, D.C.H., and Tong, s., 2007, *On the Profile Design of Transmission Splines and Keys* Journal of Mechanism and Machine Theory, Vol.42, P.P.82-87.

Yeung, K.S., 1999, *Analysis of a New Concept in Spline Design for Transmission Output Shafts*", Ford Motor Company, Dearborn, MI, 24121, USA.

http://en.wikipedia.org/wiki/Paris'_law
http://en.wikipedia.org/wiki/Spline-(mechanical)
http://www.facebook.com/pages/Rotating-spline/143902598956699?sk=wiki

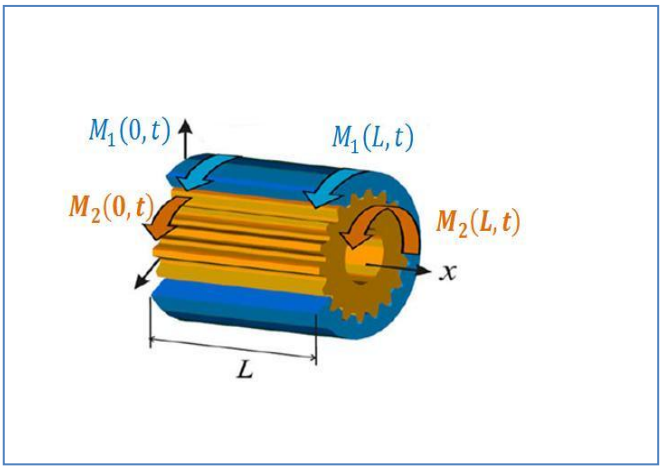

Figure 1. Schematic figure of the spline coupling.

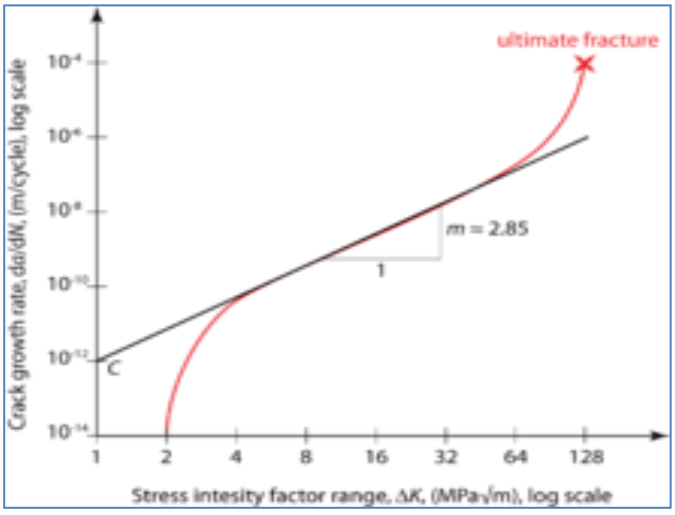

Figure 2. Schematic plot of the typical relationship between the crack growth rate and the range of the stress intensity.

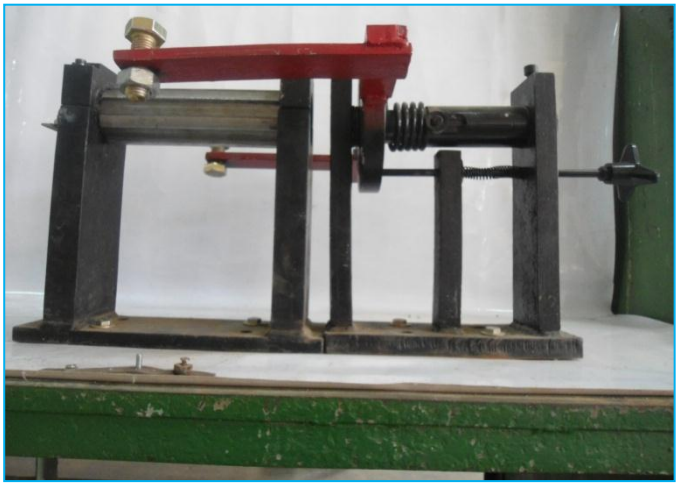

Figure 3. The fixing plate and the impact.

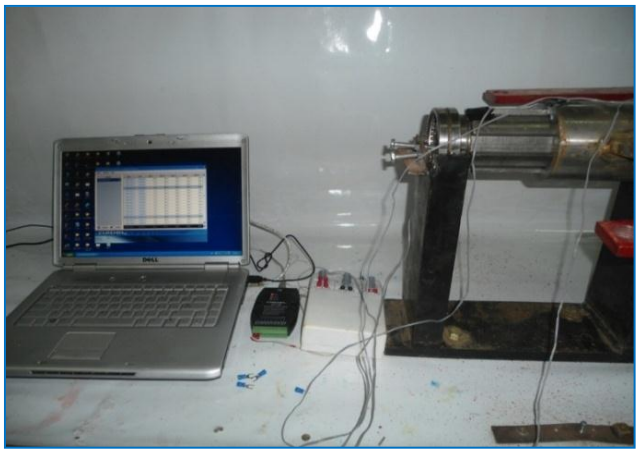

Figure 4. The measuring instruments.

.

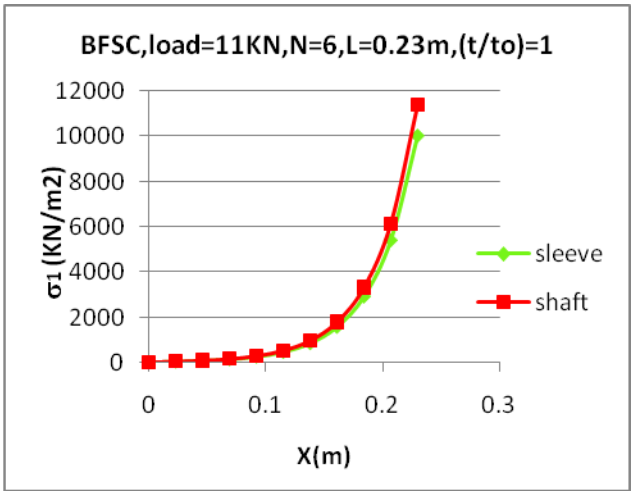

Figure 5. Principal stress distribution along the axial direction of a (bfsc) tooth due to impact load.

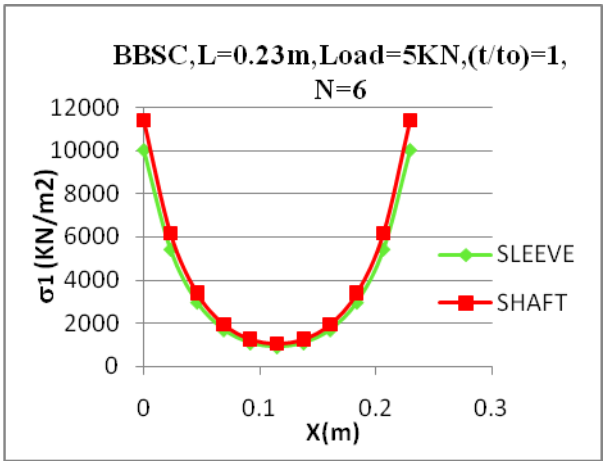

Figure 6. Principal stress distribution along a (bbsc).

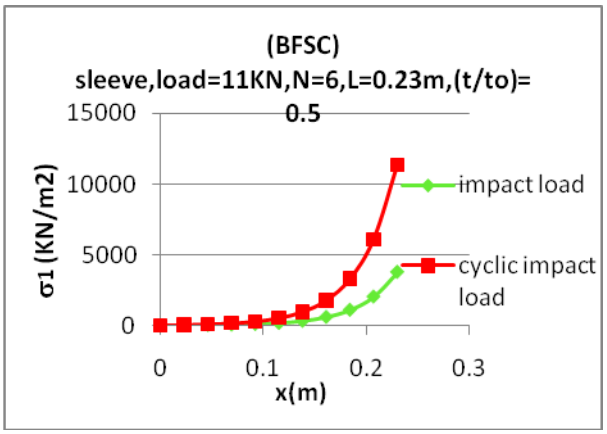

Figure 7. Effect of cyclic impact load on the principal stress values.

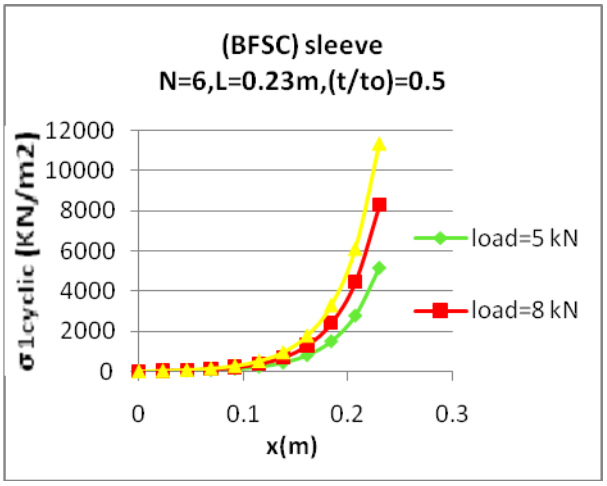

Figure 8. Principal Stress Distribution along a (BFSC) Sleeve for 3 Different Cyclic Loads.

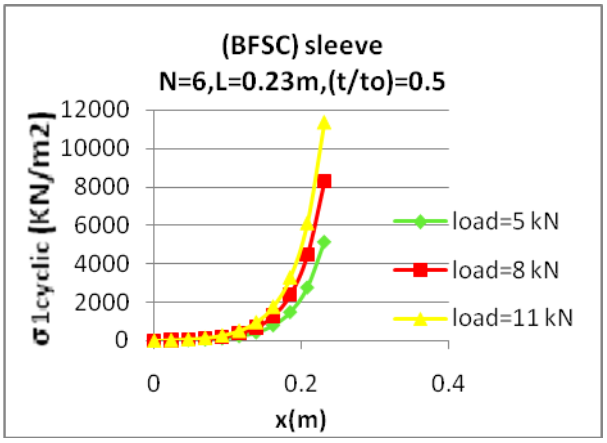

Figure 9. Principal stress distribution along a (bfsc) sleeve for 3 different cyclic loads.

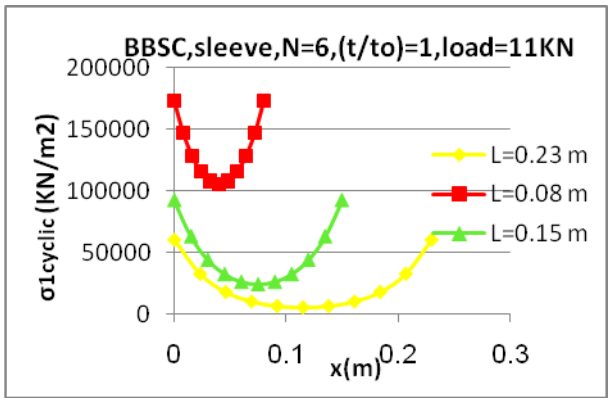

Figure 10. Stress distribution along a (bbsc) sleeve for 3 different engagement lengths.

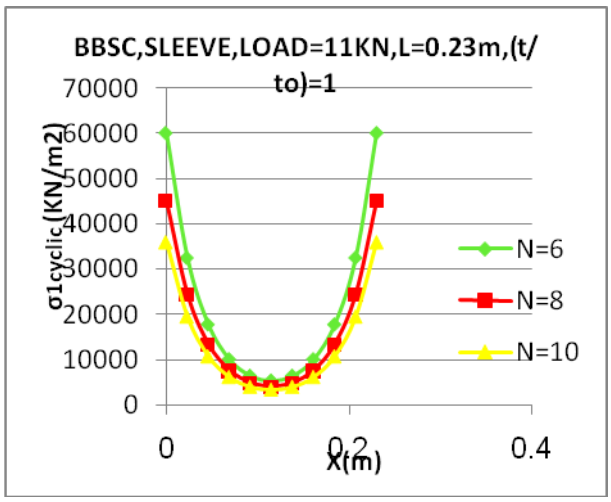

Figure 11. Stress distribution along a (bbsc) sleeve for 3 different numbers of teeth.

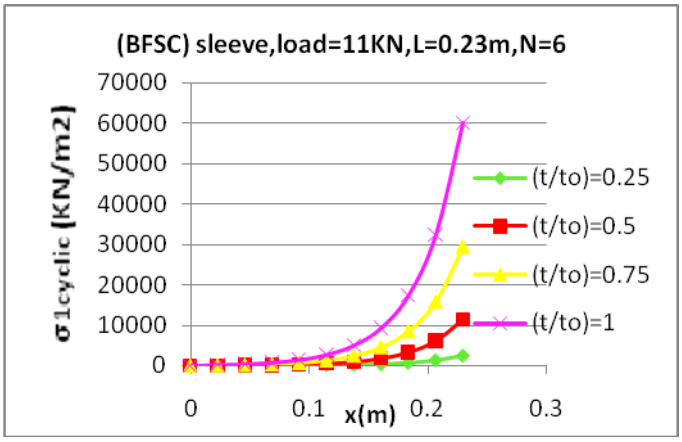

Figure 12. Stress distribution along a (bfsc) sleeve at 4 different wave propagation times.

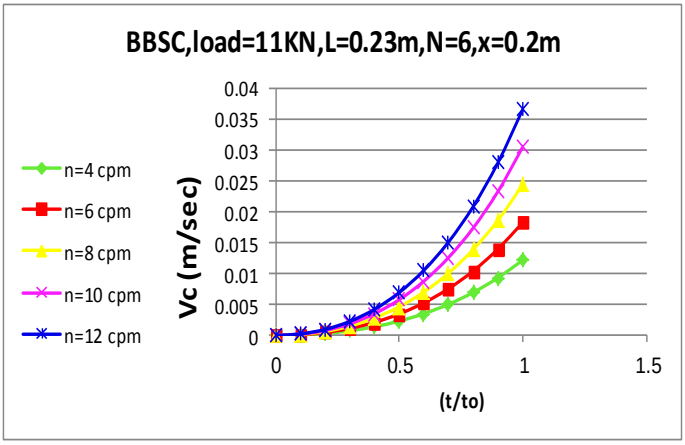

Figure 13. Velocity of crack propagation due to cyclic impact load for 5 different numbers of cycles.

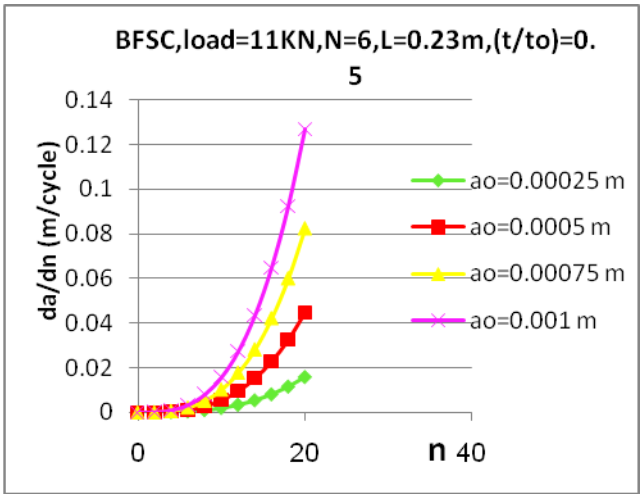

Figure 14. Cyclic crack growth rate variation with number of cycles.

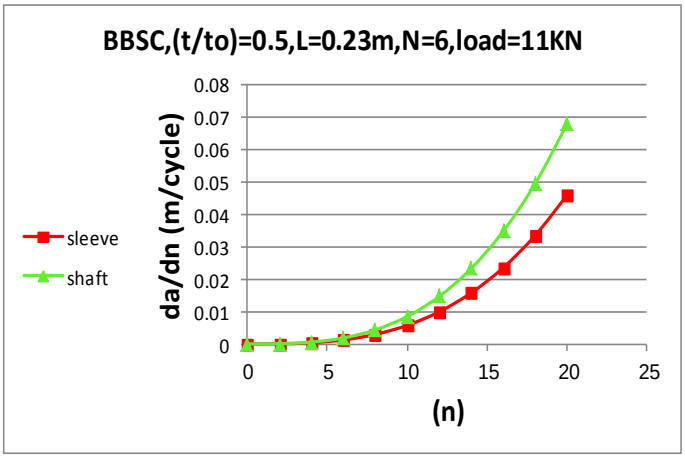

Figure 15. Cyclic crack growth rate for 4 different initial crack lengths.

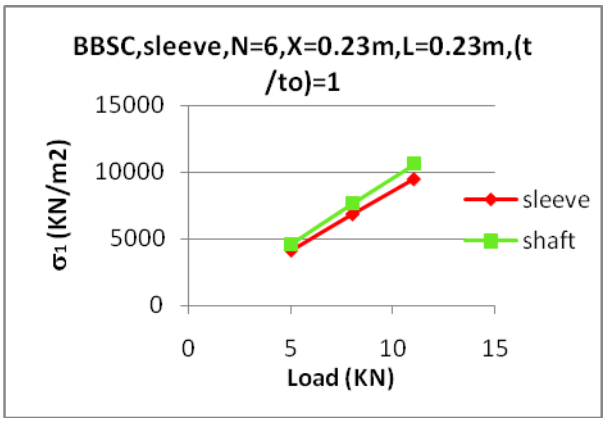

Figure 16. Principal stress variation with amount of applied load.

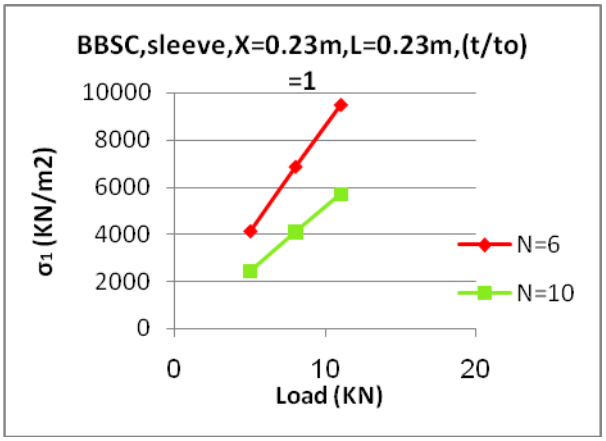

Figure 17. Principal stress variation with the amount of applied load for 2 different number of teeth.

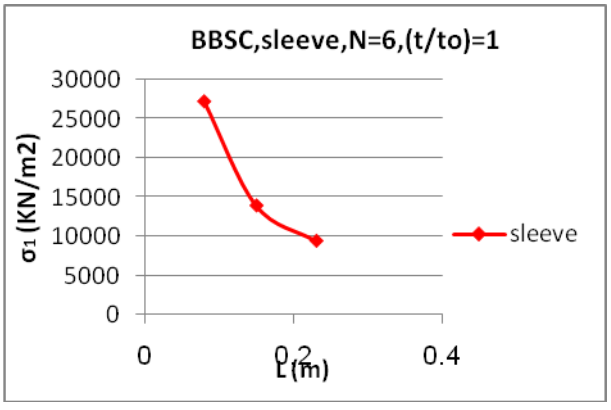

Figure 18. Principal stress variation with the engagement length.

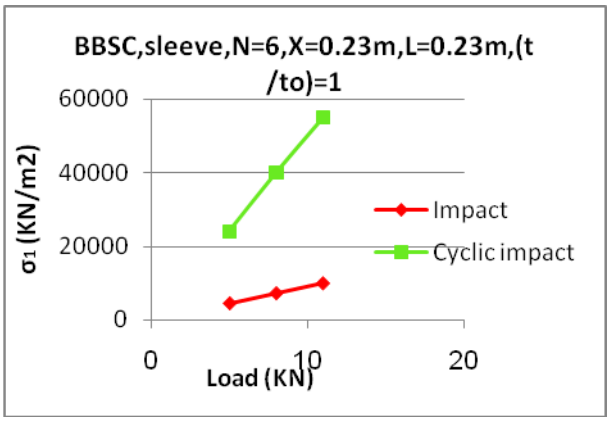

Figure 19. Principal stress variation with the amount of applied load for impact and cyclic impact load.

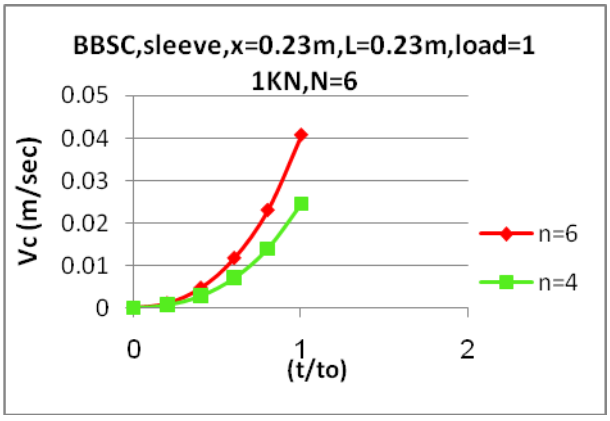

Figure 20. Variation of velocity of crack propagation with wave propagation time for 2 different numbers of cycles.

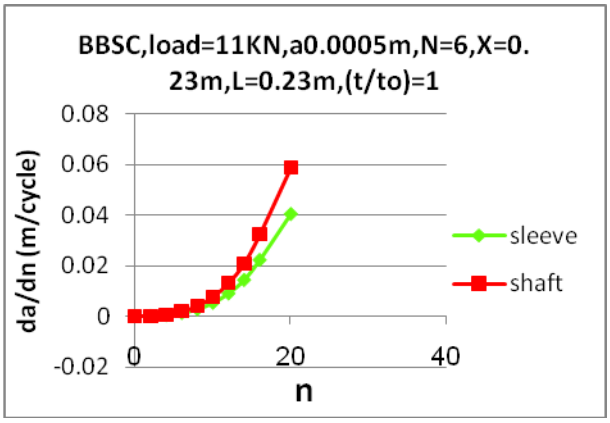

Figure 21. Cyclic crack growth rate variation with the number of cycles.

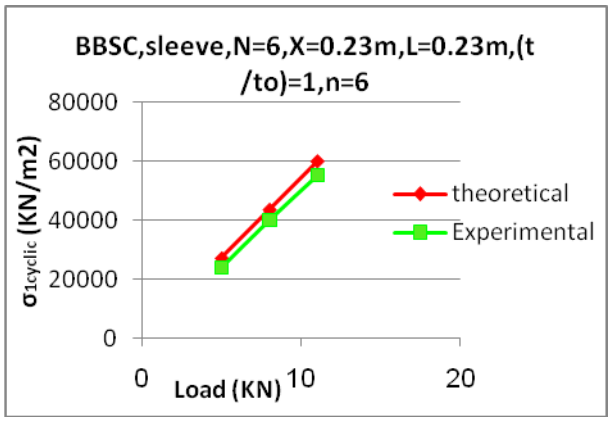

Figure 22. Comparison between the experimental and theoretical results for the principal stress variation with the amount of cyclic impact load.

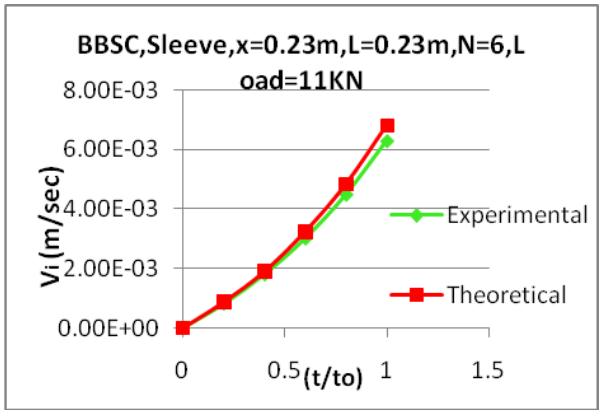

Figure 23. Comparison between the experimental and theoretical results of velocity of crack propagation variation with the wave propagation time**.**

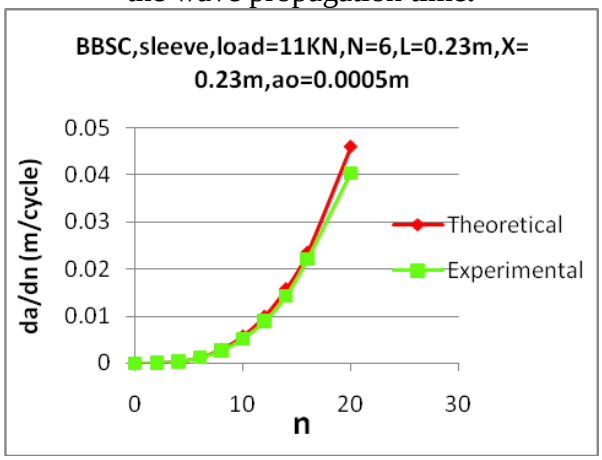

Figure 24. Comparison between the experimental and theoretical results of the cyclic crack growth rate variation with the number of cycles.

Study of Dynamic Sorption in Adsorption Refrigeration Cycle

Adil A. Al-Hemiri
Proffessor
Eng. College
Baghdad University
E-mail : adilawad2001@yahoo.com

Mohammed A. Atiya
Assistant Professor
Research & Development Department
Ministry of Higher Education & S.R.
E-mail : mohatiya1965@gmail.com

Farkad A. Lattieff
Assistant instructor
Research & Development Department
Ministry of Higher Education & S.R.
E-mail : farkad400@yahoo.com

ABSTRACT

This paper shows the characteristics of temperature and adsorbed (water vapor) mass rate distribution in the adsorber unit which is the key part to any adsorption refrigeration system. The temperature profiles of adsorption/desorption phases (Dynamic Sorption) are measured experimentally under the operating conditions of 90^{o}C hot water temperature, 30^{o}C cooling water temperature, 35^{o}C adsorption temperature and cycle time of 40 min. Based on the temperature profiles, The mass transfer equations for the annulus adsorbent bed are solved to obtain the distribution of adsorption velocity and adsorbate concentration using non-equilibrium model. The relation between the adsorption velocity with time is investigated during the process of adsorption. The practical cycles of adsorption and desorption were stated dependent on the variables obtained from the experiment and equations calculations.

The results show that the adsorption velocity is diminished after a period of 20 min. The maximum value of the adsorbed water vapor concentration on silica gel is 0.12 kg water/kg adsorbent (adsorption phase) and the minimum value of the water content into silica gel is 0.04 kg water/kg adsorbent (desorption phase) producing a dynamic sorption of $\Delta x = 0.08$ kg water/kg adsorbent.

Key words: adsorption, refrigeration, silica gel-water, mass transfer

دراسة ديناميكية الامتزاز في دورة التبريد الآمتزازية

ا.د. عادل احمد عوض
كلية الهندسة
جامعة بغداد

ا.م.د. محمد عبد عطية
دائرة البحث والتطوير
وزارة التعليم العالي والبحث العلمي

م.م فرقد علي لطيف
دائرة البحث والتطوير
وزارة التعليم العالي والبحث العلمي

الخلاصة

يعرض هذا البحث خصائص توزيع الحرارة وجريان الكتلة للمادة الممتزة (بخار الماء) في وحدة الآمتزاز والتي تمثل الجزء المفتاح لآي منظومة تبريد أمتزازية. إن شكل التوزيع الحراري لأطوار الآمتزاز والانبعاث (ديناميكية الامتصاص) تم قياسه عمليا" تحت ظروف تشغيلية من درجة حرارة 90 ^{o}م للماء الساخن ودرجة حرارة 30 ^{o}م للماء البارد ودرجة حرارة 35 ^{o}م للامتزاز وزمن دورة 40 دقيقة. اعتمادا على شكل التوزيع الحراري فأن معادلات انتقال المادة لحشوة الحبيبات الدائرية قد حلت للحصول على توزيع سرعة الامتزاز وتركيز المادة الممتزة باستعمال موديل اللاتوازن. كذلك العلاقة بين تغير سرعة الامتزاز مع الزمن قد تم التحقق منها إثناء عملية الامتزاز. تم تحديد الدورة العملية للامتزاز والانبعاث بالاعتماد على على المتغيرات التي تم الحصول عليها من التجربة وحسابات المعادلات.

النتائج بينت ان سرعة الامتزاز تتلاشى بعد مرور 20 دقيقة . كانت أعلى قيمة لتركيز بخار الماء الممتز في السليكا جل 0,12 كغم ماء/كغم مازه (إثناء الامتزاز) وأوطأ قيمة كانت 0,04 كغم ماء/كغم مازه في السليكا جل (إثناء الانبعاث) مولدة" ديناميكية امتزاز 0,08 كغم ماء/كغم مازه.

الكلمات الرئيسية : الامتزاز, التبريد, السيلكا جل-ماء, انتقال المادة

1. INTRODUCTION

Adsorption (solid–vapor) refrigeration is analogous to liquid–vapor absorption, except the refrigerant is adsorbed onto a solid desiccant (freeze dried) rather than absorbed into a liquid (dissolved) as in liquid– vapor heat pumps. The adsorption cycle **Fig. 1** proceeds as follows **Lambert, 2007.**

1. At state 1, a cool canister filled with adsorbent, an adsorber, is saturated with refrigerant at slightly below P_e. The adsorber is heated and desorbs refrigerant vapor isosterically (i.e., at constant total mass in the adsorber), pressurizing it to state 2, slightly above P_c ,which opens a one-way valve to start pumping refrigerant vapor into the condenser.
2. Isobaric heating desorbs more refrigerant, forcing it into the condenser until state 3 is attained, at which the adsorber is nearly devoid of refrigerant.
3. The hot adsorber is then cooled isosterically (at constant total mass) causing adsorption and depressurization, until the pressure drops below P_e (state 4), opening another one-way valve to allow refrigerant vapor to enter the adsorber from the evaporator.
4. Isobaric cooling to state 1 saturates the adsorbent, completing the cycle.

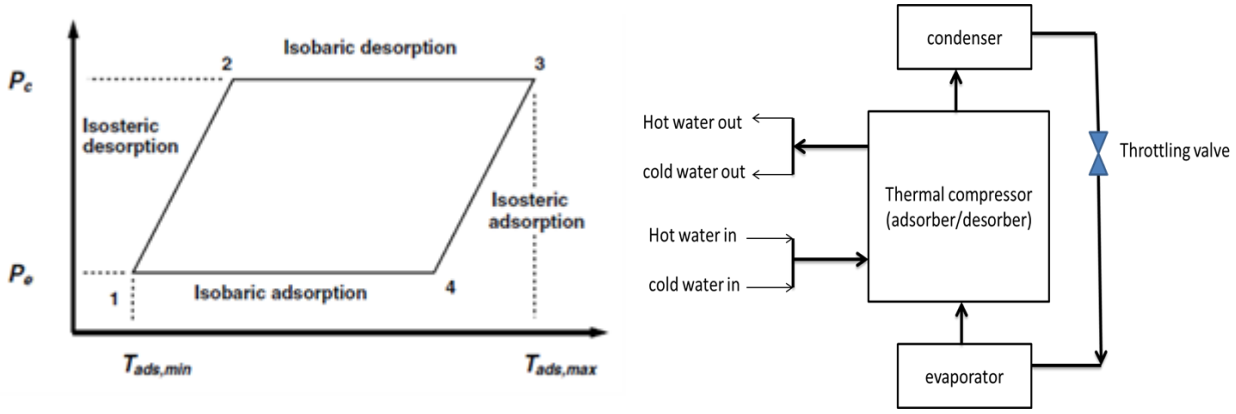

Figure 1. Thermodynamic cycle of the adsorption refrigeration **,Lambert, 2007.**

Wang, D., 2014, showed that the adsorption capacity of the silica gel was influenced by many factors. But pollution by solid particulates was the primary factor to decline the adsorption capacity.

Aristov, et al., 2012, investigated, using an intermittent cycle, the effect of the relative duration isobaric adsorption/desorption stages to maximize the coefficient of performance and the specific cooling power of the cycle. They found that the desorption phase is faster than the adsorption one and this should be considered as a routine case for adsorption refrigeration cycles, probably, because desorption occurs at higher temperature and pressure and hence, they suggested practical

Sapienza, et al., 2012, used a new composite sorbent to operate at low regeneration temperature (< 70^{o}C). Adsorption equilibrium measurements demonstrated that the new composite, $LiNO_3$ / Vermiculate exchange about 0.4 kg water/kg adsorbent in an exceptionally narrow temperature range, 33-36^{o}C (Adsorption at 12.6 mbar) and 62-65^{o}C (desorption at 56.2 mbar).

Gong et al., 2011, evaluated the composite material based on lithium chloride on silica gel as adsorbent and water as adsorbate in an adsorption chiller. The theoretical results showed that the COP can be increased using composite adsorbent.

Demir, et al., 2009, studied the effect of the granule size on the heat and mass transfer. The decrease of granule size enhances the contact area between the granules and consequently heat transfer rate through the bed; however it causes the increase of the mass transfer resistance.

Doau, et al., 2006, report results from an open cycle investigation aimed to determine the optimal salt content of $CaCl_2$ on the silica gel. The sorption equilibrium demonstrated that these materials can sorb 0.5-0.6 kg water/kg adsorbent at 12.3 mbar and 20^{o}C.

In porous media, adsorption process is controlled by both adsorbate transportation and diffusion in adsorbent and inner reaction with adsorbent, between the two items, the transportation of gaseous adsorbate in the tunnel of micro pores and diffusion on its surface are more dominated than the internal reaction in rare pressure **,Wang, and Wang, 2005.**

Aristov, et al., 2002, studied the adsorption capacity of selective water sorbents by confining hygroscopic salt into the open pores of silica gel. The experimental results showed that the water uptake of $CaCl_2$ –in-silica gel was about 0.75 kg/kg at the temperature of 28^{o}C while for silica gel is 0.1 kg/kg.

In this study, the attentions are focused on the mechanisms of mass transfer in the adsorbent bed of adsorption refrigeration system. The influences of temperature and cycle time on the adsorption velocity and adsorbate concentration rate are calculated. The governing equations for the mass transfer are presented and the solution method is described. The results are discussed via figures, which show the variations of temperature, adsorption velocity, and adsorption concentration in a circular bed. Finally, the practical cycle of the dynamic sorption is stated depicting all the operating conditions affected on the system.

2. ADSORPTION CAPACITY TEST

Brazilian commercial mesoporous and microporous silica gel was employed as the adsorbent for the adsorption chiller prototype **Table1.**. water free from any ions was chosen as a refrigerant. For the heating/cooling system, water is the best heat transfer fluid (HTF), with the highest C_p of any liquid and higher thermal conductivity than all.

The silica gel was saturated whenever it was regenerated in an electric oven at 120 °C for a minimum period of 24 h. After regenerating the silica gel, the adsorber was replaced immediately and was expected to cool down to room temperature, at which time and every one hour, it was weighed on a digital scale with a minimum accuracy of 5 g. The adsorptive adsorbers are coupled to the evaporator, which is a cylindrical container with a globe type valve used to control the passage of the adsorbate **Fig.1.**. Before introducing water vapor from the evaporator into the adsorber, the vapor pipe from the evaporator toward the adsorber is evacuated to remove any traces of condensed water vapor, which cause experimental errors. The difference in weight of adsorber with silica gel before and after the adsorption interval period is the adsorbed water concentration.

Table. 1 Thermophysical properties of silica gel (values supplied by the manufacturer) .

Property	Value	Unit
Apparent density	750	Kg/m^3
Average particle diameter	7	mm
Specific surface area	650-700	m^2/g
Thermal conductivity	0.198	W/m.K
Specific heat capacity	921	J/kg.K

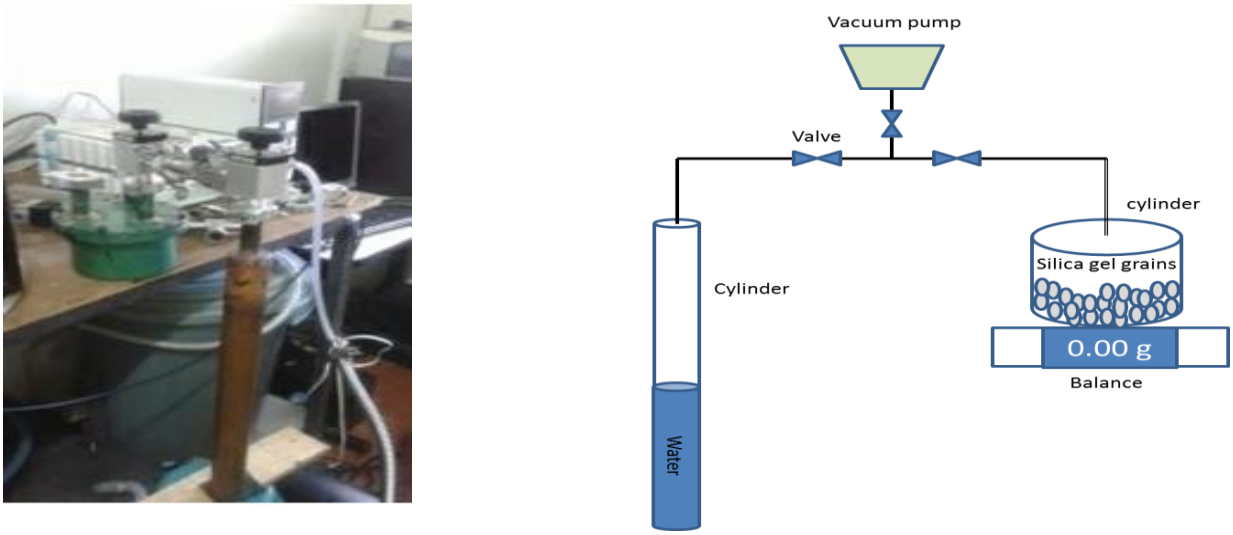

Figure 1. Equilibrium adsorption capacity apparatus.

3. DESCRIPTIONAND PROCEDURE OF EXPERIMENTAL PROTOTYPE

Fig. 2 shows photographs of the experimental adsorption chiller prototype. The adsorption chiller has a single bed, a condenser, an evaporator and a heating/cooling water system. The evaporator lies at the bottom of the chiller and the condenser is located at the upper side. The heating system is next to the adsorber. All the valves are controlled manually. The prototype is designed to test various operating conditions and operating adsorption cycle. The whole prototype is connected to a water heating system for regeneration, tap water for cooling and adsorption, and a vacuum pump.

The main parameter was measured during the experiment: temperature variation with time. All sensors were connected to a data logger and recorded every 8.5 seconds. The data measurements were taken after the cycle steady state had been reached. A computer was used to collect and process the measurement data acquired by the data logger. The flow rate of hot water and cooling water are constant at 0.04 kg/s.

Fig. 3 illustrates the schematic diagram of the testing system. The adsorber is of the shell and fin-tube configuration which is readily (easily) manufactured, and it can withstand high operating pressure and incur low inert mass. The principle innovation of this design is that of internal heat exchanger of the adsorber. Using fins and tubes made the surface area to volume ratio relatively large. The fins on the adjacent four tubes overlap slightly in order to reach all portions of the shell void.

To complete one full cycle, the adsorbent bed passes through four consecutive steps: pre-heating, desorption, precooling, and adsorption. In the adsorber, about 4 kg silica gel is filled. The hot water temperature can be controlled in the range of 85–90^{o}C. The flow rate of hot water is controlled by valve V7 and the cooling water is controlled by V8. V1 and V2 controlled the flow of the refrigerant from the adsorber to the condenser (desorption) and from the evaporator to the adsorber (adsorption), respectively. **Table. 2** reports the operating conditions of the tested adsorber where all the investigated tests conditions are displayed in terms of temperature and the duration of cycle time.

Figure 2. Pictorial of the experimental device.

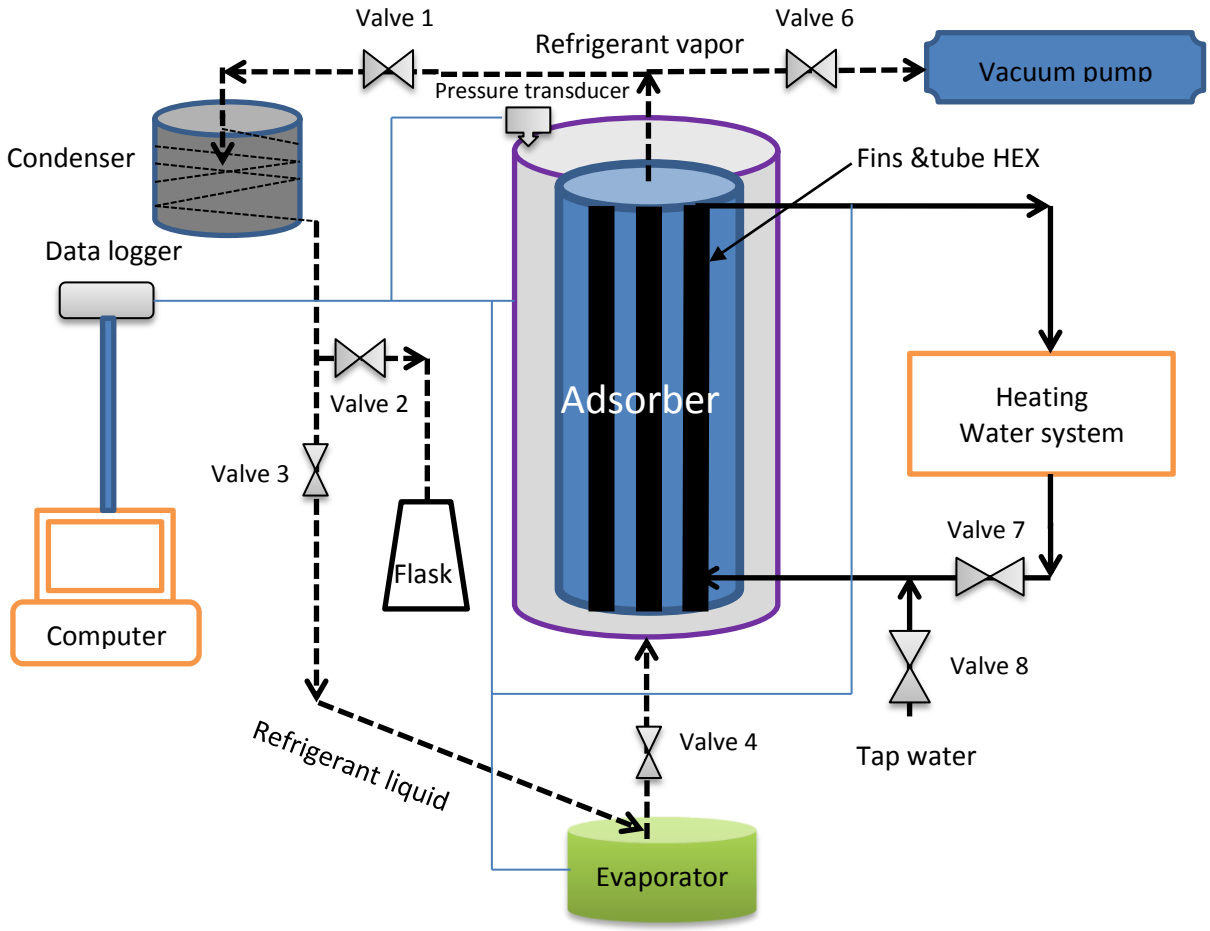

Figure 3. The schematic diagram of the experimental adsorption chiller.

Table 2. Experimental parameters for single bed silica gel-water prototype

Parameter	Value
T_e	11.2°C
T_c	30°C
T_{ads}	35°C
T_{des}	90°C
$t_{iso-heating}$	1.25 min
$t_{iso-cooling}$	1.25 min
t_{des}	18.75 min
t_{ads}	18.75 min
t_{cyc}	40 min

4. NON-EQUILIBRIUM ADSORPTION MODEL

For refrigeration applications, the adsorbent should have high adsorptive capacity at ambient temperature and low pressure, and small capacity of adsorption at high temperature and pressure ,**Leite, et al., 2004**. Two types of mass transfer are encountered in a granular adsorbent bed : mass transfer within the adsorbent granules and mass transfer through the void between the granules (i.e intra-particale and inter-particle mass transfer) **, Demir et al., 2009**. The equilibrium adsorption quantity is the amount of refrigerant adsorbed by the sorbent when the reaction time tends towards infinite, and it is an important parameter for adsorption working pairs. In general, the velocity of adsorption in adsorber is not faster than that of heat transfer, that is, the desorption rate does not reach the equilibrium value at each status point in real operation ,**Wang, and Wang, 2005**. Moreover, the actual process of adsorption/desorption is of non-equilibrium and it actually relies on the mass transport process. Therefore, actual adsorption process is not the process only dominated by the temperature of adsorbent and pressure of the adsorbate, it is involved with mass transport and diffusion, **Wang, and Wang, 2005**.

The equilibrium model for this physical adsorption concentration (x^*) is a function of adsorbent temperature and pressure, and it is written in a generic form as, **Liu, et al., 2005.**

$$x^* = f(T, P)$$

Models with different fixed parameters are as follows:

$$x^* = f(P)_T \quad Isothermal$$
$$x^* = f(T)_P \quad Isobric$$
$$P = f(T)_x \quad Isosteric$$

These functions correlate the temperature *T*, the pressure *P* and the concentration of the adsorbed phase$x$, so that *f* (T, P,x) = 0 For equilibrium of adsorption in micrporous materials with a polymodel distribution of pore dimensions, such as the silica gel-water and activated carbon-methanol pair, Dubinin and Astakohov proposed the following isotherms**, Dieng, and Wang, 2001.**

$$x^* = x_o exp\left[-K\left(RT_b * ln\left(\frac{P_b}{P_{c/e}}\right)\right)^n\right] \quad (1)$$

Where:

$P_c\ (T_c = 30°C) = 4.42\ Kpa$
$P_e\ (T_e = 7°C) \ = 1\ Kpa$

Sakoda and Suzuki, (1984) considered the influence of diffusion on the micropores surface, proposed the model of adsorption velocity as below (2). When the analysis is simplified, the lagging effect between adsorption and desorption is neglected:

$$\frac{dx}{dt} = k_m(x^* - x) \quad (2)$$

$$x(t) = x^*.(1 - e^{-k_m.t}) \quad (3)$$

$$k_m = \left(\frac{15D_o}{R_p^2}\right) exp\left(\frac{-E_a}{RT_b}\right) \quad (4)$$

The saturation vapor pressure and temperature are correlated by Antonio's equation which can be written as **,Khan, et al., 2006.**

$$P_b = 133.32 * \left(exp\left(18.3 - \frac{3820}{T_b + 273 - 46.1}\right)\right) \quad (5)$$

Firstly, the equilibrium adsorbate concentration within the adsorbent granule is evaluated by using Eq. (1) at the specified temperature and pressure Eq. 5. Eq. (4) is solved to find the adsorption rate constant. Based on all these calculations, Eq. (3) and Eq. (4) are solved to find the adsorption velocity and the simultaneous concentration distribution. An iteration is performed before increasing a time step. The iteration is continued until the time of the phase is completed.

5. RESULTS AND DISSCUTION

The adsorption isotherm of water on silica gel (Brazilian type) is presented in **Fig. 4**.The experimental results include equilibrium water uptake when the silica gel was exposed to saturated water vapor at operating temperature, 30^{o}C. It is shown that the maximum equilibrium adsorption capacity is 0.2 kg water \ kg adsorbent.

Fig. 5 shows the temporal evolution of the isosteric cooling, isosteric heating, desorption and adsorption cycles at a steady state for the following operating conditions concluded from the experiment test**.**

The adsorption rate constant decreased when temperature was lowered, which means that the adsorption was taking longer time at lower temperatures, **Fig. 6**.

Fig. 7 shows the time change in the amount of adsorbed water vapor measured at various regeneration temperatures. As seen in this figure, the amount of adsorbed water increases with

time for the same temperature, but decreases with regeneration temperatures. However, effective adsorptivity did not reach the value equal to maximum state recorded from experimental results of water adsorption isotherm of silica gel, x^*; e.g. at 30°C, x^* is 0.13 kg/kg for 20 min, whereas x^* is 0.2 kg/kg. Using these results, it was determined that 35 % of silica gel was not effectively used in cycle operation.

The experimental values of the adsorption velocity (dx/dt) as a function of adsorption time using a single adsorber bed are reproted in **Fig. 8**. The operating conditions selected are the following: T_c =30°C, T_{ads} =35°C, and T_{des} =90°C. Results obtained demonstrated that the adsorption velocity was diminshed after 20 mins. There is a very low value of adsorption velocity after 20 mins, and it may not be enough to keep the temperatre of the water inside the evaporator at the designed value.

Desorptoin process is very close in concentration change to adsoption process, and many researches assume both are the same in adsorption refrigeration process. It is clear from experimental results that after 20 mins, the concentration of water into silica gel reaches 0.048 kg water/kg adsorbent **Fig. 9.** It is vey close to the calculated value, 0.04 kg/kg, by using Eq. (3) **Fig 10.**

Based on this non-equilibrium model Eq.(3), some calculations using experimental results have been done to discover the effect of non-equilibrium adsorption on adsorption refrigeration **Fig. 10**. It could be observed that the non-equilibrium deviates from the equilibrium particularly for a time shorter than 40 min., and for the first time, this deviation does not seem very big. For example, the value of non-equilibrium adsorption rate at 20 min. is 0.12 kg/kg while for the equilibrium rate; it is 0.124 kg/kg. This difference of 0.004 kg water/kg adsorbent can produce a cooling power of 9.908 kJ/kg adsorbent. Without doubt, the non-equilibrium model is closer to the real process of adsorption refrigeration and should not be neglected on designing cycle adsorption chiller, especially when the cycle is short because in real short cycle, the adsorbed refrigerant could not be sufficient due to the non-equilibrium adsorption process **, Wang and Wang, 2005.** In the same figure **Fig. 10.** , the non-equlibrium desorption process is very close to the equilibrium and the reason is simply because of the high rate constant of the desorption process.

Fig. 11 aims to determine the dynamic water sorption, which represents the amount of water involved in one adsorption-desorption cycle. The experiment has consisted of loading adsorbent with water under a temperature of 35°C, then the adsorbent were, afterwards, desorbed at the temperature of 90°C in the same duration as the adsorption time. The difference between adsorbent loading at the end of the adsorption, x= 0.12 kg/kg, and its loading at the end of desorption, x = 0.04 kg/kg, constitutes the dynamic water sorption.The measurment of the adsorpion capacity of this type of silica-gel showed that it is able to exchange a large amount of water of 0.08 kg/kg under operating conditions so it is typical for air conditioning applictions as well as to be driven by hot water temperaure of 90°C.

A complete cycle of adsorption/desorption for the silica gel-water adsorber is shown in **Fig. 12**. During the adsorption phase, the maximum value reached is 0.12 kg/kg after the first half-cycle of 20 mins, and the minimum is 0.04 kg/kg during the second half-cycle of 20 mins. this value is perhapes the target to get the best performance of the system.

To demonstrate the practical cycle of adsorption chiller using a silica gel-water system, **Fig 13** presents the calculated data using Eqs. (1-5) at two worked isobar pressure ranges, namely the vapor pressure of evaporator (T_e= 7°C, P_e = 1 kpa), A-D curve, and the condenser (T_c=30°C, P_c = 4.2 kpa), B-C curve, where A-B and C-D lines represent isostering cooling and heating phases respectively. Measuring isobars of water adsorption/desorption is useful for drawing a temporary cycle of the adsorptive chiller and determining the boundary temperatures for the adsorption and desorption processes. Isobars of water adsorption at P = 1 kpa and desorption at P = 4.2 kpa

measured for the sorpent of silica gel-water represent the isobric stages of a typical chiller cycle **Fig 6.12**. The highest desorption temperature was fixed at 90^{o}C, that determined the content of the water, with x = 0.04 kg/kg. Desorption of water started at 60.5^{o}C, and finished at 90^{o}C (isobar line B-C). The lowest adsorption temperature of 35^{o}C resulted in the maximal adsorbed amount of x = 0.124 kg/kg. Adsorption of water started at 62^{o}C, and finished at 35^{o}C (isobar line D-A). This shows the properties of this type of silica gel to exchange 0.084 kg/kg is very close to the experimantal result obtained by the practical test work **Fig. 11.** As mentioned above, **Fig. 13** will help us to assess the level of temperatures of alternating adsorption to desorption and vice versa, but it is still not able to compare it with the experimental cycle because there is no instrument that can measure the change of water concentration into silica gel with the temperature directly.

5. CONCLUSIONS

The mass transfer in a cylindrical annulus bed packed with silica gel granules during the adsorption/desorption process were analyzed. The measurement of adsorption rates using a non-equilibrium model shows that this type of silica gel is able to exchange an amount of 0.08 kg water/kg adsorbent under the operating conditions of 90^{o}C desorption temperature, 35^{o}C adsorption temperature, and cycle time of 40 min. the practical cycle indicated that the system has the ability to work under different operating system due to its dynamic sorption variation. Thus, this type of adsorbent should be a good candidate for various thermal applications driven by low temperature heat sources.

REFERENCES

- Aristov Y.I., Sapienza A., Ovoshchnikov D.S., Freni A., and Restuccia G., 2012. *Reallocation of Adsorption and Desorption Times for Optimisation of Cooling Cycles*. Internal journal of refrigeration, Vol. 35, PP. 525-531.

- Aristov Y.I., Restuccia G., and Parmon V.N.,2002, *A Family of New Working Materials for Solid Sorption Air Conditioning Systems*, Applied thermal engineering, Vol. 22, PP.191-204.

- Dauo K., Wang R.Z., and Xia Z.Z., 2006, *Development of a New Synthesized Adsorbent for Refrigeration and Air Conditioning Applications*, Applied Thermal Engineering, Vol. 26, PP. 56-65.

- Demir H., Mobedi M., and Ulku S., 2009, *Effect of Porosity on Heat and Mass Transfer in a Granular Adsorbent Bed*, International communications in Heat and Mass Transfer, Vol. 36, PP. 372–377.

- Dieng A.O., and Wang R.Z., 2001, *Literature Review on Solar Adsorption Technologies for Ice-Making and Air Conditioning Purposes and Recent Developments in Solar Technology*. Renewable and Sustainable Energy Reviews, Vol. 5, PP. 313–342.

- Gong L.X., Wang R.Z., Xia Z.Z., Chen C.J., 2011, *Design and Performance Prediction of a New Generation Adsorption Chiller Using Composite Adsorbent*, Energy Convers Mange, Vol. 52, PP. 2345-50.

- Khan M.Z.I., Alam K.C.A., Saha B.B., Hamamoto Y., Akisawa A., and Kashiwagi T., (2006), *Parametric study of a Two-Stageadsorption Chiller using Re-Heat-the Effect of Overall*

Thermal Conductance and Adsorbent Mass on System Performance. International Journal of Thermal science, Vol. 45, PP. 511-519.

- Lambert M. A., 2007, *Design of Solar Powered Adsorption Heat Pump with Ice Storage*, Applied Thermal Engineering, Vol. 27, PP. 1612–1628.
- Leite A.P., Grilo M.B., Belo F.A., and Andrade P.R., 2004, *Dimensioning, Thermal Analysis and Experimental Heat Loss Coefficients of An Adsorbtive Solar Icemaker*, Renewable Energy, Vol. 29, PP. 1643-1663.
- Liu Y.L., Wang R.Z. and Xia Z.Z., 2005. *Experimental Performance of a Silica Gel–Water Adsorption Chiller*. Applied Thermal Engineering, Vol. 25, PP. 359–375.
- Sapienzaa A.l., Glaznevb I.S., Santamariaa S.A., Frenia A.N., and Aristov Y.I., 2012, *Adsorption Chilling Driven by Low Temperature Heat: New Adsorbent and Cycle Optimization*, Applied Thermal Engineering, Vol. 32, PP.141-146.
- Wang D., Zhang J., Yang Q., Li N., and Sumathy K., 2014, *Study of Adsorption Characteristics in Silica Gel–Water Adsorption Refrigeration*, Applied Energy, Vol.113, PP.734–741.
- Wang, W. and Wang, R., 2005, *Investigation of Non-Equilibrium Adsorption Character in Solid Adsorption Refrigeration Cycle*, Heat Mass Transfer, Vol. 41, PP. 680-684.

NOMENCULATUR

b =	bed
D_o=	surface reference diffusivity constant, 2,5*10^{-4} m^2/s
E_a=	diffusion activation energy, 2.33*10^6 J/kg
HTF =	heat transfer fluid
K =	coefficients of the D–A equation = 0.004912 kg/J
k_m =	adsorption rate constant, m^2/s
n =	linear driving force relation constant (for the Brazilian silica gel = 1)
P_c=	condensing pressure, kpa
P_e =	evaporating pressure, kpa
R=	ideal gas constant, 0.462 J/kg.K
$R_{p=}$	radius of adsorbent particle, m
T_{ads} =	adsorption Temperature, ^{o}C
T_{des} =	desorption temperature, ^{o}C
T_c =	condensing temperature, ^{o}C
T_e =	evaporating temperature, ^{o}C
$T_{iso-cooling}$ =	isosteraing cooling temperature, ^{o}C
$T_{iso-heating}$ =	isosteraing heating temperature, ^{o}C
t $_{cycle}$ =	cycle Time, min
x =	adsorbate concentration, kg water/kg adsorbent
x_o =	maximum adsorption capacity, kg water/kg adsorbent
x^* =	equilibrium adsorption capacity, kg water/kg adsorbent
Δx =	difference of adsorbate content, kg water/kg adsorbent

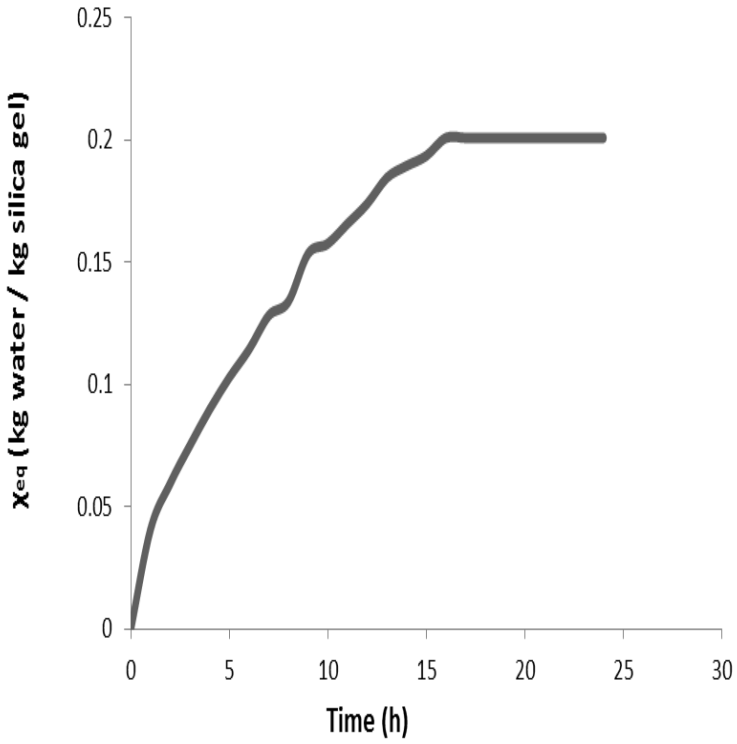

Figue 4. Equilibrium water uptake on silica gel adsorbents at 30^{o}C.

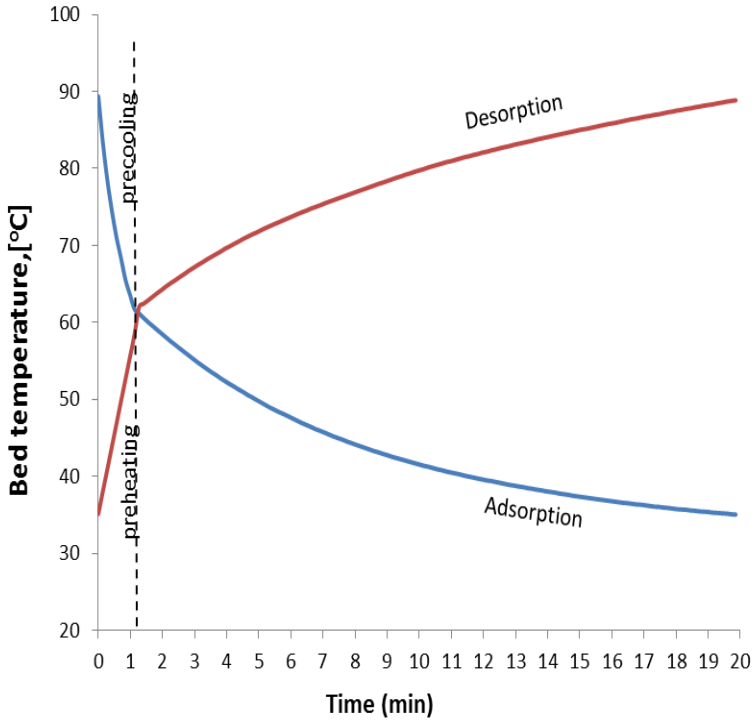

Figure 5. Preheating+ desorption/ precooling + adsorption temporal variation with time.

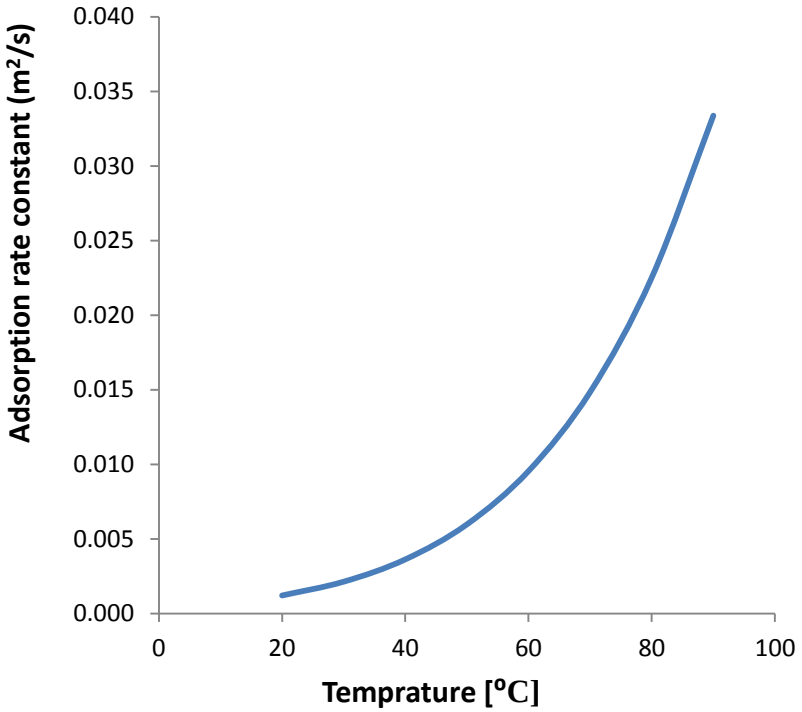

Figure 6. Adsorption rate constant variation with temperature.

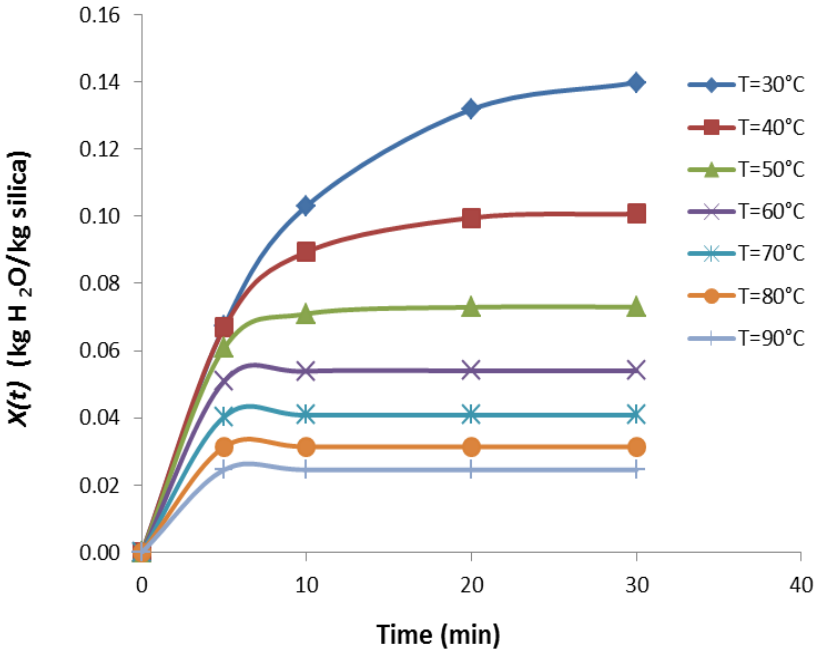

Figure 7. Adsorption uptake variation with time at constant temperature.

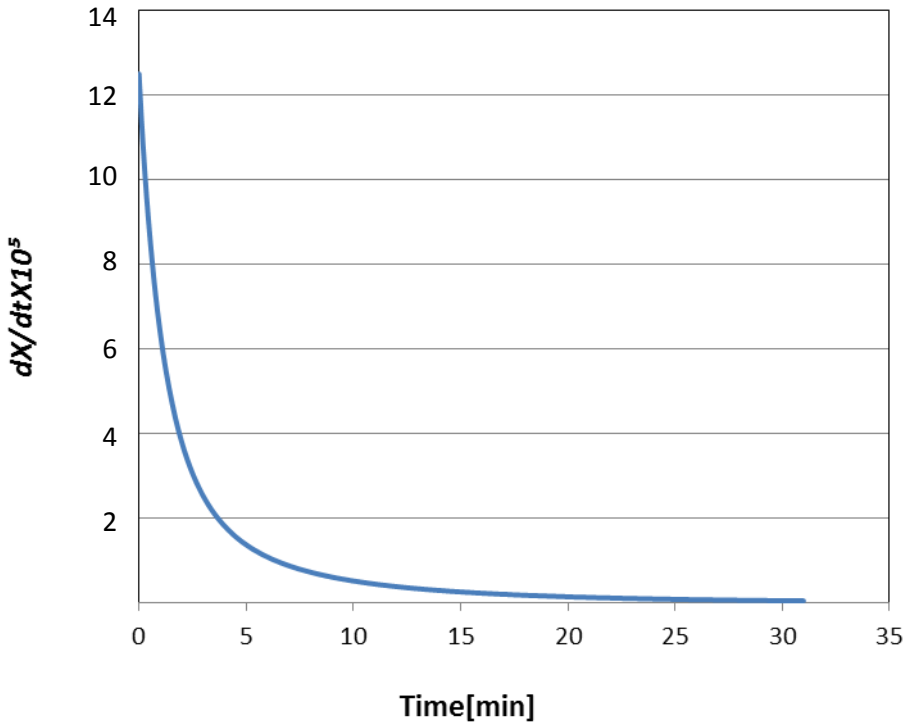

Figure 8. Adsorption velocity variation with time (T_c =30°C, T_{ads} =35°C, T_{des}=90°C).

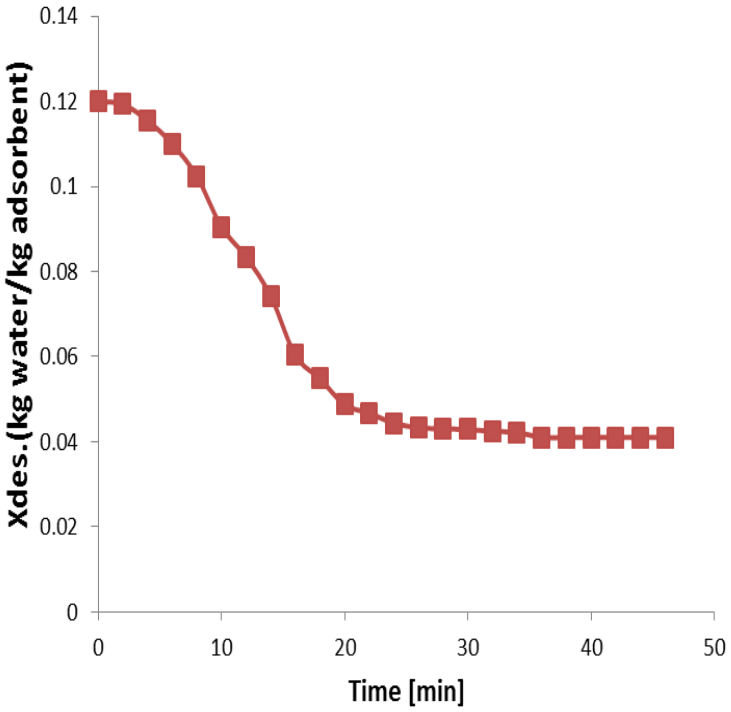

Figure 9. Experimental desorption results variation with time at 90°C hot water.

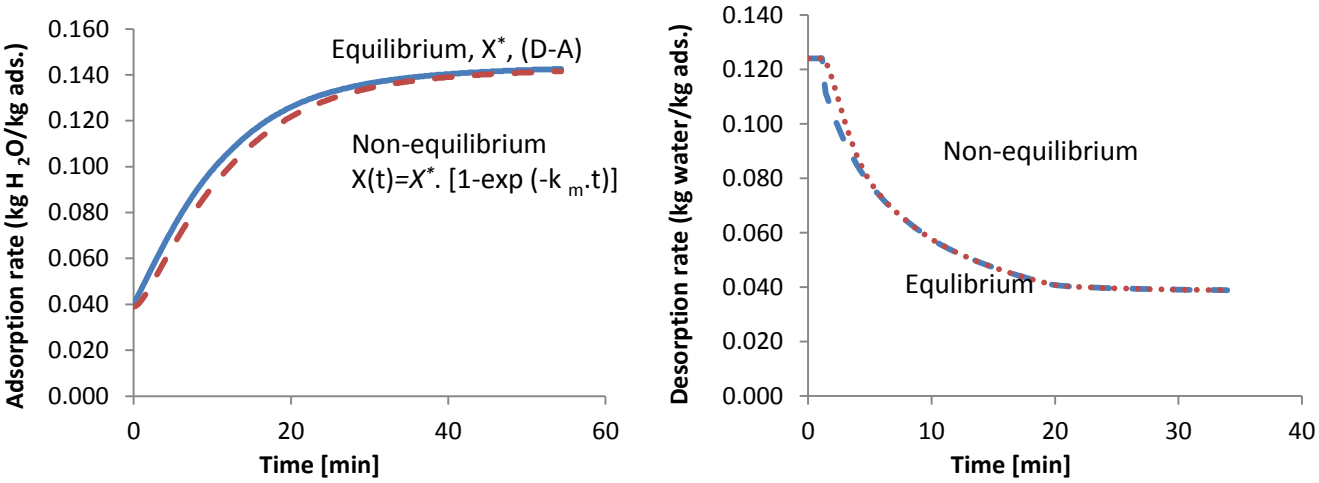

Figure 10. Comparison between equilibrium and non-equilibrium models.

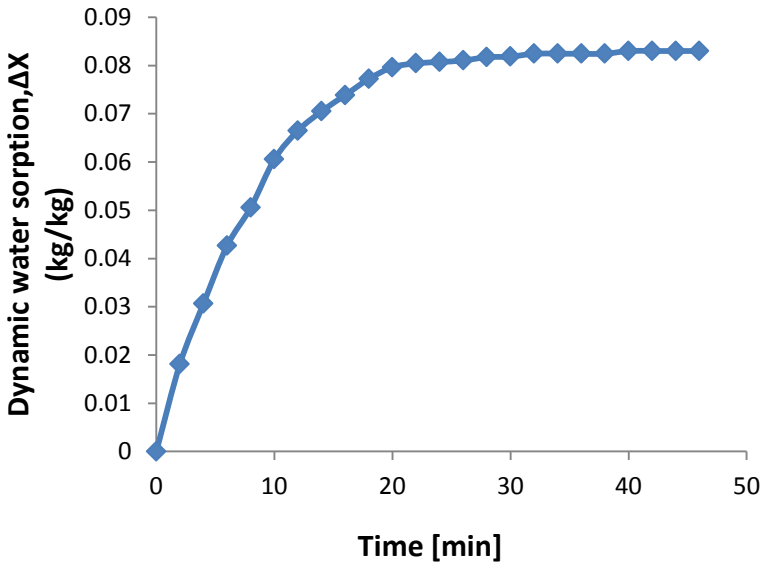

Figure 11. Dynamic water sorption.

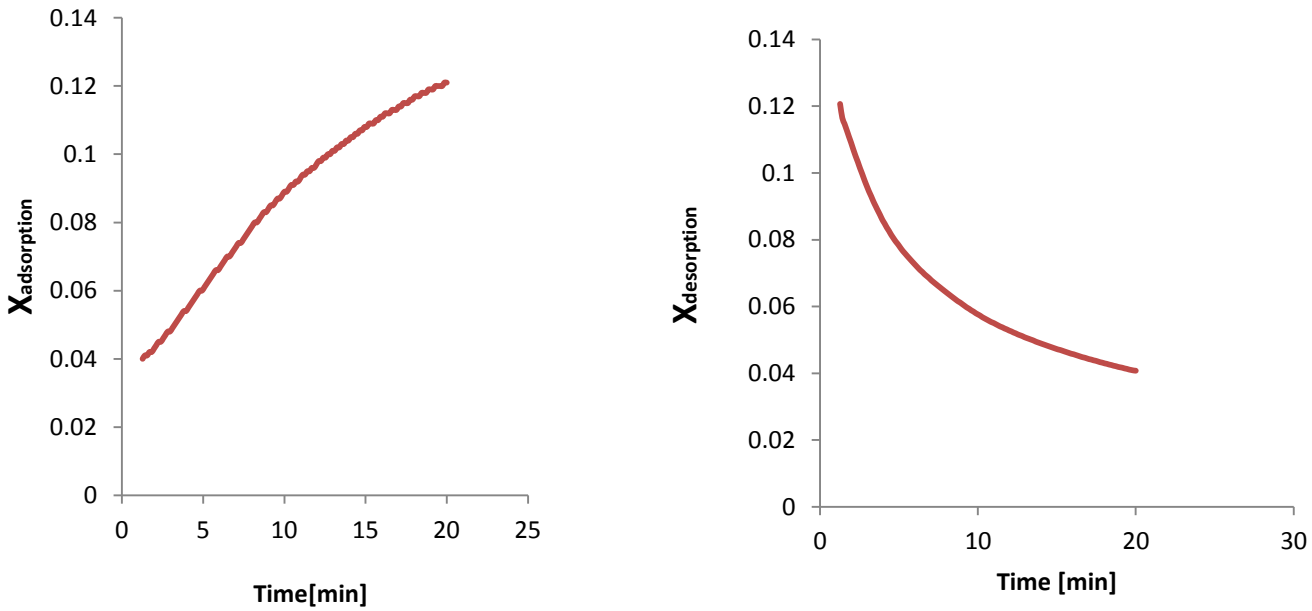

Figure12. Adsorption/Desorption rate variation with time.

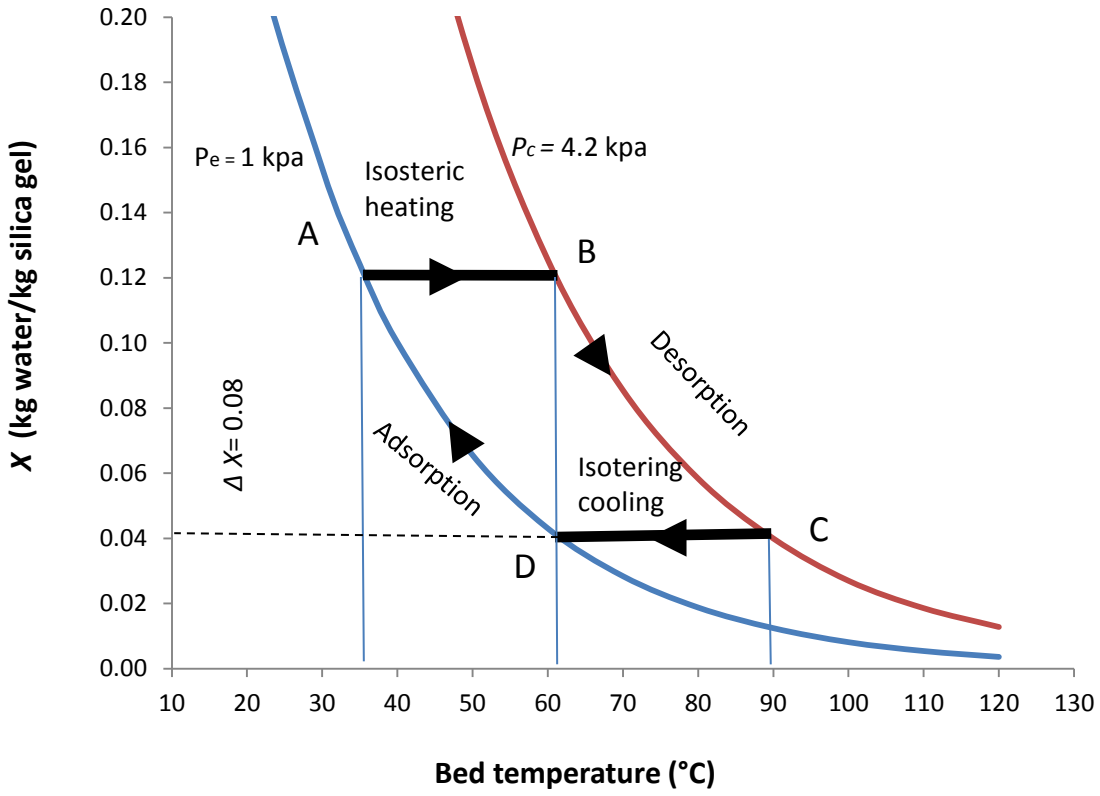

Figure 13. Practical cycles of adsorption and desorption (T_{des}=90°C, T_{ads}=35°C).

The Effect of Hydraulic Accumulator on the Performance of Hydraulic System

Dr.Jafar Mehdi Hassan
Prof. Machines and Equipment . Eng. Dep.
University of Technology
Email- Jafarmehdi1951@yahoo.com

Moayed Waleed Moayed
M.S.c Machines and Equipment. Eng. Dep.
University of Technology
Email- Moayed_w@yahoo.com

ABSTRACT

The purpose of this paper is to depict the effect of adding a hydraulic accumulator to a hydraulic system. The experimental work includes using measuring devices with interface to measure the pressure and the vibration of the system directly by computer so as to show the effect of accumulator graphically for real conditions, also the effects of hydraulic accumulator for different applications have been tested. A simulation analysis of the hydraulic control system using MATLAB.R2010b to study was made to study the stability of the system depending on the transfer function, to estimate the effect of adding the accumulator on stability of the system. A physical simulation test was made for the hydraulic system using MATLAB to show the effect of the accumulator when it's connected to the system for different parameters and compare it with a PID controller. The hydraulic system has been simulated and tested using Automation Studio (AS) to measure different data such as the linear speed of hydraulic cylinder and the effect of connecting the accumulator to the system. All the results showed that the hydraulic accumulator has a great benefits and a large enhancement to the hydraulic system.

Keywords: hydraulic system, accumulator, directional valve, relief valve, energy storage

تأثير مجمع الضغط الهيدروليكي على أداء منظومه هيدروليكيه

مؤيد وليد مؤيد
ماجستير.قسم هندسة المكائن والمعدات – الجامعه التكنلوجية

أ.د جعفر مهدي حسن
أستاذ. قسم هندسة المكائن والمعدات – الجامعه التكنلوجية

الخلاصة

في هذا البحث تم دراسة تأثير اضافة مجمع الظغط على مختلف التطبيقات. محاكاة تحليلية لنظام التحكم الهيدروليكي للمنظومة باستخدام برنامج (MATLAB. R2010b) لدراسة استقرارية النظام أثناء العمل اعتمادا على دالة الانتقال وذلك لتقدير تأثير إضافة مجمع الضغط الهيدروليكي على استقرار النظام. وقد تم عمل محاكاة للمكونات الفيزيائية للنظام باستخدام برنامج(MATLAB). لإظهار أثر مجمع الضغط عندما يكون متصلا بها ولعدة قيم مستنتجه ومقارنتها في حالة اضافة وحدة تحكم للمنظومة, تحليل و محاكاة النظام الهيدروليكي باستخدام برنامج المحاكاة Automation Studio ولنفس المنظومة التي تم اختبارها عمليا حيث تم بناءها واختبارها على جهاز الحاسوب لقياس بيانات مختلفة مثل سرعة المكبس الهيدروليكي الخطية ودراسة تأثير ربط مجمع الضغط الهيدروليكي على النظام. وأظهرت النتائج أن مجمع الضغط الهيدروليكي لديه اهميه في تعزيز وتحسين أستقراية النظام الهيدروليكي .

كلمات رئيسيه: منظومه هيدروليكيه, مجمع ضغط, صمام اتجاهي, صمام تنفيس, خزان للطاقه.

1. INTRODUCTION

In the modern world of today, hydraulics plays a very important role in the day-to-day lives of people. Any device operated by a hydraulic fluid may be called a hydraulic device, but a distinction has to be made between the devices which utilize the impact or momentum of a moving fluid and those operated by a thrust on a confined fluid, i.e. by pressure. This leads us to the subsequent categorization of the field of hydraulics into:

- Hydrodynamics
- Hydrostatics, **Ravi 2005.**

The most susceptible components in any hydraulic system are the pump, valves, rotary actuators (motors) or linear actuators (cylinders), reservoirs and connection lines. In addition, some systems that have a **hydraulic accumulator, Arthur 2006.** A hydraulic accumulator is a device which stores pressurized hydraulic fluid. That way, the pump does not have to be powerful enough to cope with a sudden surge in demand. Instead, it can keep steadily pumping hydraulic fluid and rely on the accumulator to provide extra hydraulic fluid when it is needed.

Accumulators can perform several functions for hydraulic systems such as:

- Supply oil for high transient flow demands when pump can't keep up.
- Help to reduce pump ripple and pressure transients.
- Absorb hydraulic shock waves (due to valve closures or actuators hitting stops).
- Used as a primary power source for small (low demand) systems.
- Help system to accommodate thermal
- Compensate for system leakage expansion of the fluid **,Isaiah 2009.**

There are three main types of accumulators as shown in **Fig .1** bladder, diaphragm bladder and piston The choice of accumulator to use in a given application depends on required speed Of accumulator response, weight, reliability and cost.

The bladder accumulator is commonly used in hydraulic systems because of the main advantages of a bladder accumulator such as, fast acting, no hysteresis, not susceptible to contamination and consistent behavior under similar conditions. Hence, bladder accumulators are the best choice for pressure pulsation damping. **web1,2012.** So we choose this type of accumulator to be used in my experimental branch test. **Yudong X., Y. 2009,** presented a dynamic design of electro -hydraulic control valve with accumulator based on a physical simulation model, he found That velocity oscillation of the electro-hydraulic actuator results from the inter coupling effect of the flow pressure pulsation. In order to reduce the velocity overshoot of the hydraulic actuator, an accumulator can be used to absorb the pressure pulsations to weaken the inter coupling effect. **Xiangdong, k., 2010,** presented a simulation and experimental study on the effects of adding accumulator to the fast forging hydraulic control system. By using the mathematical model of fast forging system and do simulation study, **Minav,T.A et.al. 2012,** presented how to use the hydraulic accumulator as a energy storage device that recovered from an electro-hydraulic forklift truck. The braking energy can be stored in the hydraulic accumulator for a long time, and the efficiency of the system increase from 5% to 32%.

2. THEORETICAL MODELING AND SIMULATION

Theoretical model for the main parts of the hydraulic system will be studied, to determine the transfer function for the system.i-Four-way directional valve controlled cylinder modeling:

The directional valves are one types of the spool valve; the general relations and performance for the valve have been derived and studied.

Considering power matching of hydraulic cylinder and directional valve, **Fig. 2** shows a schematic diagram was made using (Auto CAD 2012) of a valve-piston combination. If orifices area of slide valve is matching and symmetrical as shown in **Fig.2,** with zero lap, then the flow pressure equation in the valve is: **Herbert, 1967.**

$$Q_L = C_d A_1 \sqrt{\frac{1}{\rho}(P_S - P_L)} - C_d A_2 \sqrt{\frac{1}{\rho}(P_S + P_L)} \quad (1)$$

$$Q_S = C_d A_1 \sqrt{\frac{1}{\rho}(P_S - P_L)} + C_d A_2 \sqrt{\frac{1}{\rho}(P_S + P_L)} \quad (2)$$

Where, the sum of the line pressures **(P_1)** and **(P_2)** is approximately equal to the supply pressure **(P_s)**. and the same for the supply flow. **Valdmier, 2006.** Applying the continuity equation to each chamber of the cylinder yields,

$$Q_1 - C_{ip}(P_1 - P_2) = \frac{dV_1}{dt} + \frac{V_1}{\beta_e}\frac{dP_1}{dt} \quad (3)$$

$$C_{ip}(P_1 - P_2) - C_{Ep}P_2 - Q_2 = \frac{dV_2}{dt} + \frac{V_2}{\beta_e}\frac{dP_2}{dt} \quad (4)$$

The equations above solved simultaneously gives,

$$Q_L = A_P S X_P + C_t P_L + \frac{V_t}{4B_e} S\, P_L$$

$$= K_q X_V - K_C P_L \quad (5)$$

Now by applying Newton's second law to the forces on the piston, the resulting force equation Laplas transformed, is

$$F_g = A_P P_L = M_t S^2 X_P + B_P S X_P + K X_P + F_L \quad (6)$$

$$P_L = \frac{F_g}{A_P} = \frac{M_t S^2 X_P}{A_P} + \frac{B_P S X_P}{A_P} + \frac{K X_P}{A_P} + \frac{F_L}{A_P} \quad (7)$$

Now substitute Eq. (7) into Eq. (5) gives,

$$A_P S X_P + C_{tp}\left[\frac{M_t S^2 X_P}{A_P} + \frac{\beta_e S X_P}{A_P} + \frac{K X_P}{A_P} + \frac{F_L}{A_P}\right] + \frac{V_t}{4B_e} S\left[\frac{M_t S^2 X_P}{A_P} + \frac{\beta_e S X_P}{A_P} + \frac{K X_P}{A_P} + \frac{F_L}{A_P}\right] \quad (8)$$

$$= K_q X_V - K_{ce}\left[\frac{M_t S^2 X_P}{A_P} + \frac{\beta_e S X_P}{A_P} + \frac{K X_P}{A_P} + \frac{F_L}{A_P}\right]$$

Where, $k_{ce} = k_c + c_{ip} + c_{ep}/2$

The hydraulic natural frequency

$$\omega_h = \sqrt{\frac{4\beta_e {A_P}^2}{V_t M_t}} (rad/\sec) \quad (9)$$

And the damping ratio, is

$$\delta_h = \frac{K_{ce}}{A_p}\sqrt{\frac{\beta_e M_t}{V_t}} + \frac{B_p}{4A_p}\sqrt{\frac{V_t}{\beta_e M_t}} \quad (10)$$

Now substitute Eqs. (9) and (10) into Eq. (8) and simplify, the transfer function of the valve controlled cylinder is given by :

$$G_{v,c}(s) = \frac{X_P}{X_v} = \frac{\frac{K_q}{A_P}}{S(\frac{S^2}{{\omega_h}^2} + \frac{2\delta_n}{\omega_h} S + 1)} \quad (11)$$

3.THE LONG PIPE LINE MODELING

The precise model of fluid transmission pipeline is a dissipative friction model which is related to the frequency, and it includes a complex Bessel function and a hyperbolic function, as a result, it is very difficult to get accurate analytical solutions. Therefore, in engineering, the influences of pipeline for hydraulic system dynamic dynamic behavior are always neglected, which is unfavorable for system control under the situation of long pipeline. Considering fluid motion feature and physical properties in pipeline such as mass, damping and pressure, **Jiang, 2006**. So that the simple mass-spring-damping dynamic model can be used to simulate the liquid in pipeline. The model is shown in **Fig.3.**(m_o) denotes liquid mass,(B_o) damping coefficient, (K_o)spring rate, ($F_{(t)}$)external force and ($X_{(t)}$) displacement. The transfer function model is derived as follows,

$$G_p(s) = \frac{\frac{1}{K_0}}{\frac{s^2}{\omega_0} + \frac{2\delta_0}{\omega_0} s + 1} \quad (12)$$

Where, **(ω_o)** is natural frequency of long pipeline, $\omega_o = \sqrt{\frac{K_o}{m_o}}$, **(δ_o)** damping ratio,

$$\delta_o = \sqrt{({B_o}^2/4 m_o K_o)}.$$

4. PRESSURE RELIEF VALVE MODELING

Fig. 4 shows a schematic diagram was made using**, Auto CAD, 2012**. of a single-stage pressure control valves (relief valve). The equations describing spool motion**, Herbert, 1967.** is,

$$F_1 - AP_c = M_v s^2 x + K_e x \quad (13)$$

And, the linearized continuity equations at the sensed pressure chamber being controlled are

$$Q_c = K_1(P_s - P_c) = \frac{V_c}{\beta_e} s P_c - A_s x \quad (14)$$

$$Q_P - Q_L - K_l P_s - K_c P_s - K_1(P_s - P_c) + K_q x = \frac{V_t}{\beta_e} s P_s \quad (15)$$

Where,

$K_c = \frac{\partial Q}{\partial P} = \frac{C_d w x_0 \sqrt{2/\rho}}{\sqrt{P_{s0} - P_{R0}}} = \frac{Q_0}{2(P_{s0} - P_{R0})}$ = Flow-pressure coefficient of main orifice.

$K_q = \frac{\partial Q}{\partial x} = C_d w \sqrt{\frac{2}{\rho}(P_{s0} - P_{R0})}$ = flow gain of main orifice.

Now, solving Eq. 14 for **(P_c)**, and substituting into Eq. (15) yields after some manipulation, the transfer function of pressure control valve **(relief valve)** is,

$$G_r(s) = \frac{x}{F_1} = \frac{\frac{1}{K_e}(1+\frac{s}{\omega_1})}{\frac{s^3}{\omega_m{}^2 \omega_1} + \frac{s^2}{\omega_m{}^2} + (\frac{1}{\omega_1} + \frac{1}{\omega_2})s + 1} \quad (16)$$

Where,

$\omega_1 = \frac{\beta_e K_1}{V_c}$ Break frequency of sensing chamber.

$\omega_2 = \frac{\beta_e K_{ce}}{V_t}$ Break frequency of main volume.

$K_e = K_c + K_l$ Equivalent flow-pressure

$\omega_m = \sqrt{\frac{K_e}{M_v}}$ Mechanical natural frequency

5. ACCUMULATOR MODELING

According to gas law **web1,2012.**

$$P_{xo} v_{xo}{}^n = P_a v_a{}^n \quad (17)$$

So that $P_a = P_{xo} v_{xo}{}^n v_a{}^{-n}$ (18)

When the state of accumulator changes from condition **o** to **a**, **Fig.5** the pressure increment is:

$$\Delta p = P_a - P_{xo} = P_{xo} v_{xo}{}^n v_a{}^{-n} - P_{xo} \quad (19)$$

Now for accumulator modeling one can regard accumulator as a gas spring aerodynamic damping model **{9},** and the state can be considered adiabatically, ***n*=1.4**. So that the equation of accumulator is,

$$(P_s - P_a) = \frac{m_a \ddot{V}_a + B_a \dot{V}_a + C_a \dot{V}_a + K_a V_a}{A^2} \quad (20)$$

And, the resulting equation Laplas transformed, is

$$P_s - P_a = \frac{m_a s^2 x + B_a s x + C_a s x + k_a x}{A^2} \quad (21)$$

$$G_a(s)\frac{x}{P_s - P_a} = \frac{{A_a}^2}{m_a s^2 + B_a s + C_a s + k_a} \quad (22)$$

Now, by combining Eqs. **(**11), (12), (16) and (22), the Transfer function for the hydraulic system can be derived:

1- Transfer function for the hydraulic system with accumulator for short pipe.

$$G_{(s)} = \frac{x_p}{P_s} = \frac{\frac{K_q}{A_p}\frac{1}{K_e}\left(1+\frac{s}{\omega_1}\right){A_a}^2}{s\left(\frac{s^2}{{\omega_h}^2}+\frac{2\delta_h}{\omega_h}s+1\right)\left(\frac{s^3}{{\omega_m}^2\omega_1}+\frac{s^2}{{\omega_m}^2}\right)\left(\frac{1}{\omega_1}+\frac{1}{\omega_2}\right)s(m_a s^2 + B_a s + C_a s + k_a)} \quad (23)$$

2- Transfer function for the hydraulic system without accumulator for short pipe

$$G_{(s)} = \frac{x_p}{P_s} = \frac{\frac{K_q}{A_p}\frac{1}{K_e}\left(1+\frac{s}{\omega_1}\right)}{s\left(\frac{s^2}{{\omega_h}^2}+\frac{2\delta_h}{\omega_h}s+1\right)\left(\frac{s^3}{{\omega_m}^2\omega_1}+\frac{s^2}{{\omega_m}^2}\right)\left(\frac{1}{\omega_1}+\frac{1}{\omega_2}\right)s} \quad (24)$$

3- Transfer function for the hydraulic system with accumulator for long pipe.

$$G_{(s)} = \frac{x_p}{P_s} = \frac{\frac{K_q}{A_p}\frac{1}{K_0}\frac{1}{K_e}\left(1+\frac{s}{\omega_1}\right)}{s\left(\frac{s^2}{{\omega_h}^2}+\frac{2\delta_h}{\omega_h}s+1\right)\frac{s^2}{\omega_0}+\frac{2\delta_0}{\omega_0}s+1\left(\frac{s^3}{{\omega_m}^2\omega_1}+\frac{s^2}{{\omega_m}^2}\right)} \cdot\cdot$$

$$\cdot\cdot\frac{{A_a}^2}{\left(\frac{1}{\omega_1}+\frac{1}{\omega_2}\right)s(m_a s^2 + B_a s + C_a s + k_a)} \quad (25)$$

4- Transfer function for the hydraulic system without accumulator for long pipe. $G_{(s)} = \frac{x_p}{P_s} =$

$$\frac{\frac{K_q}{A_p}\frac{1}{K_0}\frac{1}{K_e}\left(1+\frac{s}{\omega_1}\right)}{s\left(\frac{s^2}{{\omega_h}^2}+\frac{2\delta_h}{\omega_h}s+1\right)\frac{s^2}{\omega_0}+\frac{2\delta_0}{\omega_0}s+1\left(\frac{s^3}{{\omega_m}^2\omega_1}+\frac{s^2}{{\omega_m}^2}\right)\left(\frac{1}{\omega_1}+\frac{1}{\omega_2}\right)s} \quad (26)$$

Fig. 6 shows a simple block diagram of the system.

6. RESULT AND DISCUSSION

The hydraulic accumulator has many benefits to the hydraulic system and some of these benefits which have been tested experimentally are:

1-The use of accumulator as an storage device energy

Fig.7 represents the time required the hydraulic cylinder to extend for both cases with and without accumulator and it's clearly shows that the time is decreased when the accumulator is used. The time required the hydraulic cylinder to extend at system pressure **(40 bar)** is **(2.26 sec),** without using the accumulator and at the same pressure but with connecting the accumulator to the system the time is **(1.72 sec)**. the decreasing in time required is about **(33%)**.the same result shown at system pressure

(**30, 20 and 10** bar). **Fig 8** represents the speed of extending of hydraulic cylinder with pressure for both cases with and without accumulator, and it clearly shows that the speed increased when the accumulator connected to the system. This has been happened because the potential energy stored in accumulator

2- The use of accumulator as a leakage compensator:

The accumulator acts as a compensator, by compensating for losses due to internal or external leakage that might occur during the operation. Also pressure losses happened due to the friction in pipes and connections, also due to the increase in oil temperature which affect on the performance of the hydraulic system. At pump pressure**s** of **40, 30, 20 and10 bars,** the decreasing in pressures drop are about **13.3%, 13 %, 12.7% and 12.5%**respestivly ,as shown in **Fig.9.**

3-The use of accumulator to cushion the vibration of the system:

In this test the effect of adding the accumulator on the vibration of the system have been studied. **Figs. 10** and **11** show the velocity and acceleration of vibration with and without using the accumulator .At system pressure **40 bar**, the velocity and acceleration of vibration is **1.6** ***mm*/sec** and **4.3**m/sec^2 respectively, So it's clearly that the accumulator cushions the vibration of the system, also the same results at system pressures **(30, 20 and 10 bar)**. Also a graphical test using vibration meter with interface software **(sw-u801wn)** by **(lutron company)**. was made at point before the relief valve with system pressure **10 bars, Figs. 12** and **13**. From the results above it's clearly that the accumulator reduced the vibration of the system.

4-The use of accumulator as shock absorber:

One of the most important industrial applications of accumulators is in the elimination of high-pressure pulsations or hydraulic shocks. **Quan, 2007.** To test this Phenomena using a graphical chart display using the pressure meter with interface software **(sw-u801 wn)** to view the behavior of pressure at the cylinder when it's suddenly stops at the end of the stroke. The set pressure is **30 bars,** as shown in **Fig.14.** When the cylinder reached the end of the stroke, the stop without using the accumulator is suddenly happened and very fast and causes a hydraulic line shock, but with using the accumulator and from **Fig.15.** it can be seen that the cylinder stops at the end of the stroke fluently. So the benefits of adding accumulators to the system are to damp pressure spikes from pumps

.

7. THE SYSTEM STABILITY TEST USING MATLAB PACKAGE V1.1(R2010B):

Fig .16 represents the Bode diagram for the system without connecting the accumulator for short pipeline, and the result shows that the system is unstable because of the pulsation at the system response and the over shoot is big. **Fig.17** represents the Bode diagram for the system with connecting the accumulator for the short pipeline, and the result shows that the system is stable with phase margin of **87.2 deg** at frequency of **0.06 rad/sec .**Also for a long pipeline **Fig.18** represents the bode diagram for the system without connecting the accumulator and the result shows that the hydraulic system is unstable. **Fig.19** represents the bode diagram for the system with connecting the accumulator, and the result shows that the system is stable with phase margin **of 180 deg.** at frequency of **10.7 rad/sec**.

The physical simulations for the hydraulic system using Matlab V7.11 (R2010b):

A simulation **Fig.20** shows the effect of the accumulator when it's connected to the system for different parameters like cylinder pressure, cyl- inder load, and displacement of cylinder, and the simulated results are shown in **Figs. 21, 22 and 23** respectively. To compare the effect of accumulator and a PID controller to the system the effect of PID controller are shown in **Figs.24, 25 and 25** which makes a self tuner to the system. The self - tuned parameters are found using MATLAB as **P= 0.9, I= 1.2 and D= 0.1.** But when we connected the accumulator the system become more stable and less fluctuation, as shown in **Figs. 7, 28 and 29**. From the figures above it's clearly that the accumulator makes the system steadier than the PID controller; for this case.

The Simulation analysis with automation studio package V5.2

The hydraulic system has been built with Automation Studio Package V5.2**(AS 2008)** to measure different data, such as the linear speed of hydraulic cylinder and to study the effect of connecting the accumulator to the system. **Figs . 30** and **31.** show a compression between the effect of connecting or disconnecting the accumulator on the linear speed at set pressure **of 40 bars**. The results of simulation shows that the liner speed increases by **(31%)** and the response become much faster. Also to estimate the effect of using the accumulator as shock absorber, **Fig. 32** shows the response of the cylinder pressure at the end of stroke. It's clearly that the hydraulic cylinder stops suddenly and so fast which causes a pressure shock at the cylinder, but when the accumulator is connected to the system the rise of the pressure until the cylinder reached to the end of the stroke become more smoothly as shown in **Fig.33** the set pressure is 10 bar.

8. CONCLUSIONS

The present, theoretical simulation analysis and experimental investigation show several conclusions these conclusions can be summarized as below:-

1-The experimental tests showed that the performance of the hydraulic system clearly improvement by connecting the accumulator to the system and the results showed that the accumulator can be used in a wide variety of applications such as:

a- Energy storage
b- Leakage compensation
c- Cushion the vibration
d- Emergency operation
e- Shock absorption

It's found that the effect of accumulator as an energy storage is the most common application than the others.

2- A model equation for the hydraulic system combination has been derived. The theoretical simulation analysis using the bode diagram showed that the system become stable with connecting the accumulator.

3- A physical simulation test using *Matlab V7.11 (R2010b)* was made for the hydraulic system to show the effect of the accumulator when it's connected to the system for the different parameters, the results showed that when the accumulator is connected, the system become more stable and less fluctuation also than the PID Controller, for this case.

4- The practical results and simulation using (AS) program are clearly convergence. This leads us to the possibility of using this program for testing and analysis and design of any hydraulic system.

REFERENCES

-Arthur Akers**,** 2006. *Hydraulic System Analysis*, *Iowa* State University Ames, Iowa, U.S.A .

-Automation Studio, 2008. (AS) *Automation Studio Circuit Design Simulation Software*, Fluid Power and Automation Technologies. user manual

-Herbert E.Merrit**,** 1967, *Hydraulic Control System***,** John Wiley and Sons Inc, New York, US, first edition.

- Isaiah David**,** 2009, *Hydraulic Accumulators Work***.**

-Jiang Ming, Ming Yali, and Yuan Zhejun**,** 1999,*The Model And Dynamic Characteristics Analysis of Long Tubes*, Journal of Harbin Institute of Technology, vol. 31, no 4, pp. 103-106.

-Minav T.A.**, 2012,** *Storage of Energy Recovered from an Industrial Forklift***,** LUT Energy, Lappeenranta University of Technology, P.O. Box 20, 53851 Lappeenranta, Finland.

- Quan Lingxiao, Kong Xiangdong, and Gao Yingjie,2007, *Theory And Experimental Research on Accumulator Absorbing Impulsion without Considering Entrance Characteristics***,** Chinese Journal of Mechanical Engineering, 43(9):28-32.

- Ravi Doddannavar and Andries Barnard, 2005, *Practical Hydraulic Systems*, Linacre House, Jordan Hill, Oxford.

-Valdmier M, 2006, *Design and Modeling of a New Electro Hydraulic Actuator* , National Library of Canada, M.Sc thesis, Mechanical engineering, Toronto, Canada.

-Xiang dong, 2010, *Research of the Influence Factors of the Accumulator Fast Forging Hydraulic Control System*, Heavy Machinery Fluid Power Transmission and Control Key Laboratory of Hebei Yanshan University Qinhuangdao, China, pp.414-417.

-Yudong Xie, 2009, D*ynamic Design of Electro-hydraulic Control Valve Based on Physical Simulation Model*, School of Mechanical Engineering, Shandong University Jinan, China, pp.388-391.

-Web1:2012, *Hydraulic Accumulators*, Retrieved from Web Site, www. Hydraulic Accumulators.com.

NOMENCLATURE

A_1 ,A_2	orifice area gradient
A_p	piston Surface area
A_a	area of accumulator plan
A_s	Spool end area
B_p	viscous damping coefficient of piston
P	proportional gain
P_L	load
P_c	chamber pressure
P_s, P_a:	pressure at system and condition a
P_1, P_2	pressure of Port A and B
P	pressure difference
Q_1 ,Q_2	the flow through proportional valve
$Q_{p\ ideal}$	ideal flow rate of the hydraulic pump
$Q_{p\ actual}$	actual flow rate of the hydraulic pump
Q_L,Q_s	load and system flow
c_a	gas damping factor
C_d	discharge coefficient of the valve
C_{ip} , C_{ep}	internal and external leakage coefficient
D_p	volume displacement rate
D	derivative gain
F_L	load force on piston
F_g	force generated by piston
I	integral gain
k_q	valve flow gain
k_e	equivalent spring rate
k_a	gas stiffness factor
k_o	spring rate of pipe
K_c	valve pressure gain
K_{ce}	total flow-pressure coefficient
K_1	flow-pressure coefficient of restrictor
K_l	leakage coefficient
m_a	liquid equivalent mass
M_t	total mass of piston
M_v	spool mass
N	rotational speed of pump
t	time
V_t	total hydraulic oil volume in cylinder
V_1 , V_2	forward and return chamber volume
V_c	sensing chamber volume
V_o	gas volume
V_a	volume of accumulator
X_p	piston displacement
X_v	valve displacement
x	spool displacement

GREEK SYMBOLS

δ Damping coefficient

δ_0 Damping ratio of pipe

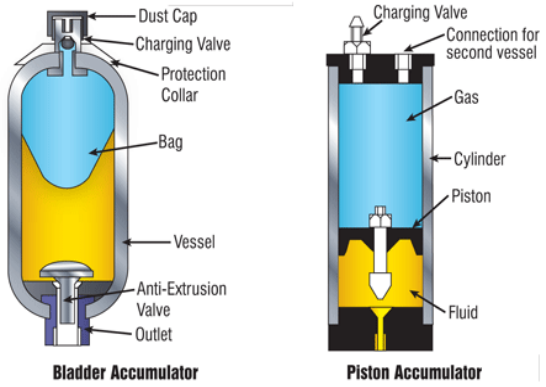

Bladder Accumulator **Piston Accumulator**

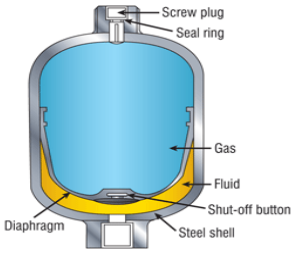

Diaphragm Accumulator

Figure 1. The main types of accumulator**, Automation Studio, 2008.**

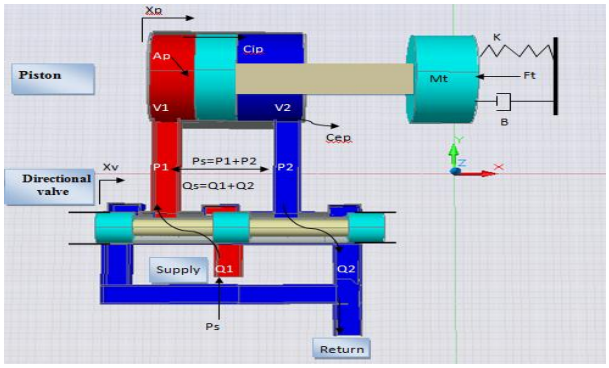

Figure2. Schematic of a valve-piston combination**.**

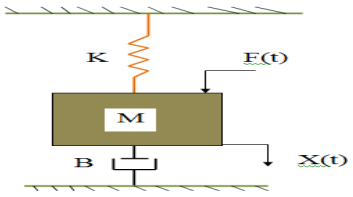

Figure3. Simulation model of liquid in pipeline, **Xiang dong, 2010**.

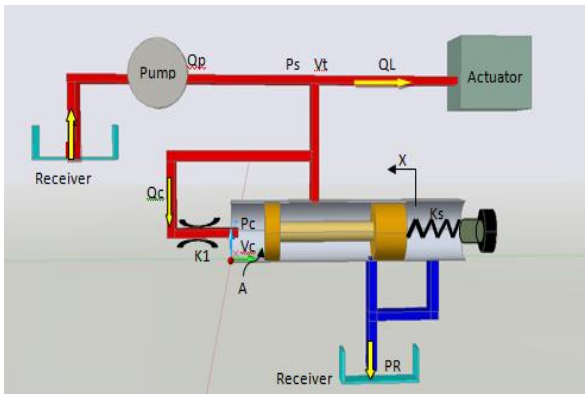

Figure4. Schematic of a single-stage pressure relief valve**.**

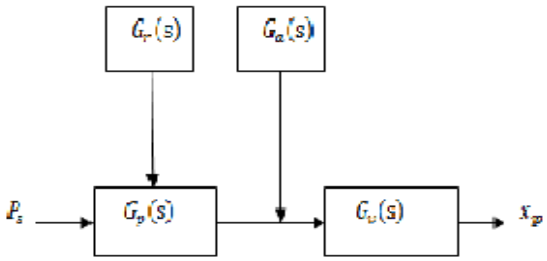

Figure5. Bladder type hydraulic accumulator, **Isaiah David, 2009.**

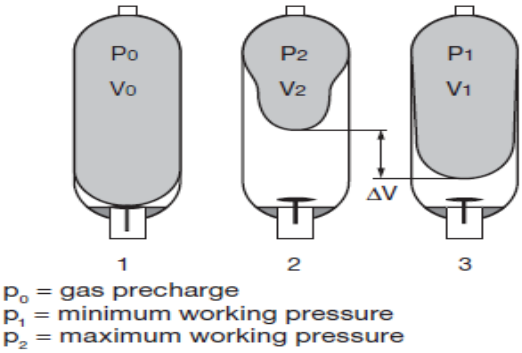

Figure.6 Simple block diagram for the hydraulic system.

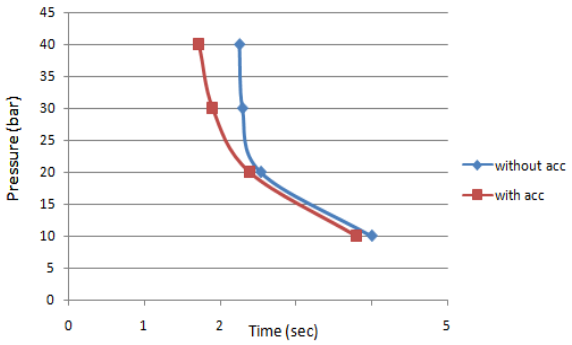

Figure7. The time required the hydraulic cylinder to extend for both cases with and without accumulator.

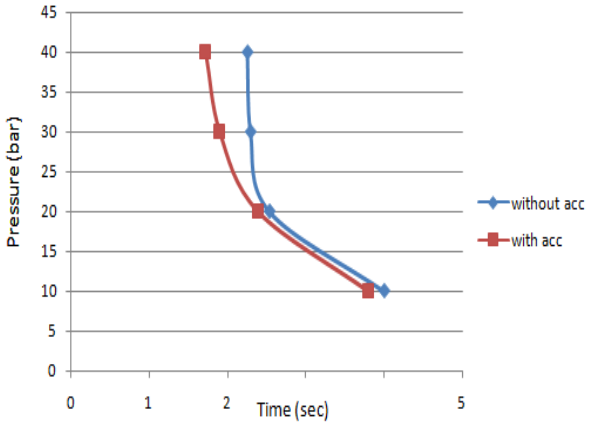

Figure8. The speed of extending of hydraulic cylinder for both cases with and without accumulator.

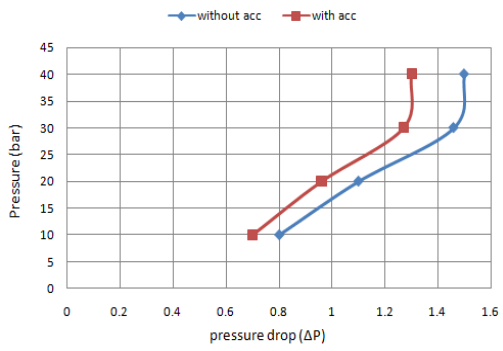

Figure9. The pressure drops across the hydraulic system.

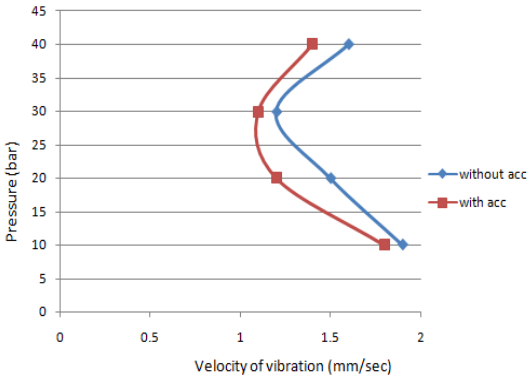

Figure10. The velocity of vibration for both cases, with and without connecting the accumulator.

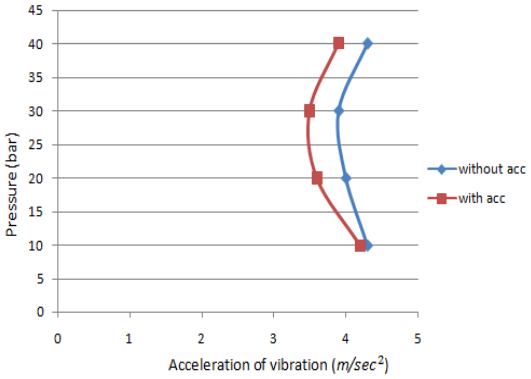

Figure11. The acceleration of vibration for both cases, with and without connecting the accumulator.

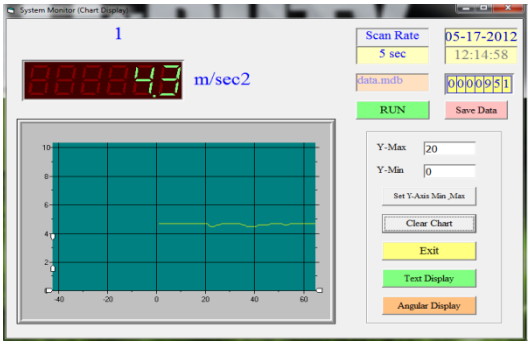

Figure12. Acceleration of vibration at set pressure (10) bar without connecting the accumulator.

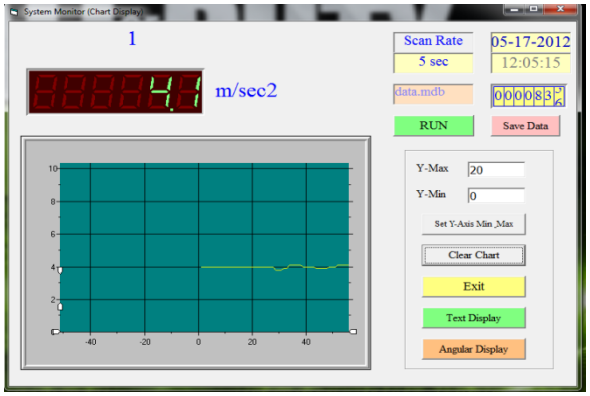

Figure13. Acceleration of vibration at set pressure (10) bar with connecting the accumulator**.**

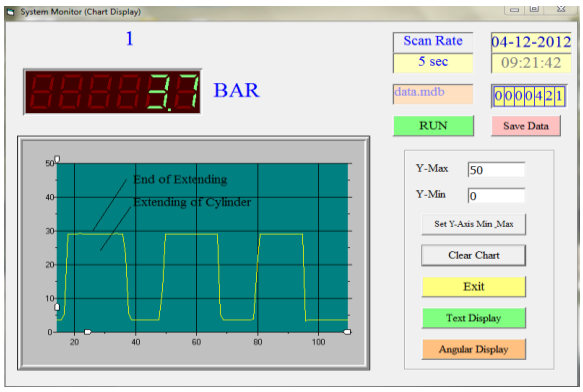

Figure14. Pressure measured at the cylinder without connecting the accumulator, the set pressure is 30bar.

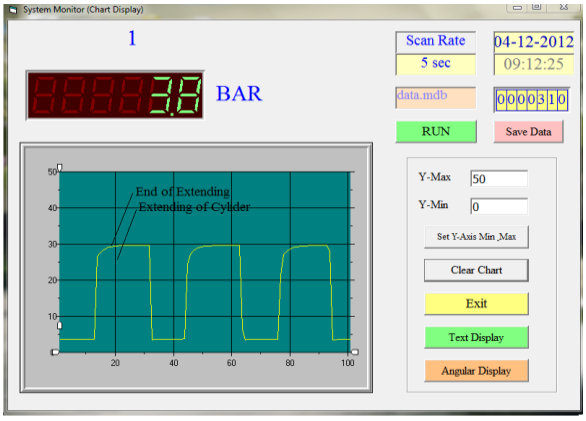

Figure15. Pressure measured at the cylinder with connecting the accumulator.

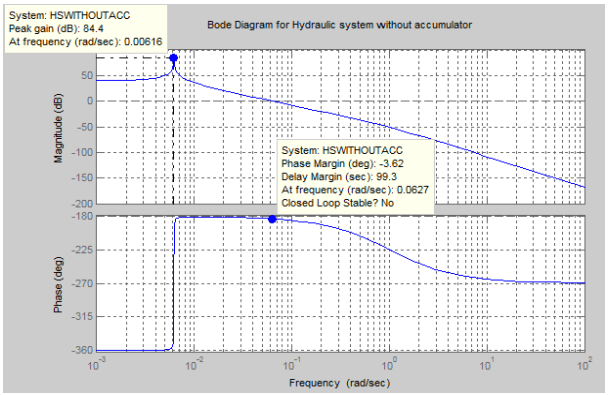

Figure16. The bode diagram for the (tf) of the hydraulic system without connecting the accumulator for short pipeline.

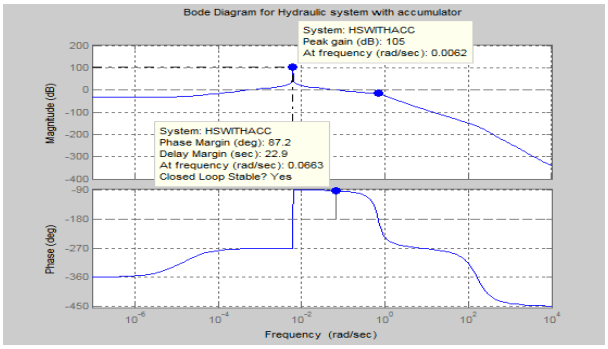

Figure17. The bode diagram for the (tf) of the hydraulic system with connecting the accumulator for short pipeline.

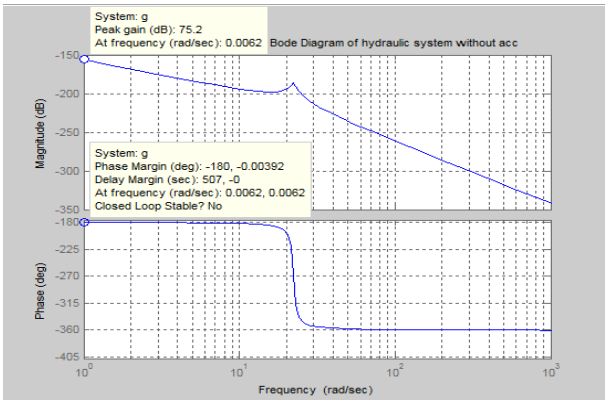

Figure18. The bode diagram for the (tf) of the hydraulic system without connecting the accumulator for long pipeline.

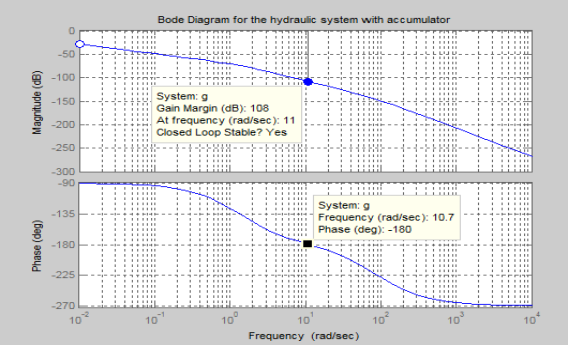

Figure19. The bode diagram for the (tf) of the hydraulic system with connecting the accumulator for long pipeline.

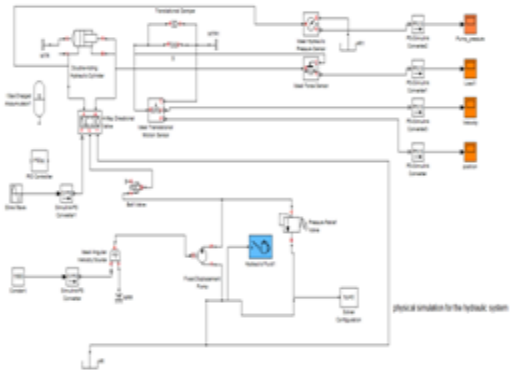

Figure20. Physical simulation for the hydraulic system.

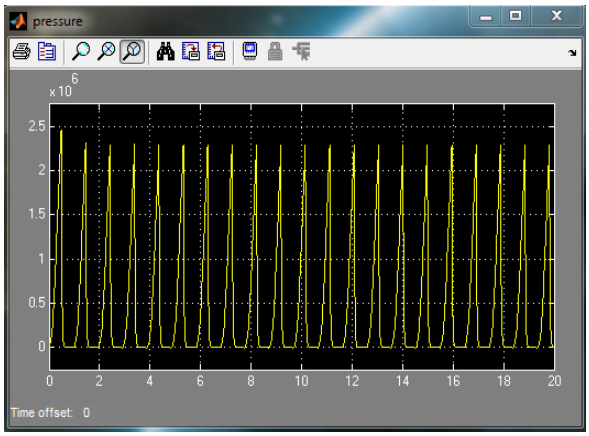

Figure21. The cylinder pressure of hydraulic system without the pid controller or the accumulator.

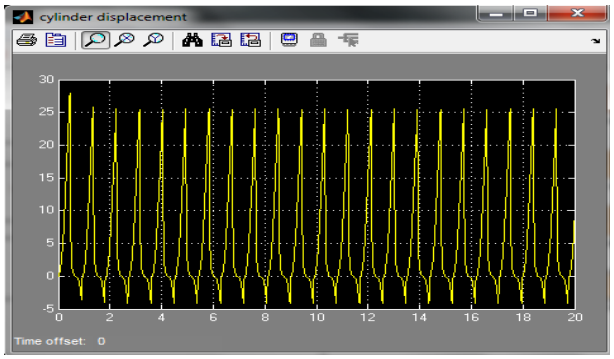

Figure22. The cylinder load of hydraulic system without the pid controller or the accumulator.

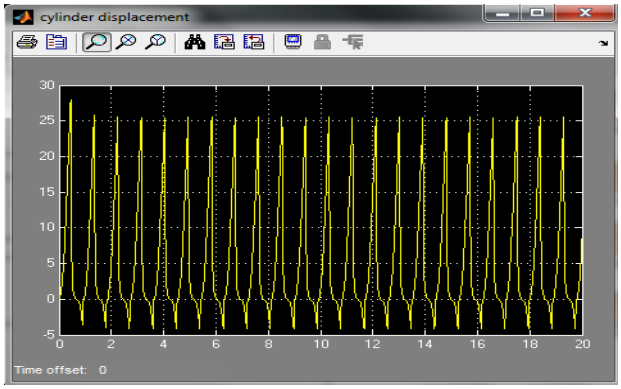

Figure23. The cylinder displacement without connecting the pid controller or the accumulator.

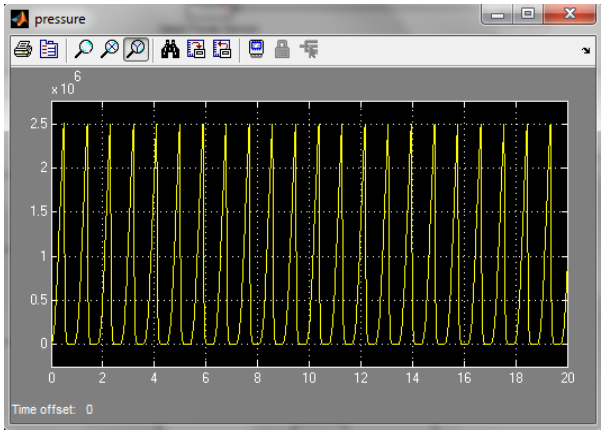

Figure24. The cylinder pressure of hydraulic system with connecting the pid controller.

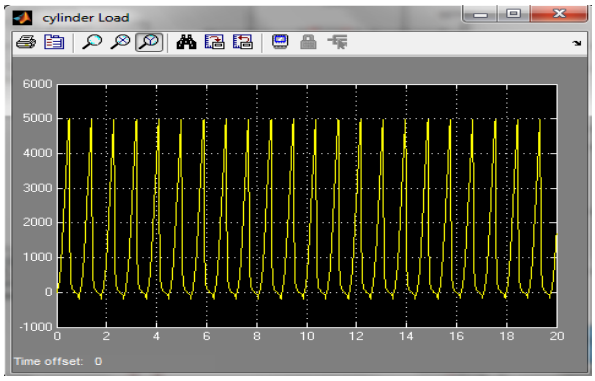

Figure25. The cylinder load of hydraulic system with connecting the pid controller.

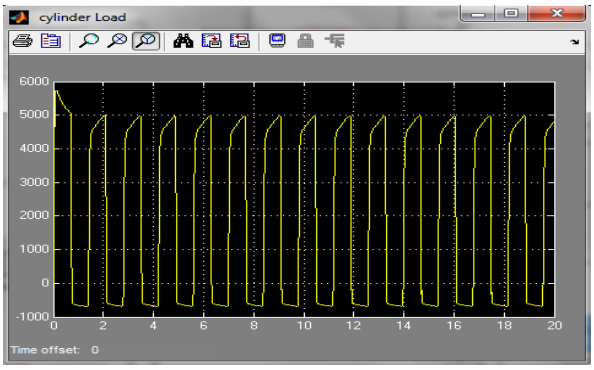

Figure28. The cylinder displacement of hydraulic system with connecting the pid controller.

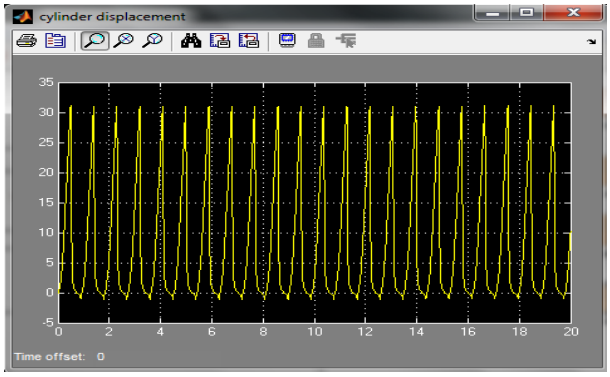

Figure26. The cylinder displacement of hydraulic system with connecting the pid controller.

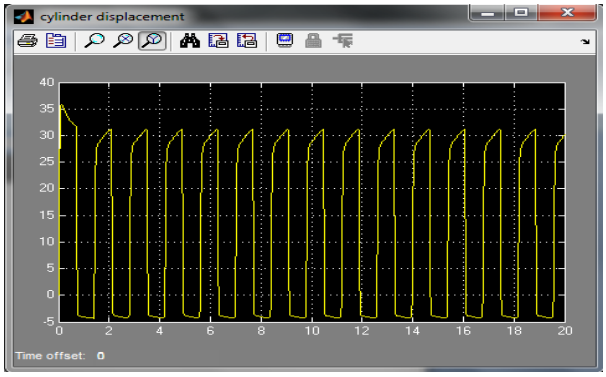

Figure29. The cylinder displacement of hydraulic system with connecting the accumulator.

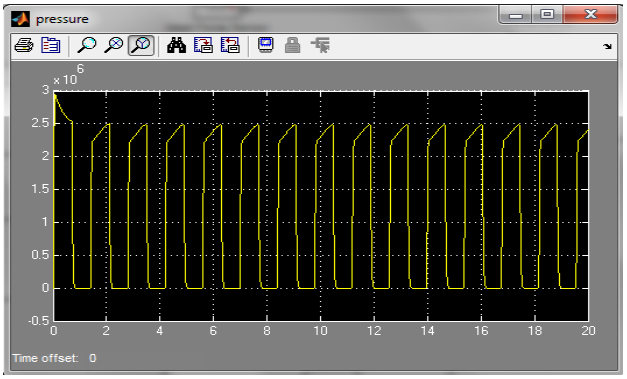

Figure27. The cylinder pressure of hydraulic system with connecting the accumulator.

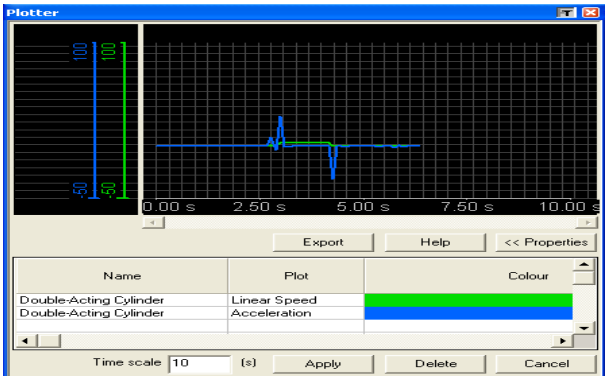

Figure30. The linear speed and acceleration of cylinder without connecting the accumulator using (as).

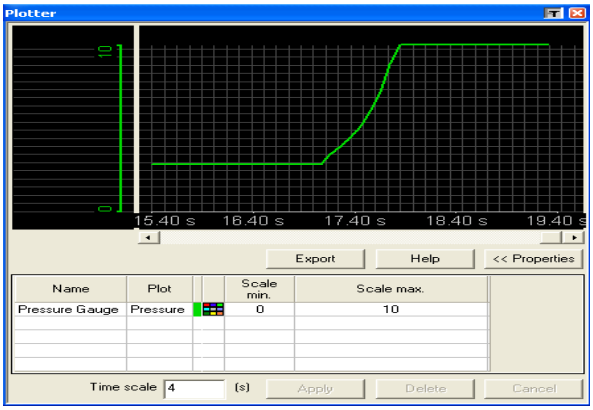

Figure31. The linear speed and acceleration of hydraulic with connecting the accumulator using (as **).**

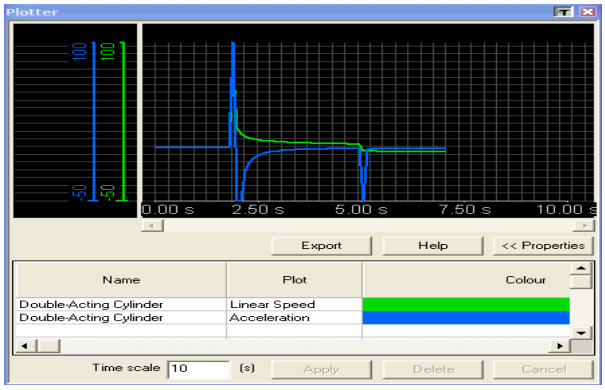

Figure32. The cylinder pressure at the end of stroke without connecting the accumulator using (as).

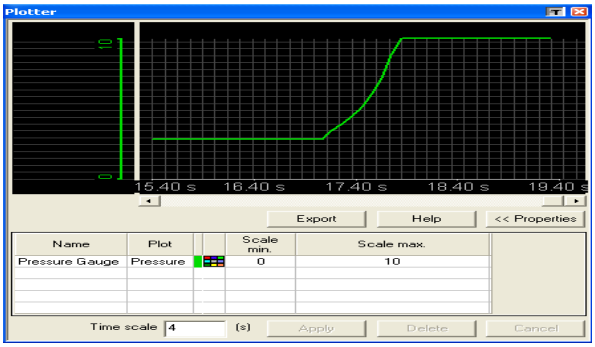

Figure 33. The cylinder pressure at the end of stroke with connecting the accumulator using (as).

Forward-Reverse Osmosis Processes for Oily Wastewater Treatment

Hasan Farhood Makki
Chemical Engineering Department – College of Engineering – University of Baghdad – Iraq
hs_fmfm@yahoo.com

Noor Hammood Zghair
Chemical Engineering Department – College of Engineering – University of Baghdad – Iraq
nn_h_zz@yahoo.com

ABSTRACT

In this study, the feasibility of Forward–Reverse osmosis processes was investigated for treating the oily wastewater. The first stage was applied forward osmosis process to recover pure water from oily wastewater. Sodium chloride (NaCl) and magnesium chloride ($MgCl_2$) salts were used as draw solutions and the membrane that was used in forward osmosis (FO) process was cellulose triacetate (CTA) membrane. The operating parameters studied were: draw solution concentrations (0.25 – 0.75 M), oil concentration in feed solution (FS) (100-1000 ppm), the temperature of FS and draw solution (DS) (30 - 45 °C), pH of FS (4-10) and the flow rate of both DS and FS (20 - 60 l/h). It was found that the water flux and oil concentration in FS increase by increasing the concentration of draw solutions, the flow rate of FS and the temperature for a limit (40^oC), then, the water flux and oil concentration decrease with increasing the temperature because of happening the internal concentration polarization phenomenon. By increasing the oil concentration in FS and the flow rate of the DS, the water flux and oil concentration in FS decreased, while it had a fluctuated behavior with increasing pH of oily wastewater. It was found also that $MgCl_2$ gives water flux higher than NaCl. So the values of resistance to solute diffusion within the membrane porous support layer were 55.93 h/m and 26.21 h/m for NaCl and $MgCl_2$ respectively. The second stage was applied reverse osmosis process using polyamide (thin film composite (TFC)) membrane for separating the fresh water from a diluted (NaCl) solution using different parameters such as draw solution concentration (0.08–0.16 M), feed flow rate (20–40 l/h).

Keywords: membranes separations, forward- reverse osmosis, oily wastewater.

عمليات التنافذ الامامي–العكسي لمعالجة المياه الملوثة بالزيوت

د. حسن فرهود مكي
جامعة بغداد/ كلية الهندسة /قسم الكيمياوي

الباحثه نور حمود زغير
جامعة بغداد/ كلية الهندسة /قسم الكيمياوي

الخلاصة

في هذه الدراسة, تم بحث مدى ملائمة عمليات التنافذ (الامامي– العكسي) لمعالجة المياه الملوثة بالزيوت. في المرحلة الاولى طبقت عملية التنافذ الامامي لاسترجاع الماء النقي من المياه الملوثة بالزيوت. استخدمت كل من املاح كلوريد الصوديوم (NaCl) و كلوريد المغنيسيوم ($MgCl_2$) كمحاليل سحب, واستخدم غشاء السليلوز تراي اسيتيت خلال عملية التنافذ الامامي. الظروف التشغيلية التي تم دراستها هي : تركيز محاليل السحب (0,25 – 0,75مول / لتر), تركيز الزيت في محلول القيم (100 – 1000 جزء بالمليون), درجة حامضية اللقيم (4 – 10),

درجة حرارة محلول اللقيم ومحلول السحب (30 - 45 م^{o}) و معدل الجريان الحجمي لكل من محلول اللقيم ومحلول السحب (20 - 60 لتر/ساعة) , وجد ضمن مدى الظروف التشغيلية التي تم دراستها, ان معدل تدفق الماء وتركيز الزيت في محلول اللقيم يزداد بزيادة تركيز محلول السحب , معدل الجريان الحجمي لمحلول اللقيم و درجة الحرارة لمحاليل اللقيم والسحب لغاية (40 م^{o}), بعد ذلك, يقل معدل تدفق الماء وتركيز الزيت في محلول اللقيم مع زيادة درجة الحرارة بسبب حدوث ظاهرة استقطاب التركيز الداخلي. بزيادة تركيز الزيت في محلول اللقيم و معدل الجريان الحجمي لمحلول السحب, يقل معدل تدفق الماء وتركيز الزيت في محلول اللقيم. بينما وجد ان له سلوك متذبذب بزيادة درجة حامضية اللقيم. كذلك وجد بأن املاح كلوريد المغنيسيوم تعطي معدل تدفق ماء اعلى من املاح كلوريد الصوديوم. كانت قيم المقاومة لانتشار المذاب داخل الطبقة الداعمة المسامية للغشاء (55,9 ساعة/ م) و (26,2 ساعة/ م) لكل من كلوريد الصوديوم و كلوريد المغنيسيوم على التوالي. المرحلة الثانية تم تطبيق عملية التنافذ العكسي لفصل الماء النقي من محلول كلوريد الصوديوم المخفف باستخدام متغيرات مختلفة كتركيز محلول السحب (0,08 – 0,16مول / لتر) ومعدل الجريان الحجمي لمحلول السحب (20 -40 لتر/ساعة).

1.INTRODUCTION

One of the most challenging problems today is the removal of oil from wastewater. Large amounts of wastewater are generated by industrial companies that produce or handle oil and other organic compounds, both immiscible and miscible in water. Oily wastewater discharged into the environment causes serious pollution problems since the biodegradability of oil is very low and oily wastewater hinders biological processing at sewage treatment plants , **Mohammed et al., 2011**. Oily wastewater is defined as liquid waste either from automotive workshop or oil industry and known as a combination of water with some surface oil, oil sludge or sediments which contained lubricants, cutting fluid and heavy hydrocarbon such as tars, grease and diesel oil, bacteria and light hydrocarbon at concentration that may vary from a few hundred parts per million to as much as 1 to 10 percent by volume , **Bujang et al., 2012**. Oil and grease in wastewater can exist in several forms: free, dispersed or emulsified. The differences are based primarily on size ,**Cheryan and Rajagopalan, 1998**. Based on the form of the oil in the water, different methods have been applied to its removal. Conventional oily wastewater treatment methods include gravity separation and skimming, dissolved air flotation, de-emulsification, coagulation and flocculation, which have several disadvantages such as low efficiency, high operation costs, corrosion and recontamination problems ,**Yan et al., 2006**. Osmosis a physical phenomenon extensively studied by scientists in various disciplines of science and engineering. In a FO process, water diffuses spontaneously through a semi-permeable membrane from a feed solution (FS) with low osmotic pressure to a draw solution (DS) with high osmotic pressure , **Zhao and Zou**, 2011. The osmotic driving forces in FO can be significantly greater than hydraulic driving forces in RO, theoretically, leading to higher water flux rates and recoveries. Besides low or no

hydraulic pressure requirements for FO process, high rejection of a wide range of contaminants, lower membrane fouling, and simplicity of equipment used in the process are additional advantages of FO ,**Bamaga et al., 2011 and Kim et al., 2012**.

In 1886, van't Hoff formulated an equation to calculate osmotic pressure (π), based on data for sugar solution and the similarity of dilute solutions to ideal gases ,**Thain, 1967.**

$$\pi = \Phi \, i \, R_g \, T \, C \qquad (1)$$

where C is the concentration of solute, T is the temperature of solution, R_g is the gas constant, i is number of dissociated ions per molecule, and Φ is osmotic coefficient. Basically, the FO desalination process involves two steps. In the first step, the fresh water is extracted from the raw water source using a suitable draw solution (osmotic agent having a high osmotic pressure). The second step deals with separation of the osmotic agent from the fresh water , **Bamaga et al., 2011**. The diluted draw solution that was produced from FO process is subsequently desalinated by RO to produce fresh water suitable for beneficial uses , **Xie et al., 2012**.

The main goal in this study was to investigate the technical feasibility and the efficiency of FO– RO processes for treating the oily wastewater. The first stage is application forward osmosis process to recovery of water from oily wastewater using FO process. In the second stage, a technically reverse osmosis process was employed to treat the diluted draw solution outlet from forward osmosis using polyamide and the effect of (NaCl) concentration in feed solution and feed flow rate were studied on water flux for RO process.

2.CONCENTRATION POLARIZATION

Concentration polarization is the term used to describe the accumulation of rejected solute at the surface of a membrane so that the solute concentration at the membrane wall is much higher than that of the bulk feed solution , **Ahmed, 2007**. Because asymmetric FO membranes are comprised of a dense layer on top of a porous support layer, concentration polarization occurs externally at the feed–membrane and draw solution–membrane interfaces, and internally in the porous support layer of the membrane ,**Achilli et al., 2010**. Below, these two concentration polarization phenomena are quantitatively described.

2.1 External Concentration Polarization

In osmotic processes, concentration polarization can occur on both sides of the membrane. Concentrative external concentration polarization occurs in forward osmosis when the feed solution is placed against the active layer of the membrane. To account for this phenomenon, the extent of concentration polarization was calculated from film theory. The concentrative external concentration polarization moduli at each permeate flux, J_w, could be calculated using ,**Ahmed, 2011.**

$$\frac{\pi_{F,m}}{\pi_{F,b}} = \exp\left(\frac{J_w}{k}\right) \quad (2)$$

Where, J_w is the experimental permeate water flux, k is the mass transfer coefficient and $\pi_{F,m}$ and $\pi_{F,b}$ are the osmotic pressures of the feed solution at the membrane surface and in the bulk, respectively. Note that the exponent is positive, indicating that $\pi_{F,m} > \pi_{F,b}$ (**McCutcheon and Elimelech**, 2006). The mass transfer coefficient, k, is:

$$k = \frac{Sh\ D}{d_h} \quad (3)$$

Where, Sh is Sherwood number, D is the solute diffusion coefficient and d_h is hydraulic diameter.

Simultaneously, the draw solution in contact with the permeate side of the membrane is being diluted at the permeate-membrane interface by the permeating water. This is called dilutive ECP , **Digman**, **2010**. Dilutive external concentration polarization can be calculated also from film theory. The external concentration polarization modulus ($\pi_{D,m}/\pi_{D,b}$) is calculated using:

$$\frac{\pi_{D,m}}{\pi_{D,b}} = exp\left(-\frac{J_W}{k}\right) \quad (4)$$

where $\pi_{D,m}$ is the osmotic pressure at the membrane surface and $\pi_{D,b}$ is the bulk osmotic pressure of the draw solution. J_W is negative in this equation because the water flux is in the direction of the more concentrated solution and the concentration polarization effect is dilutive ($\pi_{D,m} < \pi_{D,b}$). To model the flux performance of the forward osmosis process in the presence of external concentration polarization, we start with the flux equation for forward osmosis, given as ,**Achilli et al.**, **2009.**

$$J_w = A\ \sigma\ (\pi_{D,b} - \pi_{F,b}) \quad (5)$$

Here, A is the pure water permeability coefficient, σ is the osmotic reflection coefficient, has a value of 1. Eq. (5) predicts flux as functions of driving force only in the absence of concentrative or dilutive ECP, which may be valid only if the permeate flux is very low. When flux rates are higher, this equation must be modified to include both the concentrative and dilutive ECP , **McCutcheon and Elimelech, 2006**.

$$J_w = A\left[\pi_{D,b} \exp\left(-\frac{J_w}{k}\right) - \pi_{F,b} \exp\left(\frac{J_w}{k}\right)\right] \quad (6)$$

2.2 Internal Concentration Polarization

Internal concentration polarization (ICP) is closely related to external concentration polarization (ECP) at the surface of the active layer as shown in **Fig. 1** ,**Alsvik and Hägg**, **2013**. The ICP phenomenon occurs on the permeate side. We refer to this as

dilutive ICP since the draw solution is diluted by the permeate water within the porous support of the membrane ,**McCutcheon and Elimelech**, **2006**. **Loeb et al., 1997.** similarly described flux behavior in the FO mode ,**Cath et al., 2006**.

$$K = \left(\frac{1}{J_w}\right) \ln \frac{B + A\pi_{D,b}}{B + J_w + A\pi_{F,m}} \quad (7)$$

where K is the resistance to solute diffusion within the membrane porous support layer which is a measure of how easily a solute can diffuse into and out of the support layer and thus is a measure of the severity of ICP, is defined as:

$$K = \frac{t\tau}{D\varepsilon} \quad (8)$$

where t is the membrane thickness, τ is the tortuously of the membrane porous support layer, ε is porosity of the porous support layer, and D is the diffusion coefficient of the solute. Because t, τ, and ε are fixed for our FO membrane, K is dependent only on D ,**Gray et al., 2006.**

When assuming that B = 0, $\sigma = 0$ (i.e., the salt permeability is negligible) and the equation (7) is rearranged, an implicit equation for the permeate water flux is obtained:

$$J_w = A\left[\pi_{D,b} \exp(-\mathrm{J_w}K) - \pi_{F,m}\right] \quad (9)$$

Here, $\pi_{D,b}$ is now corrected by the dilutive ICP modulus, given by:

$$\frac{\pi_{D,i}}{\pi_{D,b}} = \exp(-\mathrm{J_w}K) \quad (10)$$

where $\pi_{D,i}$ is the osmotic pressure of the draw solution on the inside of the active layer within the porous support. The negative exponent is indicative of dilution at this point, or $\pi_{D,i} < \pi_{D,b}$.

By substituting Eq. (2) into (9) ,**Cath et al., 2006.**

$$J_w = A\left[\pi_{D,b} \exp(-\mathrm{J_w}K) - \pi_{F,b} \exp\left(\frac{J_w}{k}\right)\right] \quad (11)$$

In this study assuming that the salt permeability coefficient (B) is equal to zero and the small value of the flux (J_W) compared to osmotic pressure of draw solution, therefore the Equations (8) it can simplify as follows:

$$J_W = \frac{1}{K} \ln\left(\frac{\pi_{D,b}}{\pi_{F,b}}\right) \quad (12)$$

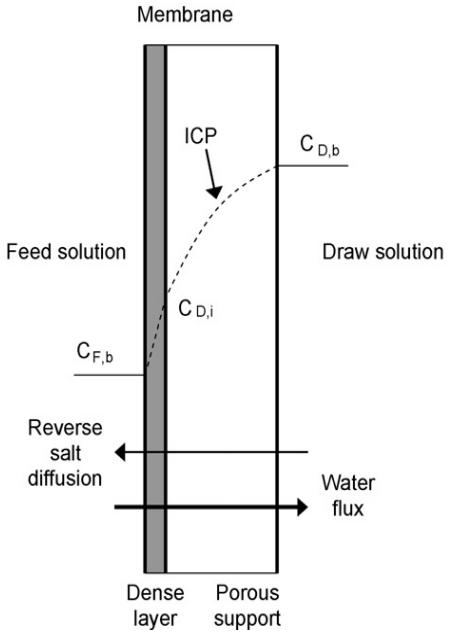

Figure 1: Concentration polarization in an asymmetric membrane in FO (concentrative ECP and dilutive ICP) **,Achilli et al., 2010.**

3. MATERIALS AND METHODS

3.1 The membranes

An asymmetric FO membrane acquired from Hydration Technology Innovations (X-Pack^{TM} supplied by Hydration Technology Inc., Albany, OR) was used for forward osmosis experiments in this study. The membrane that was used is a cellulose triacetate casted onto a non-woven back support consisting of polyester fibers individually coated with polyethylene. The physical characteristics of this specific CTA membrane are unique compared with other commercially available semi-permeable membranes and has been acknowledged to be the best available membrane for most FO applications ,**Choi, 2011**. The CTA membrane lacks a thick support layer with thickness of the membrane is less than 50 μm and membrane salt rejection is (95-99 %). While a thin film composite membrane (TFC) was used in RO process. TFC membrane is an aromatic polyamide consisting of three layers: polyester support web (120 μm), micro porous poly sulphone interlayer (40 μm), and ultra thin polyamide barrier layer on the top surface (0.2 μm). The specifications of the TFC membrane are salt rejection (96 – 99 %), maximum operating pressure (6 – 9 Mpa), maximum operating temperature 45 ^{o}C and pH range for continuous operation (2 – 11).

3.2 Feed and draw solutions preparation

Gasoline and diesel engine oil was used for preparation of the O/W emulsion with total volume was 5 liters. The O/W emulsion was prepared by vigorous mixing of oil and

deionized water using a stirrer at an agitation speed of 2000 rpm for 15 min. The concentrations of oil that was prepared for the feed solution were 100, 500 and 1000 ppm. The phycical specifications of the oil are given in Table 1. Whereas two types of salts (NaCl and $MgCl_2$) were used for preparing the draw solutions in FO experiments. The concentrated draw solution was made by dissolving a solid salt in deionized water with concentrations of 0.25, 0.5, and 0.75 M. The chemical analysis of the salts (NaCl and $MgCl_2$) is given in Table 2. The total draw solution volume was 5 liters. These chemicals were chosen in preparation of draw solutions for their relatively low molecular weight, high solubility, high osmotic pressure that can be given by this solution, easily and economically separated and recycled, and previous interest or utilization in FO research.

Table 1. Typical physical characteristics of oil (Shell Helix HX5**)**.

Viscosity grade	15W-40
Kinematic viscosity (40 °C)	105.4 c St
Kinematic viscosity (100 °C)	13.9 c St
Viscosity index	132
Density at 15 °C	0.885 kg/l
Flash point PMCC	220 °C
Pour point	-30 °C

Table 2. Chemical Specifications of Draw Solutions

Sodium Chloride (NaCl) MW = 58.44	Assay 99.5% min. Max. limits of impurities (%) Ammonia 0.002 Iron 0.002 Lead 0.0005 Potassium 0.02 Sulphate 0.02
Magnesium Chloride ($MgCl_2$) MW = 95	Assay 98% min. Max. limits of impurities (%) Sulfate 0.002 Copper 0.002 Lead 0.005 Iron 0.0005 Zinc 0.0005 Cadmium 0.005

4. EXPERIMENTAL SYSTEMS

4.1 Forward Osmosis System

Experiments were conducted using a laboratory-scale FO system consists of two cylindrical QVF glass vessels with a capacity of 7 liters were used as a feed and draw solutions vessels, **t**wo centrifugal pumps were used to pump the feed and draw solutions from vessels to high pressure pumps. Each with flow rate rang of 11.4-54.6 L/min, a head of 3-13.7 m. Then, the draw solution and feed solution that supplied from centrifugal pumps were pumped using high pressure pumps 125 psi (MAX PRESSURE)) to forward osmosis cell. The forward osmosis cell was circular plate and frame membrane cell and it consisted of two semi-cells which were made of Teflon. It was designed with two flow channels and the diameter of each circular channel was 12.5 cm with a depth of 3 cm in draw solution side and 4 cm in the feed side whereas the total effective for CTA membrane area was 165 cm^2. To measure the volumetric flow rate of feed and draw solutions, two calibrated rotameters were used each of ranged (10 - 60 l/hr). While two submersible electrical coils (220 Volt, 1000 Watt) and thermostats of range (0- 80^oC) were used to control temperatures on the solutions. The pH of FS was adjusted to the required value by addition of (NaOH) or (HCl) and the acidity of O/W emulsion was measured using pH meter (Model 2906, Jenway Ltd, UK) and a pH probe. Digital laboratory conductivity meter was used to measure the concentration of the draw solution, range (0-2 × 10^6 µs/cm), operating temperature (0-55 °C), accuracy (± 0.5 % Full Scale), also the concentration of oil in water was measured using spectrophotometer (Genesys 10 UV, Wave length = 1090 – 190 nm).

4.2 Experimental Procedure

In the typical orientation of forward osmosis process, the draw solution was placed against the support layer and the feed solution was on the active layer. The feed and draw solutions were operated in a counter-current flow configuration (feed and draw solution flowing tangential to the membrane but in opposite directions). This mode of operation provides constant $\Delta\pi$ along the membrane module and makes the process more efficient. The outlet streams of feed and draw solutions were recycled back to the main vessels. All experiments were carried out with applying a pressure of 0.5 bar across the membrane sheet in the feed side. The time of experiment was five hours. For every one hour, water flux into the DS was calculated. Also oil concentration in FS was measured. **Fig. 2** shows the schematic diagram of forward osmosis system.

For cleaning the membrane, osmotic backwashing was made in order to remove oil droptets that accumulated on or in the pores of the membrane. In the backwashing process, the direction of water permeation across the semipermeable membrane was reversed and the DS was replaced with a deionized water and FS was replaced with 0.5 M of a brine. So the same pressure was applied in the permeate side. Dionized water flows through draw side channel, the osmotic pressure gradients are formed in an opposite direction and permeate (i.e. backwash water) flows

from draw side (dionized water) to feed side (brine). Therefore, foulants on the membrane surface are detached by this opposite flow and then are removed from the membrane surface.

4.3 Reverse Osmosis System

For recovery of pure water, the diluted draw solution was treated using reverse osmosis unit that was run in a closed loop. QVF glass vessel with a capacity of 30 liters was used as a feed solution vessel and high pressure pump was used to pump the feed solution (or diluted draw solution) from the QVF vessel to spiral wound module. The spiral – wound element are adopted and operated with only one stream (the feed stream) flowing under direct control of its flow velocity tangential to the membrane, (membrane type is thin film composite (TFC), membrane length is 115 cm, membrane width is 21cm, diameter is 3 in., number of membrane is 2 and membrane active area is 4830 cm^2.

The feed solution in RO process was prepared by dissolving the solid salt (NaCl) in 15 liters of deionized water and was placed in the QVF glass vessel. Pressure gauge measured the pressure that was maintained 9 bars at the inlet module. Then the feed inter the spiral wound module in order to separate draw solution into two streams; one contained pure water and the other contained concentrated solution that was recycled to main feed vessel. The time of experiment was 2 hr, so for every a quarter hour, the water flux was calculated. An experimental rig of reverse osmosis unit was constructed in the laboratory as shown schematically in **Fig. 3.**

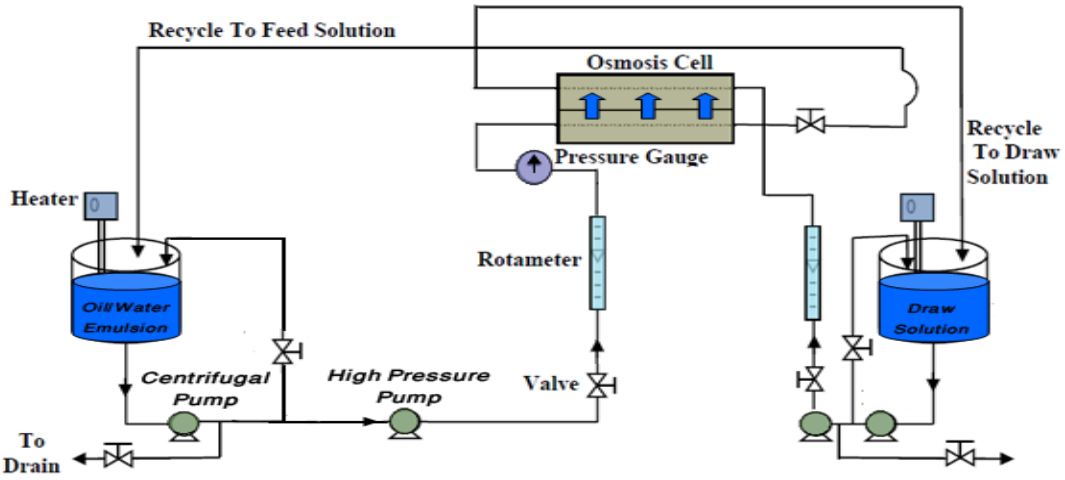

Figure 2. The schematic diagram of the laboratory scale forward osmosis membrane apparatus.

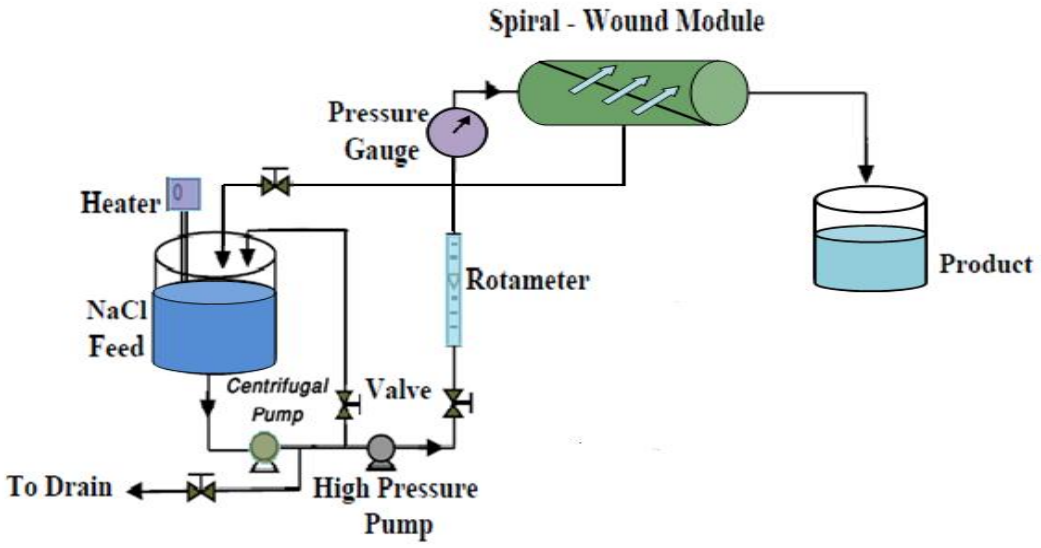

Figure 3. Schematic diagram of spiral-wound reverse osmosis process.

5. Results and discussion

5.1 Forward Osmosis

5.1.1 Effect of Draw Solution Concentration

The effect of draw solution concentration of (NaCl) and ($MgCl_2$) on water flux is shown in Figures 4 and 5. When the concentration of draw solution increased, the water permeation across the membrane increased, as a result, the water flux increased. This is expected and attributed to the increasing in the osmotic pressure difference across the membrane with an increase in the concentration of draw solution, which results in an increase in the driving force) for water transport through the membrane. Also with increasing of draw solution concentration, the concentration of O/W emulsion increases because of the increasing in water transport across the membrane as in **Fig.s 6 and 7.** From **Figs. 4, 5, 6 and 7**. it can be seen that the flux of water and oil concentration using $MgCl_2$ solution as draw solution were greater than that using NaCl solution because it has osmotic pressure higher than the osmotic pressure for NaCl and the osmotic pressure depends on the number of dissociates and osmotic coefficient of the solute (as in Eq (1)).

5.1.2 Effect of Oil Concentration in Feed Solution

Generally, the higher concentration of oil in feed is the lower amount of the permeate flux as observed in Figures 8 and 9. When the concentration increased from 100 to 1000 ppm, the adsorption of oil droplets increased and formed an accumulated layer of oil on the membrane surface (active layer). This causes easily great resistance for permeating water across the membrane and this layer cannot be removed by hydrodynamic action of flow. While at lower concentrations, the accumulation oil on the membrane surface was lower and can be removed by hydrodynamic action of flow. So the increase of oil

concentration was increased the osmotic pressure of feed solution and decrease of driving force ($\Delta\pi$) as shown in van't Hoff equation. The O/W emulsion lost quantities of pure water and this increased concentration of the oil in emulsion as in **Figs .10 and 11.**

5.1.3 Effect of Temperature

When the temperature increased from 30 to 40°C, the water permeation increased through the membrane. As a result, the water flux and the concentration of oil in the feed solution increased with this range of temperature as observed in **Fig's (12, 13, 14 and 15).** The increase in temperature of both feed and draw solutions reduces the viscosity of solutions and increases the diffusion rate of water through the membrane leading to lower resistance against passage of flow, which results the increasing in the volume of water that passed into the draw solution. Additionally, thermal expansion of active layer of the membrane could also be a reason for an increase in the permeate flux with increasing temperature , **Alturki, 2013.**

Also according to van't Hoff equation, increasing in the temperature can be increased the osmotic pressure of a salt solution. The water flux decreased when the temperature of oil/water emulsion and draw solution were rose from 40 to 45°C. This means that the increasing in temperature from 40 to 45°C accounted for a fall in effective osmotic pressure difference inside the membrane as an inherent result of higher internal concentration polarization or may be attributed for specifications of the oil that was used. The results obtained here are in good agreement with , **Aydiner et al., 2012.**

5.1.4 Effect of Feed Solution pH

The performance of FO process was highly dependent on the pH of O/W emulsion so it was affected not only by the characteristics of membrane but also by the performance of the solute (droplet). **Figs. 16 and 17** indicated that the flux increased sharply with increase the pH from 4 to 7.3, then reduced with the increase of pH from 7.3 to 10. In general, the flux under various pH values was affected by the properties of the solute (oil droplets) especially zeta potential of the emulsion.

The coagulation of emulsion droplets on membrane happened under low values of pH (i.e. pH = 4) as the zeta potential of emulsion droplet was low in absolute value and this led to decrease the inter-droplet repulsion. Therefore, the lower level of flux was observed at low pH. While the emulsion droplets had the higher negative charge at higher pH values. The oil layer became more "open" at high pH due to the inter-droplet repulsion, and this increased the permeability, resulting in higher permeate flux. Meanwhile, the inter-droplet repulsion prevented the particle from depositing, and led to the reduction of the thickness of cake layer. The results obtained here are in good agreement with ,**Hua et al., 2007**. So the oil concentration in the feed solution also fluctuates with increasing the pH of the emulsion according to the fluctuation of water flux in the same manner as shown in **Figs. 18 and 19.**

5.1.5 Effect of Draw Solution Flow Rate

Figs. 20 and 21 show the effect of draw solution flow rate on water flux with time for NaCl and $MgCl_2$ respectively. Increasing the draw solution flow rate from 20 to 60 l/hr increased the extent of hydrodynamic mixing and prevented the concentration buildup in the solution at the vicinity of the membrane surface (support layer), and resulting in decrease the driving force. Thus, water flux decreased with increasing draw solution flow rate. As observed in **Figs. 22 and 23**, the oil concentration in feed solution decreased also with increasing the flow rate of draw solution due to this decreasing in water transport across the membrane with this range of draw solution flow rate.

5.1.6 Effect of Feed Solution Flow Rate

Figs. 24 and 25 present the effect of feed solution flow rate on the FO process efficiency. The water flux increased with increasing the feed solution flow rate. The increase in the feed solution flow rate near the membrane surface increases the extent of hydrodynamic mixing and increases Reynolds number and this enhances turbulence over the active layer of the membrane. As a result, it increases mass transfer coefficient in the concentration boundary layer and this can reduce accumulation of the oil droplets (i.e reducing the external concentration polarization). Therefore, the oil droplets on the membrane surface diffuse back to the bulk solution and this causes increase water permeation across the membrane. The oil concentration in feed solution increased as a result of the increasing transmission of water from feed solution through the membrane as shown **in Figs. 26 and 27.**

5.1.7 The Analysis of Concentration Polarization

In **Figs. 28 and 29**, the water flux (J_W) is presented as a function of logarithm of the ratio of draw and feed solutions osmotic pressures ($\ln(\pi_D/\pi_F)$) (Equ. (12)). It was found that the slope of line represents the inverse of the solute resistivity for diffusion within the porous support layer (K). K can be used to determine the influence of internal concentration polarization on water flux and to describe how easily solute can diffuse in and out of the support layer. Osmotic pressure was calculated according to the Eq. (1), where numbers of dissociated ions for NaCl, $MgCl_2$ and oil are (i = 2, 3, 1) respectively and the osmotic coefficient for ideal solution is ($\Phi = 1$). The value of (K) for NaCl was found 55.93 h/m, while its value for $MgCl_2$ was equal to 26.21 h/m. This is meaning that NaCl (monovalent) diffused through the membrane more rapidly than the $MgCl_2$ (divalent) because of its relatively small hydration radius. Therefore the influence of internal concentration polarization on water flux for NaCl solution was higher than for $MgCl_2$ solution.

6. REVERSE OSMOSIS

6.1 The Effect of NaCl Concentration

The influence of NaCl feed concentration on water flux is shown in Figure 30. According to the results, the lower salt concentration is the higher permeation flux of the membrane. These results are attributed to the increasing in osmotic pressure with increasing the NaCl concentration and formation of a salt layer on the membrane surface with thickness increases with increasing feed concentration.

6.2 Effect of Feed Flow Rate

Fig31. shows the effect of feed flow rate on the water permeate flux of diluted NaCl draw solution. As shown increasing flow rate from 20 to 40 l/h leads to increase permeate flux rate. This behavior may be attributed to the fact that increasing cross flow velocity leads to the increase of turbulence and mass transfer coefficient. This weakens the effect of concentration polarization and reduces accumulate of the salt which essentially acts as a dynamic membrane, as a result the salt on the membrane surface diffuse back to the bulk solution and increases the permeate flux. The results obtained here are in good agreement with ,**Shamel and Chung , 2006).**

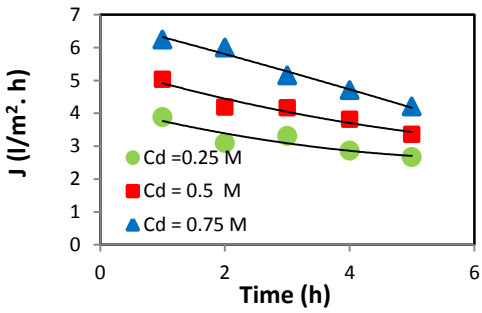

Figure 4. Water flux J (l/m^2.h) with time at different concentration of DS for NaCl (C_{oil}= 500 ppm,Temp. of FS & DS = 30 °C and pH of FS = 7.3, Q_d = 50 l/h, Q_f = 60 l/h, P = 0.5 bar).

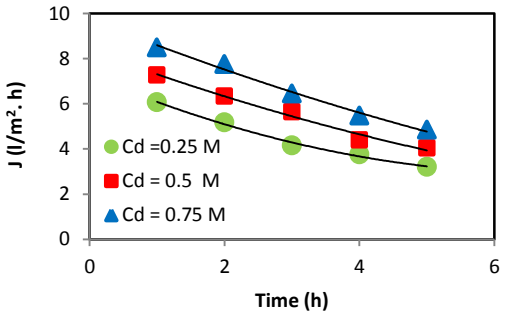

Figure 5. Water flux J (l/m^2.h) with time at different concentration of DS for $MgCl_2$ (C_{oil}= 500 ppm, Temp. of FS & DS = 30 °C and pH of FS = 7.3, Q_d = 50 l/h, Q_f = 60 l/h, P = 0.5 bar).

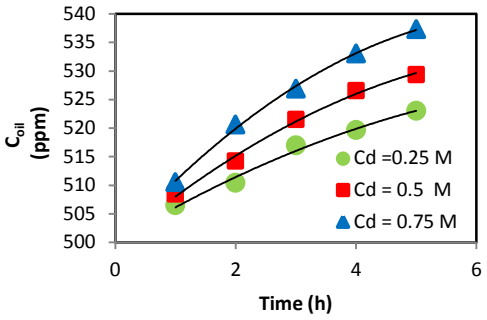

Figure 6. The oil concentration C_{oil} (ppm) in FS with time at different concentration of DS for NaCl (C_{oil}= 500 ppm, Temp. of FS & DS = 30 °C and pH of FS = 7.3, Q_d = 50 l/h, Q_f = 60 l/h, P = 0.5 bar).

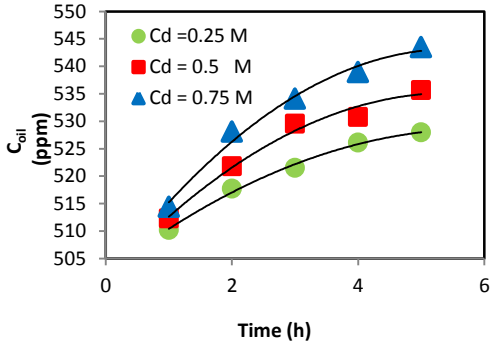

Figure 7. The oil concentration C_{oil} (ppm) in FS with time at different concentration of DS for $MgCl_2$ (C_{oil}= 500 ppm, Temp. of FS & DS = 30 °C and pH of FS = 7.3, Q_d = 50 l/h, Q_f = 60 l/h, P = 0.5 bar).

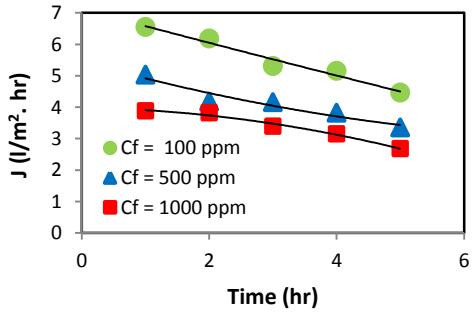

Figure 8. Water flux J (l/m^2.h) with time at different oil concentration of FS for NaCl (C_d = 0.5 M, Temp. of FS & DS = 30 °C and pH of FS= 7.3, Q_d = 60 l/h, Q_f = 60 l/h, p = 0.5 bar).

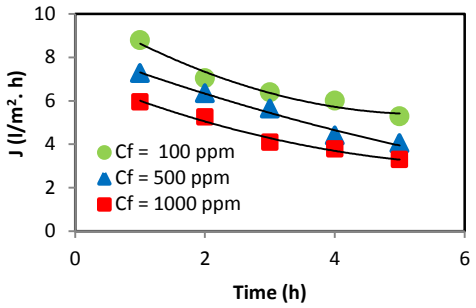

Figure 9. Water flux J (l/m^2.h) with time at different oil concentration of FS for $MgCl_2$ (C_d = 0.5 M, Temp. of FS & DS = 30 °C and pH of FS= 7.3, Q_d = 60 l/h, Q_f = 60 l/h, p = 0.5 bar).

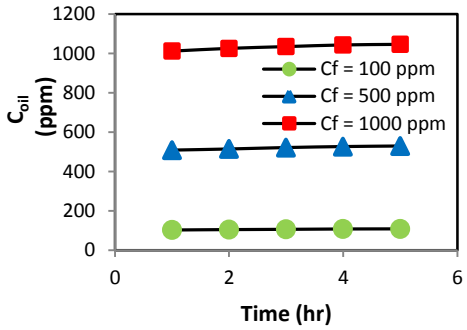

Figure 10:. The oil concentration C_{oil} (ppm) in FS with time at different oil concentration in FS for NaCl (C_d = 0.5 M, Temp. of FS & DS = 30 °C and pH of FS= 7.3, Q_d = 60 l/h, Q_f = 60 l/h, p = 0.5 bar).

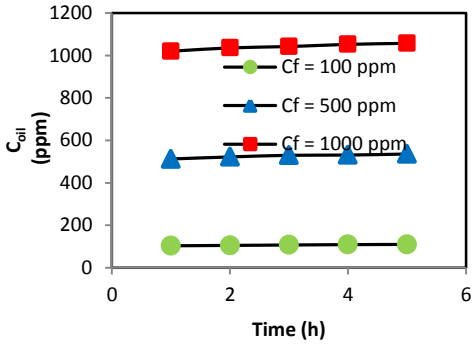

Figure 11. The oil concentration C_{oil} (ppm) with time at different oil concentrati Figure on in FS for $MgCl_2$ (C_d = 0.5 M, Temp. of FS & DS = 30 °C and pH of FS= 7.3, Q_d = 60 l/h, Q_f = 60 l/h, P = 0.5 bar).

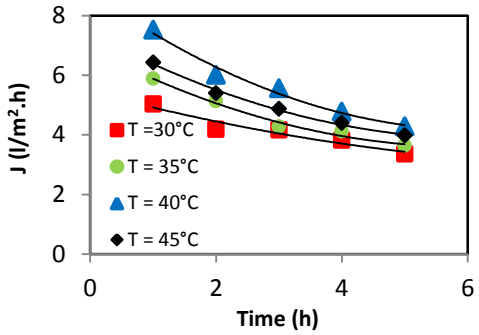

Figure 12. Water flux J (l/m^2.h) with time at different Temp. of FS & DS for NaCl (C_d = 0.5 M, C_{oil}= 500 ppm and pH of FS = 7.3, Q_d = 60 l/h, Q_f = 60 l/h, P = 0.5 bar).

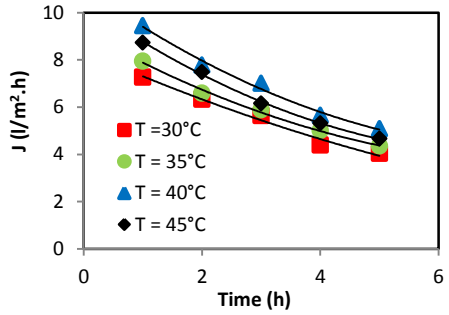

Figure 13. Water flux J (l/m^2.h) with time at different Temp. of FS & FS for $MgCl_2$ (C_d = 0.5 M, C_{oil}= 500 ppm and pH of FS = 7.3, Q_d = 60 l/h, Q_f = 60 l/h, P = 0.5 bar).

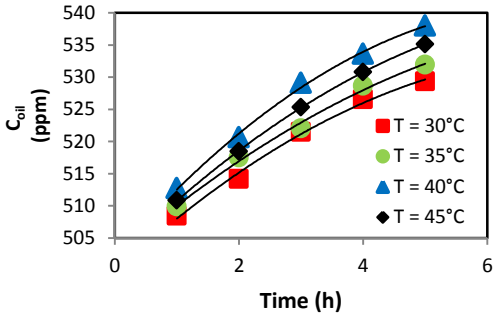

Figure 14. The oil concentration C_{oil} (ppm) in FS with time at different Temp. of FS & DS for NaCl (C_d = 0.5 M, C_{oil}= 500 ppm and pH of FS = 7.3, Q_d = 60 l/h, Q_f = 60 l/h, P = 0.5 bar).

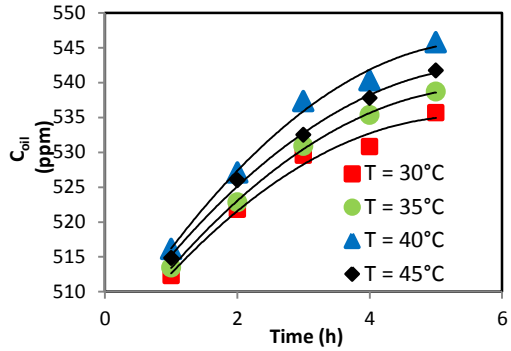

Figure 15.The oil concentration C_{oil} (ppm) with time at different Temp. of FS & DS for $MgCl_2$ (C_d = 0.5 M, C_{oil}= 500 ppm and pH of FS = 7.3, Q_d = 60 l/h, Q_f = 60 l/h, P = 0.5 bar).

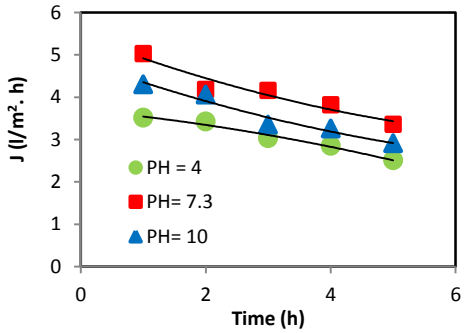

Figure 16. Water flux J (l/m^2.h) with time at different pH of FS for NaCl (C_d = 0.5 M, C_{oil}= 500 ppm and Temp. of FS & DS = 30 °C, Q_d = 60 l/h, Q_f = 60 l/h, P = 0.5 bar).

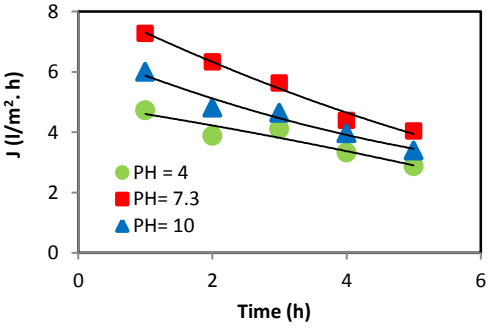

Figure 17. Water flux J (l/m^2.h) with time at different pH of FS for $MgCl_2$ (C_d = 0.5 M, C_{oil}= 500 ppm and Temp. of FS & DS = 30 °C, Q_d = 60 l/h, Q_f = 60 l/h, P = 0.5 bar).

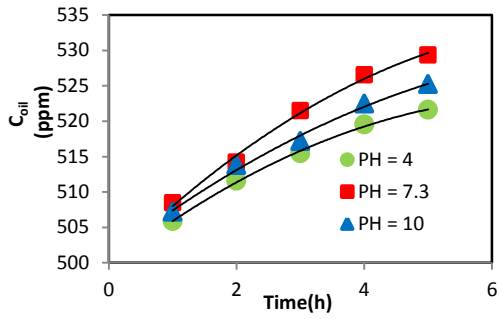

Figure 18. The oil concentration C_{oil} (ppm) with time at different pH of FS for NaCl (C_d = 0.5 M, C_{oil}= 500 ppm and Temp. of FS & DS = 30 °C, Q_d = 60 l/h, Q_f = 60 l/h, P = 0.5 bar).

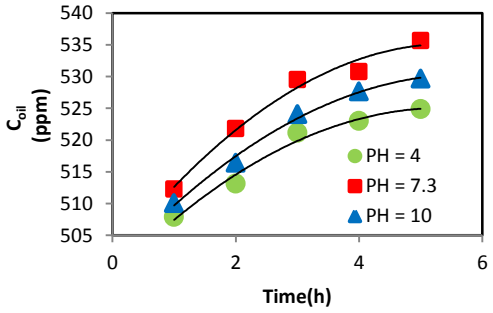

Figure 19. The oil concentration C_{oil} (ppm) with time at different pH of FS for $MgCl_2$ (C_d = 0.5 M, C_{oil}= 500 ppm and Temp. of FS & DS = 30 °C, Q_d = 60 l/h, Q_f = 60 l/h, P = 0.5 bar).

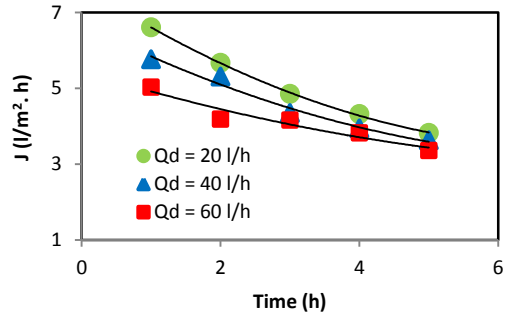

Figure 20. Water flux J (l/m^2.h) with time at different draw solution flow rate (Q_d) for NaCl (C_d = 0.5 M, C_{oil}= 500 ppm and Temp. of FS & DS = 30 °C, pH of FS = 7.3, Q_f = 60 l/h, P = 0.5 bar).

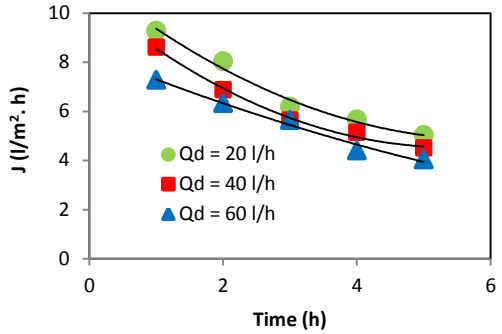

Figure 21. Water flux J (l/m^2.h) at different time at different draw solution flow rate (Q_d) for $MgCl_2$ (C_d = 0.5 M, C_{oil}= 500 ppm, Temp. of FS & DS = 30 °C, pH of FS = 7.3, Q_f = 60 l/h, P = 0.5 bar).

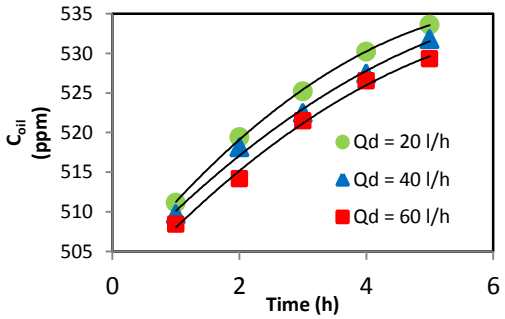

Figure 22. The oil concentration C_{oil} (ppm) in FS with time at different draw solution flow rate (Q_d) for NaCl (C_d = 0.5 M, C_{oil}= 500 ppm, Temp. of FS & DS = 30 °C, pH of FS = 7.3, Q_f = 60 l/h, P = 0.5 bar).

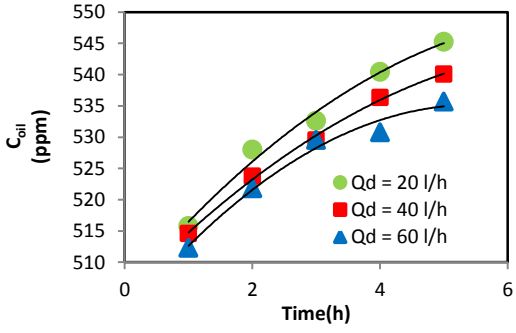

Figure 23. The oil concentration C_{oil} (ppm) in FS with time at different draw solution flow rate (Q_d) for $MgCl_2$ (C_d = 0.5 M, C_{oil}= 500 ppm, Temp. of FS & DS = 30 °C, pH of FS = 7.3, Q_f = 60 l/h, P = 0.5 bar).

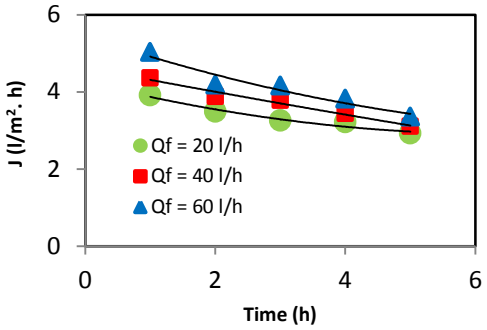

Figure 24. Water flux J (l/m^2.h) with time at different feed solution flow rate (Q_f) for NaCl (C_d = 0.5 M, C_{oil}= 500 ppm, Temp. of FS & DS = 30 °C, pH of FS = 7.3, Q_d = 60 l/h, P = 0.5 bar).

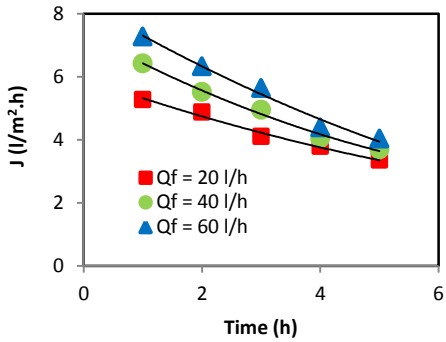

Figure 25. Water flux J (l/m^2.h) with time at different feed solution flow rate (Q_f) for $MgCl_2$ (C_d = 0.5 M, C_{oil}= 500 ppm, Temp. of FS & DS = 30 °C, pH of FS = 7.3, Q_d = 60 l/h, P = 0.5 bar).

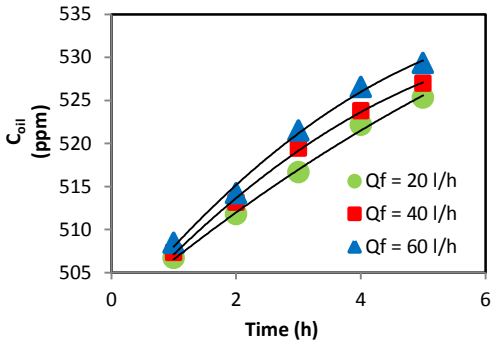

Figure 26. The oil concentration C_{oil} (ppm) in FS with time at different feed solution flow rate (Q_f) for NaCl (C_d = 0.5 M, C_{oil}= 500 ppm, Temp. of FS & DS = 30 °C, pH of FS = 7.3, Q_d = 60 l/h, P = 0.5 bar).

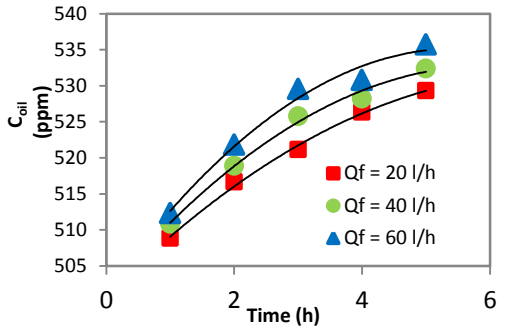

Figure 27. The oil concentration C_{oil} (ppm) in FS with time at different feed solution flow rate (Q_f) for $MgCl_2$ (C_d = 0.5 M, C_{oil}= 500 ppm, Temp. of FS & DS = 30 °C, pH of FS = 7.3, Q_d = 60 l/h, P = 0.5 bar).

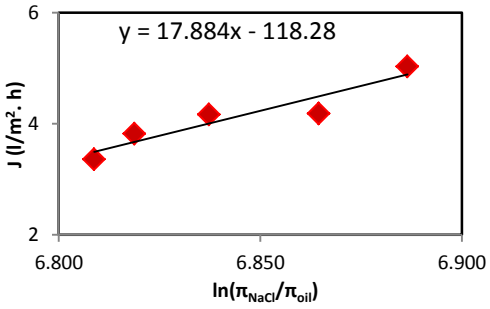

Figure 28. Water flux against the logarithm of the ratio of osmotic pressures for calculate K (C_d = 0.5 M, C_f = 500 ppm, Temp. of FS & DS = 30^{o}C, pH = 7.3, Q_d = 60 l/h, Q_f = 60 l/h, and P= 0.5 bar).

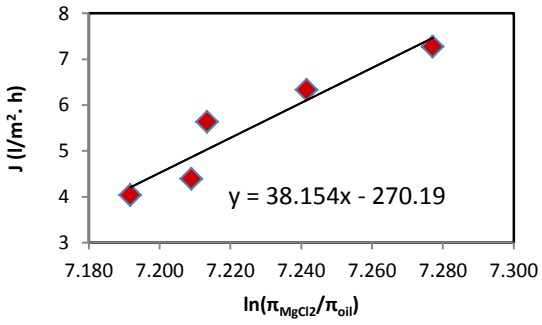

Figure 29. Water flux against the logarithm of the ratio of solution osmotic pressures for calculate K (C_d = 0.5 M, C_f = 500 ppm, Temp. of FS & DS = 30^{o}C, pH = 7.3, Q_d = 60 l/h, Q_f = 60 l/h,and P= 0.5 bar).

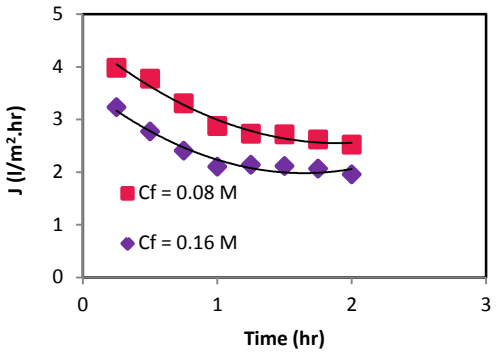

Figure 30. Water flux with time at different NaCl concentration in the FS (Flow rate of FS= 20 l/h, Pressure = 9 bar, Temp. of FS = 30 ^{o}C).

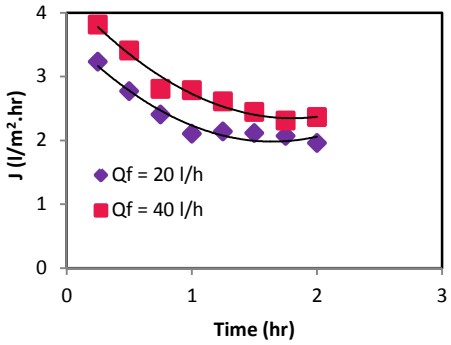

Figure 31. Water flux with time at different flow rate of FS (NaCl concentration in the FS= 0.16 M, Pressure = 9 bar and Temp. of FS = 30 ^{o}C).

CONCLUSIONS

- Forward osmosis can be used for treating the oily wastewater from different industries.
- The water flux produced from the osmosis cell and oil concentration in FS increase by increasing the concentration of draw solutions, the flow rate of feed solution, and the temperature for a limit then, it decreases with increasing the temperature and decreases by increasing the oil concentration in the feed solution and the flow rate of the draw solutions.
- The $MgCl_2$ gives water flux higher than NaCl.
- The values of resistance to solute diffusion within the membrane porous support layer were 55.93 h/m and 26.21 h/m for NaCl and $MgCl_2$ respectively.

Nomenclature

Symbols	Definition	Units
A	water permeability constant	$l/m^2.h.bar$
B	salt permeability coefficient	m/s
C	concentration	g/l
C_F	conentration of feed side	g/l
C_P	conentration of permeate side	g/l
D	solute diffusion coefficient	m^2/s
d_h	hydraulic diameter	m
i	dissociation factor	
J_w	water flux	$l/m^2.h$
J_s	reverse salt flux	$l/m^2.h$
K	resistivity coefficient	h/m
k	mass transfer coefficient	m/s
p	pressure	bar
R_g	universal gas constant	J/gmol.K
R	rejection Percent	
T	temperature	^oC

GREEK SYMBOLS

π_D	Osmotic pressure of the draw solution	bar
$\pi_{D,b}$	Osmotic pressure of the draw solution in the bulk	bar
$\pi_{D,i}$	Osmotic pressure of the draw solution on the inside of the active layer within the porous support	bar
$\pi_{D,m}$	Osmotic pressure of the draw solution at the membrane surface	bar
π_F	Osmotic pressure of the feed solution	bar
$\pi_{F,b}$	Osmotic pressure of the feed solution in the bulk	bar
$\pi_{F,i}$	Osmotic pressure of the feed solution on the	bar

	inside of the active layer within the porous support	
$\pi_{F,m}$	Osmotic pressure of the feed solution at the membrane surface	bar
π	Osmotic Pressure	bar
τ	Tortuosity of the support layer	
ε	Porosity of the support layer	
σ	Reflection Coefficient	
Φ	Osmotic Coefficient	

ABBREVIATION

Symbol	Definition
CP	Concentration Polarization
CTA	Cellulose Triacetate
DS	Draw Solution
ECP	External Concentration polarization
FO	Forward Osmosis
FO-RO	Forward-Reverse Osmosis
FS	Feed Solution
ICP	Internal Concentration polarization
O/W	Oil-in-Water
RO	Reverse Osmosis
TFC	Thin Film Composite
W/O	Water-in-Oil

Feed Solution

REFERENCES

- Achilli, A., Cath, T.Y., and Childress, A.E., 2010, *Selection of inorganic-based draw solutions for forward osmosis applications,* Journal of Membrane Science, Vol. 364: 233–241.

- Achilli, A., Cath, T.Y., Childress, A.E., 2009, *Power generation with pressure retarded osmosis: An experimental and theoretical investigation*", Journal of Membrane Science, Vol. 343: 42-52.

- Ahmed, F. H., 2007, *Performance of Manipulated Direct Osmosis in Water Desalination Process* Ph.D. thesis, Baghdad University.

- Ahmed, F. H., 2011, *Forward and Reverse Osmosis Process for Recovery and Re-use of Water from Polluted Water by Phenol*, Journal of Engineering, Vol. 17, No. 4: 912-928.

- Alsvik, I. L., and Hägg, M-B., 2013, *Pressure Retarded Osmosis and Forward Osmosis Membranes: Materials and Methods*, Polymers, Vol. 5: 303-327.

- Alturki, A., 2013, *Removal of trace organic contaminants by integrated membrane processes for indirect potable water reuse applications*, Ph. D thesis, University of Wollongong.

- Aydiner, C., Topcu, S., Tortop, C., Kuvvet, F., Ekinci, D., Dizge, N., and Keskinler, B., 2012, *A novel implementation of water recovery from whey*: Forward–reverse osmosis" integrated membrane system", Desalination and Water Treatment iFirst: 1–14.
- Bamaga, O.A. , Yokochi, A. , Zabara, B. , and Babaqi, A.S. , 2011, *Hybrid FO/RO desalination system: Preliminary assessment of osmotic energy recovery and designs of new FO membrane module configurations*, Desalination 268 (2011) 163–169.

- Bujang, M., Ibrahim, N. A., and a/l Eh Rak, A., 2012, *Physicochemical Quality of Oily Wastewater from Automotive Workshop in Kota Bharu, Kelantan Malaysia*, Australian Journal of Basic and Applied Sciences, Vol. 6, No. 9: 748-752.

- Cath, T.Y., Childress, A.E., and Elimelech, M., 2006, *Forward Osmosis: Principles, Applications, and Recent Developments", Journal of Membrane Science*, Vol. 281: 70–87.
- Cheryana, M., and Rajagopalan, N., 1998, *Membrane processing of oily streams. Wastewater treatment and waste reduction*, Journal of Membrane Science, Vol. 151: 13-28.

- Choi, J., 2011, *Efficient production and application of volatile fatty acids from biomass for fuels and chemicals*,Ph.D. thesis, Kaist University.

- Digman, B.R., 2010, *Surface Modification of Polybenzimidizole Membranes for Forward Osmosis*, M. Sc. thesis, The University of Toledo.

- Farah, A. Y., 2013 *Application of Forward Osmosis Process in Whey Treatment*, M.Sc. thesis, University of Baghdad.

- Gray, G.T., McCutcheon, J.R., and Elimelech, M., 2006, I*nternal concentration polarization in forward osmosis: role of membrane orientation*, Desalination, Vol. 197: 1–8.
- Hua, F.L., Tsang, Y.F., Wang, Y.J., Chan, S.Y., Chua, H., and Sin, S.N., 2007, *Performance study of ceramic microfiltration membrane for oily wastewater treatment*, Chemical Engineering Journal, Vol. 128:169–175.

- Kim, C., Lee, S., Shon, H.K., Elimelech, M., and Hong, S., 2012, *Boron transport in forward osmosis: Measurements, mechanisms, and comparison with reverse osmosis*", Journal of Membrane Science 419–420: 42–48. Loeb, S., Titelman, L.,

- Korngold, E., and Freiman, J., 1997, *Effect of porous support fabric on osmosis through a Loeb-Sourirajan type asymmetric membrane*, Journal of Membrane Science, Vol. 129: 243–249.

- McCutcheon, J.R. and Elimelech, M., 2006, *Influence of concentrative and dilutive internal concentration polarization on flux behavior in forward osmosis*, Journal of Membrane Science, Vol. 284: 273-247.

- Mohammed, S.A., Faisal, I., and Alwan, M.M., 2011, *Oily Wastewater Treatment Using Expanded Beds of Activated Carbon and Zeolite*, Iraqi Journal of Chemical and Petroleum Engineering, Vol.12 No.1.

- Shamel, M.M., and Chung, O.T., 2006, *Drinking Water from Desalination of Seawater: Optimization of Reverse Osmosis System Operating Parameters*, Journal of Engineering Science and Technology, Vol. 1, No. 2: 203-211.

- Thain, J.F., 1967, *Principles of Osmotic Phenomena*", W Heffer & Sons Ltd, London.

- Xie, M., Price, W. E. and Nghiem, L. D., 2012, *Rejection of pharmaceutically active compounds by forward osmosis: Role of solution pH and membrane orientation*, Separation and Purification Technology, Vol. 93: 107-114.

- Yan, L., Li, Y.S., Xiang, C.B., and Hong, L.J., 2006, *Treatment of oily wastewater by organic–inorganic composite tubular ultrafiltration (UF) membranes*, Desalination, Vol. 196: 76–83.

- Zhao, S., Zou, L., 2011, *Effects of working temperature on separation performance, membrane scaling and cleaning in forward osmosis desalination*, Desalination, Vol. 278: 157–164.

قـائـمـة الـمـحـتـويـات

القسم العربي:

معالجة المياه المطروحة من مصافي بيجي لأعادة تدويرها للأغراض الزراعية

رافع جمال يعقوب
مدرس
قسم العمليات النفطية– كلية هندسة النفط والمعادن – جامعة تكريت
E-mail: rafijamalalgawi33@yahoo.com

الخلاصة

يهدف البحث الى معالجة المياه الصناعية المطروحة من مصافي بيجي من خلال أضافة مرحلة ثالثة وهي أضافة وحدتين الاولى الترسيب بالألواح المتوازية ووحدة الأمتزاز بالكاربون المنشط لاعادة استعمالها مرة ثانية وخصوصا للاغراض الزراعية حيث تبلغ كمية المياه المطروحة بحدود 2000 م^3/ساعة وتحتوي على مواد عضوية وعناصر ثقيلة غير مسموح بيئيا طرحها الى النهر.

تم الحصول على نتائج جيدة في تخليص المياه من المواد الضارة دون الوصول الى المواصفات المطلوبة حيث كانت نسبة الأزالة بحدود 90% مما تطلب اعادة التجارب بأستخدام متعدد كلوريد الحديديك لغرض الوصول الى المواصفات العالمية اللازمة لاعادة استخدام المياه.أن الطريقة الكيمياوية بحقن مادة متعدد كلوريد الحديديك في وحدة الترسيب بالألواح المتوازية بينت كفاءتها العالية في ازالة المواد السامة وخصوصا الفينول حيث تم الوصول الى المواصفات المطلوبة للمياه لغرض أعادة تدويرها للأستخدام للاغراض الزراعية.

الكلمات الرئيسية :–معالجة مياه المصافي،الأمتزاز بالكاربون المنشط،الترسيب بالصفائح المتوازية،أعادة أستعمال المياه المعالجة.

Baji Refinery Water Treatment to Reuse for Agricultural Purposes

Rafi Jamal Yacoup
Lecturer
University Of Tikrit-College of Petroleum&Minerals Engineering
E-mail: rafijamalalgawi33@yahoo.com

ABSTRACT

The purpose of this research is to treat Baiji refinery waste water by adding tertiary treatment which consist of two units:-Lamella precipitators & adsorption by activated carbon,and reuse it for agricultural purposes.The treatment covers 2000 m^3/hr of water which contains organic and heavy metals impurities not recommended to drain to

river according to Environmental rules. Good results were gained in this research and the removal was 90% by adsorption & Lamella precipitation .This result is not according to environmental rules so we treat the waste water by using poly ferric chlorides to remove all the remaining phenol and be written the environmental limits for reuse the water for agriculteral purposes.

Keywords: refinery waste water treatment,adsorption by activated carbon,lamella precepitation ,water reuse

المقدمة

تعتبر المواد الهايدروكاربونية من اخطر الملوثات الصناعية على الإطلاق في الوقت الحاضر وذلك لعدة أسباب منها: ضخامة كمياتها وصعوبة تحللها عن طريق البكتريا اضافة الى أن العديد منها تعتبر مواداً مسرطنة .تتوفر في جميع المصافي العديد من الوحدات لمعالجة المياه الصناعية الملوثة ولكن في اغلب الأحيان تكون هذه الوحدات غير قادرة على جعل المياه الصناعية ضمن المواصفات المطلوبة لذلك استلزم الأمر التفكير بإضافة وحدات أخرى يمكنها التعامل مع المواد الهايدروكاربونية، ومن هذه الوحدات وحدات الامتزاز باستخدام الكاربون المنشط. ومصفى بيجي يعاني من ارتفاع تراكيز المواد الهايدروكاربونية في المياه الخارجة من وحدات معالجة المياه الصناعية بحيث تتخطى الحدود المسموح بها وفق المواصفات العراقية لذا استوجب دراسة إمكانية معالجة هذه المياه لازالة المواد الهايدروكاربونية باستخدام الكاربون المنشط الحبيبي(**لطيف.1988**)

يمكن تقسيم طرق معالجة مياه الفضلات إلى ثلاث طرق:-

1- المعالجة الأولية. 2- المعالجة الثانوية. 3-المعالجةالمتقدمة.

حيث تستخدم المعالجة الأولية لإزالة المواد الصلبة العالقة من مياه الفضلات سواء كانت هذه المواد قابلة للتحلل أو غير قابلة للتحلل فيمكن إزالة المواد الصلبة العالقة بعملية الترسيب مع إضافة بعض المخثرات أو تتم إزالتها باستخدام المناخل أو المرشحات والمعالجة الثانوية تكون بطريقة التطويف. وأخيراً وحدات المعالجة المتقدمة حيث تقوم هذه الوحدات بإزالة الملوثات التي يتعذر إزالتها بالطرق السابقة ومن أهم طرق المعالجة المتقدمة هي عمليات الامتزاز والتبادل الأيوني والتناضح العكسي وضخ الكلور والأوزون.

الامتزاز بواسطة الكاربون المنشط تقنية مفيدة وفعالة لمعالجة المياه الملوثة الصناعية وكمعالجة متقدمة للمواد الخارجة من وحدات المعالجة البايولوجية. تستخدم تقنيات الامتزاز بشكل واسع في مجال إزالة كميات صغيرة من الملوثات الموجودة في حجم كبير من المائع. تتم معالجة المواد الخارجة من مصافي النفط والتي تحتوي على الفينول والفورفورال وعناصر سامة والامونيا بطرق مختلفة مثل الأكسدة الكيميائية والفصل الفيزيائي والمعالجة البايولوجية (**اسماعيل 2008**) استخدمت المنشط الحبيبي لإزالة الفينول والامبرلايت مع XAD4 لإزالة صبغة ألمثيلين الزرقاء لإزالة إضافة نسب مختلفة من حبيبات الزجاج كمادة غير مازة مع الكاربون المنشط ومع الامبرلايت لجعل عملية الامتزاز أكثر كفاءة بزيادة المساحة السطحية للامتزاز، وجدت الباحثة ان إضافة 5% من حبيبات الزجاج إلى الكاربون المنشط الحبيبي والامبرلايت بالتعاقب تقلل الوزن لكل مادة مازه بمقدار 5% وزيادة لزمن التشغيل بمقدار 80%. ان زيادة نسبة حبيبات

الزجاج الكروية أكثر من 60% لكلا المادتين يجعل عملية الامتزاز غير كفوءة مقارنة مع استخدام المادة ألمازة بمفردها وقد وجدت الباحثة أن علاقة التوازن مطابقة لمعادلة (لونكماير)لكل من الفينول وصبغة المثيلين الزرقاء.

قام الباحثان **(حميد و رحمن 2008)** باستخدام الكاربون المنشط المصنوع من نشارة خشب جوز الهند لإزالة الفينول من المياه وقد تم إجراء التجارب عند درجة حرارة 30 ^{0}م ودرجة حامضية (3–10) وتراكيز فينول (25–200) ملغم/لتر وجد الباحثان توافقاً بين النتائج المختبرية والنماذج الرياضية (لونكماير) و (فريندلج)..

ووجد**(رادوشكفج ودبلنن 2009)** أن أقصى سعة امتزاز مقدارها 149.25 ملغم/غم واثبتت النتائج ان الكاربون المنشط مادة مازه فعالة لإزالة الفينول.

قام **(ديليناس و دايامادوبولص2008)** بتصنيع وحدة ترشيح تجريبية لمعالجة المياة الملوثة في اليونان وقد تم اجراء ثلاثة تجارب الاولى عملية ترشيح فقط والثانية عملية ترشيح وتخثير بالشب اما التجربة الثالثة والاخيرة فكانت تشمل اضافة الكاربون المنشط بنوعيه (المسحوق والحبيبي) خلال عملية الترشيح. تم ازالة المطلب الكيمياوي للاوكسجين بنسبة 19% وازالة المطلب الحيوي للاوكسجين بنسبة 25% وازالة الكدرة بنسبة 90% وكذلك كانت هنالك ازالة للعناصر الثقيلة ، وعندما تم مزج عمليتي الترشيح والتخثير كانت النتائج مشابهة لنتائج عملية الترشيح بدون تخثير. اما في حالة اضافة مسحوق الكاربون المنشط فان ازالةالمطلب الحيوي أكثر من 60% ولكن كان هنالك زيادة بالضغط على سطح غشاء الترشيح . ونتج في حالة أضافة الكاربون الحبيبي فأن أزالة المتطلب الحيوي بنسبة 36% بدون ان يسبب ارتفاعاً في الضغط وقد تم ازالة فعالة جداً للعناصر الثقيلة أيضاً عند استعمال الكاربون المنشط الحبيبي

بينت**(أبتسام 2011)** إمكانية إزالة هذه المواد بالكامل من مياه الفضلات باستخدام أعمدة من الكاربون المنشط. كذلك بينت النتائج أن زمن الاختراق وزمن الاستنزاف يتناسبان عكسياً مع تركيز الملوثات الداخلة وسرعة السائل الفراغية وطردياً مع سمك الكاربون المنشط. كذلك فقد تبين بأن سعة الامتزاز تتناسب طردياً مع تركيز الملوثات الداخلة وسرعة السائل الفراغية وقد وجد أيضا أن سمك مجال الامتزاز الذي تم إيجاده في هذه الدراسة يتناسب طردياً مع سرعة السائل الفراغية.

درس **(مدائني2013)** أداء الترشيح المايكروي والأغشية الأنتقائية في معالجة مياه المصافي المطروحة وضمن الحدود البيئية لغرض أعادة أستخدامها للأغراض الزراعية وقد حصل على نسبة أسترجاع بجدود 95% مع وجود كمية من المياه الملوثة وبتركيز عالي بنسبة 5%

قام **(توني مكين مع أخرين 2010)**بمعالجة المياه الملوثة بأستخدام الألواح المتوازية كمرسب وبأستخدام مادة الألمنيوم كلورو هيدريت كمادة مخثرة ووجد أن نسبة أزالة المواد الصلبة بحدود 57% ونسبة أزالة المتطلب الحيوي للأوكسجين 30% ومع فعالية عالية في أزالة عناصر الفسفور والنتروجين.

قامت**(زينة ورافع 2013)** بأستخدام الألواح المتوازية في معالجة المياه الملوثة وبكفاءة عالية بأستخدام مواد طبيعية كبديل عن أستخدام الشب. وتبين كفاءته العالية في تخليص المياه من التلوث.

أستخدم متعدد كلوريد الحديديك كمادة مزيلة للفينول من قبل عدد من الباحثين**(ولديرير وأخرين2014)** تبين وصول الكفاءة في الأزالة 99.7% وفاقت هذه الكفاءة على أستخدام متعدد سلفات الحديديك وكلوريد الحديديك.

الفحوصات الكيمياوية للمياه الملوثة

تم الحصول من شركة مصافي الشمال في بيجي على كمية ماء بحدود (1 م^3) من الماء المطروح إلى النهر لغرض إجراء التجارب العملية عليه. ولغرض معرفة طرق المعالجة الإضافية لتحسين الماء المطروح إلى النهر لابد من إجراء فحوصات مختبرية في مختبرات جامعة تكريت , حيث تم أستخدام جهاز لقياس قيمة الرقم الهيدروجيني ويسمى موديل 410 من صنع شركة (ثيرمو أورينت)

وجهاز الأشعة فوق البنفسجية المستخدم لقياس التراكيز عند الأطوال الموجية المعينة ومن خلال إجراء المعايرة نتمكن بواسطته قياس تركيز المواد الهايدروكاربونية في المياه وهو من (Model530 UV Spectrophotometer)(V-) وهو ياباني المنشأ. وتم عمل معايرة للأمتصاصية مع تركيز الفينول. ونتائج فحوصات موضحة في الجدول رقم (1)

الأجهزة ألمختبرية وطريقة العمل

تم بناء منظومة البحث وحسب ما هو موضح في الشكل رقم (1) المنظومة البحثية لعملية الامتزاز والتي تم اعتماد الاعتبارات التصميمية في بناء المنظومة وأجريت تجارب عديدة لتقليل نسبة الفينول في المياه.

مع الأخذ بنظر الاعتبار عند بناء الجهاز ألمختبري إمكانية التحكم بأهم العوامل التي تؤثر على عملية الامتزاز وهي كل من سرعة السائل الفراغية المرتبطة بمعدل الجريان ومساحة المقطع العمودي على الجريان وسمك طبقة الكاربون وتركيز الملوثات الداخلة للجهاز. أما درجة الحرارة فقد أنجزت جميع التجارب ضمن درجة حرارة المختبر لكون ذلك هو واقع الحال في المؤسسات الصناعية حيث يشكل رفع أو خفض درجات الحرارة للمياه الملوثة قبل معالجتها كلفة اقتصادية عالية لا يمكن تحملها.

تم تصنيع عمود الامتزاز بطول 50سم وقطره يساوي 2سم وهو دائري الشكل مصنوع من مادة البايركس ، و للتحكم بسمك طبقة الكاربون التي تستقر فوق قطعةخزفية مثقبة يتم اعادة تدوير الماء للحصول على ارتفاع اضافي (60 سم و 90 سم). وقد تم اختيار معدل الجريان بالاعتماد على الأعتبارات التصميمية وتتراوح ما بين 2-6 لتر/ساعة. أما بالنسبة لطول العمود أن كل أعمدة الامتزاز يتم ترك مسافة للأسفل وتترك مسافة للأعلى وهذا للغسل العكسي يحتاج إلى فراغ فوق الطبقة المحشوة يصل إلى 10سم لذلك تركنا هذا الفراغ في العمود.

يوضح الشكل رقم (2) مخططاً لجهاز الترسيب بالألواح المتوازية والشكل يمثل صورة للجهاز الذي يتألف من عدة أجزاء يمثل الجزء الأول منها حجرة التخثير والجزء الثاني يمثل حجرة التلبيد ، أما الجزء الثالث فيمثل حجرة الترسيب التي تحتوي على صفائح مائلة بزاوية 60. تفصل بين صفيحة وأخرى مسافة متغيرة حيث تكون بالقسم الأول 4 سم أما في القسم الثاني فتكون المسافة بين الصفائح 2 سم.

يحتوي الجهاز إضافة لذلك على خزان الماء المراد معالجته وخزان الماء المعالج ، إضافة إلى مضخة وعدد من الصمامات للسيطرة على جريان الماء. الجدول (3) يبيّن مواصفات جهاز الترسيب ذي الصفائح المائلة المستخدم

طريقة العمل في جهاز الترسيب ذو الصفائح المائلة

تم تهيئة الماء الملوث أو الماء الخارج من وحدة الأمتزاز بالكاربون المنشط .

– تم إضافة كميات محددة من المواد الكيمياوية المستعملة في البحث (مثل مادة الشب او متعدد كلوريد الحديديك) إلى حجرة المزج السريع ، ينتقل الماء بعدها إلى حجرة التلبيد .

– بعدها يدخل الماء إلى حجرة الترسيب وبمعدل جريان يتم السيطرة عليه بواسطة المضخة.

النتائج والمناقشة

إن أهم العوامل التي تؤثر على عملية الامتزاز هي معدل الجريان وسمك طبقة المادة ألمازة وطبيعة وتركيز المادة الممتزة (تم أستخدام الماء الملوث المطروح من مصافي النفط في بيجي الى النهر وبتركيز ثابت مفحوص وهو 8 (ملغم /لتر) ولمادة الفينول.

إن زمن التماس عامل مهم في تصميم عمود الامتزاز ذي الطبقة الثابتة ولذلك فأن سمك الطبقة وسرعة السائل الفراغية هما العاملان الرئيسيان في التصميم.

نلاحظ من الشكل رقم (3) انه عند زيادة معدل الجريان بثبوت سمك الطبقة فأن تركيز الفينول الخارج يزداد وذلك لعدة أسباب منها عدم وجود الوقت الكافي لحدوث الامتزاز و وجود مساحات معينة وحجم معين من الكاربون غير مغطاة ولذلك لا يحدث الامتزاز عليه وبذلك تتكون مناطق نقية من الكاربون المنشط أي مواقع أمتزاز فارغة. ولكن عندما يكون معدل الجريان قليلة أي وقت التماس كبيراً فأن ذلك سيؤدي إلى إتاحة الوقت الكافي لامتزاز كمية اكبر من الملوثات وهذا يؤدي إلى شبه تشبع الكاربون المنشط بالمواد الملوثة قبل الانتقال إلى الجزء الأخر من الطبقة مما يعني إن كمية المادة الممتزة تكون اكبر في هذه الحالة.

إن سمك طبقة الكاربون أهمية كبيرة في عملية الامتزاز , ويتضح من الشكل رقم(4) أن قلة سمك الطبقة تؤدي إلى زيادة تركيز الفينول الخارج. أما زيادة سمك طبقة الكاربون فأنها تعني زيادة كمية الكاربون أي زيادة المواقع المتاحة للامتزاز وهذا ما يقلل من تركيز تركيز الفينول الخارج كذلك زيادة السمك تؤدي إلى تقليل ظاهرة ترك مساحات فارغة لكونه يتيح وقت أكثر للماء الملوث للتماس مع الكاربون.

ان زيادة سمك طبقة الكاربون تؤدي إلى امتزاز كمية مواد هايدروكاربونية أكثر وبالتالي يتم استهلاك الكاربون بصورة كاملة والذي يؤدي إلى استنزاف الكاربون وبذلك يفقد عمود الامتزاز فائدته بحيث يخرج الماء الملوث بدون معالجة وتتساوى تراكيز الملوثات الداخلة والخارجة وعندها يحتاج

الشكل رقم (5) وهي تمثل منحنيات الامتزاز للفينول عند سمك كاربون منشط مقداره 35سم. نلاحظ من هذه الأشكال انه عند زيادة سرعة السائل الفراغية بثبوت سمك الطبقة فأن نقطة الاختراق ستظهر مبكرة أي يحدث الاختراق بسرعة وذلك لعدة أسباب منها عدم وجود الوقت الكافي لحدوث الامتزاز و وجود مساحات معينة وحجم معين من الكاربون غير مغطاة ولذلك لا يحدث الامتزاز عليه وبذلك تتكون مناطق نقية من الكاربون المنشط أي مواقع أمتزاز فارغة. ولكن عندما تكون قليلة أي وقت التماس كبيراً فأن ذلك سيؤدي إلى إتاحة الوقت الكافي لامتزاز كمية اكبر من الملوثات وهذا يؤدي إلى شبه تشبع الكاربون المنشط بالمواد الملوثة قبل الانتقال إلى الجزء الأخر من الطبقة مما يعني إن كمية المادة الممتزة تكون اكبر في هذه الحالة. ومن الملاحظ أيضاً أن زيادة سرعة السائل الفراغية تقلل حجم الماء المعالج إلى أن يتم حدوث الاختراق وتقلل زمن التماس بين المادة المذابة والمـادة ألمازة وهذا متوافق مـع ما توصلت إلـيه(**أبتسام2011**).أن تشبع الكاربون المنشط بالملوثات يتم أعادة تنشيطه بالتسخين

أما حوض الترسيب بالألواح المتوازية فأن تشبعه بالملوثات فيتم التخلص منها من خلال تفريغ الحوض ودفع المياه الملوثة والمشبعة بالملوثات الى أحواض تجفيف بالطاقة الشمسية وهي عملية أقتصادية وفعالة للتخلص من المياه الملوثة.

تم ربط منظومة الترسيب بالألواح المتوازية مع الخارج من وحدة الأمتزاز بالكاربون المنشط وتم أضافة متعدد كلوريد الحديديك وبتركيز قليل(10-25 ملغم /لتر) لغرض أزالة الكمية المتبقية من الفينول وتم الحصول على مياه معالجة تنطبق عليها شروط المياه المستخدمة للأغراض الزراعية وحسب الجدول رقم(2) النوع (ب) مع الأحذ بنظر الأعتبار أن تركيز الفينول يقترب من الصفر..وجميع هذه التجارب أجريت في منظومة الألواح المتوازية من خلال حقن كمية محددة من متعدد كلوربد الحديديك وتم الأكتفاء بقياس نسبة الفينول في المياه الخارجة من منظومة الألواح المتوازية وكانت قريبة الى الصفر وهي تتطابق مع نتائج الباحثين(**ولديرير وأخرين2014**).

الاستنتاجات

1- إن تركيز الملوثات المدروسة لمياه مصفى بيجي الخارجة من جميع وحدات المعالجة لا تزال مرتفعة جداً وهي خارج الحدود المسموح بها وفق المواصفات العراقية.

2- إمكانية تقليل تراكيز قسم محدد من الملوثات إلى الحدود المسموح بها وفق المواصفات العراقية باستخدام الكاربون المنشط الحبيبي ولكن ضمن هذه المواصفات لا يمكن استخدام هذه المياه للإغراض الزراعية وحسب الجدول رقم(2).

3- أن أفضل معدل جريان هو 2 لتر/ساعة.

4- ان معدل الجريان التي لها علاقة بزمن التماس وسمك الكاربون المنشط لها تأثيراً مهما على عملية الامتزاز.

5- يتناسب تركيز الفينول الخارج عكسيا مع سمك طبقة الكاربون المنشط وطردياً مع معدل الجريان.

6- أن أستخدام مادة متعدد كلوريد الحديديك يساعد على أزالة الكمية المتبقية من الفينول

المصادر

لطيف حميد علي، "التلوث الصناعي"، دار الكتب للطباعة والنشر جامعة الموصل، صفحة (184- 188) ، 1987.

Dialynas, E. and Diamadopoulos, E, "Integration of Immersed Membrane Ultra-filtration with Coagulation and Activated Carbon Adsorption for Advanced Treatment of Municipal Waste Water", Department of Environmental Engineering, Technical university of crete, chania, Greece, 2008.

Hameed, B. H., and Rahman, A., "Removal of phenol from aqueous Solution by Adsorption onto Activated Carbon Prepared from Biomass Material", Applied science publishers LTD, Essex, chapter 3, PP. (49-84), 2008.

Ibtisam A. Jaddo," Study of Using Granular Activated Carbon For Removing Phenol, Parachlorophenol, and Benzene From Wastewater of Baiji Refinery", Department of chemical engineering, University of Tikrit, 2011.

Ismail, Sh., "Evaluation of Heterogeneous Adsorbents Bed for the Removal of Organic Materials from Water", Ph. D. Thesis, university of Baghdad P. (4-39), Iraq, 2008.

Madaeni S.S,"Membarance Treatment of Oily Waste Water From Refinery Processes",Asia Pacific Journal of Chemical Engineering,8,(45-53), 2013.

Wilderer,A."Evolution of Sanitation & waste treatmenttechnologies through the centeries", 2014, ISBN9781780404844.

WWW.ress.com,vol.113,IssB,1,25

جدول رقم1 .نتائج الفحوصات المختبرية للمياه المطروحة إلى النهر من مصافي بيجي

الفحص	القيمة	الفحص	القيمة
pH	8.65	Cd, mg/l	<0.1
Cond., ms	2.39	Cr, mg/l	<0.1
Cl^- ,mg/l	122	Cu, mg/l	0.19
Hardness ,mg/l	640	Fe, mg/l	0.6
SO_4^- ,mg/l	80	Pb, mg/l	<0.1
OH^- ,mg/l	zero	Ni, mg/l	0.15
(HCO_3^-, CO_3^-),mg/l	120	Ag, mg/l	<0.05
Phenol, mg/l	8	Oil	7.5

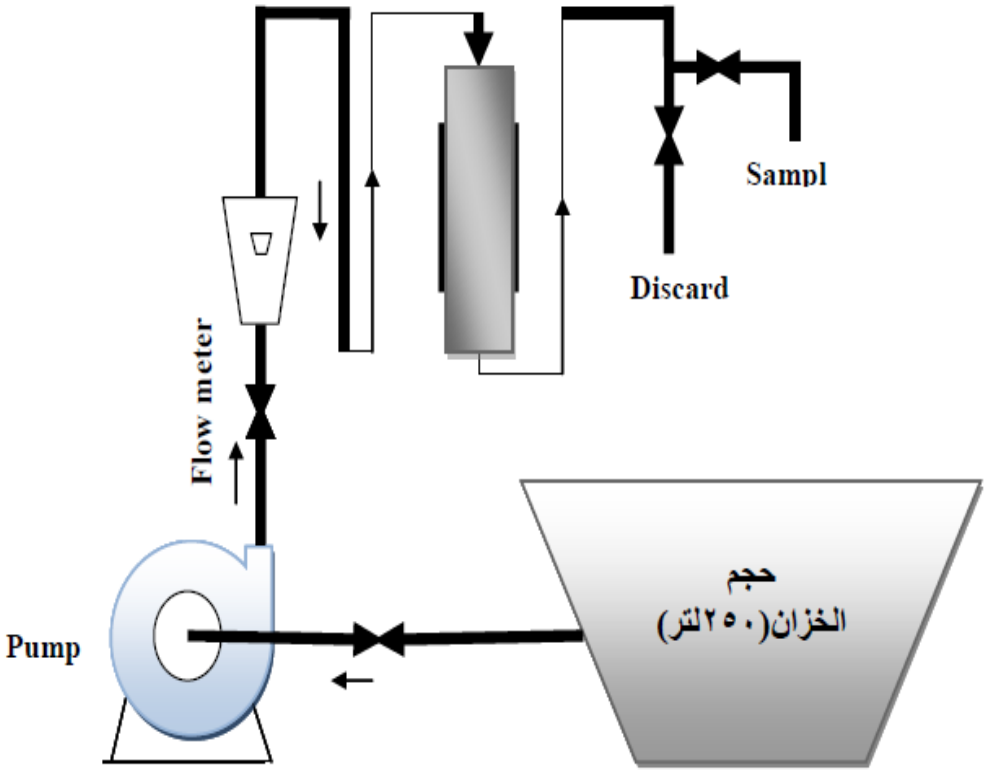

شكل رقم 1 . مخطط لجهاز الأمتزاز

جدول رقم 2 . الحدود القصوى المسموح بها للمعايير القياسية الخاصة بالمياه المعالجة المستخدمة لأغراض الري

المؤشر	الخضار المطبوخة	المتنزهات والملاعب	الملاعب الرياضية	الأشجار المثمرة	جوانب الطرق الخارجية	المسطحات الخضراء	الحبوب والمحاصيل العلفية	المحاصيل الصناعية	الأشجار الحرجية
المؤشر	أ			ب				ج	
BOD_5(mg/l)	30			100				150	
COD(mg/l)	75			200				300	
DO(mg/l)	أكبر من 4			–				–	
TDS(mg/l)	15000			1500				–	
SS(mg/l)	50			150				150	
SAR	9								
pH	9–6								
CL2residual	0.5			–				–	
NO_3–N (mg/l)	20			25				25	
NH_4–N (mg/l)	3			5				–	

جدول رقم 3 . مواصفات جهاز الترسيب ذو الصفائح

زاوية ميل الصفائح	60°
معدل الجريان	(55– 24)لتر /ساعة
ارتفاع الجهاز	100 سم
مساحة الترسيب لحجرة الترسيب	12837 سم^2
عرض الجهاز	120 سم
سمك الجهاز	25 سم

شكل رقم2. جهاز الترسيب ذو الصفائح

جدول 4. بعض الخواص الفيزياوية للكاربون المنشط الحبيبي

الخاصية	القيمة
الكثافة	482.025 كغم/م^3
المسامية	0.41
قطر الحبيبية	(2–3) ملم
المساحة السطحية	1175.62م^2/غم

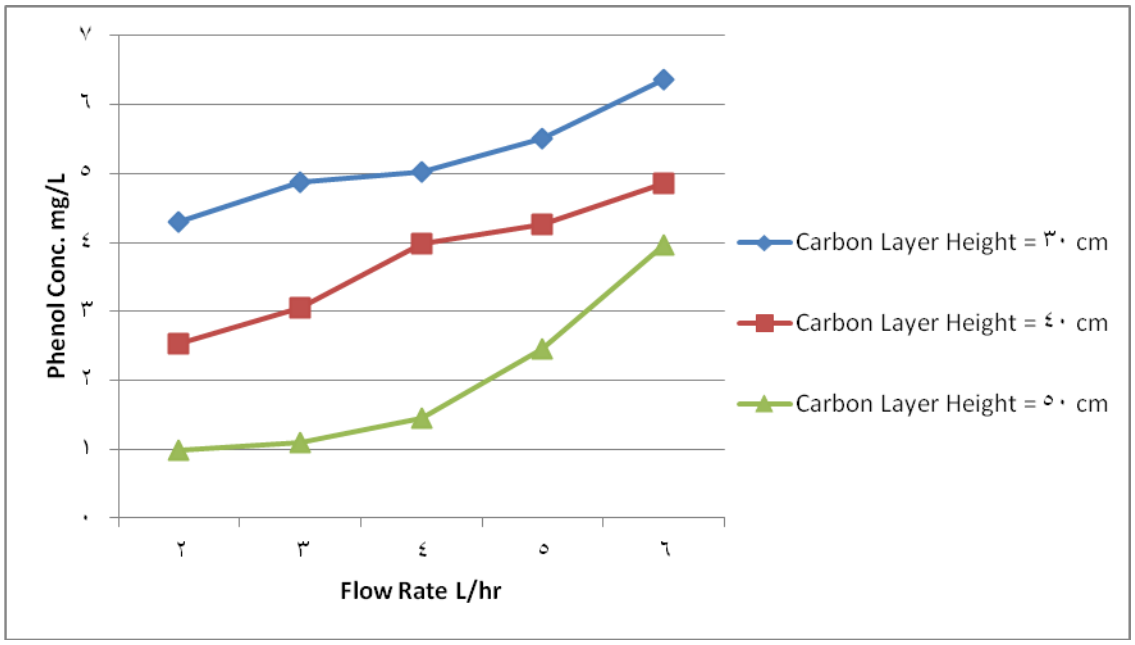

شكل رقم 3. تأثير معدل التدفق على تركيز الفينول المزال من الماء الملوث

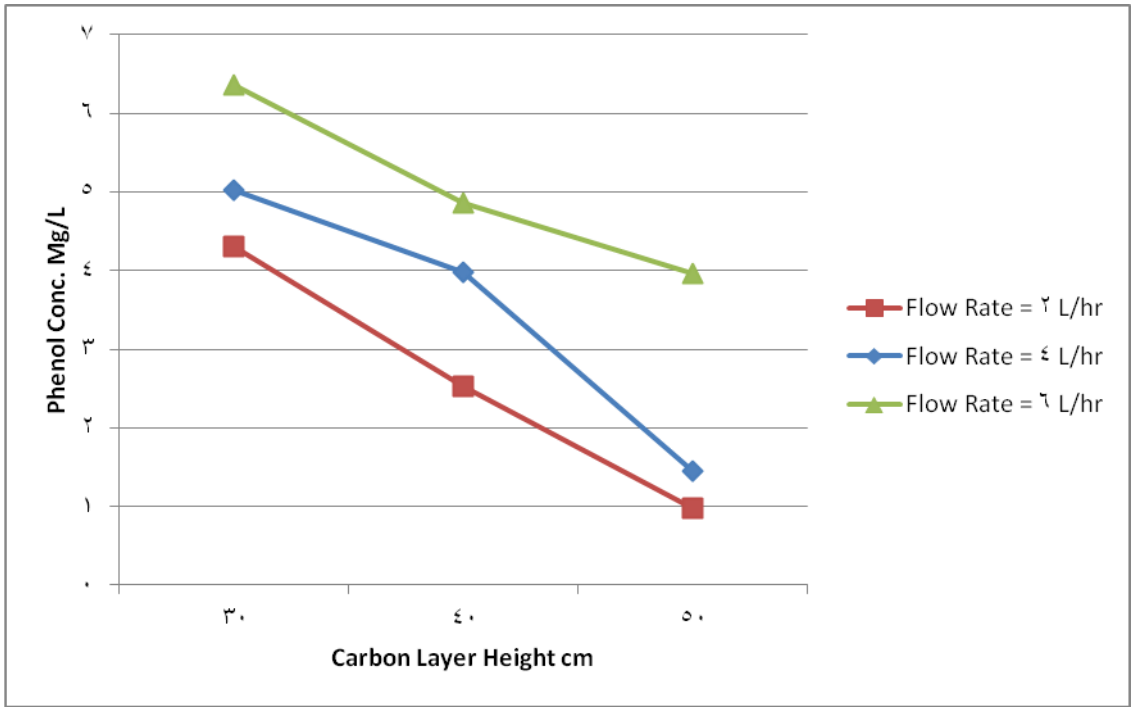

شكل رقم4. تأثير سمك طبقة الكاربون على تركيز الفينول المزال من الماء

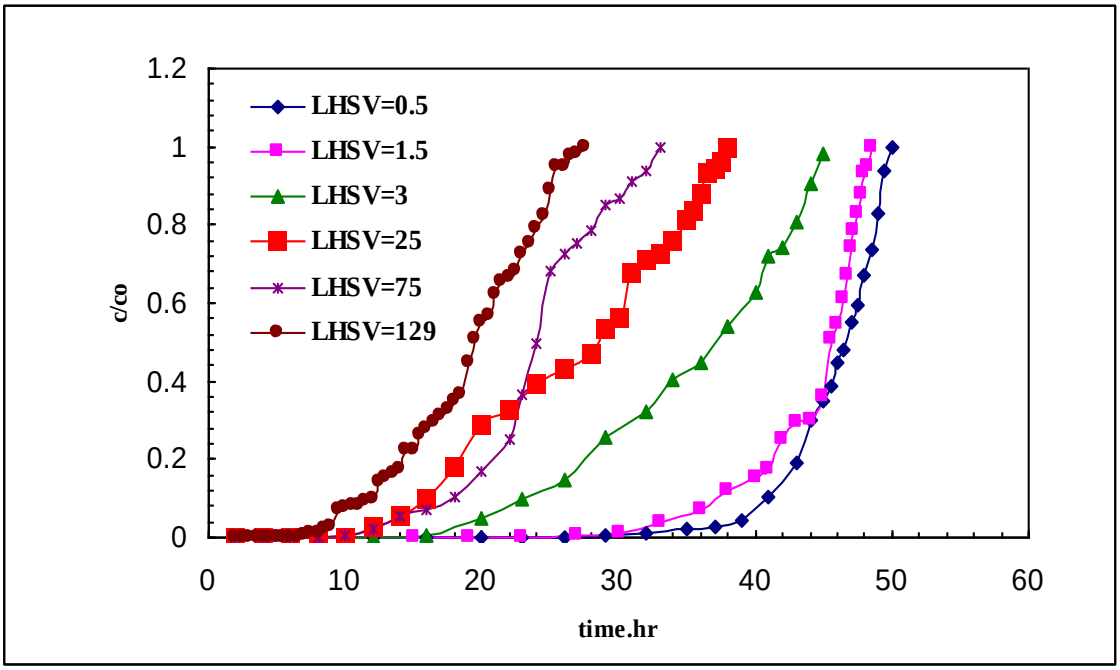

شكل رقم 5. منحنيات الامتزاز للفينول على الكاربون المنشط (السمك =35سم)